GEOCHEMICAL, SPATIAL, AND TEMPORAL RELATIONSHIPS OF THE INTRUSIVES AND META-INTRUSIVES OF THE POGO DEPOSIT, EASTERN INTERIOR, AK

By

William D. Thompson, B.S.

A Thesis Submitted in Partial Fulfilment of the Requirements

for the Degree of

Master of Science

in

Geology

University of Alaska Fairbanks

December 2020

APPROVED:

Dr. Rainer Newberry, Committee Chair

Dr. Mary Keskinen, Committee Member

Dr. Jochen Mezger, Committee Member

Dr. Paul McCarthy, Chair,

Department of Geosciences

Dr. Kinchel Doerner, Dean,

College of Natural Science and Mathematics

Dr. Richard Collins,

Director of the Graduate School

Abstract

The Pogo deposit is an intrusion-related gold deposit (IRGD) located approximately 90 km southeast of Fairbanks, Alaska. It consists mainly of shallowly NW dipping quartz veins hosted in amphibolite facies paragneiss and predominately granite orthogneiss bodies. To date the deposit has produced over 4 million ounces of gold.

U-Pb zircon dating of the orthogneisses shows they have Devonian-Mississippian protolith ages. Dates from the metamorphic zircons, established by microprobe Th data and cathodoluminescence studies, constrain a mid-Cretaceous metamorphic event to ~116 Ma. Recrystallization of kyanite to sillimanite and zircon recrystallization indicates this was a large fluid flux event that predated mineralization by 10 million years.

Due to the fine-grained nature of the intrusive rocks at Pogo, identifying rocks in hand sample proved problematic. By combining XRF analysis of the rocks' major and trace elements and age data from this and previous studies, I identified and differentiated several suites of igneous rocks. The oldest is peraluminous granite, emplaced at ~2.5 ± 0.5 kb at ~109-107 Ma, predating mineralization at 104 Ma at a pressure of 2.0 kb. Non-peraluminous granite is less common and of uncertain relationship to the peraluminous granite. Next, temporally, is a body named the Football pluton (and associated dike) of granodioritic to tonalitic composition, emplaced at 2.0 ± 0.5 kb at 103 ± 2 Ma. Not only indistinguishable from age and depth of mineralization, a dike of this body is present downdip underneath the Liese veins (main zone of mineralization), making it the most likely candidate for being the causative pluton for mineralization. The final mid-Cretaceous body is the Liese pluton (and associated dikes), of quartz diorite to tonalite. This forms a large body with E-W dikes cutting the Pogo mineralization and post-dating it at 95.4 ± 0.2 Ma, emplaced at a pressure of 1.0 kb.

Thermobarometry and radiometric dating indicate a consistent uplift rate of about 0.6 mm/year during the mid-Cretaceous, 116 to 95 Ma. Initially an extensional event, subduction-related magmatism began at about 105 Ma. At the same time, the thrust faults were re-activated as low angle normal faults that apparently acted as pathways for the Liese mineralization.

Table of Contents

List of Figures

List of Tables

Page

List of Appendices

Page

1 Chapter 1 Introduction and Methods

1.1 Introduction

The "Tintina gold belt" (TGB, Fig. 1-1) is an arcuate region in Alaska and Central Yukon that contains significant gold resources, invariably hosted by (or spatially associated with) felsic intrusions. Major deposits and prospects include Fort Knox (5.4 million ounces of gold = Moz), Donlin Creek (12.3 Moz), True North (0.79 Moz), Brewery Creek (0.85 Moz), Dolphin (~ 1 Moz), Livengood (9 Moz) and many others (Gough and Day, 2007). Mineralization age, emplacement depth, size and type of associated pluton and proximity to causative pluton vary; however, all the listed deposits are generally considered (e.g., Flanigan et al., 2000) intrusion related gold deposits (IRGDs). The Pogo deposit (Fig. 1-1), 90 km SE of Fairbanks, is also widely (but not universally) believed to be an IRGD (e.g., Smith et al., 1999).

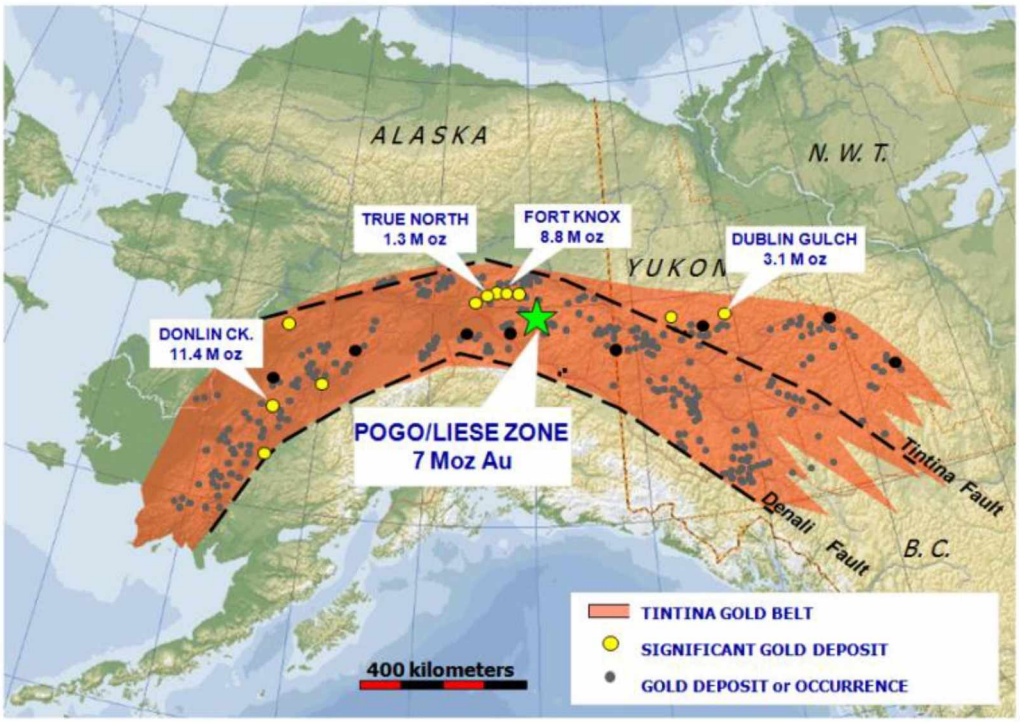

Figure 1-1:Map of Alaska and adjacent Canada showing the location of the Pogo deposit in the (orange) so-called 'Tintina Gold belt'. Modified from Gough and Day, 2007.

The Pogo deposit mainly consists of steeply and shallowly dipping quartz veins in complexly deformed metamorphic and minor igneous rocks. The deposit is complicated by a post-mineralization intrusion (and associated dikes) that cut veins and had an uncertain effect on

the deposit, as well as extensive post and syn-mineralization faulting. The original occurrence was a blind discovery, found by fortuitous drilling, and additional discoveries in the immediate area are almost exclusively drill-based. It has been the focus of multiple studies over the past two decades, which have not yet been able to explain the relations of nearby pluton(s) to the deposit.

The Pogo deposit displays characteristics of both orogenic (i.e., not related to plutons per se) deposits and IRGDs. The style of veining, lack of obvious metal zoning, associated sericite-carbonate alteration, and CO_2-bearing fluid inclusions (Smith et al., 1999) are features seen in many orogenic gold deposits as well as some IRGDs. However, the veins often cut through metamorphic fabric, and are faulted rather than sigmoidally deformed, characteristics not consistent with orogenic origins (Rhys et al., 2003). Furthermore, the mid-Cretaceous age of mineralization is similar to that of some nearby plutons, and the Au-As-Bi-Sb-W-Te geochemical assemblage is both similar to that seen in many IRGDs, and different (especially the elevated Bi) from that of typical orogenic deposits (Flanigan et al., 2000). However, the absence of the supposed causative intrusion in the immediate Liese (main ore body) area is problematic. This is further compounded by the fine-grained nature of the intrusive rocks, which makes differentiations between units difficult by typical techniques such as hand sample inspection and stained slab analysis difficult.

The two purposes of this research are to (1) classify the intrusive and meta-intrusive units through a systematic approach using chemical compositions and textural characteristics, and (2) interpret the timing of events at and near the deposit based on new U-Pb ages. The temporal and spatial relation of metamorphism to mineralization is important in consideration of the origin of the gold bearing fluids, and hence, the origin of the deposit. Determining the timing of the last prograde metamorphism "event" will help elucidate these concerns. I intend to resolve controversies raised by previous studies, such as the age and character of metamorphosed granites in the deposit. Through this research I intended to unravel some of the deposit's complex history, in hopes that better understanding will lead to additional discoveries.

1.2 Geologic Setting

1.2.1 Regional Geology

Extending over 2000 km, the Yukon-Tanana terrane (YTT) is a composite, polygenetic assemblage of rocks that represents the largest tectonostratigraphic terrane in the northern North

American Cordillera (Hansen & Dusel-Bacon, 1998). The YTT stretches from the eastern Interior, Alaska, into the Yukon, Canada, and is bounded and (or) displaced by the Tintina fault to the north and the Denali fault to the south (Fig. 1-2). It has a complex, polyphase history involving multiple deformation events affecting a multitude of volcanic, plutonic, and sedimentary units. Even the question of what belongs in the YTT is debated. For example, many consider the metamorphic rocks of the greater Fairbanks area part of the YTT (e.g., Fig. 1-2); others do not (e.g., Dussel-Bacon et al., 2015; Fig. 1-3).

Numerous attempts have been made to subdivide the YTT into smaller coherent pieces both within and outside of Alaska. A currently accepted version distinguishes metamorphic rocks in the general Pogo area as part of the 'Lake George Assemblage', characterized by amphibolite facies regional metamorphism and abundant Devono-Mississippian granitic orthogneiss bodies (Dusel-Bacon et al., 2002). These authors indicate high-P metamorphism occurred as part of a contractional event in the early Jurassic and an extensional event took place in the mid-Cretaceous, prior to local plutonism.

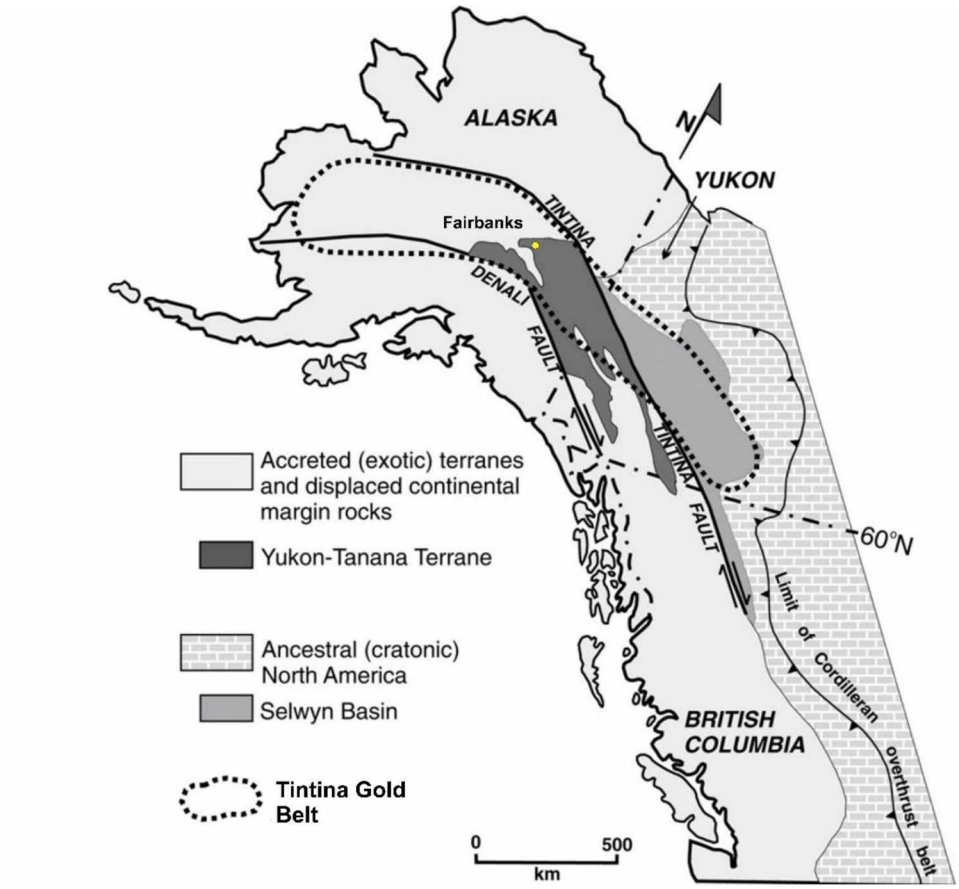

Figure 1-2: One version of the location and size of the YTT in relation to major faults and the Tintina Gold Belt. Modified from Mair et al., 2006.

1.2.2 Intrusions in YTT

Abundant intrusions occur in the YTT in general, and the Lake George assemblage (Fig. 1-3) in particular, with Devonian to Paleogene ages. The oldest (Devonian-Mississipian) are granite to tonalite bodies that were subsequently deformed into orthogneiss. Trace element compositions (e.g., Werdon et al., 2004; Dusel-Bacon et al., 2013) suggest they represent extensional, within-plate, and subduction-related tectonic environments.

Triassic and Jurassic intrusions occur in other parts of the YTT, but in the Lake George assemblage a multitude of intrusions were emplaced during the Mid- to Late-Cretaceous, many of which have been related to gold deposits within the TGB (Flanigan et al., 2000). Arc-related magmatism produced intermediate to felsic plutons of diorite to granite during the period from ~110 to 88 Ma (Werdon et al., 2004). Intrusions vary greatly in expression, from small (meter size) dikes to batholiths (Fig. 1-3).

The most recent magmatism in the YTT consists of bimodal (mafic and felsic) early Paleogene a (~50-55 Ma) plutonic, volcanic, and dike rocks (Werdon et al., 2004). Subsequent steeply dipping, NE-striking faults with significant vertical offsets (e.g., the Shaw Creek fault, Fig. 3) caused variable preservation of the volcanic and other shallow-crustal rocks in 'down-dropped' blocks.

1.3 Pogo Deposit

1.3.1 Pogo Deposit Geology

The Pogo deposit is an enormous, high-grade gold deposit located in the TGB. The original discoveries in the Pogo area were of horizontally extensive, stacked, shallow-dipping, sulfide-poor quartz veins, the so-called Liese veins (Fig. 1-4). In the last 15 years additional Liese-type veins have been discovered, both under L2, and to the north, northeast, and northwest of the Liese Creek pluton (Fig. 1-5), including steeply-dipping veins present NE of Liese Creek. The 4021 prospect, ~5 kilometers east of the Liese Zone (Fig. 1-5) consists of shallowly dipping auriferous quartz veins hosted in granitic orthogneiss, of uncertain relation to Liese veins. In comparison, the Liese veins are typically hosted by biotite-feldspar-quartz gneiss (paragneiss). Amphibolite and serpentinite are locally present adjacent to the veins.

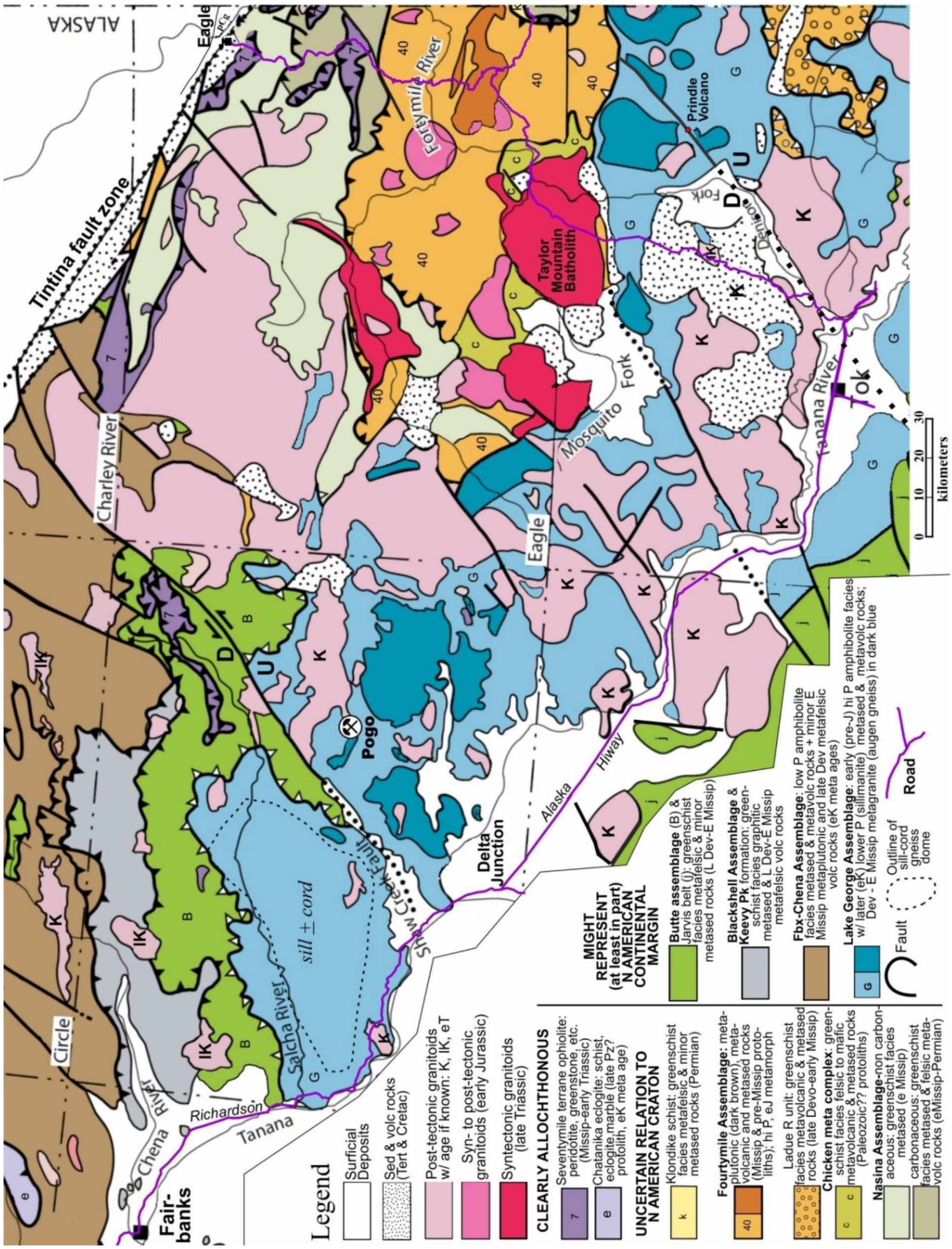

Figure 1-3: Generalized geologic map of Eastern Interior Alaska showing one version of YTT subdivisions and the location of the Pogo deposit, modified from Dusel-Bacon et al. (2015).

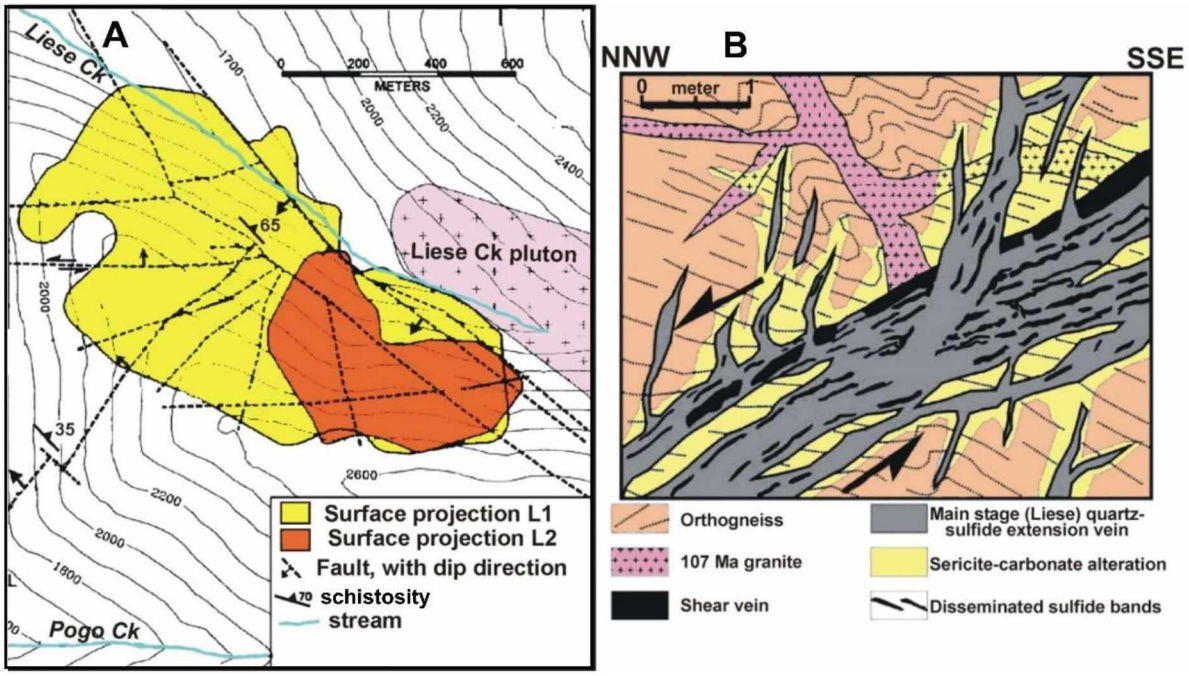

Figure 1-4:Simplified map and schematic section, Pogo area. A. Simplified map, showing projections to the surface of the major ore bodies (L1 and L2), major post-ore faults, and schistosity. The ore bodies are shallowly NNW-dipping quartz-sulfide veins. Modified from Rhys et al. (2003). B. Schematic cross-section, showing interpreted relationships between main schistosity, early Cretaceous granite, the main-stage low-angle quartz vein, and hydrothermal alteration. Modified from Rhys et al. (2003).

Previous published studies concerning the Pogo deposit include Smith et al. (1999), Rhys et al. (2003), Dilworth (2003), and Dilworth et al. (2007). Until the 21st century, the most detailed mapping was at a scale of 1:250,000. Recent 1:63,360 maps that enclose the Pogo area include those by Day et al. (2003) and Werdon et al. (2004). Dilworth (2003) also presents a simplified geologic map of the greater Pogo area. Day et al. (2003) show generalized geology in the immediate Pogo area and provide important geochronologic information. They were largely concerned with defining broad structural terranes. All three maps are dominated by gneissic units with Cretaceous intrusions. The intrusions are broken out differently on the different maps; Dilworth (2003), for example, shows a strip of Cretaceous granite separating 'tonalite' from 'diorite' and shows the orthogneiss as having a mid-Cretaceous protolith (Fig. 1-7A). Further

differences between the Dilworth (2003) and Werdon et al. (2004) maps are illustrated in Figure 1-6.

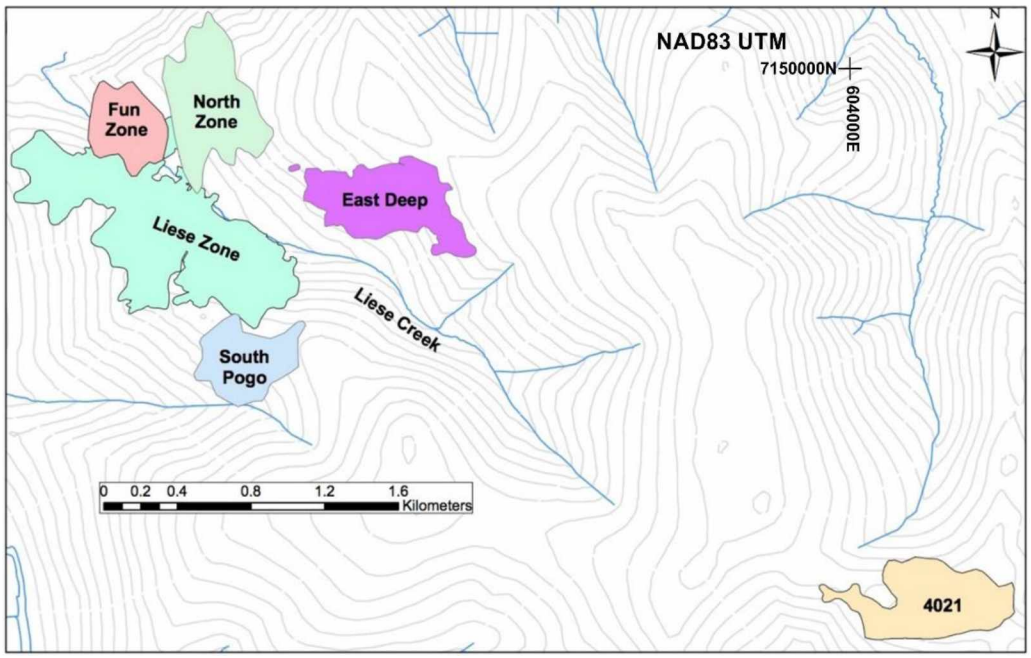

Figure 1-5:Ore zone reference map, with ore zones projected to surface.

Based on U-Pb radiometric ages and compositional data, Dilworth (2003) recognizes three major (and one minor) Cretaceous-early Tertiary igneous suites and a chronology dominated by Cretaceous events (Fig. 1-8). The oldest suite (109-107 Ma) is mostly granite, is present as dikes that parallel and are cut by low-angle quartz veins (Fig. 1-4B). These rocks locally exhibit sericite-carbonate alteration with associated mineralization (Fig. 1-4). The granites are variably deformed and can exhibit a weak mineral alignment (Rys et al., 2003).

The second oldest suite is hornblende-biotite tonalite to granodiorite. The suite is post-kinematic: U-Pb zircon age is 103 ± 2 Ma (Dilworth, 2003). Because MoS_2 from the L1 vein yields a statistically indistinguishable ^{187}Re-^{187}Os age of 104 ± 1 Ma (Selby et al, 2002) the tonalite suite is alleged to be responsible for the Pogo mineralization (Dilworth et al., 2007). No further evidence for this conjecture has been offered however. Known outcrops of the tonalite are more than 1.5 km from the Liese zone, making a genetic relationship problematic.

The youngest major suite consists of diorite to tonalite; known as the Liese Creek ‘diorite’. This body (Figs. 1-4, 1-6) has a U-Pb age of 95.4 ± 0.2 Ma. The pluton intrudes most other units

in the Pogo area and appears to cut off Liese-type veins. Rhys et al. (2003) suggest that narrow, E-W striking, "mafic" dikes in the orebody are offshoots from the Liese Creek pluton.

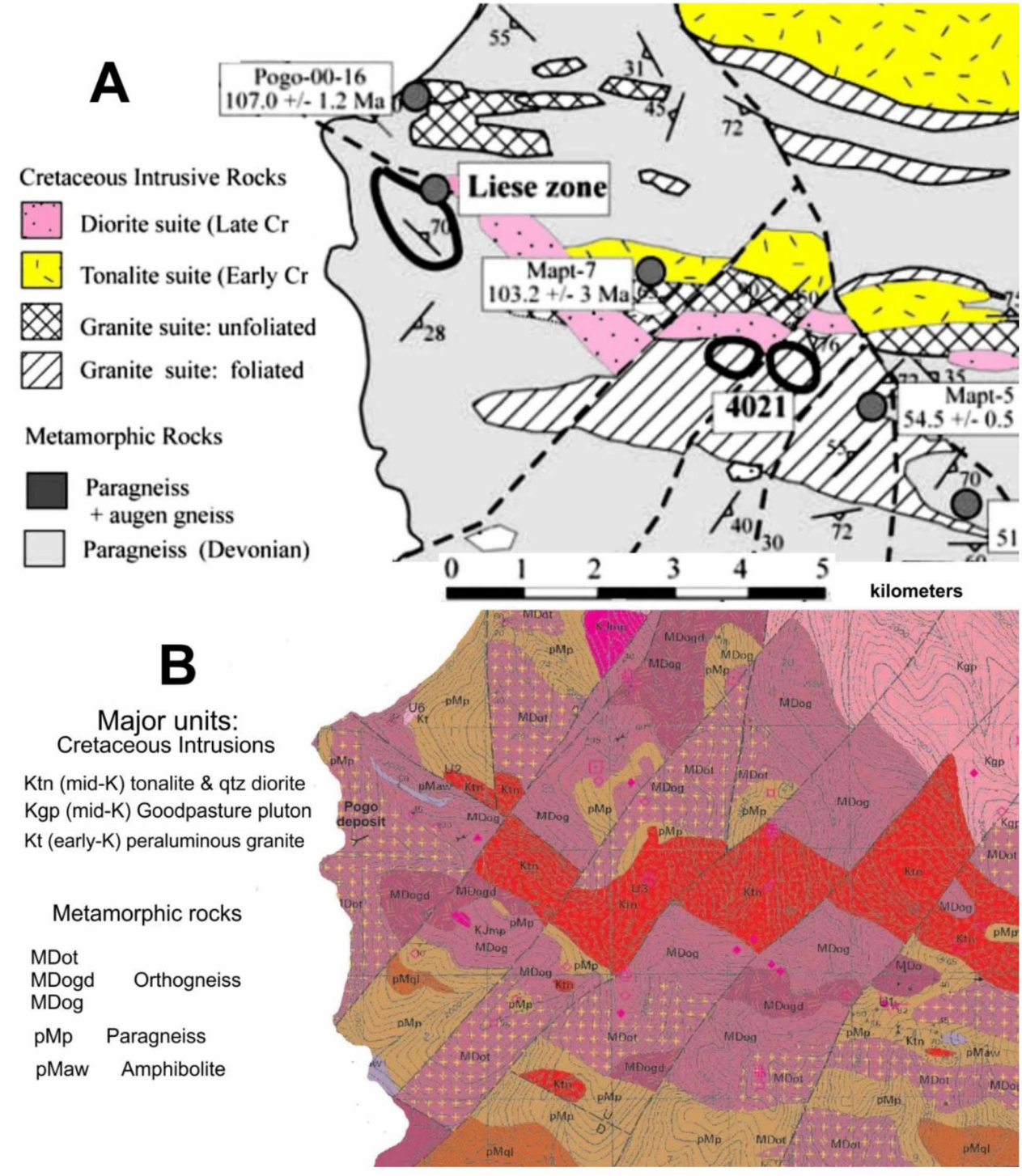

Figure 1-6: Geology of the general Pogo area as depicted (a) by Dilworth (2003) and (b) by Werdon et al. (2004). The two maps are at the same scale and show the same area, bounded to the west by the Goodpasture River. Although broadly similar, they differ in many differ in many details.

The youngest igneous suite consists of rare, bimodal, early Paleogene (ca. 50-55 Ma) mafic and felsic dikes. Werdon et al. (2004) show dikes of this suite with NNW and NNE strikes.

Mapping of the area by Dilworth (2003) shows older, E-W striking igneous bodies, cut by the NW to E-W striking Liese Creek pluton. All three are offset by NE-striking faults (Fig. 1-6A). Dilworth (2003) also shows a body of early Cretaceous granitic gneiss south of and including the 4021 prospect and several E-W striking bodies to the north. The largest body of unfoliated granite is present between tonalite and diorite. Some descriptions of samples include a so-called "meta-granite" which is only slightly foliated. None of the large 'Cretaceous' granite gneiss bodies shown by Dilworth (2003) were dated, and their age is conjectural.

Previous workers disagree about the timing of major metamorphism in the Pogo area. Because the metamorphic rocks in the immediate Pogo area include both amphibolite and garnet-biotite-muscovite (locally sillimanite-bearing) schist—commonly lacking retrograde minerals—the last major metamorphic event must have taken place under amphibolite facies conditions. That is, the last prograde metamorphism occurred at about 9 kb pressure (~30 km depth; Dusel-Bacon et al., 2002). Dilworth (2003) suggests that metamorphism—which she shows as producing large bodies of granitic orthogneiss (Fig. 1-6A) —lasted until approximately 107 Ma (Fig. 1-7). Rhys et al. (2003) show that some of the Early Cretaceous granites cut foliation in the surrounding gneiss, and are undeformed, but are cut by quartz veins (Fig. 1-4). Mineralization occurred at approximately 104 Ma (Selby et al., 2002) at a pressure of ~2 kb (Dilworth, 2003), or a depth of ~ 7 km. This interpretation would suggest an enormous uplift rate, from 30 km depth to 7 km depth in a period of approximately 2 Ma. In contrast, Day et al. (2003) present zircon rim and monazite ages and suggest the last major metamorphic event occurred at approximately 115 Ma. Based on their data for granitic gneisses approximately 10-15 km from Pogo, such bodies are of Devono-Mississippian age and are not Cretaceous. The Day et al. (2003) data would allow for an interval between regional metamorphism and hydrothermal mineralization of ~10 Ma, which requires high (~2mm/yr) but less drastic, uplift rates.

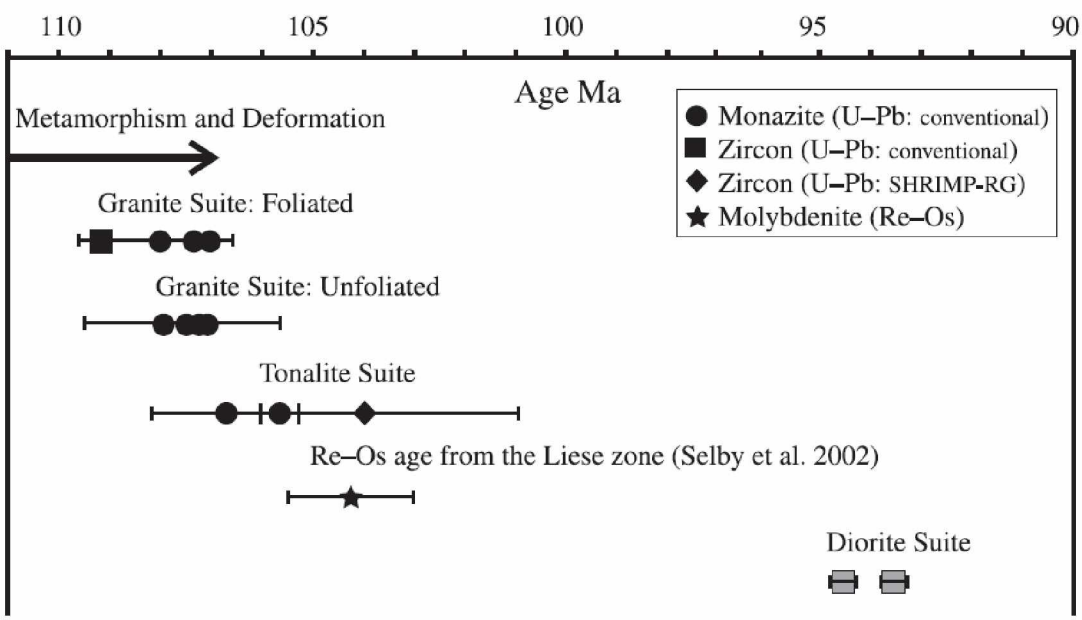

Figure 1-7:: Chronology of events in the Pogo area, as taken from Dilworth (2003).

1.3.2 Pogo Mineralization

The mineralization at Pogo is largely represented by quartz veins of the Liese zones (Fig. 1-4). The veins can be modeled as three or four tabular, gently NNW dipping bodies 1 to 20 meters thick, containing approximately 3 percent opaque minerals, including pyrite, pyrrhotite, loellingite, arsenopyrite, chalcopyrite, bismuthinite, tetradymite, various Ag-Pb-Bi ± S minerals, maldonite, native bismuth, and native gold (Smith et al., 1999). These bodies consist of 3 different types of shear veins (Rhys et al., 2003). The earliest are biotite selvage-bearing veins with low sulphide content that display top to southwest/east displacement under ductile conditions. The second, main-stage, quartz veins often exploit the shear of the earlier veining. This type of vein supplies the bulk of gold production at Pogo due to their thickness, up to 20 meters, and increased sulfide content (1-5%). Sericite-muscovite-Mg-Fe-Ca carbonate alteration commonly occurs adjacent to this type of vein, up to 10 meters from the veins, and overprints metamorphic mineral assemblages (Figure 1-4). The third type of vein occurs as steeply dipping extensions off of the main stage veins and shows evidence of top-to-the-northwest under brittle to semi-brittle conditions. Multiple lines of evidence (Rhys et al., 2003) suggest that the extension veins are coeval with the main-stage veins.

A previous study looked at amphibolite 'stratigraphy' to reconstruct the structural setting of the Liese veins (Newberry et al., 2012). Amphibolite samples were taken from the area around the upper 2 Liese veins (L1 and L2) and divided into 4 groups plus 4 sub-groups based on their immobile trace elements (Fig. 1-8). Correlation of the uniquely-identified amphibolite layers across the L1 and L2 (Fig. 1-9) shows approximately 90 meters of net thrust offset across L2 and 180 meters of thrust offset across L1. The Liese veins are former thrust faults, with small, but measurable offsets.

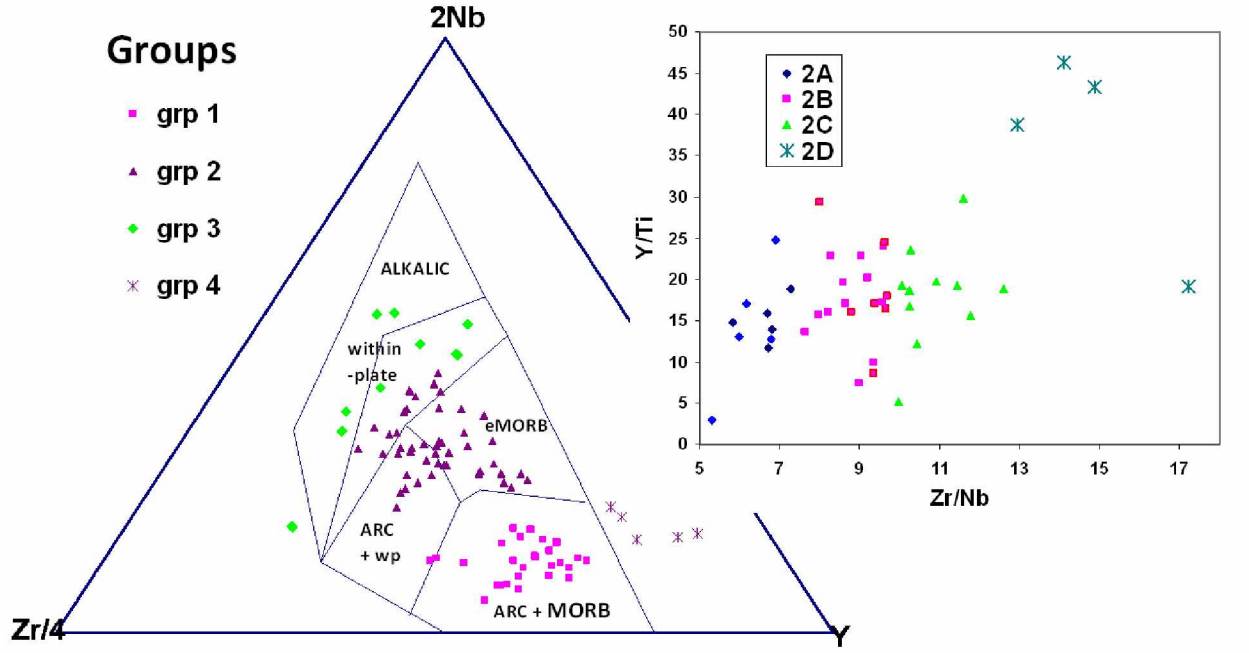

Figure 1-8: Pogo amphibolites divided into 4 groups and 4 sub-groups based on relative Nb, Zr, Y, and Ti. Modified from Newberry et al. (2012).

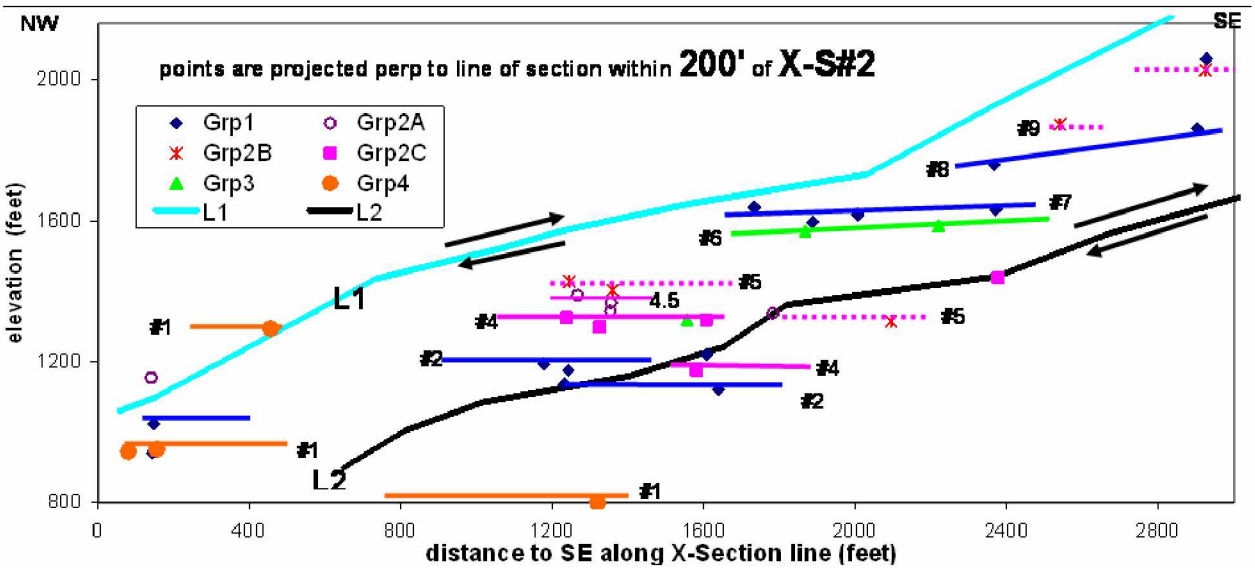

Figure 1-9: Cross section showing amphibolite bodies in relation to the L1 and L2 veins. Taken from Newberry et al. (2012).

1.4 Exploration History

Anomalous Au, As, and W concentrations were found in the vicinity of the Pogo and Liese Creeks following stream sediment and pan concentrate geochemical sampling in 1981 by WGM Inc. (Smith et al., 1999). Following the additional discovery of mineralized quartz float, claims were staked in the area in 1991 and conglomerated as the Stone Boy Venture by Sumitomo Metal Mining Arizona, Inc., and three other international companies. Subsequent prospecting and soil sampling identified a significant gold-in-soil anomaly. However, in 1993, the three other international companies withdrew and WGM remained sole operator. The Liese zone was discovered by three drill holes in 1994 and expanded by 13 holes in 1995 and 23 in 1996. The flat lying nature of the veins was determined in 1997 with the drilling of 41 holes. In the same year Sumitomo, SC Minerals, Inc., and Teck Resources, Inc., entered into agreement, with Teck becoming operator. Exploration drilling continued in the subsequent years, with an underground exploration program commencing in 1999. Full scale production at the mine began in 2006.

1.5 Objectives

The main goals of this study are to investigate the geochemical, spatial, and temporal relationships between the intrusive and meta-intrusive units at the Pogo deposit. The principal objectives to accomplish these goals will be to characterize the units present based upon their major and trace element compositions, mineralogy, and ages. Specific questions to be addressed in this study include:

- What are the immobile element distributions within intrusions and how do they relate to intrusion tectonic origins?
- Is the Liese pluton compositionally zoned and is it compositionally similar to the 'mafic' dikes?
- Can different granite bodies in/near Pogo be distinguished?
- What are the ages of orthogneiss in the Pogo deposit, including the 4021 area? Can different types be recognized and mapped?
- Can a distinct pluton with Liese mineralization age be recognized in the immediate Pogo area? If so, does it possess characteristics likely to cause mineralization?

- At what depths were the various pre-, syn- and post-intrusive units emplaced?
- When did the last period of regional metamorphism end?

Previous workers have disagreed over several distinctions among maps and within descriptions such as the location and age of orthogneiss bodies and differentiation of intrusive units (Fig. 1.6). The results of this study are intended to resolve these differing interpretations.

1.6 Methods

I have employed multiple methods of study to accomplish my objectives and goals stated above. I conducted field mapping of the intrusive and metamorphic units, focusing on areas of contention in previous mapping studies. I conducted petrographic studies in transmitted light to confirm and determine mineralogy of units. I conducted WDS electron microprobe analyses to measure trace and major elements of hornblende, plagioclase, garnet, biotite, and muscovite in order to calculate pressures and temperatures of emplacement and peak metamorphism. Additionally, I conducted analyses to measure trace elements in dated zircons in order to determine the genesis of metamorphic versus igneous material with relation to age. I utilized whole rock XRF analyses for the calculation of normative mineralogy used to identify the Pogo rocks. Finally, trace element data from the XRF analyses were used to discriminate between and to determine tectonic origins of the various rock suites.

1.6.1 Detailed Field Mapping

Detailed mapping at the Pogo deposit was completed at the 1:20000 scale over several extensive mapping efforts during the summers of 2014, 2015, and 2016. Rock stations were taken where there was reliable outcrop or subcrop with changes in lithology without significant apparent alteration. Occasional samples of float were also taken as samples. Stations were recorded with a Garmin GPSmap 62S. The NAD83 UTM coordinates of the station as well as a description (rock type, presence of foliation, alteration) was written down in a field notebook to later be manually imported. A total of 109 stations were collected.

Field data were compiled using ESRI's ArcGIS® 10.3.0. Rock stations were loaded into a map project assigned to a NAD83 UTM base. Rock stations compiled from previous studies and field mapping exercises were added as well, much of which had to be reprojected to fit the NAD83 UTM base. Map units and contacts were interpreted based upon the station data well as

structural data from previous mapping exercises and drill core data near the surface. Areas of the map not specifically mapped during this project have indeterminate lithologies and use boundaries defined by previous mapping exercises in the area. The compilation of data was re-defined into polygon and line layers. Units were assigned for each polygon and colors assigned for each map unit.

1.6.2. Petrographic study

A total of 63 thin sections were studied using reflected and transmitted light during this study. Thirty-one were produced for this study, the other 32 were obtained from a 1998 study of units at the Pogo deposit. Of the 31 produced, 9 were selected from core, 16 from field mapping, and the rest from underground face samples. The features described in the study include bulk rock texture, grain size, mineral habit, mineral mode, structural features, and alteration. Modal percentages were visually estimated and used to determine modal rock type using the IUGS igneous rock classification scheme to aid in comparison to the geochemical classification.

Additionally, a thick section of sillimanite-garnet-biotite gneiss was produced for geothermobarometry study. Mounts containing the zircons from the 4 dated rock samples were viewed through transmitted light to verify the alignment of the mounts for use in microprobe studies.

1.6.3 Mineral Chemical Analysis

I utilized 5 different sample sets for this study. I collected a set of 11 samples in the summer of 2014 from field and underground mapping that were made into polished thin sections in the fall of 2014. During the summer of 2015 I selected additional samples from core, previous field mapping, and summer 2015 field mapping that were made into polished thin sections during the fall. Selected samples from the 1998 thin section collection were analyzed as well as 3 thick sections made from core during the summer of 2016. Finally, zircons from the 4 dated samples were analyzed on their separate mounts. All samples were coated with a 250-300 Å carbon layer in order to prevent charge build-up and to be suitable for microprobe analysis.

Quantitative routines were developed for the analysis of hornblende, plagioclase, garnet, biotite, muscovite, and zircon using a wavelength-dispersive spectrometer on a JEOL JXA-

8530F electron microprobe in the Advanced Instruments Laboratory at the University of Alaska Fairbanks. Specifics for these routines and completed analyses are in Appendix A.

1.6.4 Rock slab XRF analysis

I collected three hundred and thirty two samples in the field and from core for XRF analysis. Samples were cut into approximately 37 mm diameter circular slabs. These were polished on an Ameritool polishing wheel at 60, 180, and 280 grit for 2 minutes each. Samples were then analyzed using a PANalytical Axios XRF unit for a variety of major and trace elements (SiO_2, Al_2O_3, FeO, MnO, MgO, CaO, Na_2O, K_2O, TiO_2, P_2O_5, BaO, S, Cr, Cu, Ga, Nb, Ni, Pb, Rb, Sr, V, Y, Zn, and Zr). The analysis routine utilized international press pellet standards as well as rock slab standards from the Alaska Division of Geological and Geophysical Surveys (DGGS) (9 samples) that had been commercially analyzed by 4 acid digestion, ICP-MS, and XRF. Beta and line overlap coefficients in the routine were calculated as appropriate. Complete analyses are in Appendix B.

I used five polished slabs of granitic rocks from Pogo with known chemical composition to assess the slab XRF routine (Table 1-1). For oxides present at concentrations > 10 wt%, they generally agree within 3-5% of the amount present. The % errors are larger for oxides with smaller concentrations but are relatively close in absolute concentrations. Using this method radically decreased sample preparation time and eliminated contamination problems caused by crushing and pulverizing. I have found this routine to be successful in determining major, minor and trace elements for felsic to mafic rocks with average grain sizes of ≤ 4 mm.

1.6.5 3D Modeling

I modeled the intrusive bodies using Leapfrog Geo 5.0. I assigned lithology to intervals based upon core logging information, core photos, and geochemical data when available. This lithologic assessment was then used to create a 3D model of the various intrusive bodies.

Table 1-1: Major oxide (weight percent) comparison between slab XRF and commercial laboratory analyses for 5 Pogo rocks, with percent difference shown in red.

	Sample	SiO_2	Al_2O_3	FeOt	CaO	MgO	Na_2O	K_2O	TiO_2	MnO	P_2O_5
ALS	91A	62.6	15.8	5.98	5.02	2.36	2.40	2.22	0.77	0.13	0.15
XRF Slab	91A	64.8	15.0	4.67	5.18	1.83	2.41	1.91	0.66	0.10	0.14
% Difference		**3**	**-5**	**-22**	**3**	**-22**	**0**	**-14**	**-14**	**-23**	**-7**
ALS	747	56.4	16.4	7.73	7.97	4.98	2.17	1.31	0.79	0.15	0.13
XRF Slab	747	57.5	18.0	7.19	8.56	3.99	2.33	1.25	0.82	0.14	0.12
% Difference		**2**	**10**	**-7**	**7**	**-20**	**7**	**-5**	**4**	**-7**	**-8**
ALS	1745#	73.5	13.9	0.97	0.93	0.23	2.75	5.46	0.10	0.03	0.14
XRF Slab	1745#	75.4	14.3	0.82	1.08	0.27	2.89	5.25	0.06	0.03	0.12
% Difference		**3**	**4**	**-16**	**16**	**17**	**5**	**-4**	**-40**	**0**	**-14**
ALS	1703	75.1	13.4	0.74	1.02	0.17	2.14	5.88	0.06	0.02	0.14
XRF Slab	1703	76.8	14.0	0.62	1.54	0.24	2.24	5.83	0.08	0.02	0.19
% Difference		**2**	**4**	**-16**	**51**	**41**	**5**	**-1**	**33**	**0**	**36**
ALS	772	65.1	16.0	4.74	4.29	1.46	2.47	2.11	0.73	0.10	0.17
XRF Slab	772	64.8	15.1	4.68	4.53	1.49	2.41	2.05	0.76	0.10	0.17
% Difference		**0**	**-5**	**-1**	**6**	**2**	**-2**	**-3**	**4**	**0**	**0**

2 Chapter 2 Geologic units, their compositions & distribution

2.1 Introduction

Geologic units in the greater Pogo area have been assigned inconsistent names and geologic maps of the area show different unit distributions (e.g., Chapter 1, Fig. 1-5). Naming is particularly messy for exposures below the surface, as a variety of schemes have been employed for underground mapping and core logging over the decades. I attempted to bring some order to the chaos by making unit assignments based primarily on chemical analysis and hand specimen texture. To accomplish that, I prepared > 330 polished slabs which I analyzed by Wavelength Dispersive XRF (see Chapter 1, methods). My geologic map (Fig. 2-1) is based on located XRF-identified samples; it represents my best attempt at defining the surface distribution of the major rock types. The major rock types present are Paleozoic-protolith metamorphic rocks and mid-Cretaceous intrusions (Fig. 2-1). Minor occurrences of small Paleogene felsic and mafic dikes are not shown.

2.2 Metamorphic Rocks

Conceptually, the metamorphic rocks at Pogo consist of meta-sedimentary (mostly paragneiss) and meta-plutonic (orthogneiss) types. In practice, distinguishing between the two types can be problematic, and both have been logged as 'biotite-quartz-feldspar gneiss'. That practice dodges around the problem of protolith assignment, but also makes it difficult to tease out the distribution of the two. Amphibolite occurs, especially in the Liese area (Fig. 2-1), and marble, quartzite, and serpentinite are rarely present in small intervals. The latter three were not sampled for XRF analysis.

2.2.1 Paragneiss

About a third of the gneiss present is likely paragneiss, especially common in the Liese area (Fig. 2-1). Parageniss is generally distinguished by having more mica (usually > 20%) with biotite in bands 1- 5 mm thick (Fig. 2-2) and quartz (usually > 40%) and less feldspar (usually < 30%), although distinguishing between fine-grained quartz and feldspar is often difficult. 1-5% garnet can be present. Thin sections show that sillimanite is typically present, but as thin bundles 0 .1 mm x 0.5 mm (Fig. 2-3) all-but-invisible in hand specimens.

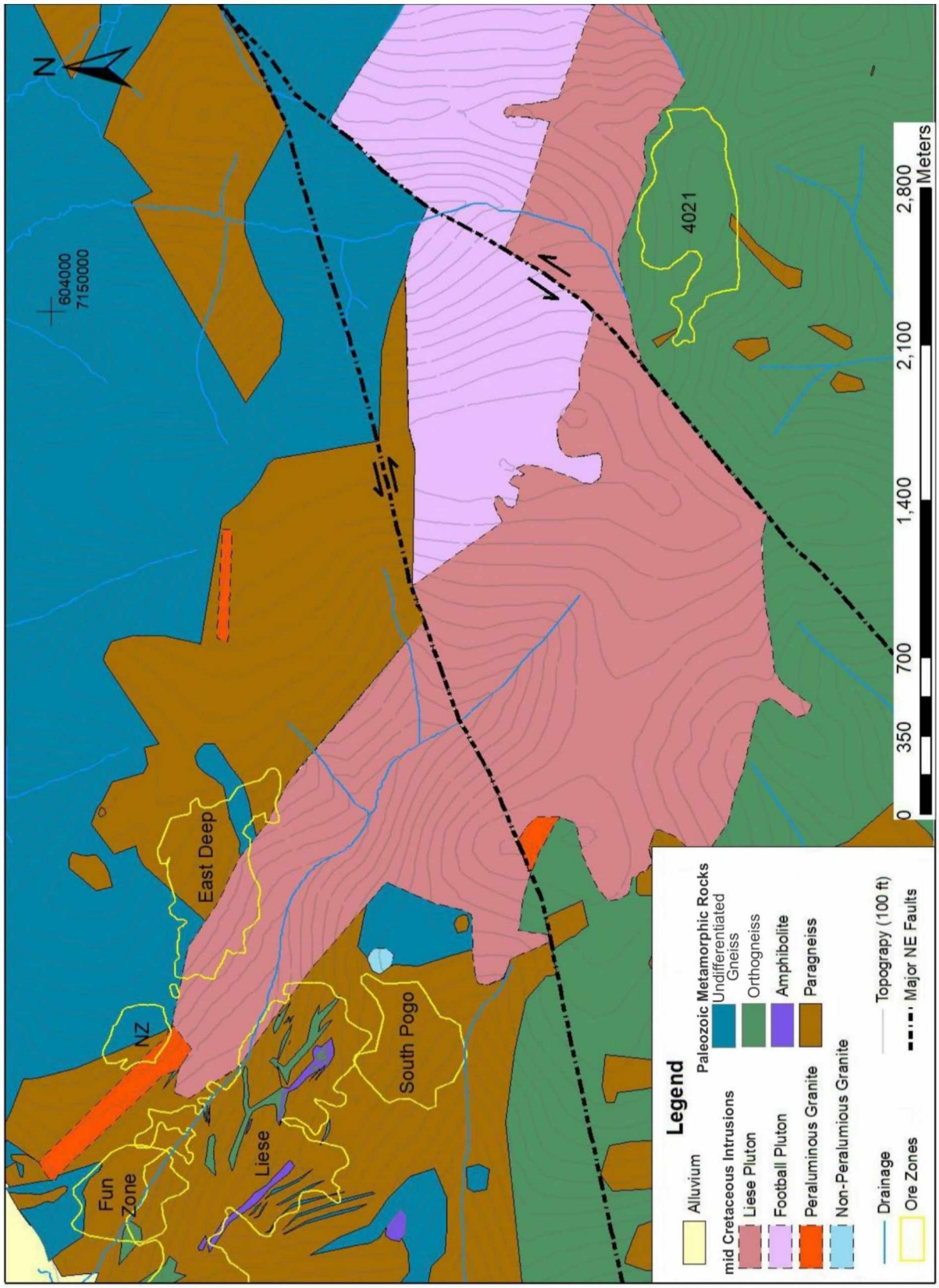

Figure 2-1: Geologic map of the Pogo Mine Area, based on surface and near-surface samples.

Figure 2-2: Representative hand specimen samples of Pogo paragneiss. Black = biotite; white = quartz > feldspar, orange = iron oxide staining.

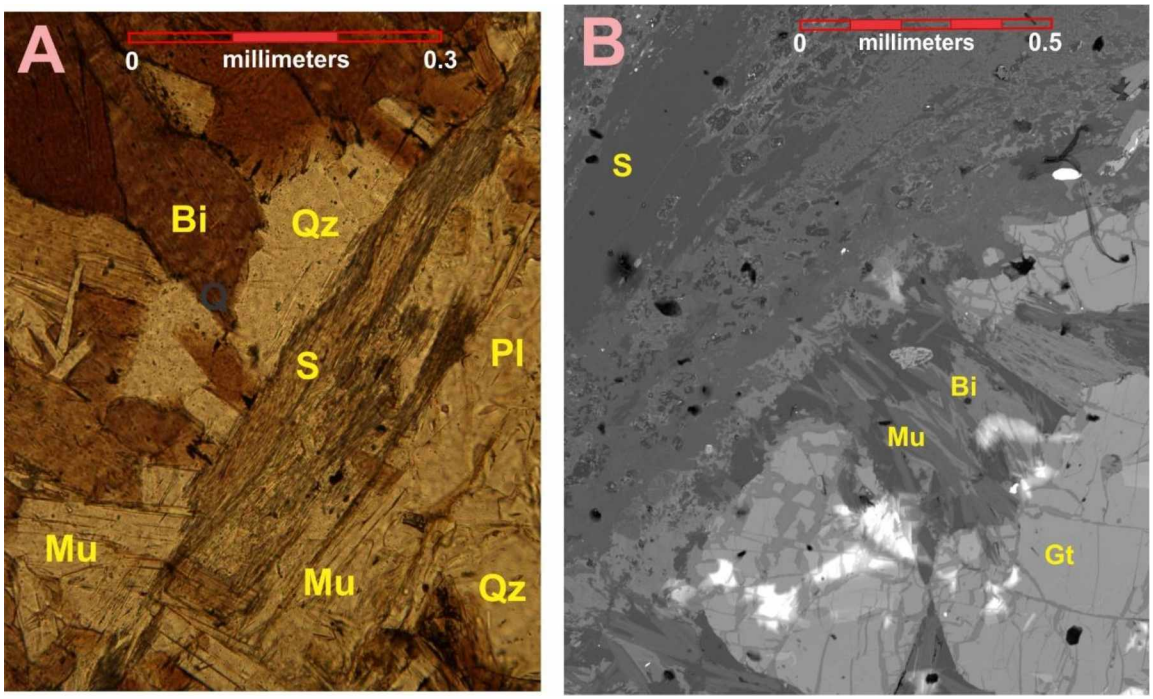

Figure 2-3: Thin section (A) and Back-scattered electron image (B) of sillimanite-bearing paragneiss, showing typical occurrence as small bundles, not readily visible by eye. S= sillimanite, Bi = biotite, Mu = muscovite, Pl = plagioclase, Qz = quartz, Gt = garnet.

Compositionally, paragneiss contains more MgO (usually > 1%) than orthogneiss (invariably < 1%) reflecting the greater abundance of biotite (and its modest Mg content, Chapter 4) in paragneiss. The more abundant mica and invariable sillimanite produce substantial normative corundum (Fig. 2-4); the higher quartz content produces generally higher normative quartz/(quartz+total feldspar) than seen in orthogneiss.

I generally avoided sampling paragneiss and 'ambiguous gneiss' for this study; however, paragneiss is an important rock type with regards to P-T conditions due to locally containing the assemblage sillimanite-biotite-muscovite-plagioclase-quartz-garnet.

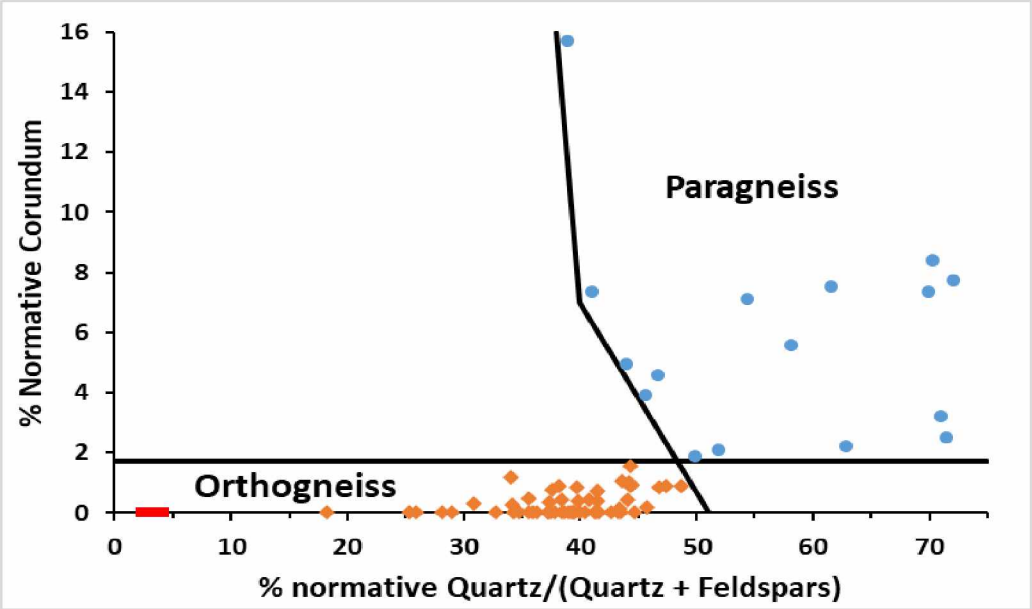

Figure 2-4: Compositional discrimination between Pogo paragneiss and orthogneiss, based on normative mineralogy. Note the much higher % normative corundum in paragneiss, reflecting its sedimentary protolith.

2.2.2 Amphibolite

Metamorphic rock rich in hornblende is present as thin layers on the surface and in drill core in the Liese area (Fig. 2-1). Such rocks are commonly easy to recognize, but fine grained and hornblende-rich varieties in drill core are commonly confused with dark dikes. Compositionally, they are readily distinguished from igneous rocks (Fig. 2-5) by virtue of their high V and Cr concentrations.

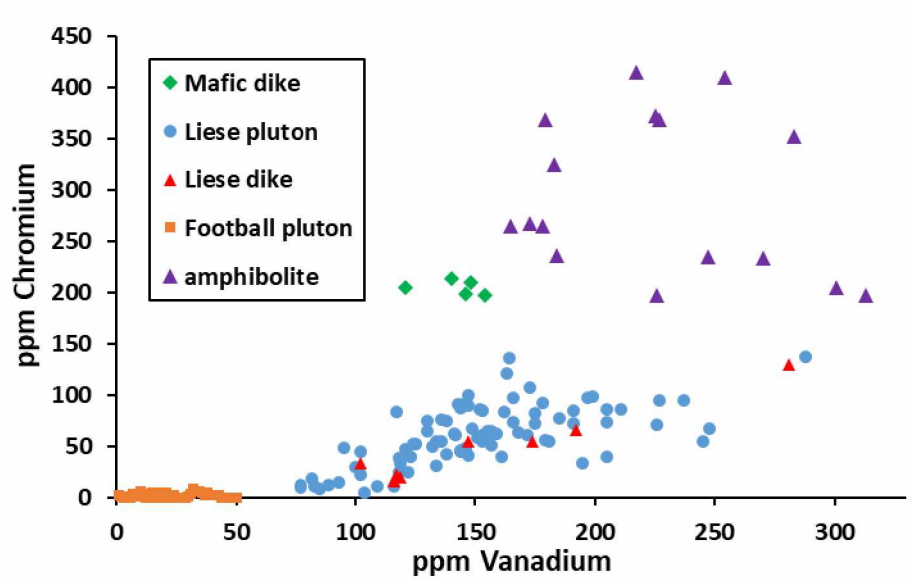

Figure 2-5: Compositional distinctions among Pogo mafic and intermediate composition rocks based on Cr and V concentrations. Note the non-overlapping fields for all but Liese pluton and Liese dikes.

2.2.3 Orthogneiss

Gneissic rocks with a felsic plutonic origin (orthogneiss) account for about a third of the metamorphic rocks in the Pogo area (Fig. 2-1), notably in the 4021 and south of the South Pogo areas. As a group the orthogneisses are poorer in biotite (commonly 10% or less) and possess larger feldspar crystals (2-5 mm) than the paragneiss. The most abundant variety is quartz-rich (Figs. 2-4, 2-6); I have found quartz-poor orthogneiss exclusively in deep drill holes of the Fun Zone (Fig. 2-1). I have broken out two sub-types of quartz-rich orthogneiss based on trace element compositions (Fig. 2-6). Unfortunately, these two sub-types are nearly indistinguishable in hand specimen.

2.2.3.1 Quartz-rich orthogneiss

The 4021B type of quartz-rich orthogneiss has lower Nb+Y (Fig. 2-7); based on CIPW normative mineralogy the protolith varied from granite to tonalite (Fig. 2-8). Unfortunately, all the feldspar at Pogo is white, so the higher plagioclase content of this type is not obvious in hand specimen. This type contains 10-15% biotite, usually well-aligned; 25-35% quartz; 3-30% K-feldspar; 25-60% plagioclase; and 0-3% garnet. K-feldspar is 1-4 mm; the other grains are typically 0.3-.5 mm. Garnet is invariably tiny (0.1-.15 mm) and essentially invisible in hand

specimen. This is apparently the most abundant orthogneiss type and is present both on the surface and in the sub-surface.

The 4021A type of quartz-rich orthogneiss has higher Nb+Y (Fig. 2-7) and is restricted to granite protoliths (Fig. 2-8). Relative to the 4021B type, it contains less biotite (typically 5-10%) and may be somewhat coarser-grained, with feldspar and quartz both 1-5 mm. It also contains tiny trace garnet, which is all but invisible in hand specimen. This type of orthogneiss is apparently restricted to the sub-surface: all of my samples are from drill holes, mostly in the 4021 area (Fig. 2-1).

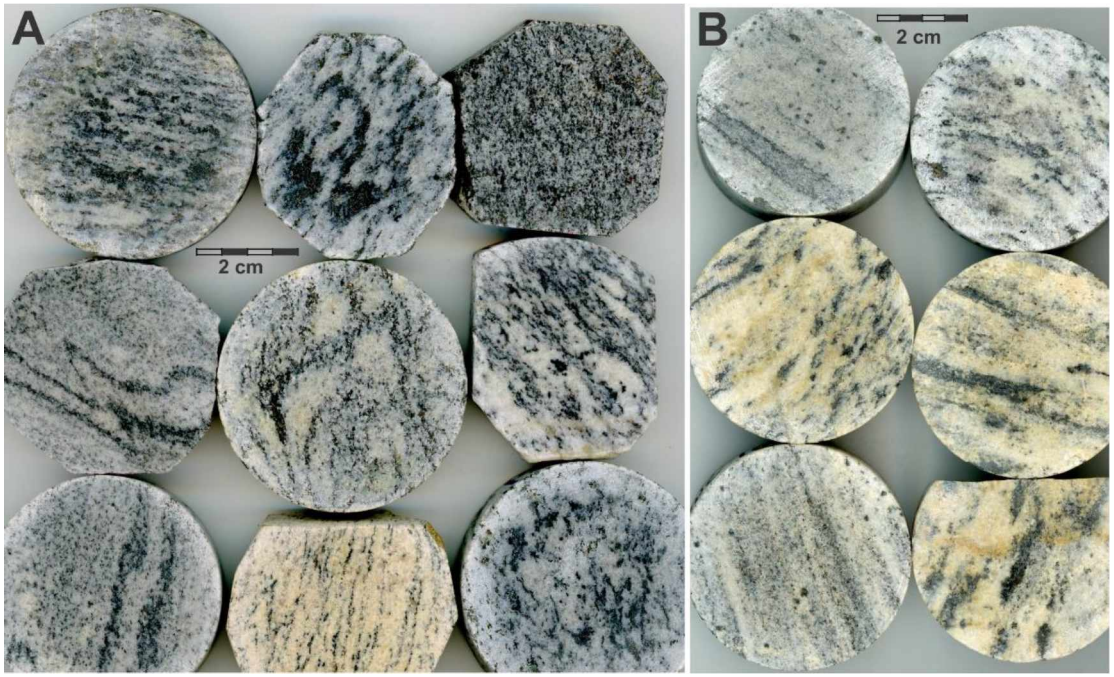

Figure 2-6:Typical hand specimens of quartz-rich orthogneiss. A volcanic arc (4021B) type. B Within-plate (4021A) type. The two are essentially indistinguishable in hand specimen.

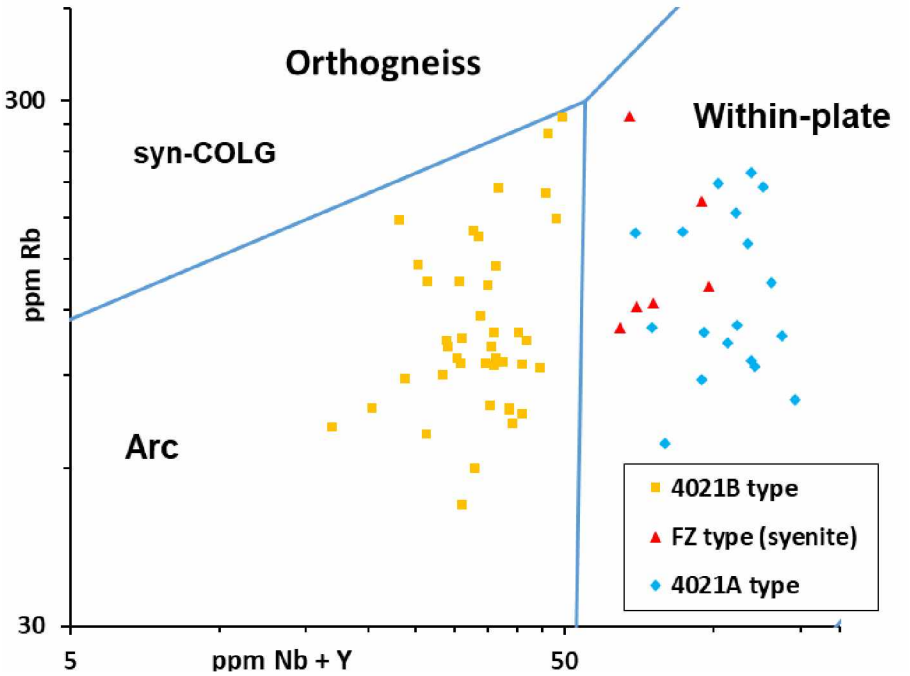

Figure 2-7: Pogo orthogneiss types distinguished on a Pearce et al. (1984) tectonic discrimination diagram. The quartz-rich types are best distinguished by Nb content, as 4021B = 3-19 ppm, 10 ppm average; 4021A = 24-87 ppm, 49 ppm average.

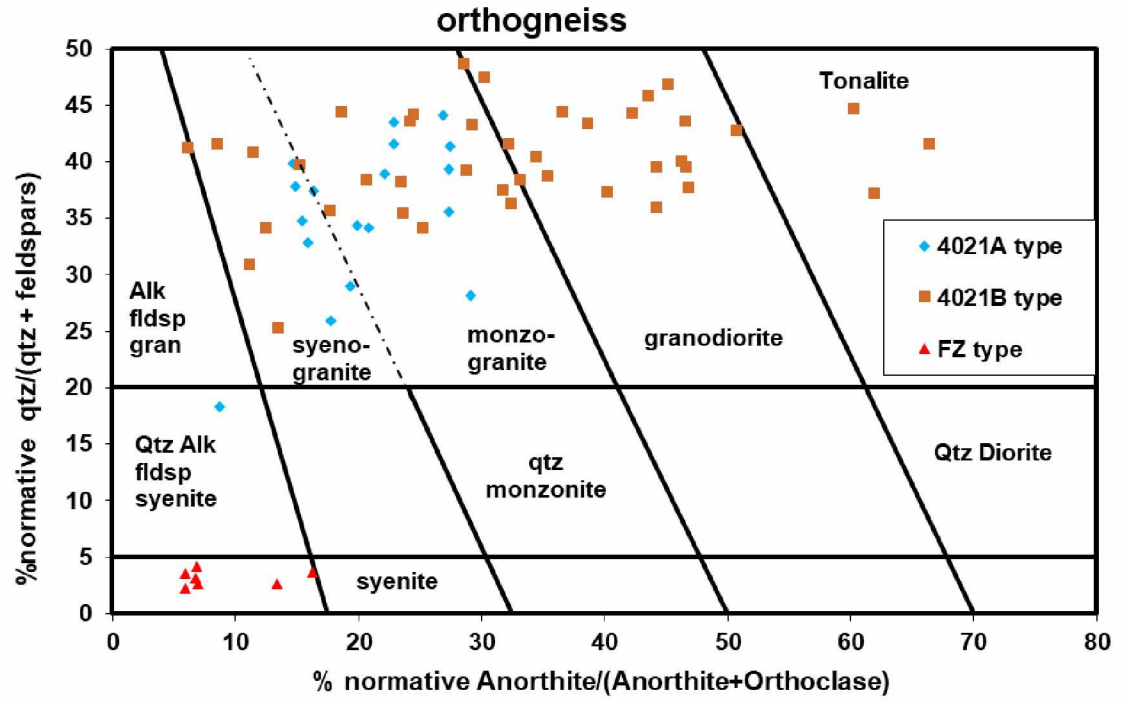

Figure 2-8: Classification of Pogo orthogneiss based on CIPW normative composition, as shown on the diagram of Streckeisen and Le Maitre (1979).

2.2.3.2 Quartz-poor orthogneiss (FZ type)

The most distinctive orthogneiss is the Fun Zone (FZ) type. It contains both biotite and hornblende (15-20% mafics), both typically coarser (1-2 mm) than in the other types (Fig. 2-9). It also displays the most consistent and distinctive gneissic banding with mafic layers 1-3 mm wide alternating with 2-5 mm wide feldspar-rich layers (Fig. 2-9). Quartz is both relatively rare (3-7%) and tiny (0.1-0.2 mm). K-feldspar (1-3 mm; 40-50%) is both coarser and more abundant than plagioclase (0.5 mm; 10-20%).

The quartz-poor orthogneiss contains elevated levels of Nb and Y, yielding a within-plate origin for the protolith ((Fig. 2-7). Calculated normative mineralogy places the protolith in the alkali feldspar syenite field (Fig. 2-8). Mineralogically, this unit is distinguished by appreciable hornblende (sub-equal in abundance to biotite), magnetite (~0.5%, 0.3-.5 mm) and accessory titanite (0.1 mm).

I have found this unit in multiple drill holes in the general Fun Zone area. Based on drill hole intersections, the FZ orthogneiss body forms a roughly tabular shape approximately 700 meters long, at least 360 meters high (limited by deep drilling), and 90-120 meters wide, oriented 280-295°/60° NNE. One thousand meters to the north is another body of similar looking orthogneiss with a similar shape and orientation (Fig. 2-10). Based on its distinctive appearance and chemical composition, the quartz-poor orthogneiss is apparently restricted to the NW corner of the Pogo map area.

Figure 2-9: Typical FZ type (low-quartz) orthogneiss, with strong schistosity defined by obvious biotite-hornblende bands. The core box is 0.76 meters long.

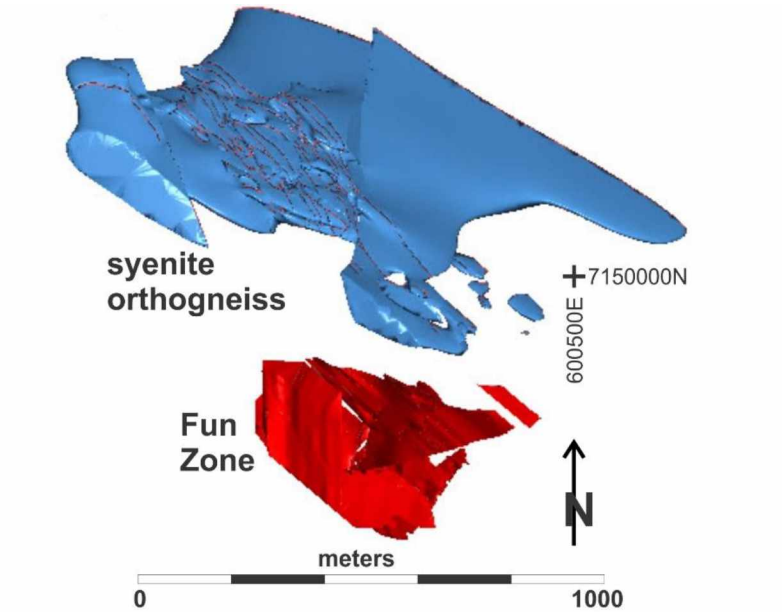

Figure 2-10: Isometric image, looking down, of an alkalic orthogneiss body (blue) north of the Fun Zone orebody (red, c.f., Fig. 2.1). The orthogneiss body dips approximately 60° NNE.

2.2.4 Undifferentiated gneiss

I did not spend much time mapping in the northernmost part of the map area. Cursory examination suggested both orthogneiss and paragneiss are present. Werdon et al. (2004) also mapped both types in this area. Rather than trying to break out several types, I called this area of mixed gneiss 'undifferentiated'.

2.3 Mid-Cretaceous plutonic rocks and dikes

Dilworth (2003) broke out three suites: granite, tonalite, and diorite suites. I changed the names, in part because tonalite is the predominant rock type in the latter two and in part because I found two different types of granite at Pogo. Dikes of both mid-Cretaceous and Paleogene ages are also present.

2.3.1 Granite

Most of the granite samples I analyzed were peraluminous (contain more Al than required to make feldspars) and are characterized by significant muscovite ± biotite. As best I can tell, these are representative of a granite suite and have U-Pb monazite and zircon ages of 109.2 ± 0.4 to 107.0 ± 0.6 Ma (Dilworth, 2003). A less common variety, apparently not dated, is not peraluminous and lacks muscovite. It occurs as a single body just E of the South Pogo area (Fig. 2-1) and in drill holes below it.

2.3.1.1 Peraluminous Granite

This rock type occurs as three small mapable bodies on the surface (Fig. 2-1) and innumerable smaller bodies in the sub-surface, especially in the vicinity of the Liese zones (Fig. 2-11). Compositionally, this unit ranges from rare granodiorite and alkali feldspar granite; quartz-rich syenogranite is the most common type (Fig. 2-12). Relatively coarse (1-2 mm) muscovite is an essential component, with 0-5% biotite (Fig. 2-13A). Grain size varies widely, with textures ranging from aplitic to pegmatitic. Garnet (1-2 mm) is common, but not ubiquitous. About half of the thin sections I have examined contain (microprobe-verified) andalusite and sillimanite. Tourmaline is less commonly present. Weak mineral alignment is variably present, but it is never sufficiently pervasive to call the rock an orthogneiss. As seen in map view (Fig. 2-1) and in an isometric diagram (Fig. 2-11) peraluminous granite tends to occur as steeply-dipping dikes that cut schistosity and are cut by the Liese zones.

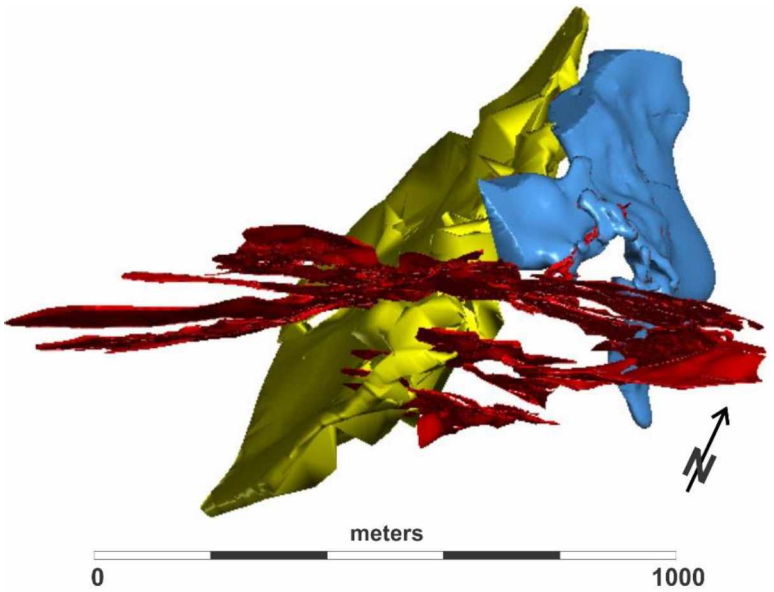

Figure 2-11:Isometric drawing, looking down-dip of the Liese zones (red) showing two peraluminous granite dikes (blue and yellow) oriented at 165/45 SW and 345/65 NE—both at high angles to the Liese zones. The schistosity in this area dips moderately NE. General location is shown on Fig. 2.1.

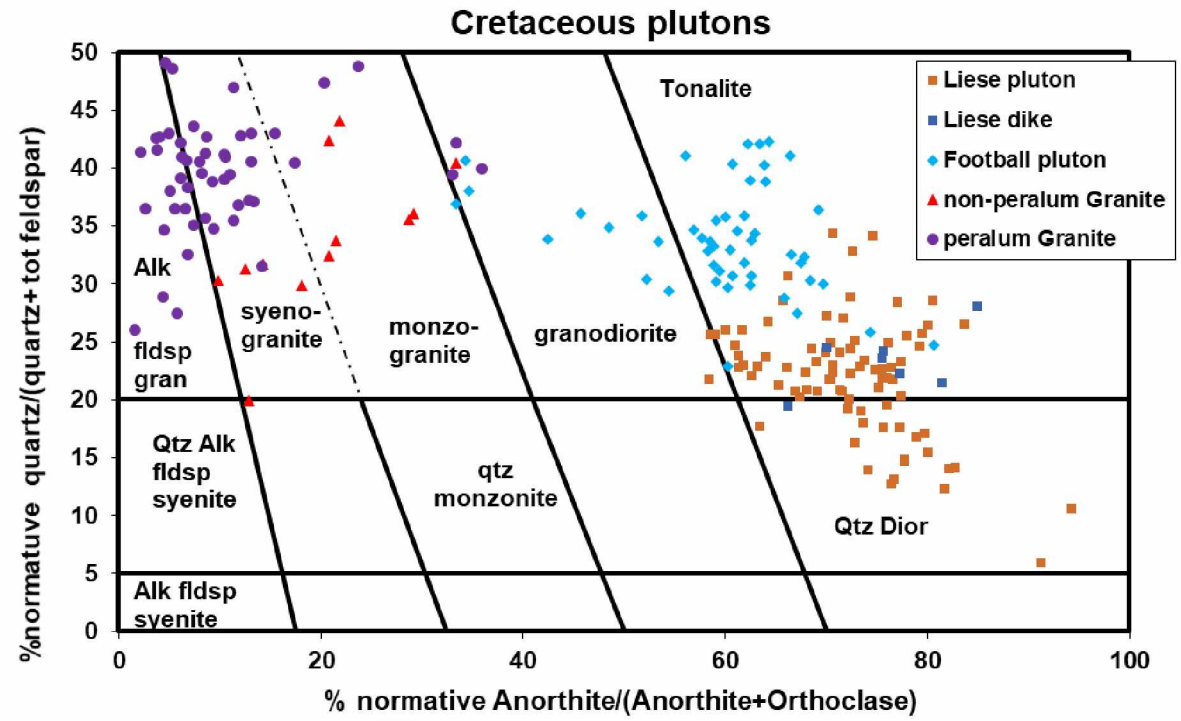

Figure 2-12: : Classification of mid-Cretaceous intrusive rocks at Pogo based on the normative scheme of Streckeisen and Le Maitre (1979).

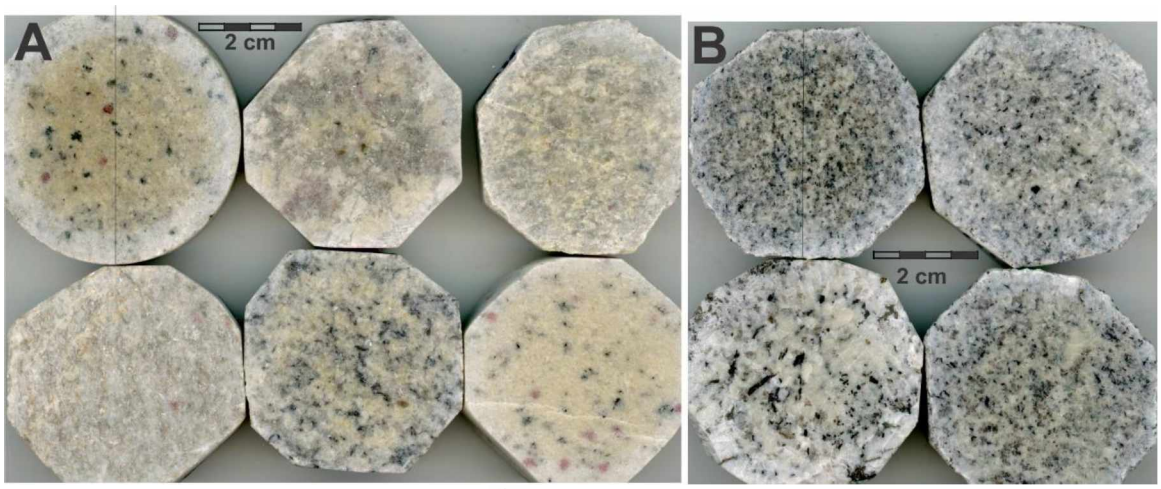

Figure 2-13: Hand specimen images of Pogo granites. A = Peraluminous granite, B = non-peraluminous granite. Red = garnet, black = biotite, white = muscovite, grey = intergrown quartz and feldspar.

Peraluminous granite commonly contains elevated Rb concentrations; that combined with low Nb+Y causes samples to plot in or near the 'collisional type granite' field (Fig. 2-14) of Pearce et al. (1984). This is problematic, as a 107 Ma collisional event is not known in the region.

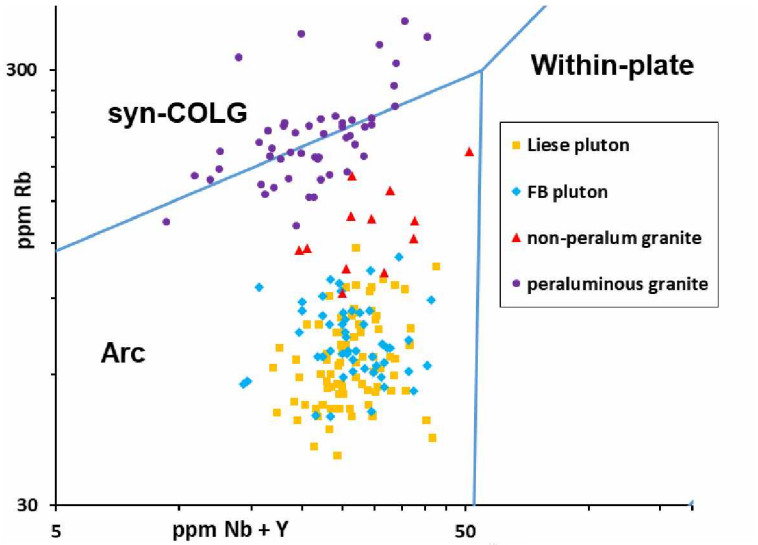

Figure 2-14: Tectonic classification of Pogo area mid-Cretaceous plutonic rocks using the trace element scheme of Pearce et al. (1984).

2.3.1.2 Non-Peraluminous (metaluminous) Granite

This rock type is much rarer than the peraluminous granite; I have found it in a small body just east of the South Pogo area (Fig. 2-1) and in drill core exposures below that. As this rock type is significantly different from the peraluminous granite, its age is uncertain, aside from being post-tectonic. Non-peraluminous granite lacks muscovite (and garnet and aluminosilicates) and instead contains 7-12% biotite (Fig. 2-13). Its composition is simply granite (Fig. 2-12). It differs from the majority granite in having little or no normative corundum and higher wt% CaO (Fig. 2-15) as well as lower Rb (Fig. 2-14).

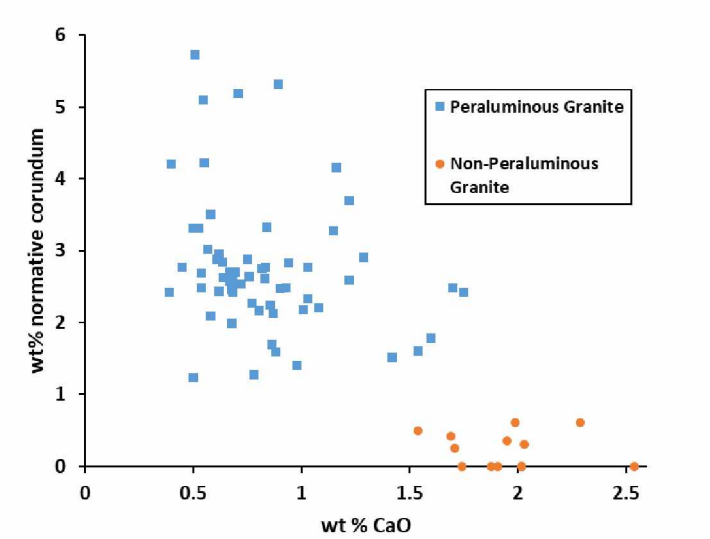

Figure 2-15: Compositional contrasts between Pogo peraluminous and non-peraluminous granite.

2.3.2 Football pluton

Dilworth classified most of the mid-Cretaceous rocks of the greater Pogo area belonging to the 'tonalite suite'. One body in particular, located 3 km SE of the Liese zones (Fig. 2-1) yielded a U-Pb zircon age indistinguishable from the Re-Os age for Pogo mineralization (both 103-104 ± 2 Ma). I have called that body the 'Football pluton' as it prominently occurs on a flat topographic bench locally known as 'the football field' (Fig. 2-1). Rocks from this body possess a distinctive texture (Fig. 2-16), mineralogy, and compositional range (Fig. 2-12).

Rocks from the Football pluton always possess small (0.3-1 mm) biotite and significant (>25%) quartz (Fig. 2-16). The latter is sufficiently coarse (1-2 mm) to be obvious on broken rock surfaces. Rocks from the pluton vary gradationally between tonalite and granodiorite (Fig. 2-12). On the surface, the granodiorite portion is restricted to the central part of the body. The

granodiorite contains 12-15 % mafic minerals (mostly biotite, with 0-3% hornblende), 40-45% plagioclase, 30-35% quartz, 5-7% K-feldspar, and trace magnetite and ilmenite. The rock is very slightly magnetic. The majority of the pluton is of tonalite composition, similar in mineralogy to the granodiorite, but with trace to 5% hornblende and accessory to 1% K-feldspar. The plagioclase in both phases is An_{40-50} (see Chapter 4). Notably (and unlike the Liese pluton) pyroxene is not present. Consistent with its intermediate to felsic composition, rocks from the Football pluton plot in the 'volcanic arc' field on the trace element diagram of Pearce et al. (1984).

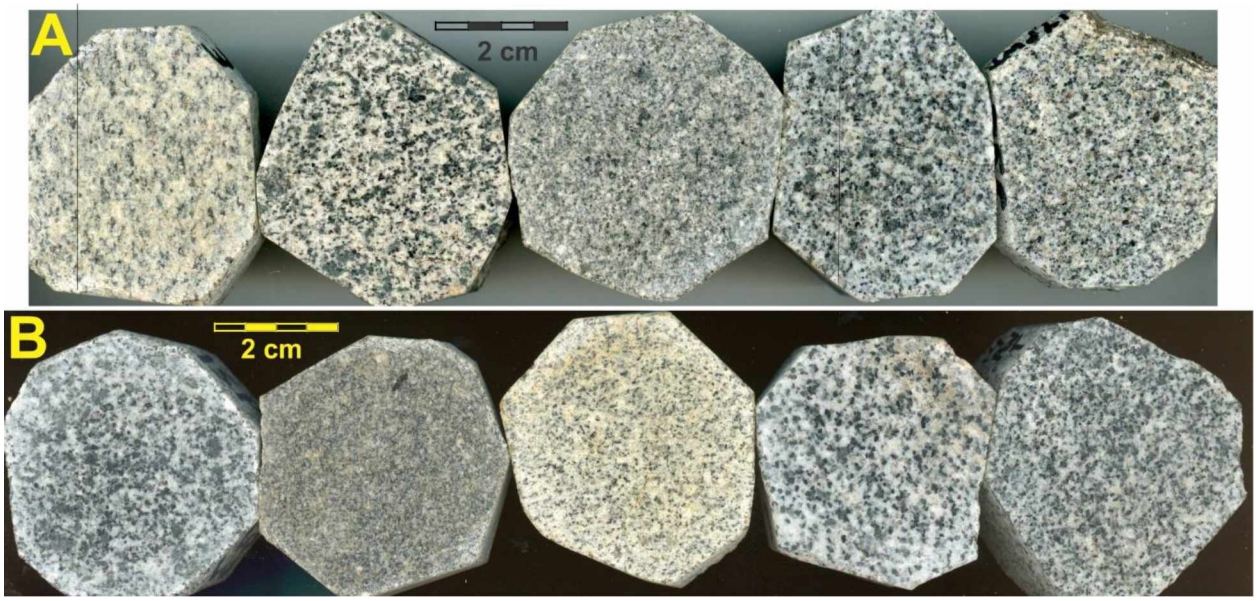

Figure 2-16: Representative hand specimens from the Football pluton. Black = mafic (mostly biotite), grey = quartz, white = feldspar (mostly plagioclase). 0.5-1 mm biotite is characteristic.

In addition to the small pluton north of the 4021 prospect, rocks with Football pluton compositions and appearance (< 1 mm biotite) plot as isolated dikes in the map area and as a coherent, dike-like body lying underneath the Liese zones (Fig. 2-17). This dike was identified by a combination of analyzed core samples and examination of core photos for characteristics seen in the Football rocks. This includes a lack of chill margins and cm scale fracture-related bleaching. Consequently, the Football pluton not only has the same age as the Liese mineralization (Dilworth, 2003), at least a dike of it lies in a position where fluids emanating from it potentially caused the mineralization.

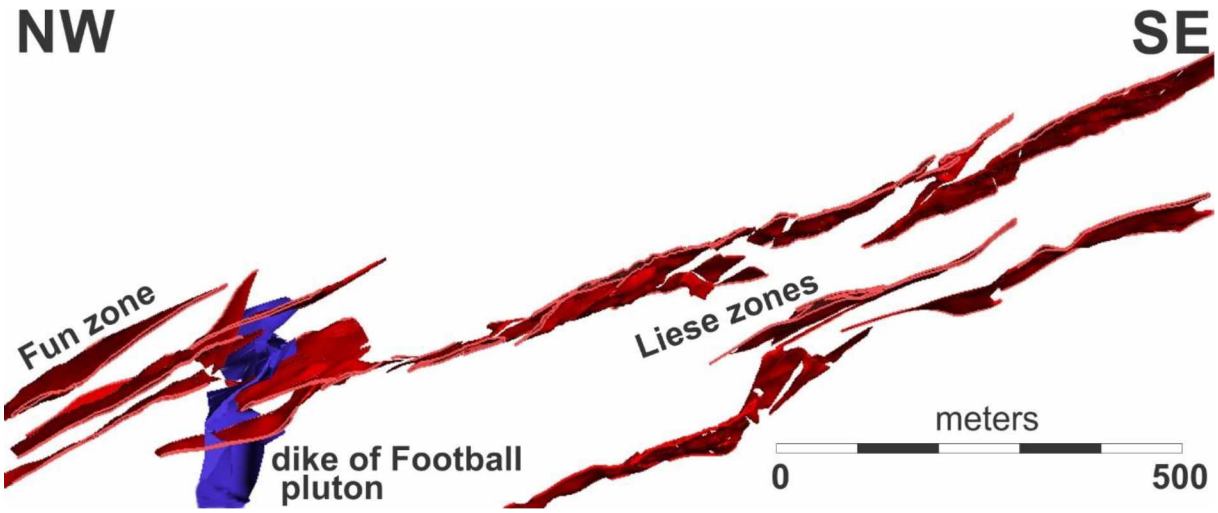

Figure 2-17: Vertical cross-section (looking 050) through the Liese veins of the Pogo deposit, showing a dike-like body of Football pluton under the veins. (Both are cut by the Liese pluton, which is not shown). The football dike is orientated approximately 50/55S and is about 1 km long and 50 m wide.

2.3.3 Liese pluton and associated dikes

The central quarter of the geologic map (Fig. 2-1) is dominated by a coherent body I have designated the 'Liese pluton', from its occurrence straddling Liese Creek. Both Pogo mine geologists and Dilworth (2003) refer to it as 'diorite', as the quartz is essentially invisible in hand specimen. Thin section petrography, however, indicates 5-20% quartz is characteristic, and the unit varies between quartz diorite and tonalite (Fig. 2-12). A U-Pb zircon age of 94.5 ± 0.2 Ma (Dilworth, 2003) indicates it is the youngest major rock unit in the Pogo area. It is readily distinguished from all other igneous rocks in the area due to its higher mafic mineral content, easily visible hornblende, and coarser (1.5-3 mm) mafic minerals (Fig. 2-18). Liese dikes are texturally different but are the only known dikes in the immediate Liese area.

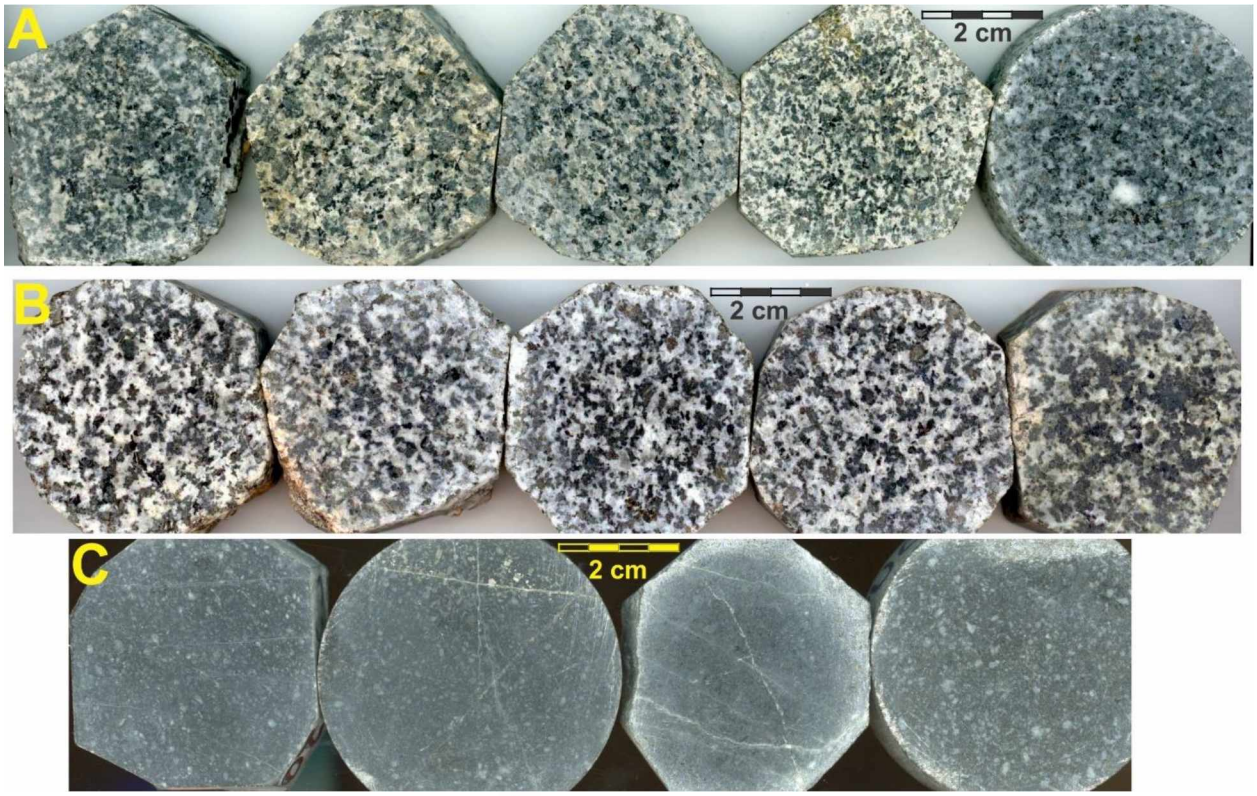

Figure 2-18: Typical hand specimens of Liese pluton (and associated dikes). A= Tonalite (most abundant), B = Quartz Diorite, C = dikes. For A & B: black = biotite, dark grey = pyroxene + hornblende, white-light grey = plagioclase + quartz. C: white = plagioclase; grey=matrix.

The Liese pluton is predominantly tonalite (Fig. 2-12); it grades into quartz diorite. The latter is mostly confined to the NE part of the body. Both varieties contain 30-45% mafic minerals (Fig. 2-18), with varying proportions of biotite, pyroxene, and hornblende. Quartz content varies from 5-10% (quartz diorite) to 15-20% (tonalite), all-but-invisible in hand specimen (Fig. 2-8), mostly due to its small size (0.3-.7 mm). In one thin section I found sub-equal amounts of biotite and pale orthopyroxene; more commonly (8 other thin sections) pyroxene is partly replaced by hornblende, yielding biotite ~ hornblende > pyroxene. Hornblende is usually the most abundant mafic mineral (and total mafic mineral abundance is a little higher) in Liese quartz diorite. The pyroxene is essentially invisible in hand specimen because it is typically mantled by hornblende ± biotite. K-feldspar is nearly absent. Abundance of opaque phases is 0.3-.5%, with sub-equal magnetite, ilmenite, and (magmatic?) pyrrhotite; these rocks are substantially more magnetic than those from the Football pluton.

Dikes emanate from the Liese pluton; these are called 'basalt' at the mine due to their dark colors and fine grain size (Fig. 2-18C). Technically, their SiO_2 concentrations (59-62 wt %) puts them in the 'andesite' field, but it seems odd to give a dike a volcanic rock name. Consequently, I refer to them as 'Liese dikes'. They have compositions indistinguishable from Liese tonalite (Figs. 2-5, 2-12, 2-14). My single thin section shows 1-2 mm plagioclase phenocrysts set in a 0.2-0.5 mm groundmass of intergrown biotite, hornblende, pyroxene, plagioclase, and quartz. In underground exposures they are easily recognized; in drill core they can be confused with fine-grained amphibolite.

A pseudo-plan map of the NE Liese pluton and associated dikes (Fig. 2-19) shows that most of the dikes strike approximately 270 (± 20°) and dip north, cutting across schistosity and ore zones. Some of these could be Paleogene mafic dikes, as I have compositional confirmation for only a few of them.

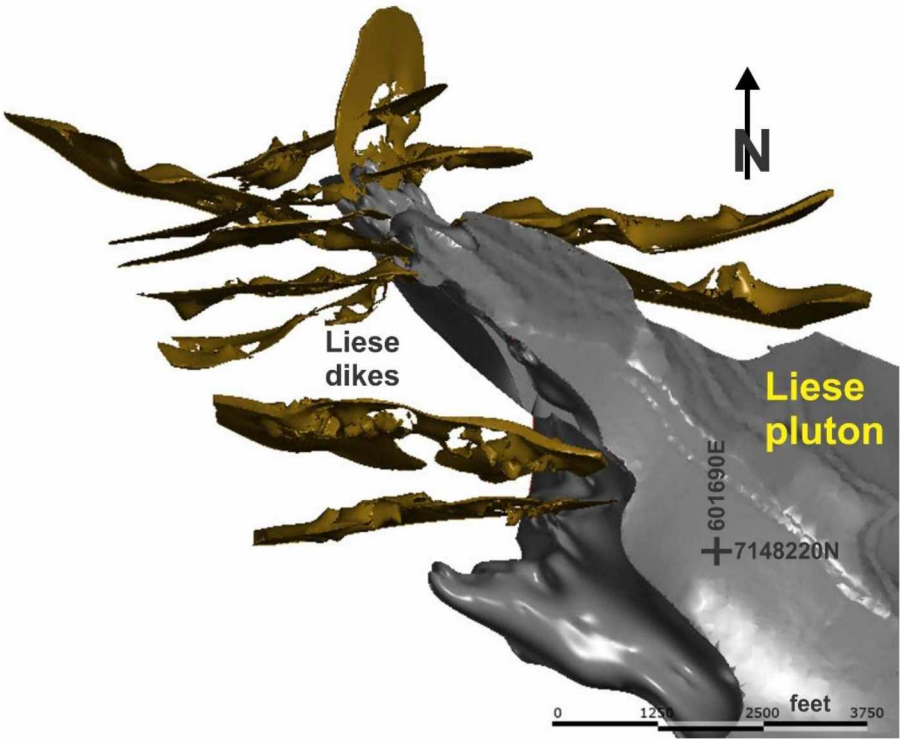

Figure 2-19: Shaded 3-dimensional view (looking down) for the NE part of the Liese pluton and vicinity, showing dikes (brown) that appear to emanate from the Liese pluton (grey). I have compositional data for only five of the dikes and am not certain that all of these dikes are Liese-related.

2.4 Paleogene dikes

Werdon et al. (2004) mapped mafic and felsic dikes with approximately N-S strikes in the general Pogo area. Dilworth (2003) provides U-Pb zircon ages (54.5 ± 0.5 and 51.8 ± 0.3 Ma) for two felsic dikes, both located east of my map area. Due to their similar strikes, it is likely that both types are of early Paleogene age. I found two such dikes on the easternmost ridge of my map area (Fig. 2-1); both are too narrow to show on the map. These dikes are dark colored and not easily distinguished (especially underground!) from the older Liese dikes. Compositionally, they contain considerably more Cr than Liese dikes (Fig. 2-5); they also contain considerably more TiO2 (~2%) than Liese dikes (0.7-0.8%). Their most distinguishing characteristic is the high abundance of (secondary) calcite which cannot be determined from core photographs. Consequently, I am not certain that all the Liese dikes shown on Fig. 2-19 are of that ilk.

2.5 Discussion and Conclusions

I have shown compositional distinctions between the various major rock types at the Pogo deposit, which (combined with textural data) allows for reliable classification of most of the rocks, using a combination of major and selected trace elements. My geologic map (Fig. 2-1) is based on the surface distribution of such compositionally-classified rocks.

Most of the 'tectonic settings' implied by trace element diagrams (Figs. 2-7, 2-14) also seem sensible: for example, at least two different origins for the Paleozoic felsic bodies that ultimately became orthogneiss. The majority appear to have been 'normal' subduction-related, volcanic arc type plutons (Fig. 2-7). Less common are bodies that require a within-plate (extensional?) setting, that may represent rifting of an arc or post-arc extension. Similarly, the bulk of the Cretaceous intrusions apparently represent subduction-related, arc-type settings; a feature common to many mid-Cretaceous intrusions in Interior Alaska.

The major 'tectonic' mystery revolves around the peraluminous granite intrusions, with ages of approximately 107 Ma (Dilworth, 2003) and apparent 'syn-collisional' setting (Fig. 2-14). Based on several lines of evidence, Dusel-Bacon et al. (2002) argue for a mid-Cretaceous extension event that preceded (or was partly contemporaneous with) subduction. If anything, their proposed early Jurassic 'high pressure' event would be collision-associated.

That the peraluminous granites represent crustal melts—or at minimum, highly crustal contaminated melts—is indicated by their major element composition and the common presence

of 'inherited' zircons (Dilworth, 2003; chapter 3). However, it is unclear why they contain such anomalously high Rb contents, causing them to plot in the 'syn-collisional' field of Pearce et al. (1984). Either small proportions of fractional melting (causing the melt to be anomalously enriched in 'incompatible' Rb) or hydrothermal alteration are possible explanations. The obvious solution to this conundrum is that granites that plot in the 'syn-collisional' field of Pearce et al. (1984) are not necessarily of collisional origins. Clarke (2019) lists eight different mechanisms for producing strongly peraluminous granites and concludes that contamination of a variety of magmas by pelitic rocks is the most effective one.

The occurrence of primary sillimanite and andalusite in granite at first seems odd, but such has been observed in countless peraluminous granites from around the world (e.g., Clarke, 1981, Zen, 1988). The problem of magmatic muscovite in such rocks relative to the stability of muscovite has also been repeatedly addressed, e.g., Clark, (1981) and Zen, (1988), who both stress that the stability of muscovite is strongly influenced by minor compositional variations and the granite solidus is strongly influenced by F and B concentrations in the melt. In other words, the mineralogy of the peralumninous granites in the Pogo area seems perfectly reasonable.

I have successfully shown (Fig. 2-17) that the Football pluton, with the same age as Pogo mineralization (Dilworth, 2003) occurs not only on the surface, about 3 km from the main Liese zones (Fig. 2-1) but also in the sub-surface, under the Liese zones. That is, it can be considered as a potential source of mineralizing fluids. The dike, however, does not explain mineralization in other areas such as the Fun Zone that is downdip from the dike. Additional Football dikes and (or) other plutons or dikes at depth would be required to explain those other mineralization areas.

The Liese pluton, in contrast, although younger than mineralization (Dilworth, 2003), seems to be unmineralized. It also ubiquitously contains pyroxene in addition to biotite and hornblende. The most likely explanation is that the melt lacked sufficient water to completely convert (anhydrous) pyroxene to (hydrous) hornblende (e.g., Naney, 1983). Such a melt would be unlikely to expel magmatic water during crystallization, and hence, be a poor candidate for causing mineralization. The Football pluton, in contrast, lacks pyroxene, and clearly contained sufficient water to only crystallize hydrous mafic minerals. It is a potential mineralizer for the Liese mineralization.

3 Chapter 3: Zircon Geochronology and Zircon Compositions

3.1.1 Introduction and Collection Methods

During the summer of 2015 I collected four rock samples from core and the surface for U-Pb zircon dating. Historically, granitic orthogneiss in interior Alaska has been treated as Devono-Mississippian, based on U-Pb dating (e.g., Werdon et al., 2004). Dilworth et al. (2007), in contrast, give Cretaceous protolith ages for 'foliated granite' and 'granite orthogneiss' in the Pogo area and indicate metamorphism took place between 107 and 109 Ma (Chapter 1). My age investigations were designed to determine (a) whether granite orthogneiss in the Pogo area is anomalously young and (b) to better constrain the age of last metamorphism. I also defined several types of orthogneiss in the Pogo area based on compositional criteria (e.g., 'within-plate' vs. 'arc related'; Chapter 2) and wished to see if these yielded significantly different ages.

LA-ICP-MS dating of zircons has been adopted as a widely, commonly used technique for determining rock ages due to its quick throughput and relatively low cost compared to conventional thermal ionization mass spectrometry (TIMS) and sensitive high mass-resolution ion microprobe (SHRIMP) techniques. The spatial resolution is intermediate between the two conventional techniques, with a spot size diameter of 20 μm typical (and for this study). The disadvantage of LA-ICP-MS is the low precision for individual ages. This can be rectified by analysis of a large number of zircon grains, giving a statistically robust age population. For this study two of the rock samples yielded 50 analyzed grains, one 49, and one 29.

Dating zircon requires that the zircon contains significant (radioactive) U and (or) Th; in addition, U/Th ratios can help distinguish zircon origins. Metamorphic zircons possess high U/Th; igneous zircons have low U/Th, although there isn't a clean cut-off value. (Based on Hoskin and Black (2000), zircons with U/Th < 3 are definitely igneous; those with U/Th > 8 are definitely metamorphic.) An accepted explanation for this phenomena is that the radius of U^{4+} is both smaller than that of Th^{4+} and closer to that of Zr^{4+}, hence U^{4+} is preferred. However, Th is considerably more abundant than U in the crust. As solid solution is more 'forgiving' at high than at low temperature, Th is typically more incorporated into igneous (higher T) than metamorphic (lower T) zircon (Hoskin and Schaltegger, 2003). Compositional zoning in zircon (as indicated by, for example, cathodoluminescence = CL) is different in metamorphic and igneous zircons (Hoskin and Schaltegger, 2003). Igneous zircons characteristically display sharp,

narrow oscillatory bands in CL; metamorphic recrystallization causes the bands to broaden and eventually disappear (Hoskin and Black, 2000).

Four rock samples were sent to GeoSep Services (GSS) in Moscow, Idaho for zircon separation and subsequent La-ICP-MS analysis by Dr. Paul O'Sullivan. Zircons were separated and analyzed as described in Hults et al. (2013). LA-ICP-MS U-Pb data collection was performed at the Geoanalytical Laboratory, Washington State University, Pullman, Washington. Collection and analysis were performed using a New Wave YP213 231 nm solid state laser ablation system and a ThermoScientific Element 2 magnetic sector mass spectrometer. The LA system used a 20 μm diameter spot size and 5 Hz laser firing rate, yielding ablation pits ~10-15 μm deep.

Following the LA-ICP-MS analysis, I was able to secure the polished mineral separates from GSS. I mapped zircons from three samples using cathodoluminescence to better understand the ages given by the zircons and used the electron microprobe to analyze zircons from two samples (4021A and FunZone) for thorium. The LA-ICP-MS analyses for several zircons from these samples indicated Th concentrations sufficiently high to be detected by microprobe. Samples were analyzed at UAF-AIL using wavelength-dispersive techniques on the JEOL JXA-8530F electron microprobe. Specific properties of the WDS routine are given in Appendix A. Electron dispersive spectroscopy (EDS) was also used on the samples, to examine its comparability to WDS results as well as to analyze for U. This was not possible with WDS due to the lack of a reliable microprobe U standard at AIL.

3.1.2 General Sample Descriptions and Characteristics

I selected samples based upon degree of schistosity, amount of Nb present in hand-held XRF analysis, and location of samples. Degree of schistosity in this context refers to whether the rock has a strong, consistent deformational fabric versus an inconsistent, weak fabric (Fig. 3-1). The amount of Nb in orthogneisses was used to infer likely tectonic setting through use of the Pearce et al. (1984) felsic rock discrimination diagram (chapter 2). A variably deformed granite sample was collected on the basis of its high Ti-Zr content and inconsistent planar fabric. The deformed granite sample was also from (as best I could determine) the same location as a Dilworth (2003) sample described as a 'foliated granite'. Sample locations and characteristics are summarized in Table 3-1.

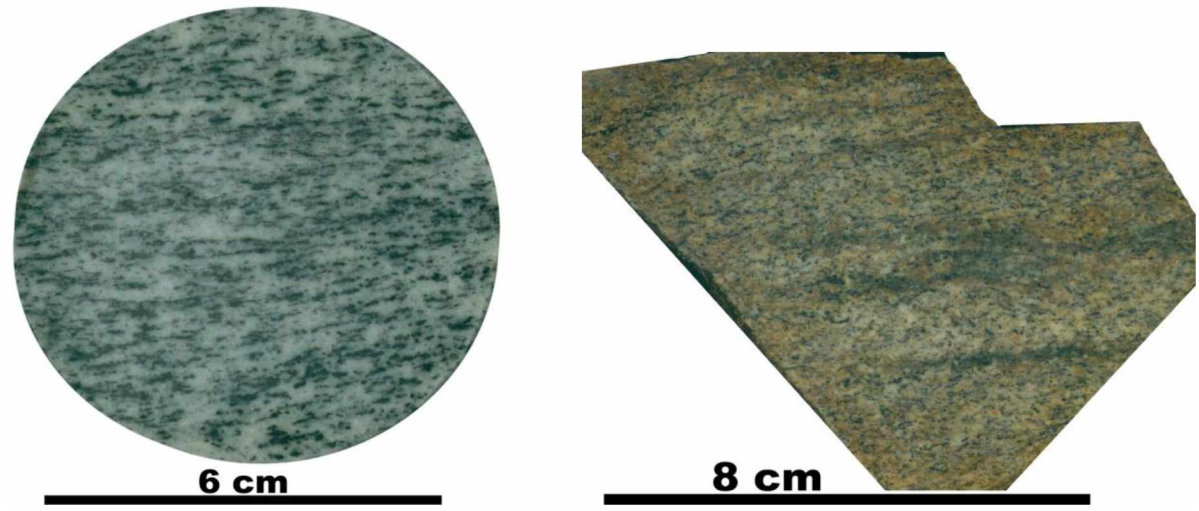

Figure 3-1: Difference in schistosity between a true orthogneiss (left) and a meta-granite (right) that has variably-developed schistosity, usually in small intervals up to a meter.

Table 3-1: Location information and descriptions of U-Pb age samples.

Sample ID	Location	UTMs	XRF Sample	Rock Type	Trace elements	Tectonic Environment
4021A	DDH 11-639 43 m	604298E, 7147153N	15PUC121	Orthogneiss	v. high Nb	Within-Plate
4021B	surface	604506E, 7147045N	15PWT27	Orthogneiss	Low Nb	Volcanic Arc
Fun Zone	DDH 15-845 427m	600050E, 7150059N	15PUC127	Orthogneiss	High Nb	Within-Plate
South Pogo	surface	601669E, 7147820N	15PWT22A	Meta-Granite	High Ti-Zr	Volcanic Arc

3.2 Individual Sample data

3.2.1 Sample 4021 A

I selected sample 4021A from DDH 11-639 at a depth of 140 feet (43 m); it is representative of high-Nb (51 ppm)-Th (22 ppm), within-plate type orthogneiss with strong schistosity and weak iron-oxidation (Fig. 3-2, left). The zircons separated are elongated to rarely sub-rounded to sub-equant, 60-80 microns long and 20-40 microns wide.

A total of 50 zircons were analyzed, yielding $^{206}Pb/^{238}$ U ages of 110 ± 2.5 to 374 ± 6 Ma (Fig. 3-3A; appendix C). A histogram of all ages (Fig. 3-3A) shows a multi-modal distribution, with a small peak at about 115 Ma, a group with a small broad range and a mode at about 325 Ma, and the majority of the data with a mode value of about 355 Ma. A histogram showing only Paleozoic ages with a tighter age interval (2 Ma, Fig. 3-3B) shows an essentially normal distribution with a mode value of 356 Ma and a long, non-gaussian 'tail' extending to 300 Ma. Exactly where the break is between the 'normal' distribution and the 'tail', however, is not entirely clear.

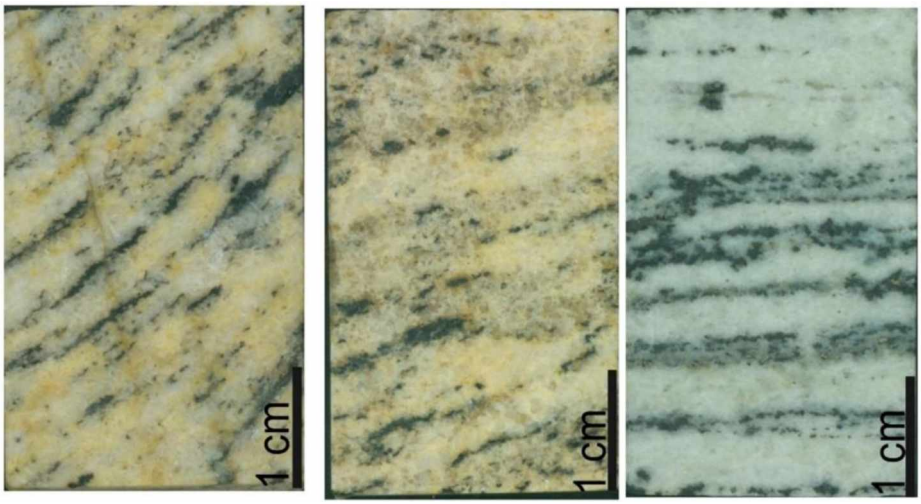

Figure 3-2: Scanned images of granite orthogneiss samples 4021 A (left), 4021B (center) and Fun Zone (right), showing well-developed mineral alignment emphasized by biotite (black).

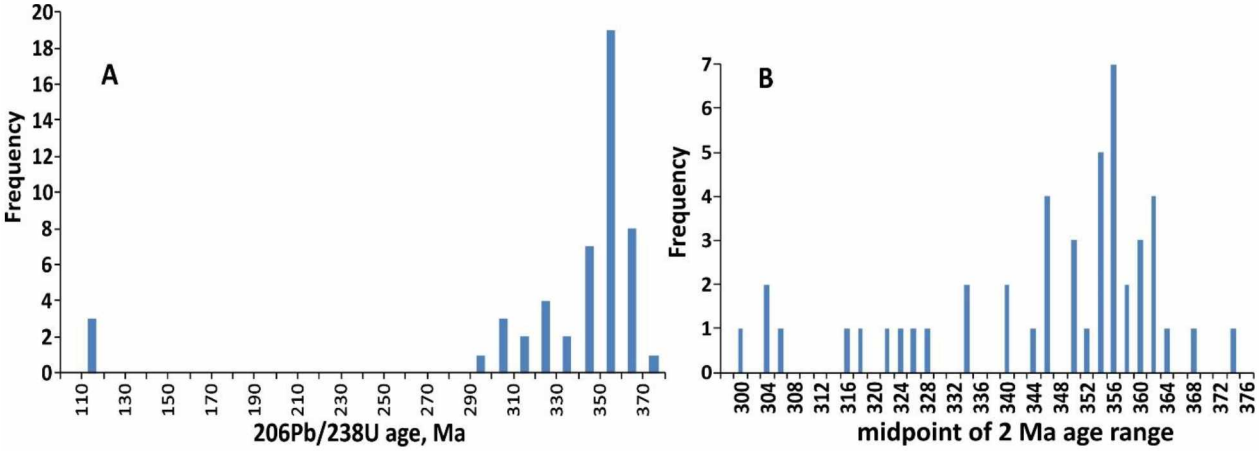

Figure 3-3: Histograms of 206Pb/238U ages for sample 4021A. A shows all data, compiled at 5 Ma intervals; B shows only Paleozoic ages, compiled at 2 Ma intervals. A mode value of 356 Ma is evident, with a long tail towards younger ages.

A cumulative histogram for the 37 analyses with $^{206}Pb/^{238}U$ ages > 330 Ma yields a median age of 355.2 + 1.4/-3.1 Ma (Fig. 3-4, left). The 29 measurements with ages of 346-367Ma plotted on a concordia diagram (Fig. 3-4, right) yield a mean age $^{206}Pb/^{238}U$ of 356 ± 1.5 Ma (very early Mississippian). All of the individual points and the mean point fall on the condordia curve (within 2 sigma errors), that is, yield statistically indistinguishable $^{206}Pb/^{238}U$ and $^{207}Pb/^{235}U$ ages. However, the mean age excludes the 3 Cretaceous and 17 Pennsylvanian and early Mississippian ages, that is, excludes 40% of the data.

A plot of ppm U/Th versus age (Fig. 3-5) for the 50 zircon spots analyzed shows that the zircon samples with Cretaceous ages possess high (>8) and the others low (<3) U/Th ratios. The group that constitutes the low-age 'tail' in the histograms (Fig. 3-3) shows an apparent relationship between age and U/Th ratio; progressively younger ages have higher U/Th. A possible explanation is that the anomalously young ages are from zircons that possess both lower U/Th 'magmatic' portions and high U/Th 'metamorphic' recrystallization zones.

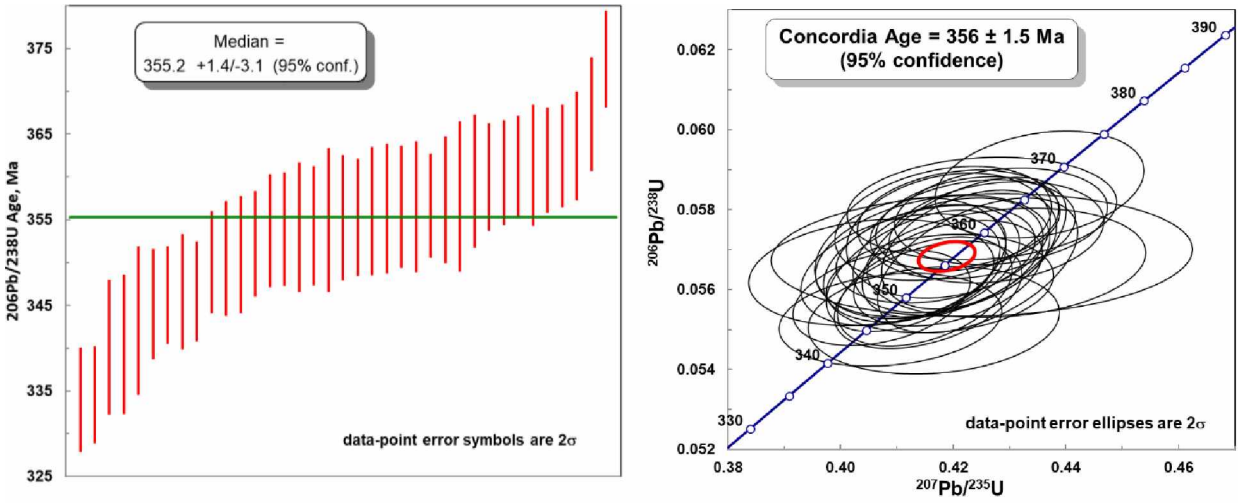

Figure 3-4: Ages for sample 4021A. Histogram of 206Pb/238U ages for the 37 analyses with ages >330 Ma (left). Concordia plot for 30 analyses with ages of 346-367 Ma (right).

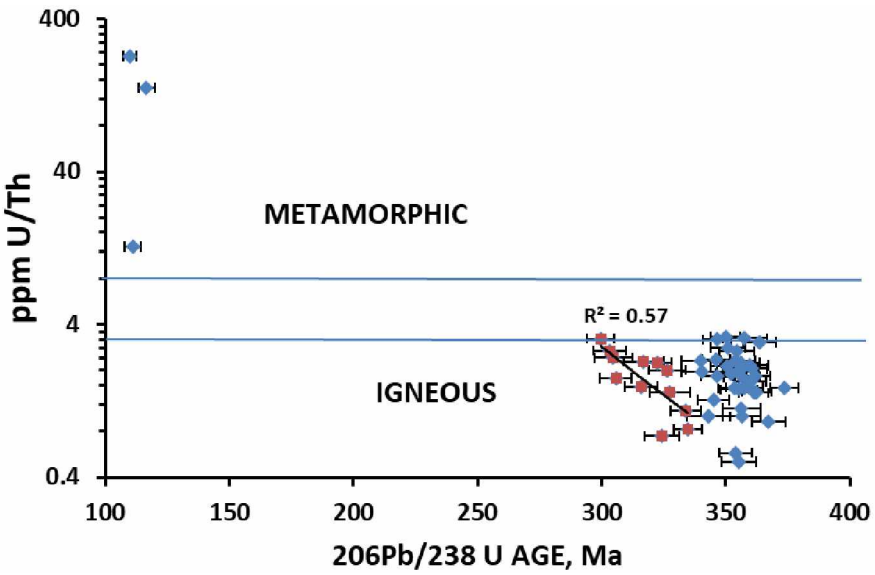

Figure 3-5: Age vs. U/Th ratios for zircon spot analyses from sample 4021A. Error bars are 2 sigma age uncertainties. The group in red represent zircon spots yielding ages of 300-335 Ma.

To test this 'metamorphic recrystallization hypothesis, I mapped 22 of the zircons using cathodoluminescence (CL) and analyzed those with highest LA-ICP-MS Th concentrations using the electron microprobe. The CL images are complicated by the fact that the image in the ablated area has been degraded by the ablation process. All CL images are given in Appendix D.

Zircons 15 and 37 (Fig. 3-6) are representative examples of those yielding Devono-Mississippian ages. Both yielded CL images with relatively sharp oscillatory zoning and a variably-developed zone of recrystallization (cutting across the oscillatory zones). The microprobe analyses indicate the recrystallized zones have low Th (below detection) whereas the oscillatory zoned parts are variably Th-enriched (Fig. 3-6). In both cases the ablation pits appear to be confined to areas lacking the low-Th recrystallization, that is, sampled exclusively igneous parts of the zircons.

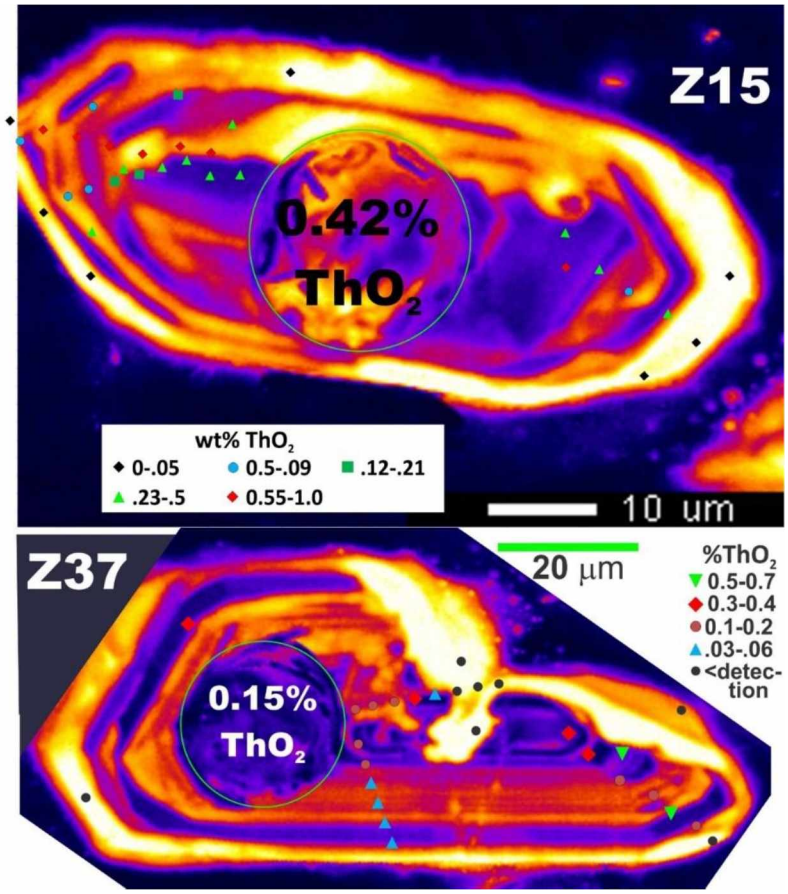

Figure 3-6: Microprobe images and data for zircon #15 and #37, from sample 4021A (~361 and 354 Ma, respectively). The calculated ThO2 concentration in the ablated core is from the LA-ICP-MS analysis and points are EMPA-derived. Note that all rim compositions yield < 0.05% ThO_2. Cathodoluminescence (CL) examination: inner parts display complex, sharp, oscillatory zonation; low-Th parts display a bright CL response and cut across the oscillatory zones. The ablation pits in these two samples are apparently confined to the regions lacking low Th recrystallization.

In contrast, zircons 18 and 48 (Fig. 3-7) yielded Cretaceous (metamorphic) ages and display CL and compositional patterns consistent with that. The CL image for zircon 48 (Fig. 3-7, right) is particularly striking, as a small, oscillatory zoned segment with elevated Th (magmatic?) is surrounded by low-Th zircon displaying no oscillatory zones. The ablation pit for this zircon was clearly in the unzoned, low-Th part, well away from the residual igneous part. Zircon 18 is more complex, but that one displays broad, largely destroyed, oscillatory zones and mostly very low Th concentrations. The original igneous oscillatory zoning was not completely destroyed, but nearly so.

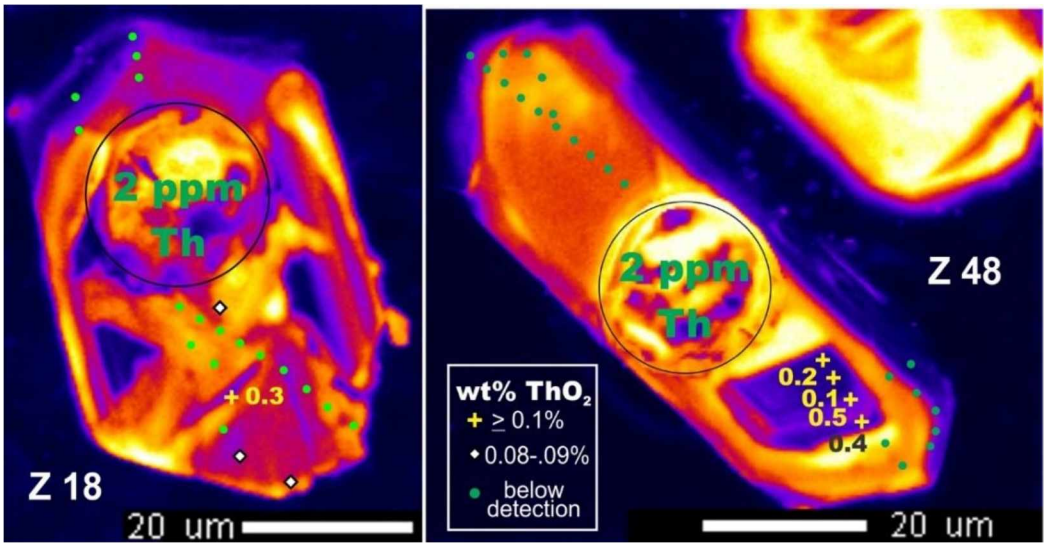

Figure 3-7: Microprobe images of zircon #18 and 48, from sample 4021A (ages of ~116 and 110 Ma, respectively). Zircon #18 (left) contains chaotic, indistinct zoning and may represent a chaotically recrystallized zircon with a large metamorphic component. Zircon #48 (left) shows a lack of zoning (homogenous color) for the majority of the grain and contains an inherited (igneous?) grain with some oscillatory zoning in the lower right. The relatively homogeneous portion with low Th most likely represents metamorphic recrystallization of an originally banded igneous zircon.

As a final contrast, zircons 6, 7, and 40 are representative of zircons (Fig. 3-8) that yielded younger (Carboniferous) Paleozoic ages (fig. 3-5). CL images of these zircons exhibit some sharp oscillatory zoning, but also line broadening and variably extensive recrystallization zones with low Th (e.g., Z6, Fig. 3-8). Most importantly, the ablation pits appear to include both clearly igneous and clearly non-igneous zones, and the typical Th concentrations of the ablated areas (.09-.13% ThO_2) are lower than those that yielded early Mississippian ages (.15-.42% ThO2, Fig. 3-5). I conclude that the ablated areas in these zircons were neither purely igneous nor purely non-igneous and the ages so generated have no geologic significance.

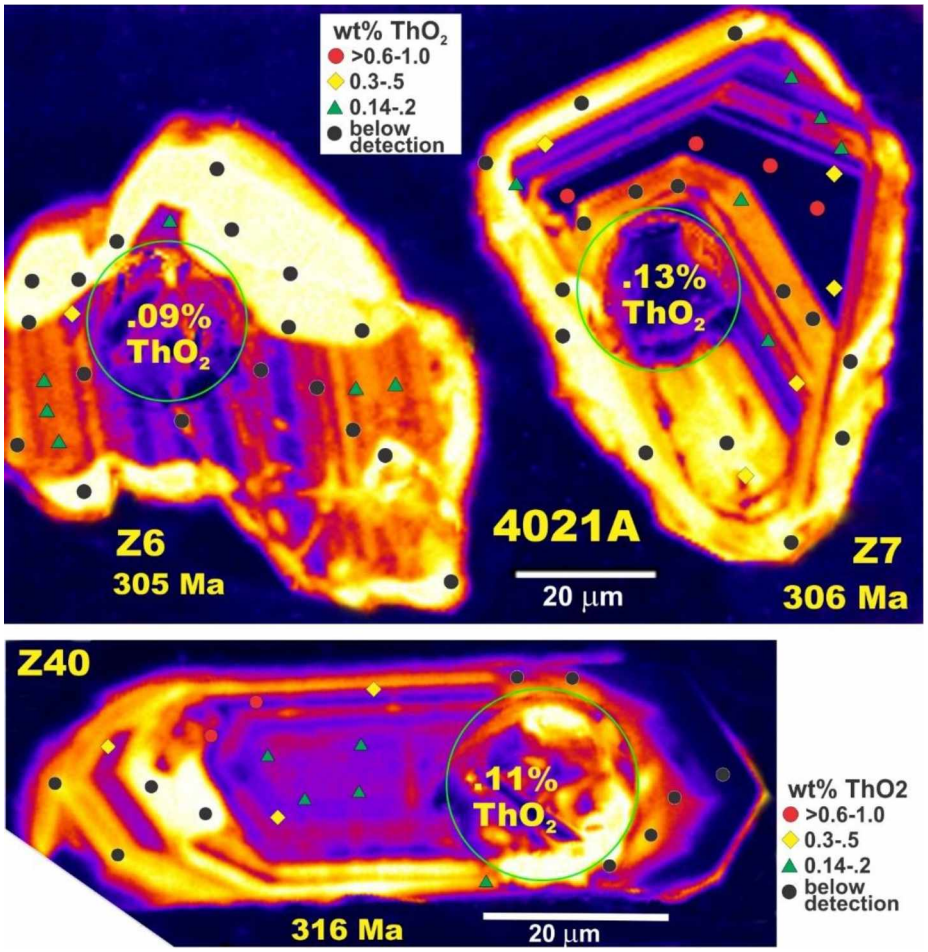

Figure 3-8: Cathodoluminescence images with microprobe spot analyses for 3 examples of zircons with 'intermediate' ages. All show remnant igneous oscillatory banding, but with some broadening and (or) replacement by homogeneous CL zircon. The 'igneous' parts are variably Th-enriched, the 'recrystallized' parts uniformly contain low Th concentrations. The ablated pits appear to have been drilled into mostly 'igneous' zircon, but with small amounts of 'recrystallized' zircon. These zircons yielded anomalously young ages, but not metamorphic ages per se. The ages presumably have no geologic significance.

3.2.2 Sample 4021 B

I collected sample 4021B from the surface at the 4021 deposit (Fig 2-1); it is representative of low-Nb (8 ppm)-Th (< 3 ppm), volcanic arc type orthogneiss (Chapter 2) with strong schistosity and weak iron-oxidation (Fig. 3-2, center). Spots from a total of 50 zircons were measured from sample 4021 B.

The zircons separated are typically elongate and sub-equant, 80-100 microns long and 30-40 microns wide. Because the age results are similar to those of sample 4021A (and the Th

concentrations much lower—making microprobe analysis problematic) I did not pursue CL imaging or attempt microprobe analyses of these.

Similar to 4021 A, three zircons yielded Cretaceous (110-113 Ma) ages (Fig. 3-9). I assume that the ablated areas on these grains were largely recrystallized, as they also yielded elevated (>6) U/Th ratios. Additionally, 4021 B contains 1 inherited zircon of Paleoproterozoic (1.6 Ga) age (not shown). Disregarding the seriously old and young ages and 3 anomalous (290-337 Ma) ages, the majority of analyses display a Gaussian distribution centered around 362 Ma (3-9, right). Analysis of the data using 42 ages (344-378) gives a weighted mean of 361 ± 2.6 Ma (Fig. 3-10, left). Further pared down, plotting 38 analyses (348-380 Ma) on a concordia diagram (Fig. 3-10 right) yields an age of 363 ± 1.6 Ma. Considering all the statistical approaches mentioned, the 'best' age for 4021 B is 362 ± 2 Ma (latest Devonian), approximately 6 Ma older than the 'best' age for 4021A.

The mid-Cretaceous aged zircon analyses included high U/Th ratios; however, two are below the metamorphic 'cut-off' ratio of 8 (Fig. 3-11), although they are above the igneous cut-off of 3. Notably, however, many of the 'igneous' zircons from sample 4021B also possess U/Th ratios >3, but < 8 (Fig. 3-11). In other words, apparently igneous zircons, and apparently recrystallized zones in zircons can yield near-identical U/Th ratios. I presume that the 3 anomalously young (Permo-Carboniferous) ages were derived from spots similar to those yielding the younger ages in sample 4021A: overlapping igneous and recrystallized zones. I consider these younger Paleozoic ages to also have no geologic significance.

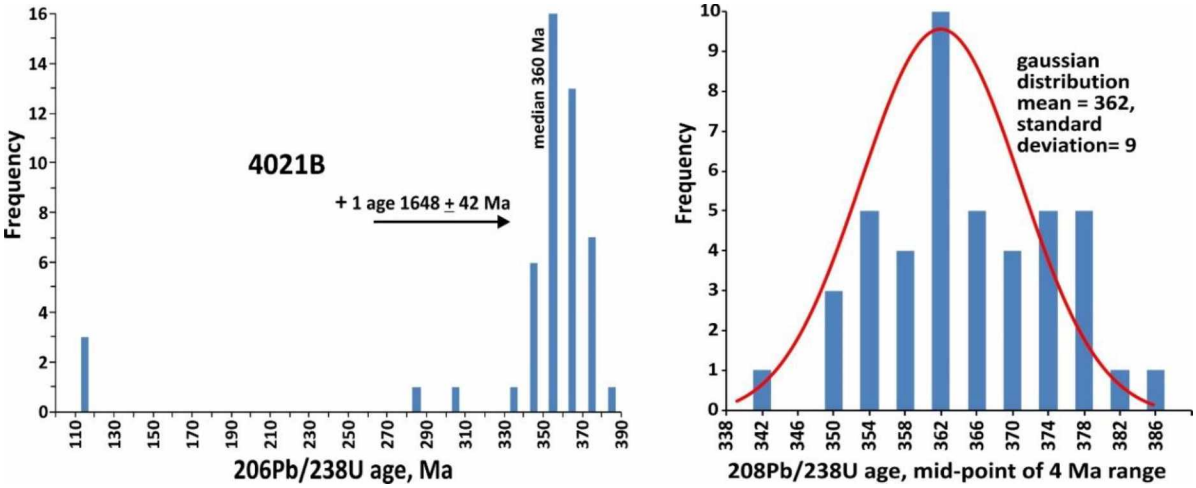

Figure 3-9: Sample 4021 B, left is an age histogram of all analyses, right an age histogram of 43 analyses (344-382 Ma) displaying Gaussian distribution centered around 362 Ma.

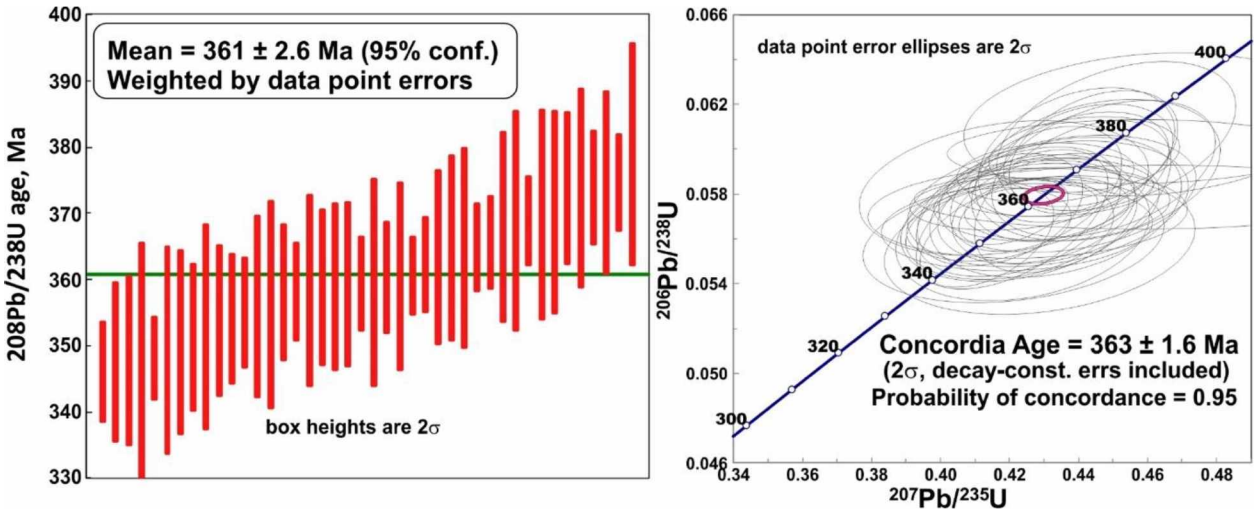

Figure 3-10: Sample 4021 B, left is cumulative histogram is for 42 ages (344-378 Ma); right is a concordia diagram for 38 ages (348-380 Ma).

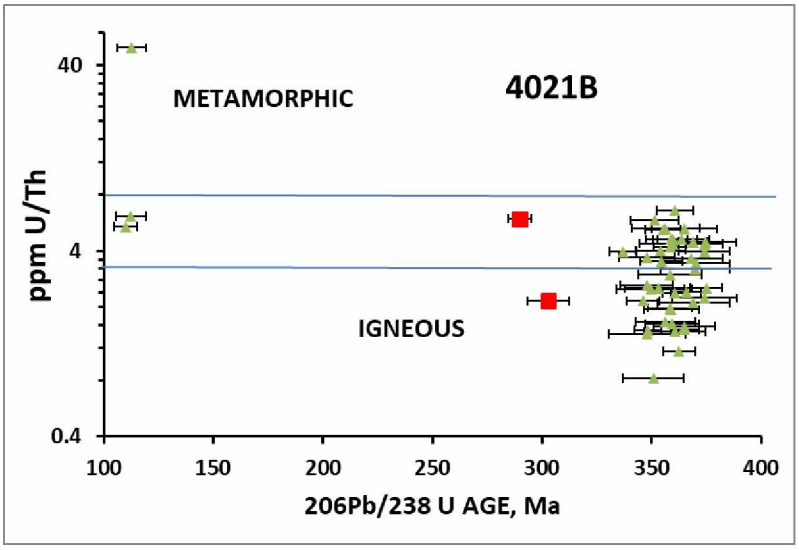

Figure 3-11: Age vs. U/Th ratio for zircon spots from sample 4021B. Error bars are 2 sigma age uncertainties.

3.2.3 Fun Zone Sample

I collected the Fun Zone sample from a diamond drill hole core targeting the Fun zone area (Fig 2-1). The sample displays strong schistosity and patchy biotite that is typical for this unit (Fig. 3-2, right). Based on its high Nb (44 ppm) content and low normative quartz, it represents an alkalic within-plate type orthogneiss (Chapter 2), with anomalous (18 ppm) Th.

Unfortunately, the heavy mineral separate from this sample was dominated by titanite and apatite, with perhaps 10% zircon (Fig. 3-12). Zircon and titanite have near-identical relief and although titanite has significantly higher birefringence, the interference colors displayed vary with grain orientation. Consequently, it can be difficult to distinguish between zircon and titanite in a heavy mineral concentrate. As a result, only 29 of 50 analyses were performed on zircons; the other 21 were on titanite (and yielded no useful data). This smaller data set yields a less robust igneous age than those of the other samples.

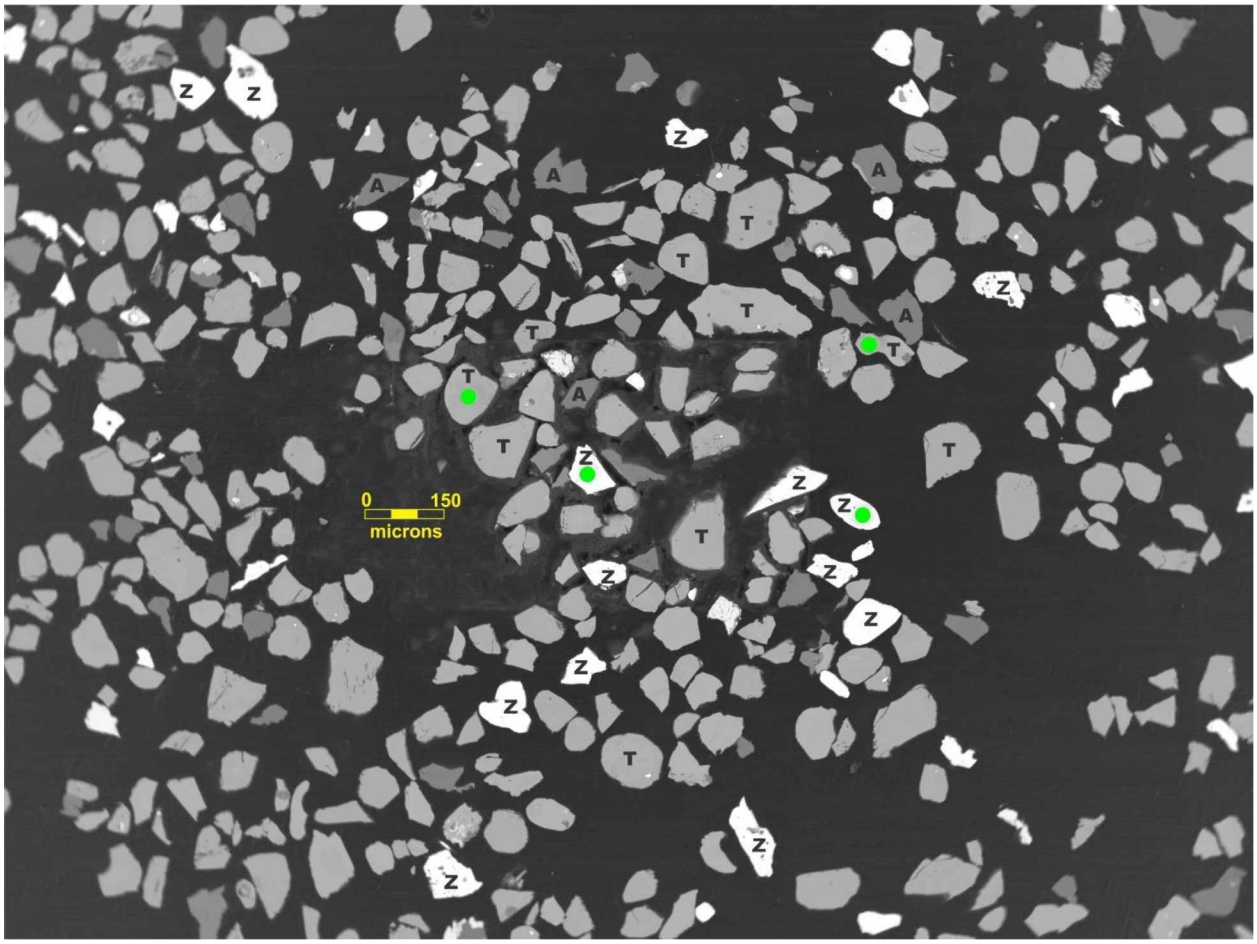

Figure 3-12: Backscattered Electron (BSE) image of a representative 2.4 m x 1.8 mm area of the heavy mineral concentrate for sample 'FunZone'. The brightest grains (many marked with 'Z') are zircons; the next brightest (several with 'T') are titanite; the least bright (several with 'A') are apatite. The black background is epoxy, variably degraded by the electron beam. The ablation pits are emphasized with green dots: two zircons and two titanites in the field of view were analyzed for U-Pb age. Approximately 10% of the grains visible are zircon; most were not analyzed.

Similar to previous samples, the data yielded three main groups of ages: mid-Paleozoic, late Paleozoic (to Triassic), and mid-Cretaceous (Fig. 3-13A). However, the older mid-Paleozoic group shows no obvious statistical symmetry (Fig. 3-13) as seen in previous samples (Figs. 3-3, 3-9). That is, rather than displaying a gaussian distribution of ages, there is a sharp break at the oldest measured age of 342 Ma (Fig. 3-13B).

The intersections of a best-fit line on a concordia diagram with the concordia (Fig. 3-14A) suggests a mixing of populations with ages of 85 ± 38 Ma and 327 ± 33 Ma. The large uncertainties are caused by the nearly parallel curves and low intersection angles. Further, the U/Th vs. age diagram reveals a general decrease in age accompanied by an increase in U/Th

(Fig. 3-14B). Such a relationship suggests that all of the zircons have been variably affected by a younger, high U/Th event.

Removing the seemingly more contaminated zircons (ages of < 330 Ma) yields a best estimated concordia age of 337.5 ± 2.0 Ma (Fig. 3-15A). Similarly, averaging all the Cretaceous ages yields a concordia age of 116 ± 1.4 Ma (Fig. 3-15B). Although the center of the error ellipse falls off the concordia, within error the point lies on it, and the age can be considered concordant.

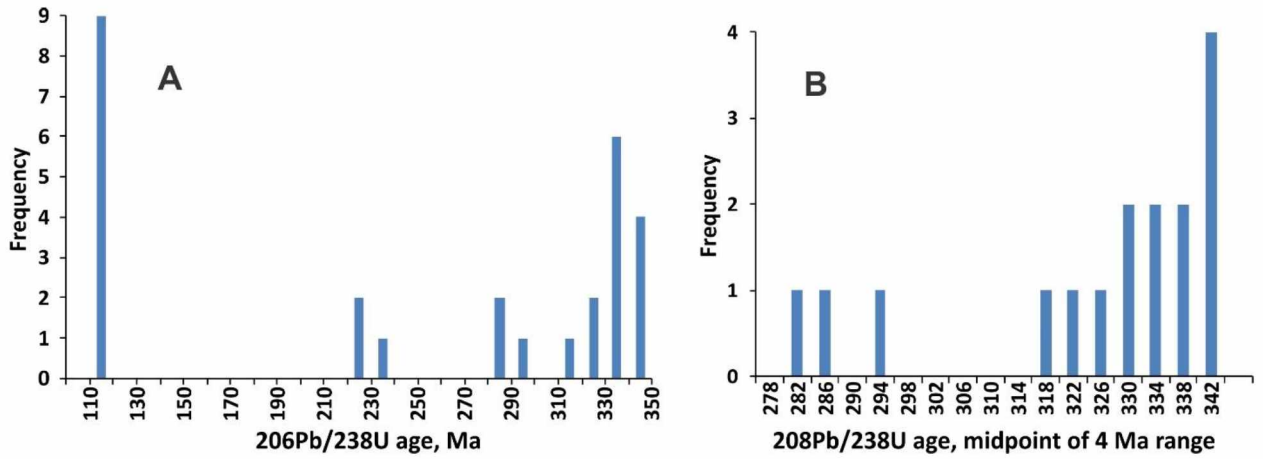

Figure 3-13:U-Pb age histograms for the Fun Zone sample: A = all ages; B = ages > 280 Ma. The smaller selection of ages (B) is apparently truncated at 342 and displays a decidedly non-gaussian distribution.

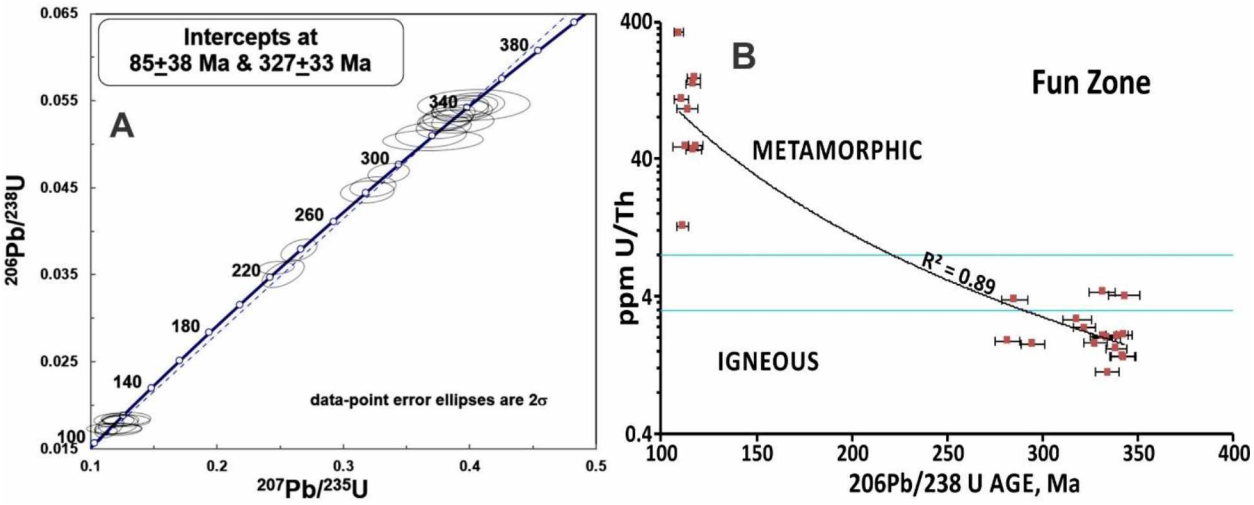

Figure 3-14: Fun Zone sample age graphics. A = all data plotted on a Concordia diagram showing intersections with the Concordia. B = age vs. U/Th for all data, showing a strong correlation between age and U/Th, suggesting that all of the ages have some 'metamorphic' component.

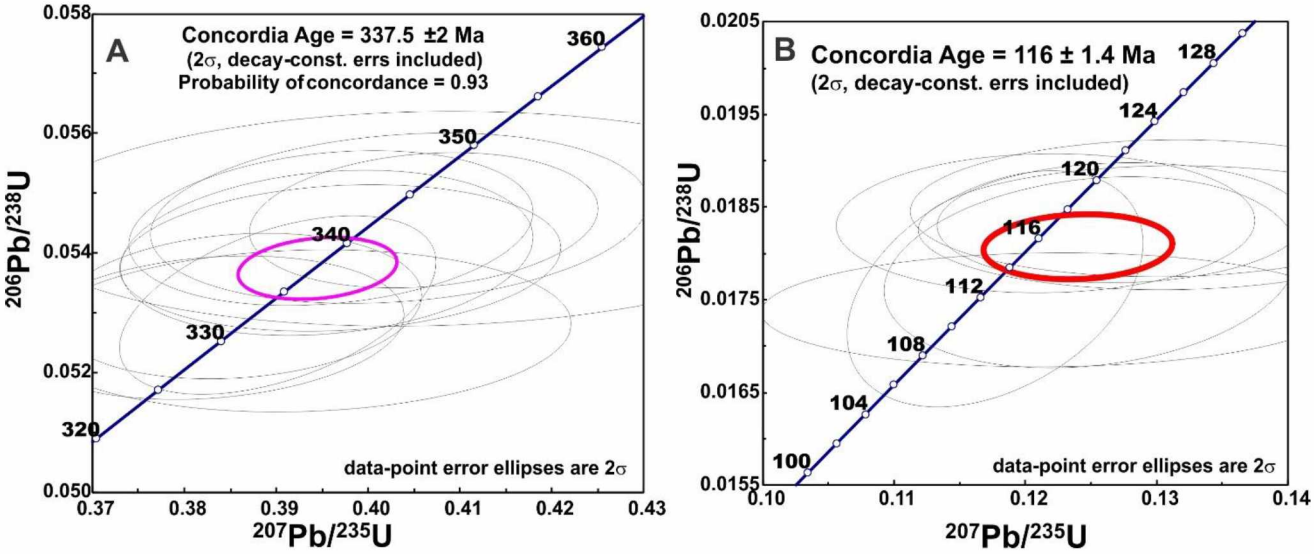

Figure 3-15: Fun Zone sample, left shows concordia for 10 measurements >330 Ma. Right image shows concordia for mid-Cretaceous ages. Within error this point lies on the concordia.

Due to the non-gaussian distribution of ages, and younger apparent ages extending to Triassic (Fig. 3-15B), the concordia age of 338 Ma should be considered a minimum age. Based on the poorly-constrained intersection of the data with the Concordia (upper intercept age of 327 ± 33 Ma, Fig. 3-17A), the igneous age could easily be as old as 360 Ma. That is, the Fun Zone orthogneiss might be as old as the 4021 orthogneisses, or it might be significantly younger.

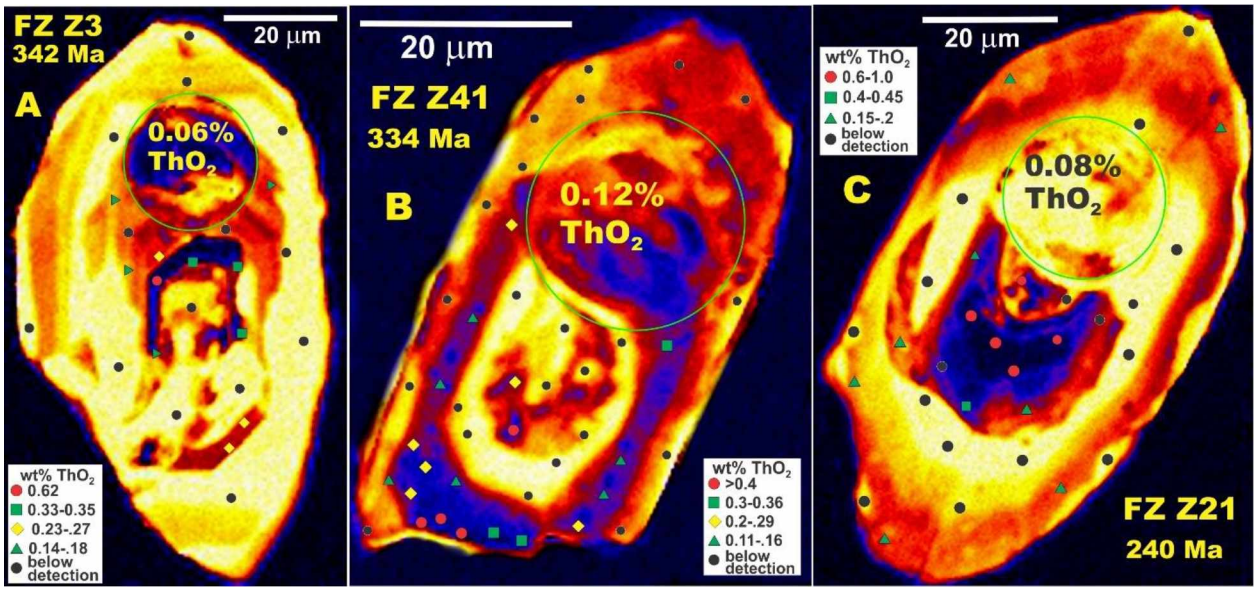

Figure 3-16: CL images and spot microprobe analyses for three Fun Zone zircons that yielded older ages, arranged from oldest (A) to youngest (C). All three images show some degree of oscillatory zoning and locally high (0.6-1%) ThO2, but compared to the images for 4021A, the zones are broad and diffuse, not sharp. Additionally, major portions of each grain do not exhibit oscillatory zoning and must represent metamorphic recrystallization.

Given the problematic ages for the Fun Zone sample, I prepared CL images for five of the zircons and performed microprobe analyses on the three with the highest ablation zone Th concentrations. Figure 3.16 shows three such grains, arranged from oldest age for the entire population (A) to a zircon that yielded a Triassic age (C). In all cases the igneous-like oscillatory zones are much broader and more diffuse than those from sample 4021A and all display extensive non-oscillatory zoned regions that--combined with their very low (<0.1%) ThO_2--are likely due to metamorphic recrystallization. The surprising part is that all of the zircons possessed zones with high (0.6-1%) ThO_2, yet the average concentrations in the ablated spots are only 0.6-0.12% ThO_2. (Through sheer bad luck, the ablation spots selected missed the higher-Th zones.) I conclude that none, even the one (Fig. 3-16A) with the oldest age, represent uncontaminated igneous ages.

In comparison, two CL images of zircons yielding Cretaceous ages (Fig. 3-17) show no sign of oscillatory zoning, and instead display nearly homogeneous CL. These are consistent with essentially complete recrystallization or else completely new zircon growth.

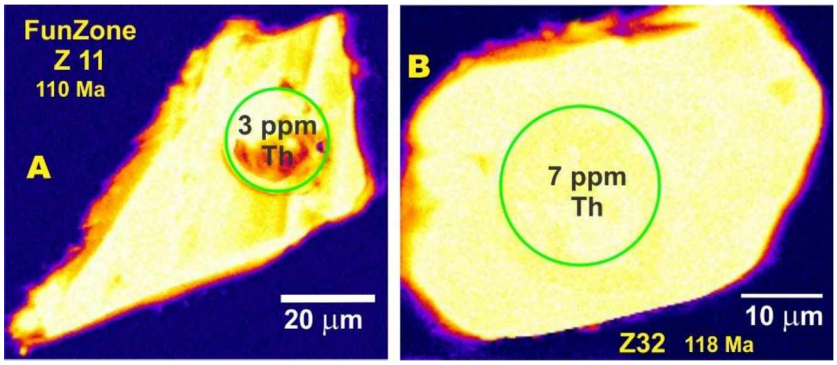

Figure 3-17: CL images of two Fun Zone zircons that yielded Cretaceous ages. The ablation pits are shown by the green circles. The featureless CL images are consistent with complete recrystallization or with growth during a metamorphic event.

3.2.4 South Pogo Sample

I collected the South Pogo sample in the South Pogo area, southeast of the Liese Ore Zone (Fig. 2-1). The hand sample collected displayed weak Fe-oxidation and variable weak foliation (e.g., Fig. 3-1). The sample was from the same outcrop (within relocation errors) as Katherine Dilworth's POGO-01-169 sample of supposed 'Cretaceous orthogneiss' (Dilworth, 2003). The zircons separated are typically elongate, 100-120 microns long and 30-40 microns wide. The rock contains relatively high Zr (137 ppm) and low Th (< 3 ppm) and is significantly peraluminous, with 2.5% normative corundum.

From the South Pogo sample 49 zircon spots were analyzed, generating 38 mid-Cretaceous dates and 11 older dates (Late Jurassic to Proterozoic; Fig. 3-18A). A simple histogram of the mid-Cretaceous ages shows a Gaussian distribution centered around 107 Ma (Fig. 3-19B). Both a weighted mean average (37 ages <113 Ma) and a concordia (38 ages <114) gives an age of approximately 107 ± 1 Ma (Fig. P20). However, the concordia average is discordant, falling off to the right, likely due to contamination by portions of the grains with residual older zircon (Fig. 3-20). Due to the inheritance problems, the igneous age of the sample may be different from 107 Ma, but probably not much different.

The South Pogo sample contains multiple generations of older zircons including Paleozoic and Proterozoic (Fig. 3-20A). These zircon ages have likely been affected by metamorphic recrystallization, as seen by their decrease in age with increasing U/Th (Fig. 3-20B). Additionally, three high U/Th ('metamorphic') zircons yield ages of 111 ± 4, 114 ± 5, and

151 ± 8 Ma. The younger two ages fit (within error) into the 'metamorphic' age defined by the other samples, however, the older (late Jurassic) ages are of uncertain origin. There is no known source for either the Jurassic nor the Proterozoic zircons in the immediate Pogo area. The zircons with Paleozoic ages could represent contamination of magma from nearby rocks, but the other ages presumably represent contamination from rocks at depth.

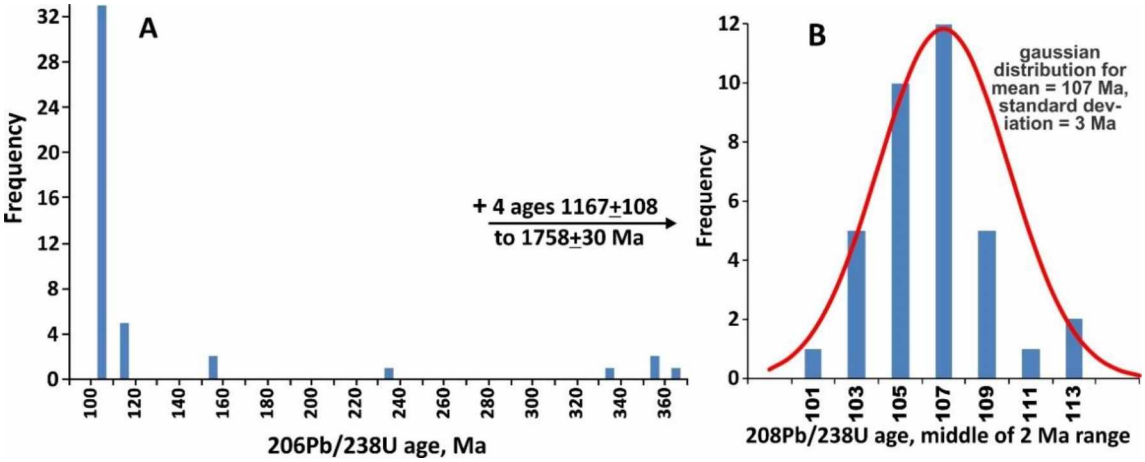

Figure 3-18: South Pogo sample, on left are all 49 analyses, on right are all 38 measurements with ages <150 Ma, with a mean of 107 Ma.

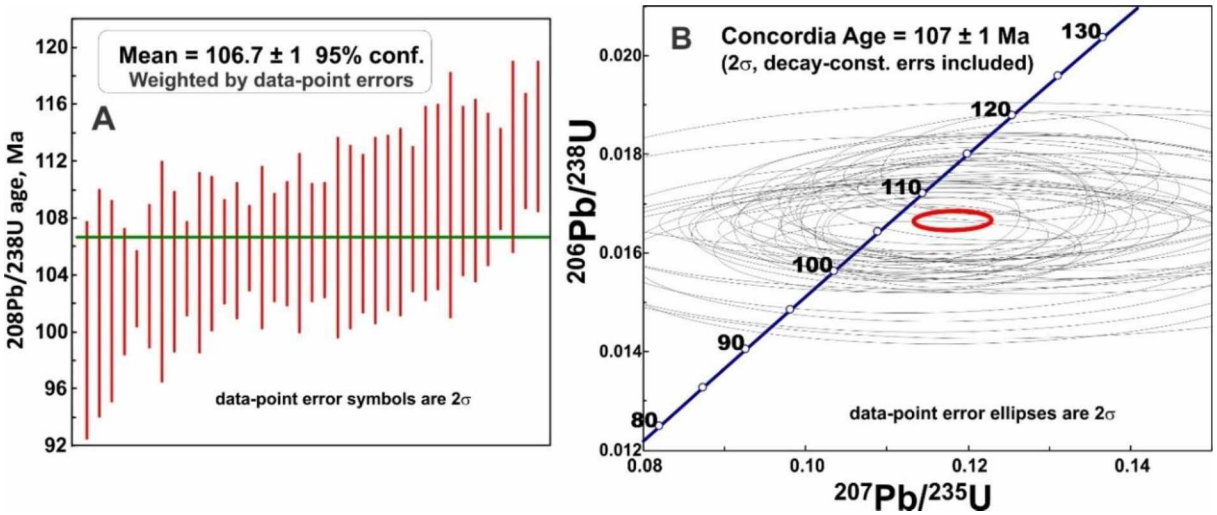

Figure 3-19: South Pogo sample, left is a cumulative histogram for 37 ages <113 Ma. The right image shows a concordia plot for 38 analyses <114 Ma, including 2 with 'metamorphic' U/Th ratios. The average does not plot on concordia, i.e., this is not a concordant age. This is likely due to contamination from older zircon cores.

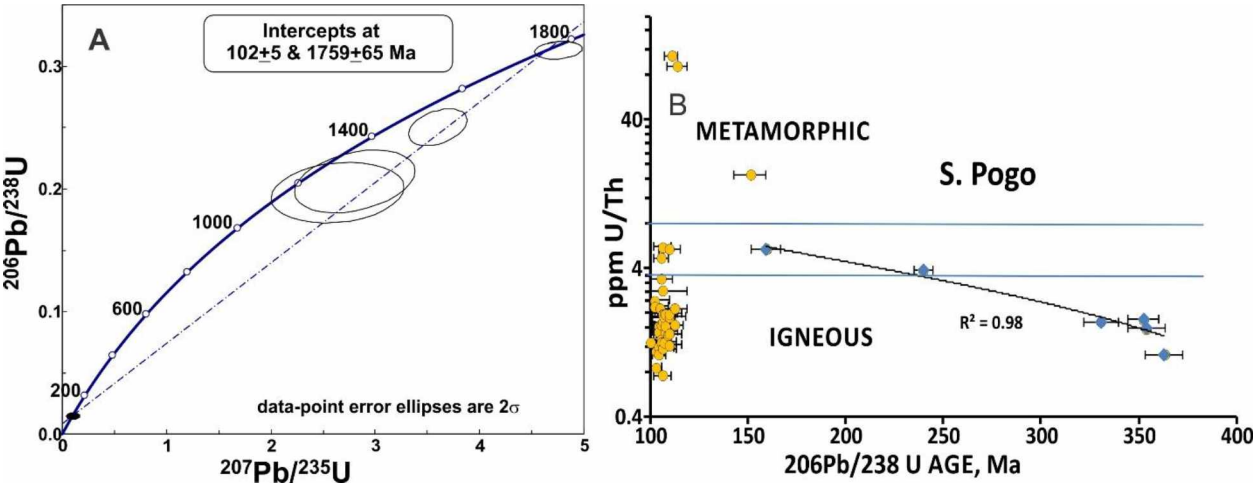

Figure 3-20: South Pogo sample, left image is a concordia diagram for the oldest and youngest zircons, showing that the 3 with ages 1100-1500 Ma are likely ca. 1.8 Ga with partial Pb loss. Right image is age vs. U/Th, showing that the 150-350 Ma 'igneous' zircons define a linear trend of decrease in age with increasing U/Th.

Cathodoluminescence (CL) images (Fig. 3-21) of representative zircons from the South Pogo pluton tell a complicated story. Those yielding mid-Cretaceous ('magmatic') ages include numerous grains with apparently metamorphic or at least partly recrystallized cores with oscillatory-zoned overgrowths (Fig. 3-21, A-C). U/Th ratios can be in the 'magmatic' range (<3) but also outside of that range. Perhaps smaller grains are truly magmatic, but most of the grains examined seemed to display predominantly non-magmatic CL textures.

The two zircons with apparently Jurassic ages similarly display cores with apparent non-magmatic CL features but variably extensive magmatic (oscillatory zoned) overgrowths. Z2 (Fig. 3-21 D) displays extensive magmatic overgrowths whereas Z21 displays virtually none. Nonetheless, they yield similar ages. Particularly in the case of zircon 21, the virtual absence of a magmatic overgrowth would suggest that the age represents a real metamorphic event.

In contrast, the example of a zircon with a Devonian age (Fig. 3-21 F) appears to contain a magmatic (oscillatory zoned) core surrounded by a recrystallized rim and in turn surrounded by a thin oscillatory zoned (magmatic) rim. Based on this morphology I think this grain likely yielded a truly Devonian magmatic age.

The zircons that yielded Proterozoic ages (Fig. 3-21, G-I) possess apparently metamorphic cores and moderately high (4-5) U/Th ratios, but also variably extensive oscillatory zoned rims. These clearly igneous rims, combined with their locations off the Concordia (Fig. 3-

20A) suggests that the ages have no geologic significance and represent partly re-set metamorphic ages. The apparent lack of correlation between width of igneous overgrowth zone and age may reflect non-uniform overgrowths.

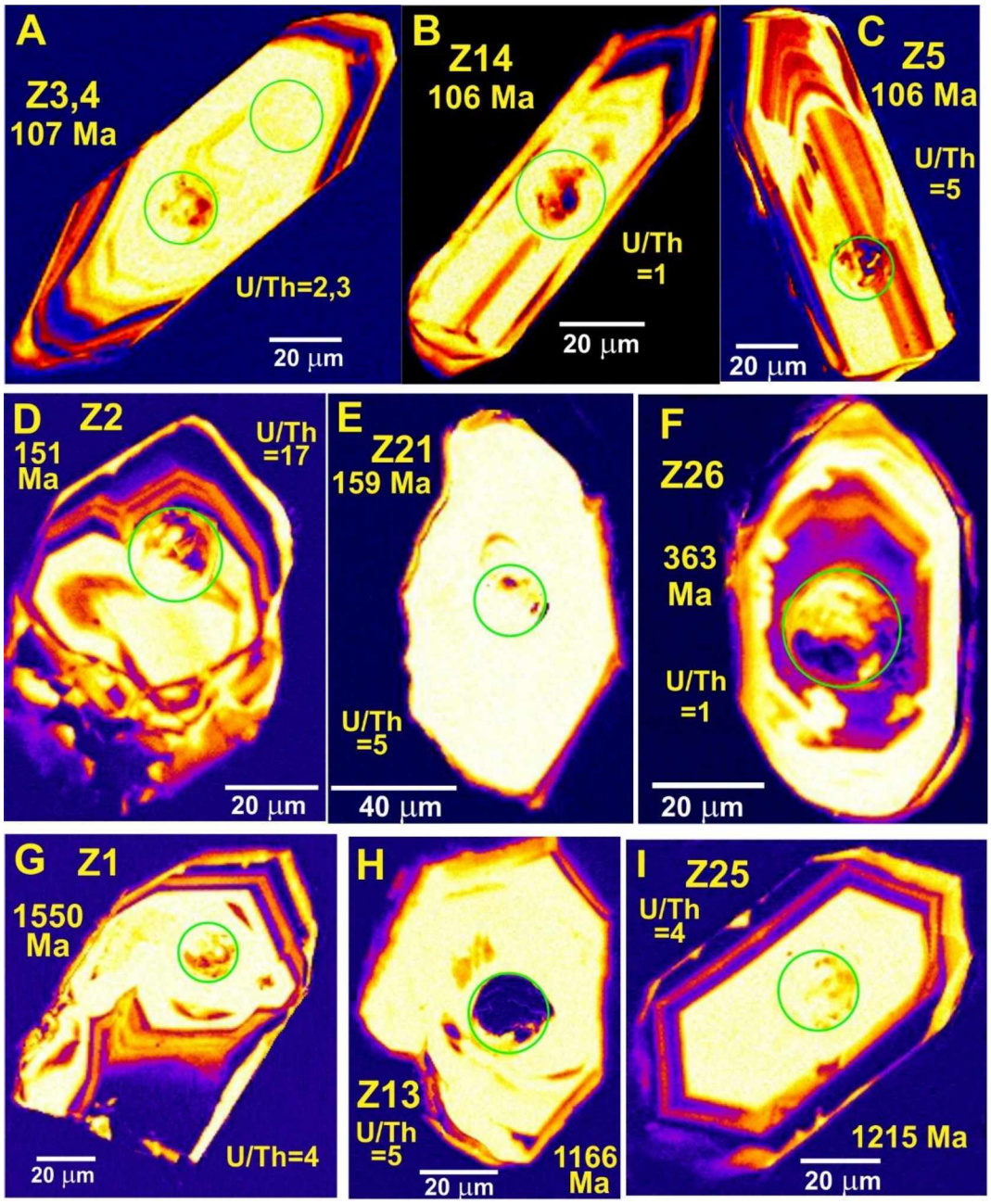

Figure 3-21: CL images from selected South Pogo zircons, arranged by apparent age. A-C = zircon spots with mid-Cretaceous (apparent magmatic) ages. D-F = zircon spots with Jurassic-Devonian ages. G-I = zircon spots with Proterozoic ages.

3.3 Discussion

At one level, the zircon geochronology is straightforward; at others, it is more complicated. The simple part is that the so-called 'early Cretaceous orthogneiss' of Dilworth (2003) and 'early Cretaceous foliated granite' of Dilworth et al. (2007) has, in fact, a Paleozoic (Devonian-Mississippian) and not Cretaceous protolith age. That is, the pervasively schistose granitic rocks are part of the Paleozoic metamorphic suite, and not deformed Cretaceous plutons. This age interpretation greatly simplifies the geologic interpretation of the Pogo area, as Dilworth et al. (2007) required that pervasive schistosity was inflicted in a very short time period, between the ages of 'foliated' and 'unfoliated' granite, both with ages of 107 ± 1 Ma. Instead, I recognize that peraluminous granite of 107 Ma age is locally sheared (as in sample 'South Pogo'), but not pervasively schistose.

Using U/Th ratios in zircon spots as indicative of zircon origin, 'clearly' igneous zircon spots (Fig. 3-22) define two age groups: Paleozoic and mid-Cretaceous (ca. 107 Ma). (However, many of the U/Th ratios fall in the 'grey zone' between 'clearly igneous' (U/Th < 3) and 'clearly metamorphic' (U/Th>8), showing that U/Th ratios are not always reliable indicator of zircon type.) In contrast, most of the 'clearly' metamorphic zircon spots yield ages of 110-118 Ma, with a median age (best defined for sample 'Fun Zone') at approximately 116 Ma (Fig. 3-22). The 'metamorphic' age is approximately 9 Ma older than the mid-Cretaceous granite. Zircon spots in orthogneiss yield a wide spread in age (~300-370 Ma) which I interpret in part to the inherent inaccuracy of a single LA-ICP-MS age determination and in part to ablation spots that overlapped 'primary' igneous zircon and recrystallized zircon.

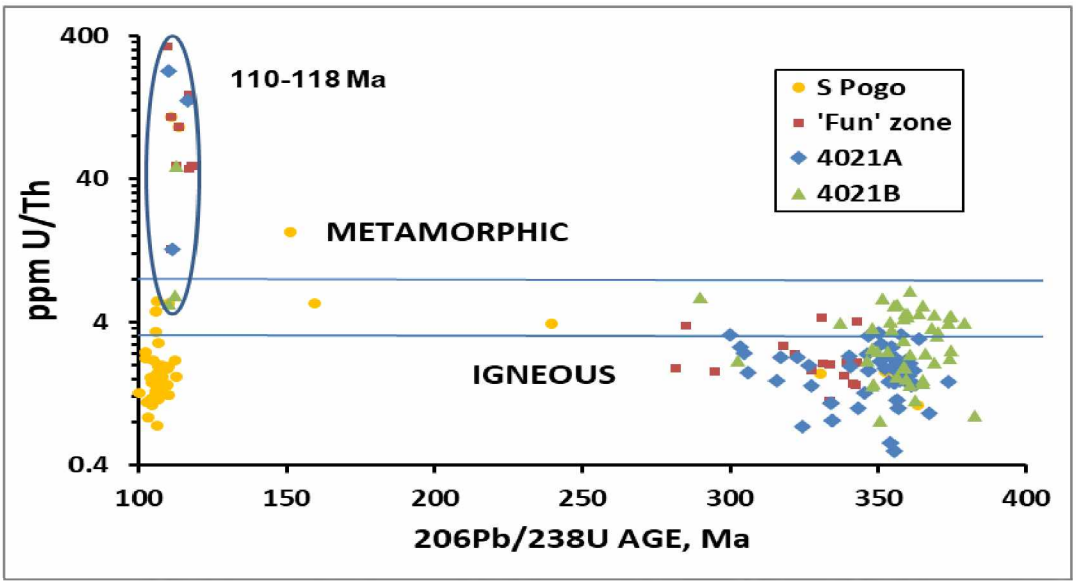

Figure 3-22: U/Th ratios versus zircon ages. The group with higher U/Th ratios represents a mid-Cretaceous metamorphic event. These have a median age of approximately 116 Ma.

The 'best' U-Pb zircon ages for the volcanic arc type orthogneiss (sample 4021 B) is 363 ± 1.5 Ma and that of the 'within-plate granite' type (sample 4021A) is 356 ± 1.5 Ma. Both ages are based on 30 or more individual analyses with a narrow age range, are statistically distinguishable, and represent different geologic events. Based on trace element considerations (Chapter 2), the older event represents subduction-related magmatism; the younger age extensional magmatism, possibly rifting of the arc.

Sample 'Fun Zone', representing alkali within-plate magmatism, yields a less robust Paleozoic age. Fewer (29) zircon spots were analyzed from this sample than the others (50) and CL indicates smaller residual igneous zones in the Fun Zone zircons than those from sample 4021A. Most of the spots analyzed showed evidence for some 'metamorphic' contamination (Fig. 3-16). A histogram of older ages from the Fun Zone sample is decidedly non-Gaussian (Fig. 3-13), with a tail extending into Triassic ages. The histogram (Fig. 3-13B) shows a mode at 342 Ma, whereas the concordia age is 338 ± 2 Ma. Perhaps the 'best' age is 340 ± 3 Ma, with the understanding that it might represent a minimum age. That is, the age of the alkalic within-plate event is probably younger than the arc event or initial rifting of the arc; it could be as much as 15 Ma younger than the initial rifting event.

In contrast, the peraluminous granite sample from the South Zone yields a Gaussian Cretaceous age histogram with a mode of 107 Ma (Fig. 3-18) and a 'concordant' age of 107 ± 1 Ma (Fig. 3-19). The error ellipse does not overlap the concordia curve (2 sigma uncertainty),

presumably due to contamination with older, inherited zircon cores. Notably, this sample shows no evidence for metamorphic recrystallization, indicating that the structural episode which created the variable fabric was not an intense one.

"Metamorphic' zones from South Zone zircons yield apparent ages of 1.55 ± .05 Ga to 110 ± 5 Ma (Fig. 3-20B). The error ellipses for the oldest samples lie far off the concordia, and a best fit line through the data yields intersections of 1.76 ± .07 Ga and 102 ± 5 Ma (Fig. 3-20A). The U/Th ratios for these are 1.1-1.5, suggesting that they represent Paleoproterozoic igneous rocks. As none such are known in Interior Alaska, the South Pogo peraluminous magma was either contaminated by melting of deeper crustal rocks or was caused by melting of deeper crustal rocks.

The South Pogo sample also yields ages of 331 ± 9 to 363 ± 10 Ma, all with 'igneous' U/Th ratios of 1.1-1.7 (Fig. 3-20B). These are (within error) indistinguishable from zircon zones analyzed from the orthogneiss samples and were presumably derived from melting of orthogneiss. Such presumably took place well below the present surface, as there are no partial melting textures seen in the orthogneiss.

Finally, rare zircon zones in the South Pogo sample yield transitional U/Th ratios of 4-5 and ages of 240 ± 5 Ma to 119 ± 8 Ma and metamorphic U/Th ratios of 17-109 and ages of 151 ± 8 to 111 ± 4 Ma (Fig. 3-20B). The former lie on a line connecting back to the Paleozoic zircon data (Fig. 3-20B) and arguably represent a mechanical mixing of Paleozoic igneous zircon and 116 Ma metamorphic zircon. That is, the zircons were originally present in orthogneiss. The 111-114 Ma metamorphic zircon spots were also likely derived from orthogneiss, as 'metamorphic' zones with such ages are present in them. The metamorphic spot analysis of 151 ± 8 Ma is problematic, as zircons with such an age are not known in the area. It was either derived from deeper rocks or represents some mixing of igneous and metamorphic regions in an orthogneiss sample.

The growth of zircon during regional metamorphism does not appear to be simple formation of an overgrowth, as the boundary between igneous (CL with oscillatory bands, low U/Th) and metamorphic (CL unbanded or irregularly banded, high U/Th) zircon is typically irregular (e.g. Fig. 3-6-3-8). The metamorphic zones are compositionally different from the igneous zones: the former have lost Pb and Th (and REEs that give rise to the CL patterns) relative to the igneous portions. Diffusion of Pb in zircon is slow; the closure temperature for Pb

diffusion in a typical-sized zircon is 900°C (Cherniak and Watson, 2001). Given the 4+ oxidation state for Th, its diffusion is much slower than that of Pb^{2+}. Consequently, the irregular zones of metamorphic zircon must represent replacements of the original igneous zircon. That is, the old zircon is dissolved, and then re-precipitated as new, Pb-free and low-Th zircon. Consequently, the 116 Ma metamorphic event documented in all of the samples must represent a significant fluid flux event.

Dusel-Bacon et al. (2002) documented an early Jurassic, high pressure, 'contraction' event (hornblende Ar-Ar ages of 181-188 Ma) and a lower-pressure, mid-Cretaceous 'extension' event (biotite and muscovite Ar-Ar ages of 113-108 Ma) in the general Pogo mine area. As the latter represent cooling to temperatures below effective Ar diffusion (300-350 °C), they are minimum ages for the younger event. Dusel-Bacon et al. (2002) also listed 5 hornblende Ar-Ar ages of 135-120 Ma, which—based on complex Ar release spectra—they interpreted as partly reset early Jurassic ages. The 116 Ma zircon age from my data presumably reflects the mid-Cretaceous extensional event. What is odd is that I found no evidence for the older, high-pressure event. I infer that the younger event wasn't necessarily of much structural significance but must represent a significant fluid flux event that overprinted any early Jurassic metamorphic zones in the meta-igneous zircons. Because the ore zones locally cut across mid Cretaceous peraluminous granites (107 Ma), this fluid flux event did not cause the Pogo deposit.

I found it difficult to interpret the various U-Pb zircon ages until I created the zircon cathodoluminescence images. Had these been prepared prior to LA-ICP-MS age analysis, it would have been possible to accurately pin-point the best spots to determine igneous and metamorphic ages in the samples. In addition, creation of back-scattered electron (BSE) images would have quickly determined which grains were—and which were not—zircon (c.g., Fig. 3-12). I would recommend both procedures prior to undertaking LA-ICP-MS age analysis.

4 Chapter 4: Geothermobarometry of Metamorphic and Intrusive Rocks

4.1 Introduction and Analytical Methods

One of the major questions I raised (Chapter 1) concerned the changes in P-T environment before, during, and after the mineralization event. Dusel-Bacon et al. (2002) documented an early Jurassic high P (9 ± 2 kb, 610 ± 50 °C) event, and Dilworth (2003) estimated mineralization pressure as 1.9 ± 0.5 kb. I have established a fluid-driven metamorphic event at 116 ± 1 Ma (Chapter 3) but conditions then and subsequently have not been constrained.

I employed different techniques for felsic vs. intermediate composition plutonic rocks: (1) plagioclase-hornblende geothermobarometry for the hornblende bearing Football and Liese plutons, (2) garnet-Al silicate-plagioclase (GASP) and garnet-Al silicate-muscovite-biotite geobarometry, garnet-tourmaline and garnet-biotite geothermometry, and granite solidus analysis for peraluminous granite, and (3) pressure-dependent water-saturated ternary composition for a Paleogene felsic dike. I used GASP geobarometry and garnet-biotite thermometry to calculate the P-T conditions for sillimanite paragneiss, representing the 116 Ma metamorphic event. Coupled with previously-determined radiometric data (Dusel-Bacon et al., 2002; Dilworth, 2003), these allow for construction of a pressure-time path for rocks in the Pogo area, for the Jurassic through Paleogene.

4.2 Metamorphic Rocks

4.2.1 Collection and Analytical Methods

During the summer of 2017 I collected diamond drill hole core samples of paragneiss that seemed relatively unaltered and contained the mineralogy conducive to GASP-Garnet-Biotite geothermobarometry. I chose from the paragneiss a sample (17PGN01) containing fine-grained fibrous sillimanite, lesser pink euhedral to fine-grained anhedral garnet, quartz, feldspar, muscovite, and biotite (Fig. 2-3). This sample contains the requisite mineralogy for thermobarometric analysis. I prepared the polished section at UAF-AIL.

To find areas for potential analyses I first employed the use of the petrologic microscope to determine coordinates of visible garnets for the JEOL JXA-8530F electron microprobe. Then, after carbon coating the section I employed EDS to locate the areas containing the requisite minerals and positively identify them.

I performed WDS analysis of the minerals garnet, plagioclase, and biotite using a modified amphibole routine developed by Ken Severin in 2014. The routine analyzed for concentrations of Si, Ti, Al, Fe, Mn, Mg, Ca, Na, and K. A total of 8 mineral clusters were analyzed. I averaged the results by mineral across the thin section (Table 4.1) and employed the Windows program PTQuick (D. V. Dolivo-Dobrovolsky, writ. Comm., 2020) to plot the results in P-T space.

Table 4-1: Average mineral compositions from sample 17PGN01.

	Weight % oxide									
Mineral	SiO_2	TiO_2	Al_2O_3	FeO	MnO	MgO	CaO	Na_2O	K_2O	Total
Biotite	34.7	4.10	18.2	23.0	0.06	7.02	0.01	0.10	9.11	96.3
Garnet	37.5	0.06	21.6	37.4	0.97	3.20	1.28	0.01	0.01	102.0
Plagioclase	59.8	0.01	25.2	0.36	0.01	0.00	6.47	7.76	0.17	99.8
	cations									
	Si	Ti	Al	Fe	Mn	Mg	Ca	Na	K	
Biotite	2.7	0.24	1.6	1.5	0.0	0.80	0.00	0.01	0.89	
Garnet	3.0	0.00	2.0	2.5	0.07	0.38	0.11	0.0	0.0	
Plagioclase	2.7	0.00	1.3	0.0	0.0	0.0	0.31	0.67	0.01	

4.2.2 Pressure-Temperature Results

I used the garnet-biotite thermometer for 17PGN01, which is based on Fe- Mg exchange between the two minerals. Older calibrations did not correct for other elements in the minerals (e.g., Mn and Ca in garnet, Ti in biotite). I employed the more recent calibrations of Bhattacharya et al. (1992), Holdaway (2000), and Kaneko and Miyano (2004).

I used the GASP geobarometer, which is based on the net-transfer reaction of plagioclase to sillimanite + garnet + quartz. I employed the two different calibrations: Newton and Haselton (1981) and Holdaway (2001). Both require that Ca(Pl) > 0.17 and Ca(Grt) > 0.09; both requirements were satisfied by my analyses (Table 4.1; Appendix A).

The geothermobarometry results, Fig. 4-1, show a tight grouping of line intersections between the thermometers and barometers with an average P-T of 4.7 kb and 690° C. The min and max P-T conditions were 685-695° C and 4.5-4.9 kb, respectively.

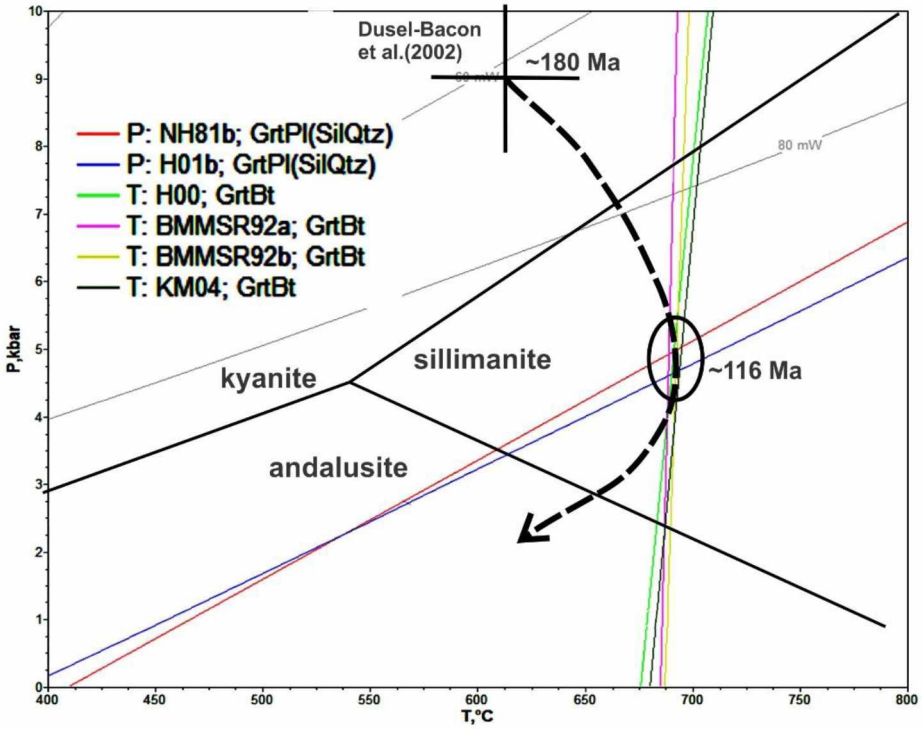

Figure 4-1: Pressure-Temperature diagram showing pathway from 180 Ma metamorphic event to the 116 Ma event with intersecting thermometry and barometry reaction lines defining the latter event. Aluminosilicate phase diagram from Bohlen et al. (1991).

4.3 Intrusive Rocks

4.3.1 Peraluminous Granite

I found andalusite, sillimanite and (rarely) tourmaline, and more common garnet, and magmatic muscovite and biotite in least-altered peraluminous granite samples (e.g., Fig. 4-2). I analyzed large, subhedral muscovite from six peraluminous granite slides to determine its origin. Most of the muscovite contained a minor celadonite component; the relative amounts of Mg, Na, and Ti (Fig. 4-3) suggest that the coarse muscovite is primary (magmatic). This is in agreement with the textural evidence that suggests the coarse muscovite is primary.

Average compositions for minerals employed in the geothermobaric analysis minerals is in Table 4-2 (WDS routine, as above). The garnet is clearly very Mn-rich, the plagioclase is Na-rich, and the muscovite contains significant celadonite (Mg-Fe) and paragonite (Na) components. GASP and GASMB geobarometry yield similar curves, as do garnet-tourmaline and garnet-biotite geothermometry combined with andalusite/sillimanite stability and the Ca-absent granite

solidus (Fig. 4-4). The best estimated conditions from these equilibria are P = 3 ± 0.5 kb and T =660 ± 20°C. The curve for muscovite + albite stability doesn't quite intersect: the presence of substantial solid solution in the muscovite (Table 4.2) increases its stability beyond the reaction curve.

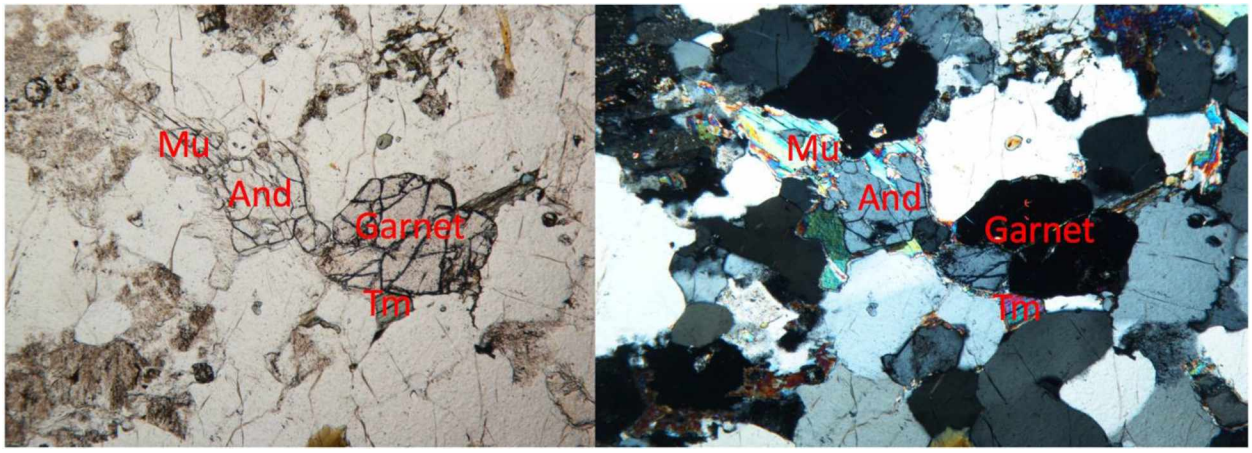

Figure 4-2: Sample 2100-4, plane (left) and polarized (right) transmitted light microphotographs showing muscovite (Mu), andalusite (And), garnet, and tourmaline (Tm). Muscovite locally replaces andalusite.

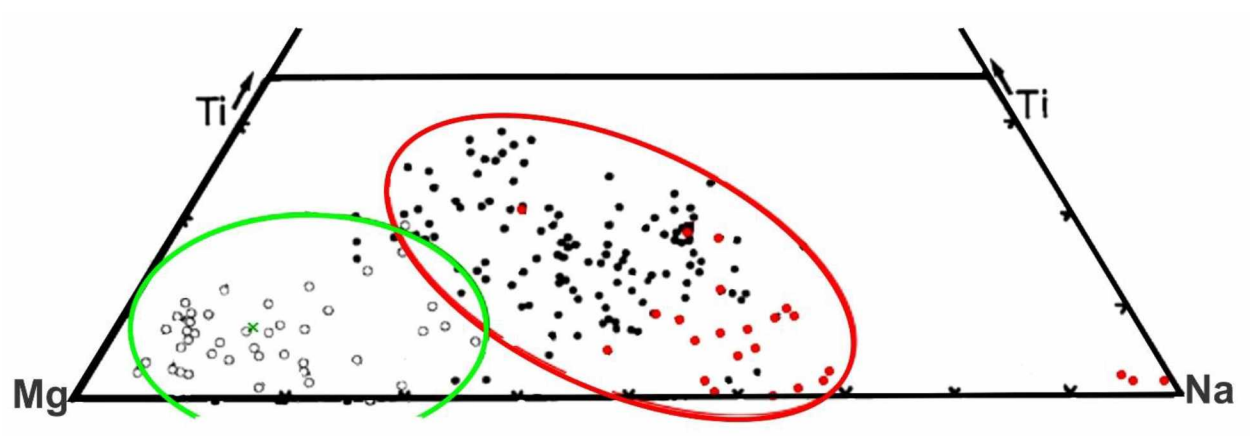

Figure 4-3: Microprobe analyses of primary (red oval) and secondary (green oval) muscovite from peraluminous granites (modified from Miller et al., 1981) with data from coarse muscovite from six different Pogo peraluminous granite slides (red dots).

Table 4-2: Average microprobe compositions for minerals from sample 2100-4.

Mineral	SiO_2	TiO_2	Al_2O_3	FeO	MnO	MgO	CaO	Na_2O	K_2O	B_2O3*	Total
Garnet	36.42		20.6	33.3	8.11	0.81	0.48				99.7
Biotite	37.24	1.94	20.96	25.8	0.56	2.07	0	0.24	8.97		97.8
Muscovite	48.42	0.14	37.32	1.24	0.10	0.22	0	0.58	10.6		98.6
Tourmaline	35.13	0.39	35.5	7.55	0.24	2.43	0.33	2.81		10.1	94.5
Plagioclase	67.23		20.99				1.63	10.96			100.8

Notes: B2O3* = B calculated from stoichiometry; each analysis is the average of > 3 points

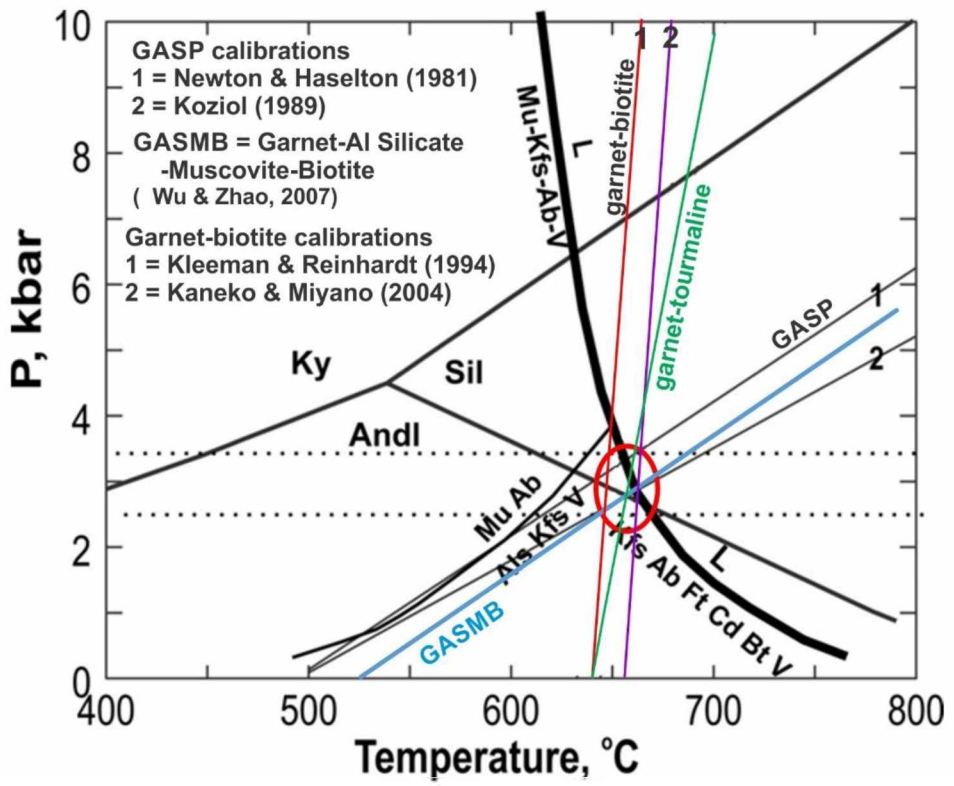

Figure 4-4: Geothermobarometry for peraluminous,granite, sample 2100-4. Numbered lines are GASP geobarometer solutions for plagioclase and garnet compositions; blue line is the GASMB barometer solution. Near-vertical lines are defined by garnet-tourmaline (Colopietro and Friberg, 1987) and garnet-biotite equilibria. Water saturated granite solidus (dark line) and muscovite vs. Al-silicate stability from Murphy (2006). Dashed lines show most likely pressure range satisfying the various equilibria and red oval shows the best overlap P-T conditions. Aluminosilicate phase diagram from Bohlen et al. (1991).

4.3.2 Football and Liese Plutons

For plagioclase-hornblende thermobarometry I used the thermometer by Blundy and Holland (1990) and the Al-in-hornblende barometer by Anderson and Smith (1995). Samples were selected from thin sections made of field surface samples which have the requisite hornblende and plagioclase minerals (e.g., Fig. 4-5). A total of 11 samples of intrusive rocks were analyzed at UAF-AIL using wavelength-dispersive techniques on the JEOL JXA-8530F electron microprobe. I analyzed as many viable plagioclase-hornblende pairs per sample as possible, 2-6 pairs per slide. The WDS routine analyzed for Si, Ti, Al, Fe, Mn, Mg, Ca, Na, K, and Cl to cover the suite of elements contained in both hornblende and plagioclase. The complete analyses are given in Appendix A. The hornblende points all plot in the compositional field for 'hornblende' (Fig. 4-6); Liese pluton points contain slightly higher Mg.

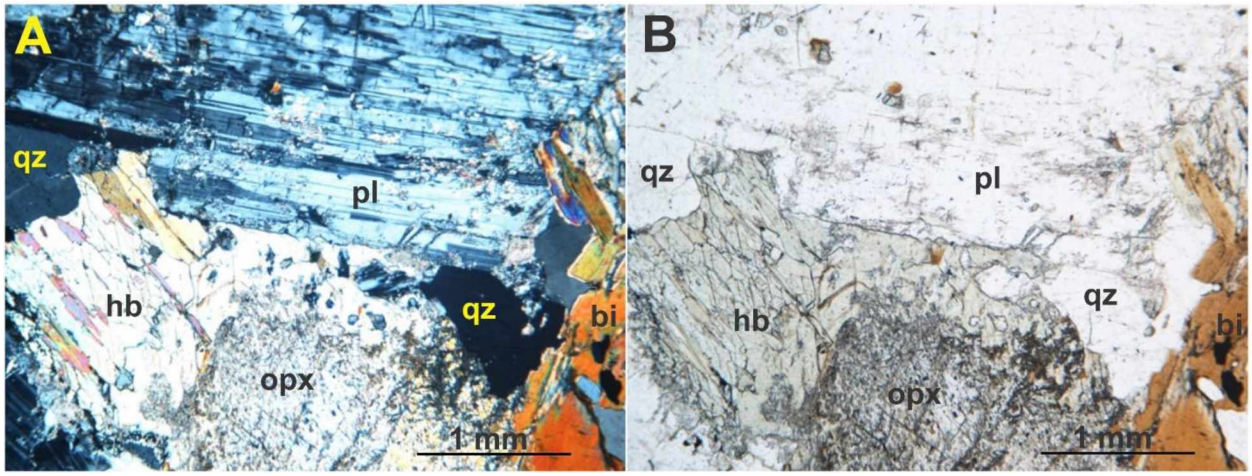

Figure 4-5: Microphotographs of sample 14PWT768, a Liese tonalite, in polarized (A) and plane (B) light. Analysis points were along the touching rims of large hornblende (hb) and plagioclase (pl) grains. Other ubiquitous minerals in Liese pluton rocks include quartz (qz), biotite (bi) and orthopyroxene (opx).

I employed a spreadsheet (J.L. Anderson, writ. Comm., 2017) that utilized thermometry calculations from Blundy and Holland (1990) and Holland and Blundy (1994) and barometry from Schmidt (1992) and Anderson and Smith (1995). Final P-T solution results were based on iteration using Anderson and Smith (1995) with various thermometers. I used the Blundy and Holland (1990) thermometry calibration as it yielded the most consistent results across a given pluton (Table 4.3). Spatial distribution of the barometry results shows no obvious patterns (Fig.

4-7) The average crystallization pressures for the Liese and Football plutons are 1.1 ± 0.3 kb and 2.0 ± 0.5 kb respectively.

Table 4-3: Calculated temperatures and pressures for Liese and Football pluton rocks using Blundy and Holland, 1990 thermometry and Anderson and Smith, 1995 barometry.

Sample	Rock Type	Average T (°C)	Average P (kb)
15PWT87	Football Tonalite	781	2.6
15PWT761	Football Tonalite	794	1.9
56	Football Granodiorite	696	1.6
15PWT771	Liese Tonalite	695	1.4
15PWT07	Liese Tonalite	746	0.8
15PUC13	Liese Tonalite	735	1.0
14PWT768	Liese Tonalite	727	1.0
15PWT14	Liese Tonalite	823	1.0
759	Liese Quartz Diorite	819	1.4
745	Liese Quartz Diorite	781	1.4

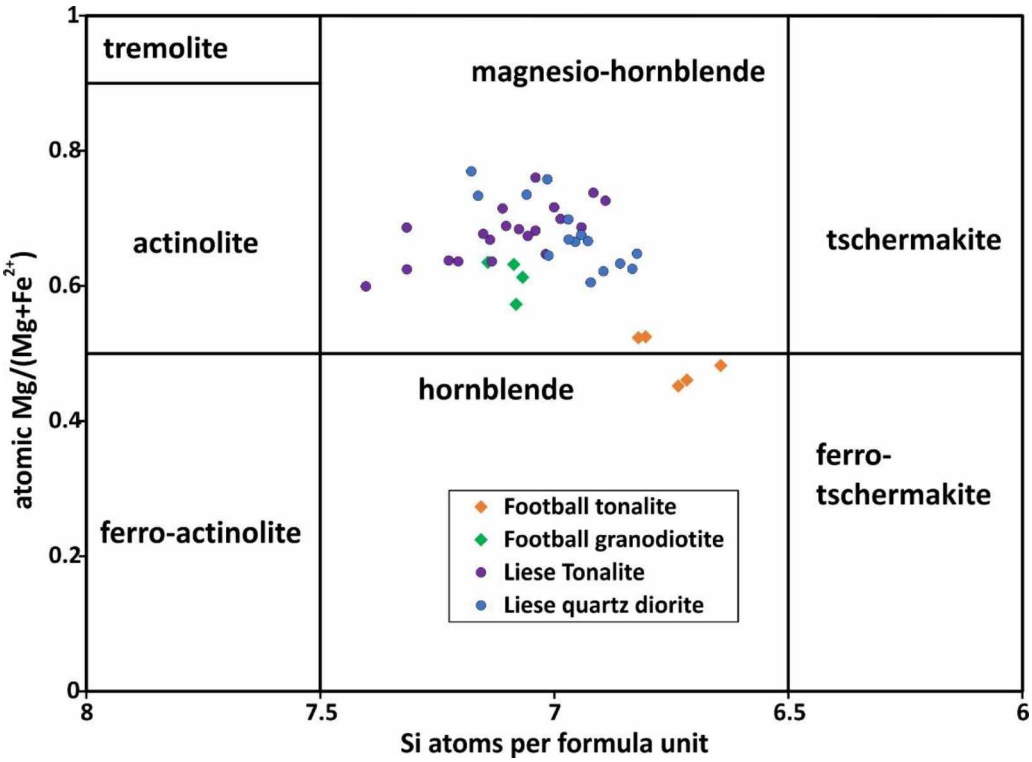

Figure 4-6: Compositional classification of the amphiboles from the Liese and Football plutons for amphiboles with Ca>1.5 and Na+K in the A site <0.5 (per formula unit), using Leake (1978).

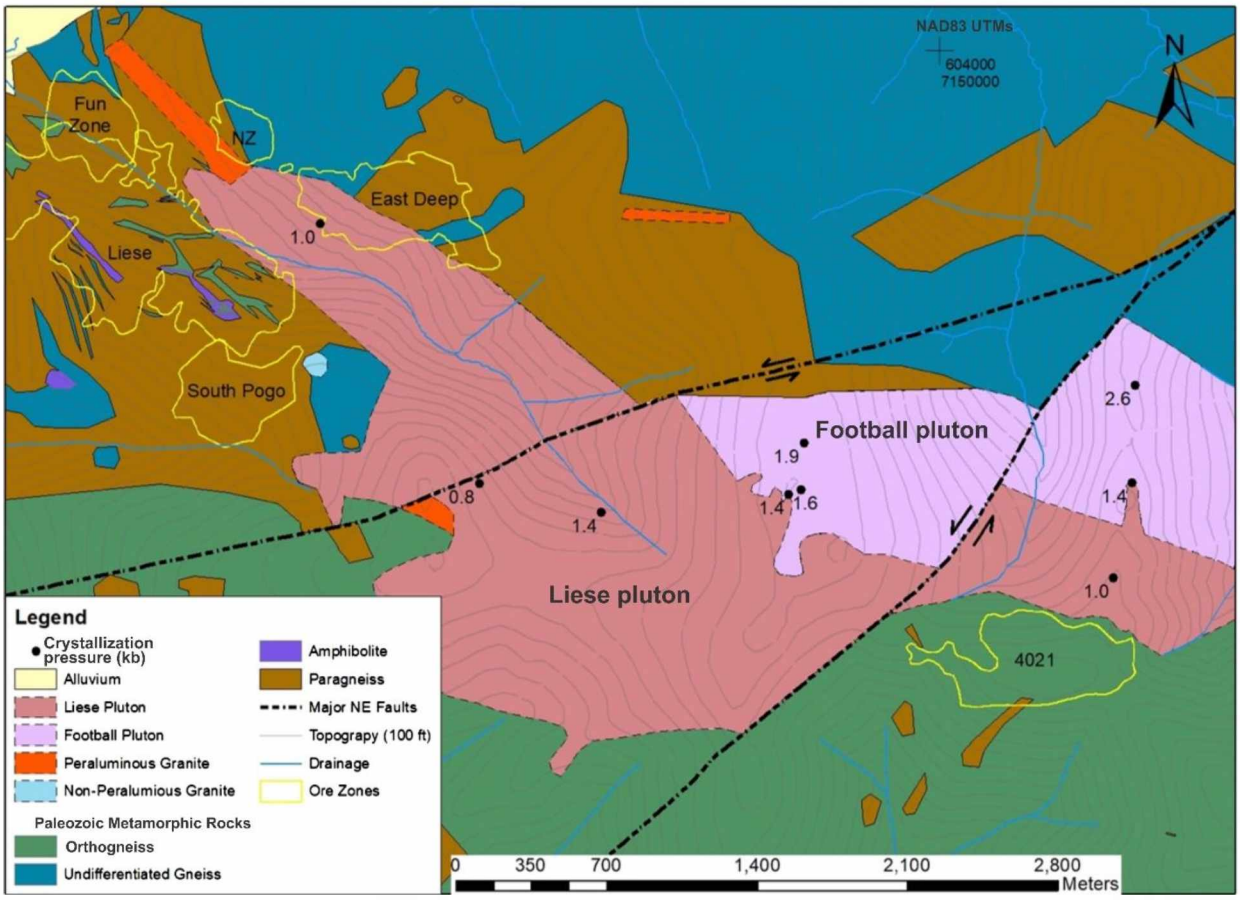

Figure 4-7: Geological map of the Pogo area with calculated crystallization pressures (kb) for Liese and Football pluton samples.

4.3.3 Paleogene felsic dike

A final geobarometer involves the pressure-dependent composition of water-saturated granite melt in the system quartz-albite-orthoclase (Tuttle and Bowen, 1958; Winkler et al., 1975). For this to be employed, the granitic rock must contain little more than quartz, albite, and orthoclase. The peraluminous and non-peraluminous granites at Pogo contain too much normative corundum and (or) too much CaO to be employed, but a Paleogene (Dilworth, 2003) felsic dike just east of my map area has an appropriate composition (Werdon et al., 2001; Table 4.4). Plotting this normative composition on the quartz-albite-orthoclase granite ternary (Fig. 4-8) falls near the 0.5 kb point. Other Interior Alaskan granites with ages similar to the Liese pluton plot at just over 1 kb, similar to the calculated pressure for the Liese pluton.

Table 4-4: Composition of Felsic dike sample 00RN830 (Werdon et al., 2001).

major oxide composition									
SiO2	Al2O3	Na2O	CaO	K2O	FeO	MgO	MnO	TiO2	P2O5
75.9	13.1	3.47	0.1	4.32	2.12	0.16	0.03	0.32	0.07
CIPW Mineral Norm									
Quartz	Albite	Orthoclase	Corundum	Hypersthene	Ilmenite	Magnetite	Apatite		
38.3	30.1	28.8	0.43	1.7	0.34	0.18	0.14		

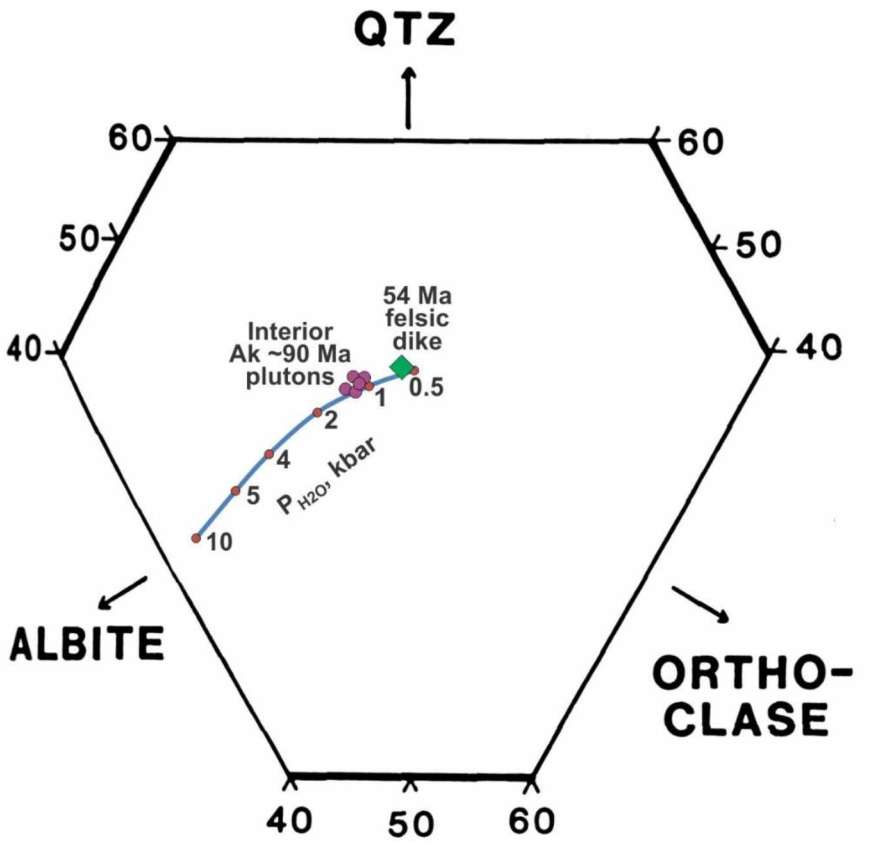

Figure 4-8: Normative composition of a Paleogene felsic dike plotted on the ternary granite diagram of Winkler et al. (1975) with data from selected Interior Alaska mid-Cretaceous granite dikes, from Newberry et al. (1990).

4.4 Discussion and Conclusions

The P-T-time path between 180 and 107 Ma (Fig. 4-9) can be followed on a single P-T diagram by combining Fig. 4-1 and 4-4. This produces the familiar 'clockwise rotation' P-T path, common to many metamorphic terranes (e.g., Philpotts, 1990). Such occurs if burial is rapid (e.g., by overthrusting): pressure increases as rock is emplaced from above, but the rocks heat up slowly by conduction. It takes significant time for the earth's heat to 'catch up' to the burial depth, and meanwhile the overthrust rocks are eroding away, causing the pressure to fall. Thus, the temperature maximum is at a significantly lower pressure than the pressure maximum.

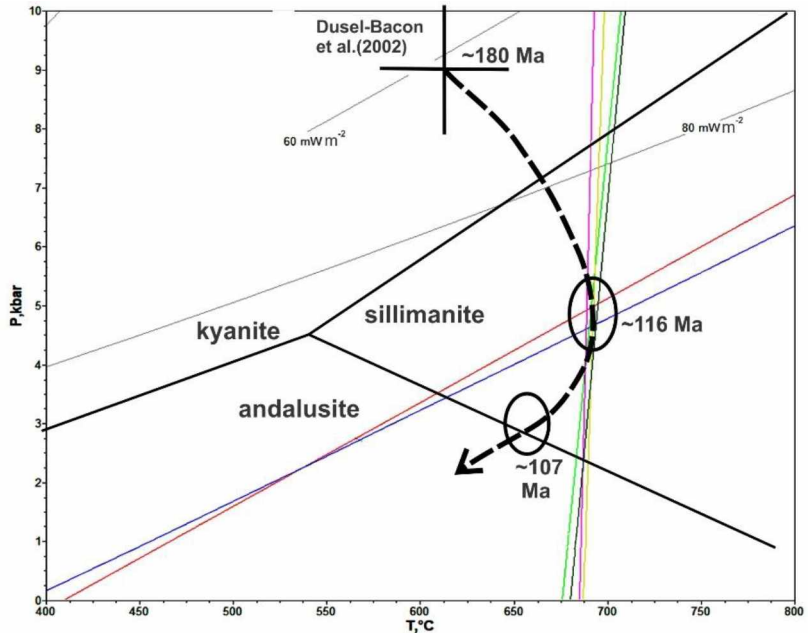

Figure 4-9: Pressure-temperature-time pathway of metamorphic events leading to peraluminous granite crystallization at 107 Ma, made from combining salient features of Figs. 4.1 and 4.4. Two typical geothermal gradients are also shown. Aluminosilicate phase diagram from Bohlen et al. (1991).

Importantly, the high-P metamorphic conditions were within kyanite stability, and Dusel-Bacon et al. (2002) record kyanite as locally present in the Pogo region. The major recrystallization event at about 116 Ma (recorded in metamorphic zircon replacements of igneous zircon in the orthogneiss samples, Chapter 3) resulted in sillimanite growth and apparently kyanite destruction. It is unclear how much (if any?) of the orthogneiss fabric developed during

the mid-Cretaceous extensional event that was recorded in the zircons, but clearly significant fluid flow occurred—both required for sillimanite formation and zircon recrystallization. Dusel-Bacon et al. (2002) envision pressure dropping during this extensional event as former thrust faults were re-activated as low-angle normal faults. Conceivably, the faults that became the Liese veins are of such origins.

Some of the quartz in the Liese veins might have been precipitated during the fluid flux event at 116 Ma, but Re-Os dating of (rare) molybdenite in the Liese veins indicates mineralization occurred at 104 ± 1 Ma (Selby et al., 2002); Dilworth (2003) indicates the pressure during mineralization (from fluid inclusion studies) was 1.9 ± 0.5 kb. The mineralization age and pressure are indistinguishable (within errors) from the 103 ± 2 Ma Football pluton (Dilworth, 2003), emplaced at a pressure of 2.0 ± 0.5 kb (Table 4.3).

Past 107 Ma, only local pressures are relevant, as the tonalitic magmas were at temperatures far hotter than the surrounding metamorphic rocks. I have converted lithostatic pressure to crustal depth, using 3.7 km/kb, to create a calculated pressure-time path for rocks of the Pogo region (Fig. 4-10). It shows a nearly linear change in depth with time for 116-94 Ma, with slope of 0.5 km/Ma or 0.5 mm/yr. Such an uplift rate is not unreasonable; for example, rocks along the San Andreas fault north of San Francisco have experienced uplift of 0.2-1.1 mm/yr (average 0.4 ± 0.2 mm/yr) for the last 0.5 million years (Grove et al., 2010).

However, extrapolation of the mid-Cretaceous rate in both directions yields zero depth at 86 Ma and the 180 Ma depth at 152 Ma instead (Fig. 4-10). Both are unreasonable and indicate that the 0.5 mm/yr uplift rates could not be true much beyond 116-94 Ma. Consequently, I propose a smaller uplift rate for 180 to about 130 Ma, and after about 90 Ma (Fig. 4-9). That is, I propose that change in depth, due to simple isostatic rebound and weathering, from 180 to about 130 Ma was relatively slow, and increased dramatically at about 130 Ma. This increase was due to the onset of extensional tectonics, causing decrease in depth from removal of overlying crust through low-angle normal faulting. Slow uplift after about 90 Ma could be due to the ending of subduction-related magmatism in Interior Alaska.

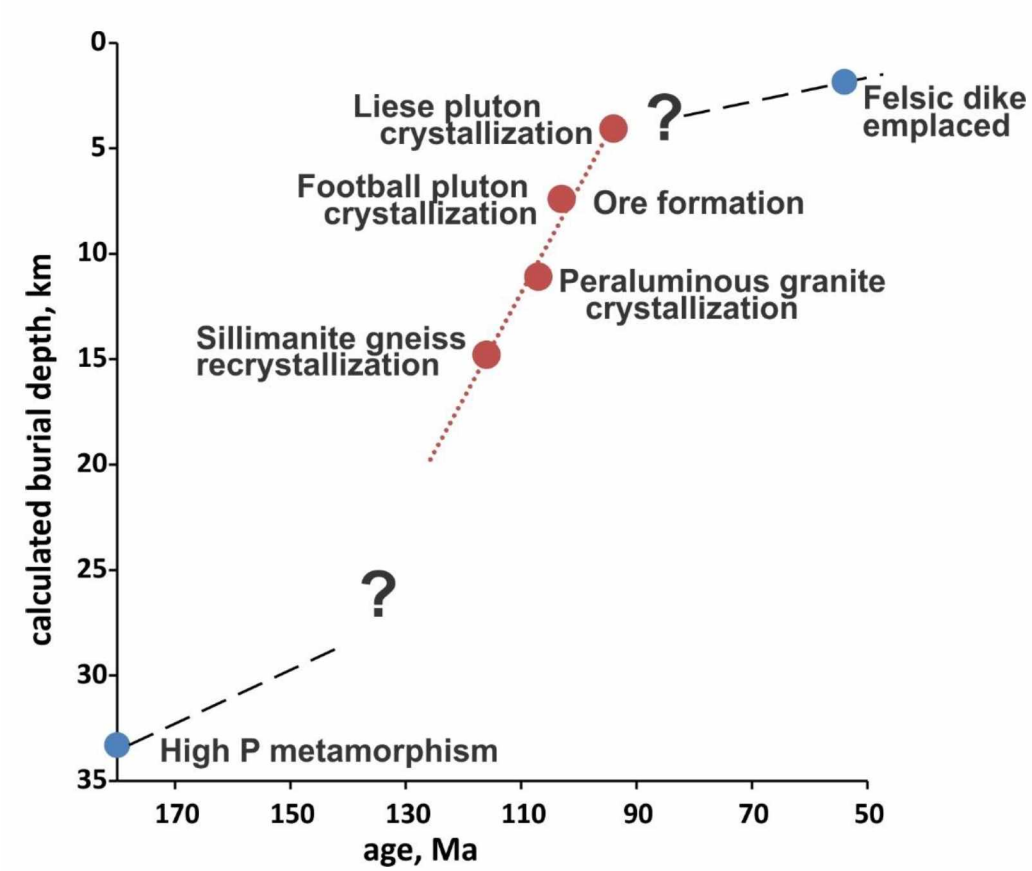

Figure 4-10: Calculated depth vs. time plot for Pogo area rocks, based on data presented in this chapter.

In any event, although the Pogo area was apparently undergoing near-constant uplift at 116 – 94 Ma, it is unclear what relevance that had to the formation of the Pogo deposit. One possibility is that the near-linear rate indicates that extension was taking place during mineralization, and extension would be vital to continued hydrothermal fluid movement along faults (e.g., the Liese zones). Normal faulting that accompanied major quartz deposition would allow the fault zones to re-open, which would allow continued fluid movement and quartz deposition. Through such means shallowly dipping quartz veins several meters thick could form.

5 Chapter 5: Summary & Conclusions

5.1 Discussion

I believe that my studies have reconciled previous disagreements over several facets of the Pogo deposit and allowed for a clearer view of its petrological framework and timeline for the genesis of the deposit. The compositional distinctions among the intrusive and meta-intrusive rocks allow for a reliable classification for most of the Pogo units using a combination of geochemical analysis and hand sample features such as schistosity. Dating of these rocks, both from my study and previous studies, allow me to put together a timeline for the deposit (Fig. 5-1). Furthermore, with the geothermobarometry results, I have put together a pressure-temperature-time pathway for the deposit.

One of the goals for this study was to determine whether the orthogneiss in the immediate Pogo area was of Cretaceous protolith age. The results from Chapter 3 show that they are decisively of Devono-Mississippan age. Analyses of the zircons also allowed for a time constraint on the last major metamorphic event, at approximately 116 Ma. Coupled with the geothermobarometry, the dating yields the rate of exhumation during 116-95 Ma (Figure 4-9). The peraluminous granites likely represent crustal melts caused by pressure decrease in the presence of water, as extension thinned the crust in the early mid-Cretaceous. The orientations of these granites and the other dikes indicate changes in the directions of extension during this prolonged event, ~107 Ma to ~55 Ma (Fig. 5-2). Thermobarometry and radiometric dating indicate a consistent uplift rate of about 0.5 mm/year during the mid-Cretaceous. Initially an extensional event, subduction-related magmatism began at about 105 Ma. Even though subduction is a fundamentally compressional event, there is always a direction of extension, leading to cracks filled by dikes. At the same time, the Liese zones (originally thrust faults, section 1.3.2) were re-activated as low angle normal faults that apparently acted as pathways for mineralization.

The question of how the mineralization at Pogo formed has long been hotly debated. Based on the results shown in my studies, the Football pluton is the most likely candidate for mineralization of the Liese zones due to timing, emplacement depth, and spatial proximity to the mineralization. It is analogous to the Tombstone suite and mineralization in the Yukon. The Liese pluton and dikes post-date mineralization and contain pyroxene, indicating a lack of water in melt which would make it hard to justify that intrusion as causative. The granites pre-date

mineralization and are cut by mineralization. Locally the peraluminous granite can be found on the footwall and hanging wall of veins but this is likely due to the low viscosity nature of peraluminous melts allowing it to exploit the same structures that the quartz veins followed. Instead the granites may have been helpful in holding the low angle structures open for mineral fluids to use. The differences between Pogo and the other IRG deposits mentioned in section 1.1 are likely due to the deeper formation of the quartz veins as well as possible addition of quartz from the 116 Ma metamorphic event.

While the Football pluton is the mostly likely candidate for mineralization of the Liese zone it does not account for other mineralization in the area such as the 4021 deposit. Although spatially proximal to Football pluton rocks, 4021 mineralization has an age contemporaneous with the Liese pluton instead (Fig. 5-1). The Liese pluton is also unlikely however, due to the anhydrous nature of the melt as mentioned above. This indicates that there must be another ~94 Ma pluton or dike at depth in that area. A similar situation is present for the Shawnee peak mineralization and other areas around Pogo that cannot currently be explained by the Football dike.

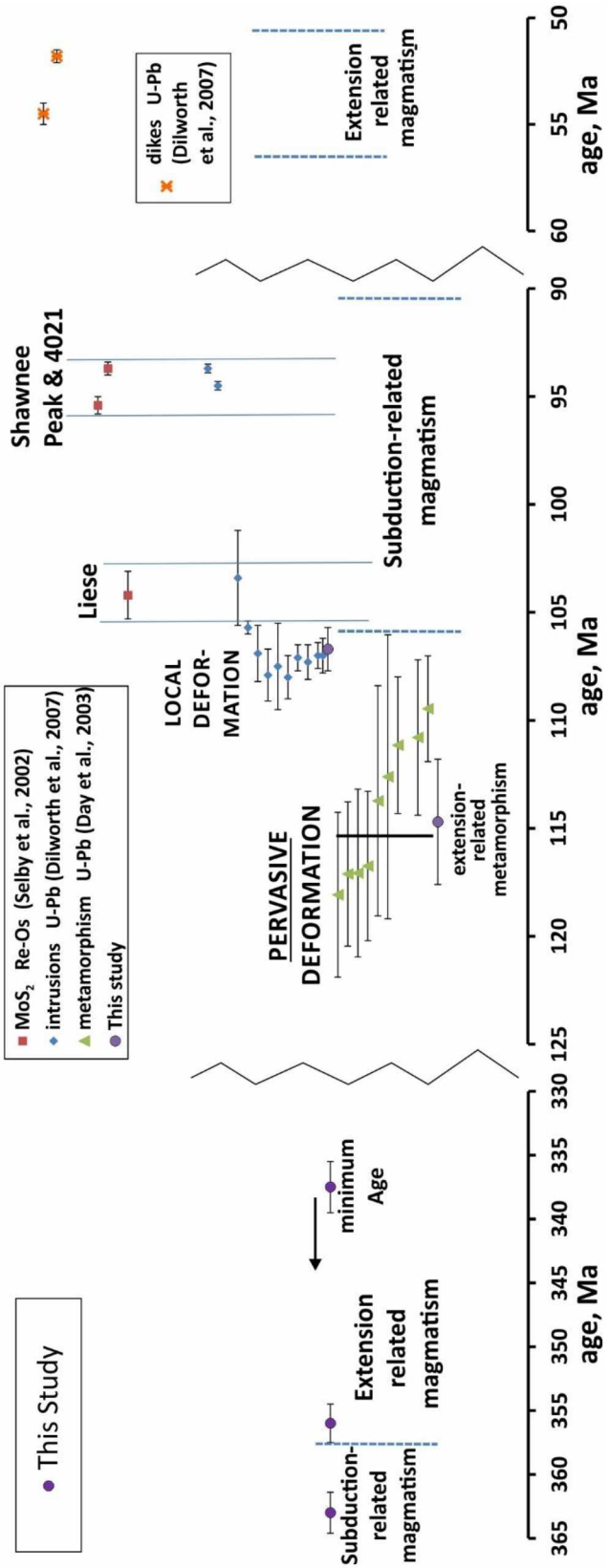

Figure 5-1: Geologic history of the Pogo area during the Devono-Mississippian, mid-Cretaceous, and Paleogene.

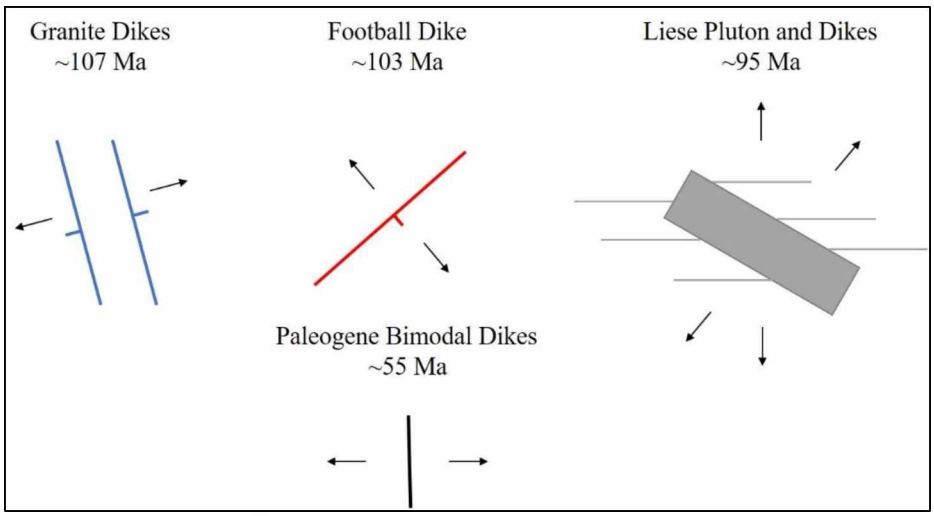

Figure 5-2: Simplified image of intrusive orientations and possible extension directions (arrows) during the emplacements of the intrusives.

5.2 Recommendations for future work

Based on the results of my findings, the following recommendations should be considered for work which could be prove useful to further understand the framework of the Pogo deposit:

- Diamond core drilling has not defined the depth of the Football pluton as seen in Fig. 2-17. Further drilling could expand the size and distribution of the pluton.
- Age dating of the Football Pluton dike to confirm age of crystallization.
- Additional dating of vein material to confirm mineralization age. Problematic due to scarcity of molybdenite in quartz veins.
- Systematic examination of core photos for evidence of more Football pluton offshoots.

5.3 Conclusions

The Pogo deposit is a mid-Cretaceous gold deposit hosted in largely amphibolite facies paragneiss with typically discrete packages of orthogneiss containing Devono-Mississipian aged protoliths. There are generally 3 different suites of Cretaceous-aged intrusive rocks in the area. The first contains peraluminous and non-peraluminous granites that intruded pre-mineralization at 107 Ma. The second, the Football suite, ranges from granodiorite to tonalite in composition, was emplaced at 103 ± 2 Ma at a pressure of 2.0 ± 0.5 kb and is present locally downdip of the Liese quartz zone. This is indistinguishable from the timing and depth of mineralization formation, indicating that the Football suite is responsible for ore formation. The last suite is

composed of rocks ranging from tonalite to quartz diorite. These post-date (95.4 ± 0.2 Ma) and cut through mineralization. This unit is multi-phasic, including a large pluton cutting through the Liese valley as well as multiple fine-grained dikes trending ~E-W.

Following the metamorphic event dated to 116 Ma that recrystallized kyanite to sillimanite and produced a large amount of fluid flux, the Pogo area experienced a consistent uplift rate of approximately 0.5 km/Ma until at least 94 Ma. This would be consistent with an extensional setting where former thrust faults could be re-activated as low-angle normal faults, becoming conduits for the thick, low angle Liese veins. During this time period intrusions were produced by subduction-related magmatism which ended about 90 Ma and was followed by slower uplift rates.

References

Anderson, J.L., and Smith, D.R., 1995, The effects of temperature and $fO2$ on the Al-in-hornblende barometer: American Mineralogist, vol. 80, p. 549-559.

Bhattacharya, A., Mohantf, L., Maji, A., Sen, S.K., and Raith, M., 1992, Non-ideal mixing in the phlogopite-annite binary: constraints from experimental data on Mg-Fe partitioning and a reformulation of the biotite-garnet geothermometer: Contrib. Mineral. Petrol., vol. 111, pp. 87-93.

Blundy, J. D. and Holland, T. J., 1990, Calcic amphibole equilibria and a new amphibole-plagioclase geothermometer: Contrib. Mineral. Petrol., vol. 104, pp. 208-24.

Bohlen, S.R., Montana, A., and Kerrick, D.M., 1991, Precise determinations of the equilibria kyanite = sillimanite and kyanite = andalusite and a revised triple point for Al2SiO5 polymorphs: American Mineralogist, vol. 76, pp. 677-680.

Cherniak, D.J. & Watson, E.B., 2001, Pb diffusion in zircon: Chemical Geology, vol. 172, pp. 5-24.

Clarke, D.B., 1981, The mineralogy of peraluminous granites; a review: Canadian Mineralogist, vol. 19, pp. 3-17.

Clarke, D.B., 2019, The Origins of Strongly Peraluminous Granitoid Rocks: Canadian Mineralogist, vol. 57, pp. 529-550.

Colopietro, M. R. and Friberg, L. M., 1987, Tourmaline-biotite as a potential geothermometer for metapelites, Black Hills, South Dakota. Geological Society of America Abstracts with Programs, vol. 19, p. 624.

Day, W.C., Aleinikoff, J.N., Roberts, P., Smith, M., Gamble, B.M., Henning, M.W., Gough, L.P., and Morath, L.C., 2003, Geologic map of the Big Delta B–2 quadrangle, east-central Alaska: U.S. Geological Survey Geologic Investigations Series I–2788.

Day, W.C., O'Neill, J.M., Aleinikoff, J.N., Green, G.N., Saltus, R.W., and Gough, L.P., 2007, Geologic map of the Big Delta B-1 quadrangle, east-central Alaska: U.S. Geological Survey Scientific Investigations Map 2975, 23 p.

Dilworth, K.M., Mortensen, J.K., Ebert, S., Tosdal, R.M., Smith, M.T., and Roberts, P., 2007, Cretaceous reduced granitoids in the Goodpaster mining district, east central Alaska: Canadian Journal of Earth Sciences, vol. 44, p. 1347–1373.

Dilworth, K. M., 2003, Geological setting, nature, and evolution of reduced intrusions and gold bearing quartz veins of the 4021 prospect, Goodpaster District, East-Central Alaska: University of British Columbia, unpublished MS thesis, 192 p.

Dusel-Bacon, C., Lanphere, M.A., Sharp, W.D., Layer, P.W., and Hansen, V.L., 2002, Mesozoic thermal history and timing of structural events for the Yukon-Tanana Upland, east-central Alaska: $^{40}Ar/^{39}Ar$ data from metamorphic and plutonic rocks: Can. J. Earth Sci., vol. 39, pp. 1013-1051.

Dusel-Bacon, C., Day, W.C., and Aleinikoff, J.N., 2013, Geochemistry, petrography, and zircon U–Pb geochronology of Paleozoic metaigneous rocks in the Mount Veta area of east-central Alaska: implications for the evolution of the westernmost part of the Yukon–Tanana terrane: Canadian Journal of Earth Sciences, vol. 50, pp. 826-846

Dusel-Bacon, C., Aleinikoff, J.N., Day, W.C., and Mortensen, J.K., 2015, Mesozoic magmatism and timing of epigenetic Pb-Zn-Ag mineralization in the western Fortymile mining district, east-central Alaska: Zircon U-Pb geochronology, whole-rock geochemistry, and Pb isotopes: Geosphere, vol. 11, no. 3, doi:10.11GES01092.1.

Flanigan, B., Freeman, C., Newberry, R., McCoy, D. and Hart, C., 2000, Exploration models for mid and late Cretaceous intrusion-related gold deposits in Alaska and the Yukon Territory, Canada, in Geology and Ore Deposits 2000: The Great Basin and Beyond, Geological Society of Nevada, pp. 138-157.

Gough, L.P., and Day, D.C., eds., 2007, Recent U.S. Geological Survey studies in the Tintina Gold Province, Alaska, United States, and Yukon, Canada: U.S. Geological Survey Scientific Investigations Report 2007-5289-F.

Grove, K., Sklar, L.S., Scherer, A.M., Lee, G., and Davis, J., 2010, Accelerating and spatially-varying crustal uplift and its geomorphic expression, San Andreas Fault zone north of San Francisco, California: Tectonophysics, vol. 495, p. 256-268.

Hansen, V.L. and Dusel-Bacon-C., 1998, Structural and kinematic evolution of the Yukon-Tanana upland tectonites, east-central Alaska: A record of late Paleozoic to Mesozoic crustal assembly: GSA Bulletin, vol. 110, pp. 211–230.

Holdaway, M.J., 2000, Application of new experimental and garnet Margules data to the garnet-biotite geothermometer: American Mineralogist, vol. 85, pp. 881-892.

Holdaway, M.J., 2001, Recalibration of the GASP geobarometer in light of recent garnet and plagioclase activity models and versions of the garnet-biotite geothermometer: American Mineralogist, vol. 86, pp. 1117–1129.

Holland, T. J. and Blundy, J.D., 1994, Non-ideal interactions in calcic amphiboles and their bearing on amphibole-plagioclase thermometry: Contrib. Mineral. Petrol., vol. 116, pp. 433-47.

Hoskin, P.W.O. and Black, L.P., 2000, Metamorphic zircon formation by solid-state recrystallization of protolith igneous zircon, J. Metamorphic Geology, vol. 18, p. 423-439.

Hults, C.P., Wilson, F.W., Donelick, R.A., and O'Sullivan, P.B., 2013, Two flysch belts having distinctly different provenance suggest no stratigraphic link between the Wrangellia composite terrane and the paleo-Alaskan margin: Lithosphere, vol. 73, pp. 255-269

Hoskin, P.W.O. and Schaltegger, U.l., 2003, The Composition of Zircon and Igneous and Metamorphic Petrogenesis, Reviews in Mineralogy and Geochemistry vol. 53, p. 27-62.

Kaneko,Y., and Miyano, T., 2004, Recalibration of mutually consistent garnet–biotite and garnet–cordierite geothermometers: Lithos, vol. 73, pp. 255-269.

Kleeman, U., and Reinhardt, J., 1994, Garnet-biotite thermometry revisited: The effect of Al^{VI} and Ti in biotite. European Journal of Mineralogy, vol. 6, 925-941.

Koziol, A. M., 1989, Recalibration of the garnet - plagioclase - Al2SiO5 - quartz (GASP) geobarometer and applications to natural parageneses: EOS, vol. 70, p. 493.

Leake, B.E., 1978, Nomenclature of Amphiboles: American Mineralogist, vol. 63, pp. 1023-52.

Mair, J.L., Hart, C.J.R., and Stephens, J.R., 2006, Deformation history of the northwestern Selwyn Basin, Yukon, Canada: Implications for orogen evolution and mid-Cretaceous magmatism: GSA Bulletin, vol. 118, p. 304–323.

Miller, C.F., Stoddard E.,F., Bradfish, L.J., Dollase, W.A., 1981, Composition of plutonic muscovite: genetic implications: Canadian Mineralogist, vol. 19, pp. 25–34.

Murphy, J., 2006, Igneous Rock Associations 7. Arc Magmatism I: Relationship Between Subduction and Magma Genesis: Geoscience Canada, vol. 33 no. 4.

Naney, M.T., 1983, Phase equilibria of rock-forming ferromagnesian silicates in granitic systems: American Journal of Science, vol. 283, pp. 993-1033.

Newberry, R.J., Burns, L.E., Swanson, S.E., and Smith, T.E., 1990, Comparative petrologic evolution of the Sn and W granites of the Fairbanks-Circle area, Interior Alaska, in Geol. Soc. Amer. Spec. Paper 246, pp. 121-142.

Newberry, R.J., Larimer, D.G., and Porritt, K., 2012, Amphibolite "stratigraphy" as key to structural reconstruction of the Liese zone, Pogo Gold Deposit, 2012 Arctic International Mining Symposium, Fairbanks Ak, abstr w/ progr. pp. 7-9.

Newton, R. C. and Haselton, H. T., 1981, Thermodynamics of the garnet- plagioclase-Al_2SiO_5-quartz geobarometer: *In* R. C. Newton, et al. Eds., Thermodynamics of Minerals and Melts, pp. 131-147, Springer-Verlag, New York.

Pearce, J.A., Harris, N.B.W., and Tincle, A.G., 1984, Trace Element Discrimination Diagrams for the Tectonic Interpretation of Granitic Rocks: J. Petrology, vol. 25, pp. 956-983.

Philpotts, A.R., 1990, Principles of Igneous and Metamorphic Petrology: Prentice-Hall, New York, 498 p.

Rhys, D., DiMarchi J., Smith, M., Friesen, R., and Rombach, C., 2003, Structural setting, style and timing of vein-hosted gold mineralization at the Pogo deposit, east-central Alaska: Mineralium Deposita, vol. 38, p. 863–875.

Schmidt, M. W., 1992, Amphibole composition in tonalite as a function of pressure: an experimental calibration of the Al-in-hornblende barometer: Contrib. Mineral. Petrol., vol. 110, pp. 304-10.

Selby, David, Creaser R.A., Hart, C.J.R., Rombach, C.S., Thompson, J.F.H., Smith, M.T., Bakke, A.A., and Goldfarb, R.J., 2002, Absolute timing of sulfide and gold mineralization; A comparison of Re-Os molybdenite and Ar-Ar mica methods from the Tintina gold belt, Alaska: Geology, vol. 30, p. 791–794.

Smith, M., Thompson, J.F.H., Bressler, J., Layer, P., Mortensen J.K., Abe, I., and Takaoka, H., 1999, Geology of the Liese zone, Pogo property, east-central Alaska: Society of Economic Geologists Newsletter, vol. 38, p. 12–21.

Streckeisen, A.L., and LeMaitre, R.W., 1979, Chemical approximation to modal QAPF classification of the igneous rocks: Neus Jahrbuch fur Mineralogie, v. 136, p. 169-206.

Tuttle, O.F., and Bowen, N.L., 1958, Origin of Granite in the Light of Experimental Studies in the System $NaAlSi_3O_8$–$KAlSi_3O_8$–SiO_2–H_2O: Geological Society of America Memoir, vol. 74, 153 p.

Werdon, M.B., Athey, J.E., Szumigala, D.J., Newberry, R.J., Grady, J.C., and Munly, W.C., 2001, Major-oxide, minor-oxide, trace-element, and geochemical data from rocks collected in the Salcha River-Pogo area in 2000, Big Delta and northwestern Eagle quadrangles, Alaska: ADGGS RDF 2001-1, 19 p., 1 sheet, scale 1:250,000.

Werdon, Melanie, Newberry, R.J., Athey, J.E., and Szumigala, D.J., 2004, Bedrock geologic map of the Salcha River-Pogo area, Big Delta quadrangle, Alaska: Alaska Division of Geological and Geophysical Surveys Report of Investigations 2004–1b.

Winkler, H.G.F., Boese, M., and Marcopoulos, T., 1975, Low temperature granitic melts: Neues Jahrbuch fur Mineralogie Monatshefte, vol. 6, pp. 245-268.

Wu, C.M., and Zhao, G., 2007, The garnet-biotite-muscovite-aluminosilicate-quartz (GBMAQ) geobarometer: Lithos, vol. 97, pp. 365-372.

Zen, E., 1988, Phase Relations of Peraluminous Granitic Rocks and Their Petrogenetic Implications: Annual Review of Earth and Planetary Sciences, vol. 16, pp. 21-51.

Appendix A: Microprobe analyses

I developed quantitative routines for the analysis of hornblende, plagioclase, garnet, biotite, muscovite, tourmaline, and zircon using wavelength-dispersive spectrometers on a JEOL JXA-8530F electron microprobe in the Advanced Instruments Laboratory at the University of Alaska Fairbanks. For these routines I used a 15kv and 10 nA beam, usually with the beam size < 1 micron. Counting times were 20 seconds on peak and 10 seconds each on the high and low backgrounds. I used well-characterized natural mineral standards, with some variations depending on the mineral analyzed. I assigned spectrometers as follows: Mg, Na = spectrometer 5, TAP; Al, Si = spectrometer 4, TAP; Cl, K = spectrometer 3, PET; Ca, Ti = spectrometer 2, PET; and Mn, Fe = spectrometer 1, LiF. I employed the standards as listed in Table A-1.

Table A-1 standards employed in most microprobe routines

element	standard(s) employed
Na	Tiberon Albite
Mg	Garnet, USNM 87375 or Hypersthene, USMN 746
Al	Orthoclase OR10 or Plagioclase, USNM 115900
Si	Scapolite , USNM R6600-1 or Tiberon Albite or Plagioclase, USNM 115900
K	Orthoclase OR10 or Biotite1
Ti	Ilmenite, USNM 96189 or Hornblende, USNM 143965 or Biotite1
Ca	Scapolite , USNM R6600-1
Cl	Scapolite , USNM R6600-1
Mn	Willimite or Spessartine
Fe	Ilmenite, USNM 96189 or Biotite1

On the following pages I list microprobe analyses by 'project', with 5 projects identified: (1) sample 17PGN01 (sillimimanite gneiss for P-T), (2) sample 2100-4 (peraluminous granite for P-T), (3) muscovite in peraluminous granite (multiple samples), (4) Liese and Football plutons P-T (multiple samples), and (5) zircon (sample FZ and 4021A). Sample locations are given in Appendix B. I use the following mineral abbreviations in these tables: Bio = biotite, Gar = garnet, Pl = plagioclase, Mu = muscovite, Tou = tourmaline, Opx = orthopyroxene, and Hbl = hornblende. All analyses are given as weight percent oxides except Cl, as weight percent element.

Table A-2: Microprobe analyses (wt% oxides) of minerals in sample 17PGN01

area	min	Na2O	MgO	Al2O3	SiO2	K2O	CaO	TiO2	MnO	FeO	sum
2	Bio	0.08	6.84	17.84	32.55	8.2	0.01	4.84	0.092	25.13	95.6
2	Bio	0.12	6.59	17.8	32.68	8.43	0.02	4.75	0.09	24.45	94.9
4	Bio	0.09	7.48	18.03	35.24	9.49	0	5.33	0.024	22.66	98.4
4	Bio	0.09	7.41	17.97	35.11	9.51	0	5.44	0.064	23.17	98.8
4	Bio	0.12	7.28	17.93	35.08	9.54	0.02	5.50	0.079	22.92	98.4
4	Bio	0.07	7.31	17.9	35.09	9.25	0.02	5.49	0.034	23.29	98.4
5	Bio	0.12	6.86	18.33	33.33	9.48	0.02	4.41	0.002	22.62	95.1
5	Bio	0.06	6.98	18.32	33.26	9.3	0.03	4.60	0.023	22.82	95.3
5	Bio	0.12	6.85	18.28	33.18	9.47	0	4.55	0.026	22.81	95.3
8	Bio	0.09	8.07	19.34	36.44	10.2	0.02	1.11	0.116	22.68	98.1
8	Bio	0.09	8.07	19.55	35.53	9.48	0.01	1.31	0.064	23.00	97.1
8	Bio	0.12	7.73	18.62	36.00	10.6	0	1.45	0.023	22.87	97.5
8	Bio	0.1	7.78	18.78	36.38	10	0.01	1.37	0.04	22.83	97.3
8	Bio	0.08	8.02	18.61	35.18	9.93	0.01	1.51	0.124	23.39	96.8
2	Gar	0.01	3.57	22.62	38.81	0.02	1.32	0.018	0.87	36.69	104
2	Gar	0.01	3.48	22.51	38.36	0	1.27	0.04	0.947	37.93	105
2	Gar	0	3.45	22.66	38.47	0	1.28	0.061	0.883	37.84	105
2	Gar	0.02	3.78	22.68	38.97	0.01	1.3	0.028	0.924	36.91	105
3	Gar	0.01	2.96	23.03	39.73	0	1.32	0.136	1.044	36.67	105
3	Gar	0	3.15	23.33	39.89	0	1.31	0.018	0.976	36.51	105
3	Gar	0.01	2.99	23.42	40.26	0.01	1.28	0.041	1.046	36.39	105
3	Gar	0.01	3.09	23.13	39.89	0.01	1.28	0.088	0.976	36.7	105
3	Gar	0.02	3.17	23	39.88	0	1.39	0.057	1.001	36.75	105
4	Gar	0.04	2.9	21.61	36	0	1.31	0.007	1.206	38.19	101
4	Gar	0.01	2.92	21.54	35.86	0	1.31	0.028	1.257	38.14	101
4	Gar	0.01	3.02	21.61	36.04	0	1.25	0.011	1.169	38.23	101
4	Gar	0.01	2.99	21.62	36.22	0	1.31	0.006	1.221	38.27	102
5	Gar	0	3.41	21.66	36.16	0.01	1.31	0.04	0.937	37.9	101
5	Gar	0	3.47	21.69	36.46	0.01	1.33	0.065	1.092	37.57	102
5	Gar	0.02	3.51	21.69	36.18	0	1.3	0.036	1.037	37.72	101
5	Gar	0.01	3.6	21.52	36.22	0.01	1.34	0.003	1.036	37.11	101
7	Gar	0.01	3.57	21.69	35.89	0.01	1.36	0.048	0.842	39.47	103
7	Gar	0.02	3.59	21.8	35.77	0	1.37	0.033	0.792	39.63	103
7	Gar	0	3.5	21.56	35.7	0.01	1.37	0.029	0.716	39.59	102
7	Gar	0.03	3.19	21.61	35.93	0.02	1.38	0.197	0.965	40.16	103
7	Gar	0	3.32	21.7	35.83	0.01	1.38	0.06	0.815	39.81	103
8	Gar	0.02	3.19	21.17	37.57	0	1.29	0.187	0.979	35.44	99.8
8	Gar	0	3.13	21.03	38.03	0	1.27	0.109	0.961	35.98	101
8	Gar	0.03	3.06	21.12	37.95	0.01	1.33	0.152	1.05	35.83	100
8	Gar	0.02	3.25	20.7	37.52	0.01	1.35	0.154	0.888	35.85	99.7

Table A-2, continued: Microprobe analyses (wt% oxides) of minerals in sample 17PGN01

area	min	Na2O	MgO	Al2O3	SiO2	K2O	CaO	TiO2	MnO	FeO	sum
1	Pl	7.15	0.03	20.24	45.82	0.13	5.85	0.008	0.015	0.355	79.6
1	Pl	7.07	0.02	20.28	45.97	0.19	5.85	0.003	0.05	0.246	79.7
1	Pl	6.93	0	20.49	45.78	0.2	5.97	0.019	0.025	0.242	79.7
1	Pl	7.04	0.01	20.31	45.51	0.19	5.93	0.019	0.037	0.28	79.3
1	Pl	7.15	0.02	20.39	46.02	0.17	5.92	0.016	0.05	0.2	79.8
2	Pl	7.5	0.01	24.71	60.98	0.26	6.31	0.004	0.005	0.277	100
2	Pl	7.52	0.01	24.24	60.93	0.25	6.24	.0001	0.028	0.394	99.6
2	Pl	7.52	0	24.16	60.53	0.26	6.27	0.016	0.037	0.402	99.2
2	Pl	7.47	0.01	24.15	60.18	0.23	6.17	0.012	0.01	0.484	98.7
3	Pl	6.84	0	28.14	56.77	0.14	8.48	0.008	0.03	0.365	101
3	Pl	6.54	0.02	27.88	55.14	0.11	8.82	0.008	0.013	0.433	99
3	Pl	6.78	0	27.16	55.95	0.15	8.08	0.016	0.01	0.483	98.6
3	Pl	6.95	0.01	26.95	55.86	0.12	7.81	0.016	0	0.457	98.1
3	Pl	6.82	0.01	27.01	56.09	0.11	8.04	0.022	0.01	0.577	98.7
4	Pl	7.06	0.02	25.49	60.6	0.15	6.97	0.027	0.01	0.349	101
4	Pl	7.05	0.01	25.85	60.14	0.17	7.34	0.033	0.02	0.358	101
4	Pl	6.94	0.01	25.69	59.63	0.18	7.39	0.009	0.01	0.439	100
4	Pl	7.19	0.01	25.4	59.75	0.16	7.09	0.006	0.04	0.364	99.9
5	Pl	6.29	0.01	27.64	55.27	0.21	9.06	0.003	0.05	0.18	98.6
5	Pl	6.29	0	27.65	55.31	0.15	9.01	0.011	0.017	0.177	98.6
5	Pl	6.21	0.01	28.25	55.42	0.12	9.23	0.009	0.04	0.256	99.5
5	Pl	6.24	0.01	27.54	55.22	0.13	9.11	0.014	0.02	0.41	98.6
5	Pl	6.44	0.01	27.73	57.03	0.18	8.39	0.018	0.02	0.422	100
6	Pl	9.31	0.03	20.72	66.38	0.05	3.11	0.053	0.053	0.796	100
6	Pl	10.2	0.01	22.29	63.38	0.06	3.22	0.02	0.013	0.702	99.8
6	Pl	9.99	0	22.54	62.78	0.07	3.39	0.006	0	0.821	99.6
6	Pl	3.37	0.02	7.291	88.27	0.01	1.06	0.006	0.032	0.749	101
6	Pl	6.74	0.01	15.46	73.04	0.02	2.64	0.007	0.01	0.924	98.8
7	Pl	11	0	21.76	66.01	0.04	2.09	0.014	0.022	0.672	102
7	Pl	10.6	0.01	22.44	65.53	0.03	2.76	0.022	0.01	0.839	102
7	Pl	11.4	0	21.91	67.96	0.05	1.72	0.019	0.015	0.923	104
7	Pl	10.7	0	22.61	65.57	0.05	2.71	0.017	0.042	0.803	102
8	Pl	8.59	0	24.74	60.88	0.3	5.51	0.002	0.04	0.259	100
8	Pl	8.09	0.01	25.07	59.2	0.23	6.12	0.008	0	0.356	99.1
8	Pl	8.54	0.01	24.46	60.62	0.27	5.63	0.014	0	0.196	99.7
8	Pl	8.32	0.01	25.06	59.51	0.23	6.25	0.017	0.028	0.419	99.8
8	Pl	8.15	0.01	24.72	59.36	0.26	6.23	0.02	0.04	0.243	98.9
9	Pl	10.2	0.05	23.09	61.69	0.07	4.04	0.008	0.02	0.757	99.9
9	Pl	9.8	0.02	23.59	61.25	0.14	4.36	0.001	0.008	0.779	99.9
9	Pl	10.2	0	22.88	61.95	0.06	3.87	0.004	0.025	0.98	99.9

Table A-3: Microprobe analyses (wt% oxides) from sample 2100-4

area	min	Na2O	MgO	Al2O3	SiO2	K2O	CaO	TiO2	MnO	FeO	sum
1	Bio	0.095	3.37	22.65	33.81	8.52	0.02	0.05	0.68	25	94.23
1	Bio	0.075	3.48	22.59	32.77	7.77	0.01	0.07	0.55	26.5	93.88
1	Bio	0.099	4.03	22.09	33.13	8.72	0	0.05	0.44	25.7	94.27
1	Bio	0.02	4.65	21.57	32.8	8.23	0.01	0.06	0.41	25.8	93.6
1	Bio	0.051	4.54	21.64	32.68	7.88	0	0.07	0.36	26.7	93.96
1	Gar	0.018	0.77	21.21	35.56	0.02	0.27	0.01	8.79	34.1	100.7
1	Gar	0	0.75	20.93	35.52	0.02	0.24	0	8.75	33.9	100.1
1	Gar	0.02	0.7	21.07	35.39	0	0.23	0.01	8.89	33.8	100
1	Gar	0.018	0.72	21.52	35.77	0	0.27	0.01	8.51	33.7	100.5
1	Gar	0.037	0.76	21.52	35.59	0	0.23	0.01	8.62	33.6	100.4
2	Gar	0.035	0.57	22.6	35.81	0.27	0.26	0	8.95	31	99.54
2	Gar	0.05	0.56	21.73	36.5	0.07	0.3	0.01	8.73	33.2	101.1
2	Gar	-0.01	0.66	21.38	35.82	0.05	0.28	0.01	8.23	34.1	100.6
2	Gar	0.025	0.61	21.59	35.94	0.04	0.26	0.01	8.41	34.3	101.1
3	Gar	0.014	0.69	21.35	35.49	0	0.26	0.04	8.35	34.4	100.6
3	Gar	0.009	0.68	21.31	35.76	0.03	0.29	0	8.42	34.5	101.1
3	Gar	0.001	0.69	21.32	35.51	0.01	0.27	0	8.37	34.2	100.3
3	Gar	0.047	0.73	21.38	35.49	0	0.29	0.02	8.1	34.5	100.5
3	Gar	0.023	0.7	21.3	35.47	0.01	0.27	0.01	8.3	34.3	100.4
4	Gar	0.013	0.75	21.13	35.92	0	0.25	0.01	8.04	34.8	100.9
4	Gar	0.044	0.72	21.02	35.49	0.02	0.25	0	8.08	34.9	100.5
4	Gar	0.031	0.71	21.11	35.78	0	0.26	0.01	8.29	35	101.2
5	Gar	0.025	0.78	21.43	35.51	0	0.27	0	8.07	34.4	100.5
5	Gar	0.034	0.77	21.28	35.64	0	0.28	0.04	8.04	34.6	100.7
5	Gar	0.011	0.79	21.33	35.57	0	0.27	0.01	8.04	34.8	100.8
5	Gar	0.042	0.82	21.25	35.71	0	0.28	0.01	7.99	34.4	100.5
5	Gar	0.018	0.8	21.38	35.6	0.01	0.28	0.02	7.98	34.2	100.3
4	Pl	10.13	0	21.28	63.99	0.17	2.08	0	0	0.03	97.65
4	Pl	10.35	0	21.11	64.51	0.21	1.86	0.01	0	0.01	98.03
4	Pl	10.24	0	21	64.2	0.19	1.91	0	0	0.04	97.54
4	Pl	10.27	0	21.36	64.2	0.19	2.11	0.01	0.02	0.02	98.11
4	Pl	10.18	0	21.3	64.21	0.18	1.92	0.01	0	0.04	97.68
5	Pl	10.42	0.01	21.16	64.58	0.11	1.83	0.02	0.16	0.4	98.7
5	Pl	10.46	0.01	21.27	64.63	0.13	1.95	0.01	0.09	0.37	98.91
5	Pl	10.51	0	21.29	64.74	0.13	1.79	0	0.08	0.34	98.9
5	Pl	10.48	0	21.21	64.67	0.1	1.77	0	0.09	0.39	98.71
5	Pl	10.45	0	21.13	64.37	0.11	1.82	0	0.06	0.31	98.25

Table A-3, continued: Microprobe analyses (wt% oxides) from sample 2100-4

area	min	Na2O	MgO	Al2O3	SiO2	K2O	CaO	TiO2	MnO	FeO	sum
2	Tour	1.8	2.57	35	34.43	0.06	0.07	0.09	0.1	11.8	85.94
2	Tour	1.7	2.78	34.57	34.18	0.27	0.1	0.14	0.11	11.5	85.3
3	Tour	1.79	2.37	35.76	34.09	0.06	0.23	0.48	0.24	12	87.05
3	Tour	1.82	2.3	35.8	34.05	0.06	0.25	0.49	0.24	12	86.96
3	Tour	1.78	2.31	35.69	34.43	0.09	0.2	0.45	0.24	12.1	87.31
1	Mu	0.69	0.05	39.32	45.32	10.8	0.01	0.06	0.01	0.62	96.85
1	Mu	0.71	0.02	39.26	45.44	10.7	0	0.05	0.01	0.63	96.89
1	Mu	0.52	0.08	38.65	45.57	10.9	0.01	0.05	0	0.69	96.48
1	Mu	0.69	0.02	39.06	45.14	10.8	0	0.02	0.02	0.55	96.26
1	Mu	0.53	0.02	38.95	45.55	10.8	0	0.02	0	0.5	96.35
2	Mu	0.49	0	39.24	45.48	11	0	0.02	0	0.41	96.66
2	Mu	0.62	0	39.41	45.6	10.7	0	0.01	0	0.38	96.67
2	Mu	0.2	0	39.15	45.79	11.3	0	0.02	0.03	0.37	96.86
2	Mu	0.59	0.02	39.21	45.52	10.8	0	0.03	0.02	0.33	96.48
2	Mu	0.63	0.01	39.52	45.49	10.7	0	0.02	0	0.27	96.59
3	Mu	0.51	0.05	38.8	45.32	10.4	0	0.05	0.05	0.94	96.17
3	Mu	0.73	0.02	38.97	45.2	10.7	0	0.04	0.02	0.51	96.18
3	Mu	0.49	0.04	38.59	45.16	10.9	0.01	0.01	0	0.49	95.63
3	Mu	0.59	0.03	39.24	45.78	10.6	0.03	0.04	0	0.42	96.76
3	Mu	0.56	0.02	38.8	45.26	10.8	0	0.03	0	0.71	96.14
3	Mu	0.7	0.02	39.03	45.16	10.6	0.01	0.01	0	0.49	96.05
1	Andl	0	0.02	65.84	35.35	0	0	0.02	0.04	0.53	101.8
1	Andl	0.01	0.01	65.74	35.11	0	0	0.01	0	0.5	101.4
1	Andl	0	0	65.99	35.56	0.01	0.01	0	0.05	0.74	102.4
1	Andl	0	0.04	66.11	35.33	0.01	0.01	0.01	0	0.64	102.1

Table A-4: Microprobe analyses (wt% oxides) of muscovite from peraluminous granites

sample	site	Na2O	MgO	Al2O3	SiO2	K2O	CaO	TiO2	MnO	FeO	sum
1631	1	0.46	0.43	35.5	49.4	10.51	0.01	0.04	0.05	1.02	97.4
1631	1	0.73	0.55	37.42	46.25	10.57	0.02	0.072	0.01	1.34	96.9
1631	1	0.73	0.47	37.36	45.77	10.62	0.02	0.32	0.03	1.33	96.62
1631	1	0.43	0.77	35.73	47.48	10.75	0	0.115	0.02	1.41	96.69
1631	1	0.52	0.39	37.46	45.79	11.08	0.01	0.375	0.04	1.14	96.79
1631	2	0.6	0.32	37.96	45.98	10.61	0.02	0.033	0.01	1.05	96.52
1631	2	0.58	0.4	38.02	45.71	10.9	0.02	0.115	0	1.25	96.98
1631	2	0.48	0.39	37.58	45.99	11.04	-0.01	0.254	0.03	1.13	96.89
1631	2	0.53	0.35	37.68	45.77	11.1	-0	0.243	0.01	1.1	96.77
1631	2	0.48	0.33	37.45	45.81	11.11	0.02	0.451	0.01	1.11	96.73
1631	3	0.77	0.56	37.1	45.88	10.55	-0	-0.02	0.02	1.74	96.58
1631	3	0.73	0.49	37.23	46.02	10.56	0.004	0.023	0.01	1.36	96.4
1631	3	0.71	0.54	36.95	45.66	10.61	-0	0.009	0.05	1.59	96.14
1631	3	0.69	0.54	36.92	46.01	10.65	0.02	-0	0	1.64	96.42
1631	3	0.65	0.57	37.31	46.17	10.71	0.03	-0.01	0.03	1.53	96.93
1631	4	0.48	0.5	35.94	47.14	10.28	0.02	0.124	0.01	1.31	95.79
1631	4	0.7	0.37	37.22	45.79	10.58	-0	0.222	0.07	1.25	96.2
1631	4	0.57	0.43	37.15	45.43	10.69	0.009	0.247	0	1.46	96.01
1631	4	0.63	0.37	37.27	46.11	10.71	0.002	0.291	0.02	1.35	96.75
1631	4	0.49	0.39	37.33	46.3	10.99	-.01	0.183	0.03	1.43	97.15
1660	1	0.43	0.32	37.76	46.07	11.06	-0.01	0.059	0.03	1.05	96.7
1660	1	0.45	0.41	37.41	45.94	11.12	0.01	0.287	0.03	1.18	96.79
1660	1	0.34	0.45	36.84	45.7	11.21	0.01	0.355	0.05	1.2	96.14
1660	1	0.42	0.65	36.69	46.12	11.21	-0.01	0.114	0.05	1.18	96.5
1660	1	0.38	0.53	36.88	45.92	11.22	0.01	0.151	0.03	1.42	96.52
1660	2	0.62	0.07	38.46	45.61	10.62	0.02	0.008	0.02	0.58	95.99
1660	2	0.61	0.1	38.85	45.85	10.81	0.02	0.023	0.03	0.57	96.82
1660	2	0.46	0.75	35.89	46.06	10.87	-0.01	0.049	0.02	1.3	95.41
1660	2	0.51	0.46	37.41	45.85	10.99	0.02	0.145	0.02	1.15	96.51
1660	2	0.38	0.7	36.61	46.01	11.1	-0.01	0.604	0.03	1.24	96.67
1660	3	0.18	0.36	37.26	46.13	10.79	0.049	0.026	0.03	0.83	95.62
1660	3	0.4	0.57	35.89	45.73	11.01	-0.02	0.468	0.02	1.12	95.21
1660	3	0.4	1.12	35.54	47.13	11.06	-0.01	1.024	0.02	1.35	97.62
1660	3	0.41	0.87	36.39	46.3	11.08	0.02	0.712	-0	1.27	97.03
1660	3	0.4	0.86	36.39	46.54	11.15	0.01	0.841	0.06	1.25	97.46
1660	4	0.71	0.42	37.45	45.12	10.47	-0.01	0.259	0	1.25	95.68
1660	4	0.5	0.42	36.84	46.29	10.59	0.019	0.161	0.02	1	95.86
1660	4	0.76	0.42	37.27	45.22	10.64	-0.01	0.288	0.04	1.28	95.93
1660	4	0.66	0.42	37.52	45.91	10.69	0.02	0.201	0	1.16	96.55
1660	4	0.55	0.39	37.36	45.46	10.84	-0	0.257	0.05	1.13	96.02

Table A-4, continued: Microprobe analyses (wt% oxides) of muscovite from peraluminous granites

sample	site	Na2O	MgO	Al2O3	SiO2	K2O	CaO	TiO2	MnO	FeO	sum
1745	1	0.58	0.57	38.36	47.45	10.77	-0	0.246	-0	1.26	99.24
1745	1	0.52	0.46	37.4	45.55	10.95	0.02	0.309	0.03	1.11	96.31
1745	1	0.46	0.62	36.95	45.99	10.96	-0.01	0.18	0.01	1.12	96.27
1745	1	0.48	0.5	37.41	46.13	11.04	-0	0.121	0	1.12	96.79
1745	2	0.44	0.47	37.41	45.85	10.99	-0.01	0.036	0.01	1.15	96.33
1745	2	0.45	0.4	37.99	45.91	11.04	-0.01	0.048	0.04	1.14	97
1745	2	0.41	0.44	37.53	46.18	11.04	-0.01	0.027	0.02	1.21	96.86
1745	2	0.42	0.37	37.97	45.87	11.05	0.006	0.03	0.05	1.13	96.91
1745	2	0.42	0.43	37.89	45.72	11.15	-0	0.011	0.03	1.23	96.9
1745	2	0.55	0.48	37.41	45.7	10.72	0.002	0.412	0.02	0.97	96.28
1745	3	0.56	0.55	37.26	45.94	10.81	-0.01	0.379	0.02	0.93	96.44
1745	3	0.5	0.46	37.28	45.53	10.88	0.02	0.73	0.05	0.98	96.39
1745	3	0.47	0.51	37.11	45.27	10.88	0.006	0.575	0.03	1.05	95.87
1745	3	0.41	0.49	37.21	45.76	11.03	0.001	0.383	0.04	0.97	96.21
1745	4	0.63	0.57	37.44	45.63	10.69	-0.01	0.012	0.05	1.34	96.35
1745	4	0.62	0.51	37.46	45.4	10.74	-0	0.003	0.01	1.28	96.04
1745	4	0.56	0.53	37.71	45.52	10.81	0.004	-0.01	0.01	1.35	96.49
1745	4	0.56	0.59	37.41	45.9	10.83	-0.01	-0.01	0.02	1.31	96.59
1745	4	0.51	0.54	37.57	45.67	10.87	-0.01	0.051	0	1.1	96.31
1745	5	0.61	0.27	38.25	45.87	10.75	-0.01	0.007	0.02	0.79	96.57
1745	5	0.61	0.48	37.57	45.72	10.76	0.01	0.044	0.05	1.12	96.36
1745	5	0.58	0.34	38.09	45.81	10.8	0.011	0.016	0	0.88	96.54
1745	5	0.53	0.23	38.09	45.6	10.83	-0.01	0.052	0.03	0.73	96.03
1745	5	0.55	0.45	37.91	45.92	10.91	-0	0.046	0.04	0.99	96.83

Table A-5: Microprobe analyses (wt% oxides) from the Liese & Football plutons

smpl#	min	Na_2O	MgO	Al_2O_3	SiO_2	Cl	K_2O	CaO	TiO_2	MnO	FeO	sum
748	opx	0.07	17.1	0.91	52.7	0.01	0	1.36	0.12	0.5	23	95.7
748	opx	0.06	17.3	0.82	52.1	0.01	0	1.3	0.11	0.47	22.9	95
748	hbl	0.68	14.2	5.93	47.4	0.02	0.43	11.5	1.3	0.18	13.1	94.7
748	hbl	0.66	14.4	5.22	48.5	0.03	0.35	11.8	1.19	0.18	13.1	95.5
748	hbl	0.73	12.7	5.75	48.6	0.04	0.45	11.5	0.57	0.38	16.5	97.4
748	hbl	0.65	12.9	5.46	48.3	0.03	0.37	10.8	0.51	0.38	17.3	96.7
748	hbl	0.61	12.7	5.21	48.6	0.02	0.37	11.8	0.47	0.35	16.7	96.8
PUC13	hbl	0.69	11.7	5.49	46.8	0.06	0.46	10.9	0.55	0.49	17.7	94.8
PUC14	hbl	0.71	11.7	6.4	46.3	0.03	0.5	11	0.65	0.41	17.4	95.1
PUC15	hbl	0.49	11.9	5.02	48.4	0.04	0.36	11.7	0.41	0.45	17	95.8
PUC16	hbl	0.63	10.8	6.12	49.7	0.05	0.46	10.5	0.61	0.49	15.9	95.3
PUC17	hbl	0.51	11.9	5.05	47.1	0.04	0.35	11.3	0.49	0.48	17	94.2
15PWT07	hbl	0.63	12.1	5.23	48.7	0.07	0.43	11.7	0.42	0.39	17.1	96.8
15PWT07	hbl	0.44	12.4	4.63	49.4	0.02	0.27	12.3	0.25	0.36	16.7	96.7
15PWT07	hbl	0.73	12.2	5.73	47.6	0.08	0.49	11.3	0.55	0.39	17.4	96.5
15PWT07	hbl	0.89	12	6.42	47.6	0.07	0.55	11.6	0.64	0.35	17.1	97.2
15PWT14	hbl	0.78	13	6.43	47.5	0.1	0.55	11.5	0.49	0.27	15.8	96.3
15PWT15	hbl	0.81	13	6.25	46.9	0.08	0.56	11.8	0.58	0.24	15.5	95.7
15PWT16	hbl	0.91	13	6.77	46.3	0.11	0.64	11.5	0.5	0.25	15.6	95.6
15PWT17	hbl	0.76	13.2	6.45	46.9	0.09	0.55	11.5	0.53	0.28	16	96.2
761	hbl	1.43	8.98	7.64	44.8	0.07	0.81	10.5	1.25	0.67	20	96.2
761	hbl	1.42	8.93	7.44	44.4	0.1	0.8	10.4	1.35	0.69	20	95.5
761	hbl	1.6	8.27	9.26	43.5	0.09	0.96	10.8	1.34	0.62	20.1	96.4
771	hbl	0.99	12.4	6.09	48.4	0.03	0.5	11.1	0.85	0.43	16.5	97.4
771	hbl	1.12	12.8	5.63	48.3	0.05	0.46	10.7	0.68	0.37	16	96.2
771	hbl	0.65	13.1	4.72	49.7	0.03	0.34	11.5	0.53	0.4	15.2	96.2
771	hbl	1.07	12.1	5.9	48.6	0.04	0.53	11.4	0.99	0.44	16.5	97.7
15PWT87	hbl	1.38	7.88	8.4	43.6	0.12	0.93	10.9	1.33	0.69	20.8	96
15PWT87	hbl	1.37	7.75	8.62	43.5	0.1	0.92	10.7	1.07	0.73	21	95.8
56	hbl	0.56	10.2	5.66	47.7	0.03	0.34	10.3	0.37	0.94	20.1	96.2
56	hbl	0.6	10.3	5.91	47.9	0.05	0.38	10.5	0.4	0.82	20.6	97.4
56	hbl	0.66	10.3	5.72	47.9	0.03	0.36	10.5	0.34	0.82	20.4	97.1
56	hbl	0.64	10.6	5.45	48.4	0.02	0.34	10.7	0.28	0.82	19.9	97.1

Table A-5, continued: Microprobe analyses (wt% oxides) from Liese & Football plutons

smpl#	min	Na_2O	MgO	Al_2O_3	SiO_2	Cl	K_2O	CaO	TiO_2	MnO	FeO	sum
56	hbl	0.78	10.3	5.72	47.8	0.04	0.44	10.6	0.45	0.71	20.1	96.9
56	hbl	0.76	10.3	5.74	47.7	0.03	0.36	10.8	0.4	0.75	20	96.8
56	hbl	0.75	10.3	5.9	47.2	0.04	0.41	10.6	0.47	0.71	20.1	96.5
56	hbl	0.77	10.3	5.8	47.5	0.04	0.41	10.7	0.5	0.69	19.9	96.7
56	hbl	0.7	9.84	6.27	47.1	0.06	0.48	11.1	0.63	0.7	19.5	96.3
56	hbl	0.65	9.94	6	47.4	0.06	0.48	11.1	0.47	0.72	19.6	96.5
56	hbl	0.69	9.98	6.2	47.3	0.04	0.48	11.3	0.48	0.68	19.8	96.9
56	hbl	0.69	10.1	5.82	47.5	0.05	0.44	10.8	0.39	0.7	20.3	96.8
56	hbl	0.63	10.1	6.01	47.7	0.05	0.47	11.1	0.47	0.67	20.1	97.3
56	Hbl	0.5	10.4	5.24	46.8	0.05	0.34	10.8	0.24	0.85	19.2	94.4
56	Hbl	0.62	10.7	5.38	48.2	0.04	0.39	10.5	0.37	0.66	19.9	96.8
56	Hbl	0.57	10.7	5.39	48.2	0.05	0.38	10.6	0.33	0.65	19.3	96.1
56	Hbl	0.6	10.8	5.48	48.5	0.05	0.4	10.6	0.31	0.71	19.8	97.2
56	Hbl	0.55	10.9	5.23	48.5	0.05	0.38	10.7	0.35	0.69	19.5	96.9
744B	hbl	0.7	14.1	5.35	49.5	0.03	0.36	11.2	1.01	0.26	14.2	96.7
744B	hbl	0.59	14.1	5.21	49.7	0.04	0.33	11.3	1.04	0.24	14.1	96.7
744B	hbl	0.66	14.4	5.2	49.7	0.04	0.33	11.2	1.07	0.29	14	97
744B	hbl	0.69	14.5	5.25	50	0.03	0.32	11.3	1.03	0.21	14.2	97.5
744B	hbl	0.86	13.8	6.45	48.1	0.06	0.48	11.3	1.3	0.23	14.1	96.7
744B	hbl	0.85	14	6.19	48.5	0.05	0.48	11.4	1.22	0.25	14.3	97.2
744B	hbl	0.72	14.2	5.56	49.3	0.05	0.36	11.3	1.05	0.17	13.8	96.5
744B	hbl	0.56	14.3	5.1	49.8	0.02	0.37	11.2	1.01	0.29	14	96.7
744B	hbl	0.61	14.5	5.21	49.7	0.03	0.35	11.3	1.01	0.2	13.9	96.7
744B	hbl	0.64	13	6.86	48.3	0.04	0.43	11.4	0.91	0.26	14.9	96.7
744B	hbl	0.6	13.5	6.23	49	0.02	0.38	11.4	0.88	0.24	14.9	97.2
744B	hbl	0.62	13.7	5.78	49.2	0.02	0.35	11.2	0.96	0.25	14.7	96.8
745	hbl	0.77	11.5	6.91	46.9	0.09	0.6	11.3	0.54	0.38	17.5	96.5
745	hbl	0.74	11.6	7.12	47.1	0.07	0.57	11.3	0.57	0.41	17.2	96.7
745	hbl	0.82	11.6	6.92	47	0.1	0.56	11.2	0.57	0.38	17.8	97
745	hbl	0.78	11.8	6.91	47.4	0.08	0.55	11.2	0.59	0.35	17.3	97
745	hbl	0.83	11.9	6.94	47.2	0.09	0.59	11.2	0.6	0.45	17.3	97.1
745	hbl	0.67	11.9	6.96	47.6	0.06	0.55	11.8	0.6	0.3	15.9	96.3
745	hbl	0.76	11.9	7.34	47.1	0.09	0.6	11.6	0.67	0.34	16.3	96.8
745	hbl	0.78	12	7.37	47.1	0.08	0.6	11.7	0.68	0.29	16.1	96.7
745	hbl	0.66	12	7.03	47.7	0.08	0.57	11.9	0.64	0.23	15.9	96.7
745	hbl	0.74	11.8	7.04	47.3	0.09	0.62	11.5	0.53	0.29	16.9	96.8
745	hbl	0.71	11.9	7.02	47.2	0.08	0.6	11.4	0.61	0.29	16.6	96.5
745	hbl	0.79	12.2	7.06	47.2	0.08	0.6	11.4	0.64	0.25	16.7	97

Table A-5, continued: Microprobe analyses (wt% oxides) from Liese & Football plutons

smpl#	min	Na_2O	MgO	Al_2O_3	SiO_2	Cl	K_2O	CaO	TiO_2	MnO	FeO	sum
745	hbl	0.78	11.7	7.6	46.9	0.11	0.67	11.3	0.56	0.37	16.5	96.4
745	hbl	0.78	11.7	7.4	47	0.12	0.6	11.3	0.48	0.35	17	96.7
745	hbl	0.81	11.8	7.64	47	0.11	0.7	11.3	0.56	0.33	17.1	97.3
745	hbl	0.76	12.3	6.9	47.5	0.06	0.63	11.4	0.53	0.32	16.4	96.9
745	hbl	0.85	12.4	6.75	47.4	0.07	0.57	11.2	0.45	0.35	16.6	96.7
745	hbl	0.89	12.4	6.75	47.4	0.06	0.58	11.3	0.44	0.35	16.8	97
745	hbl	0.86	12.6	6.84	47.5	0.06	0.59	11.3	0.46	0.38	16.3	96.9
745	hbl	0.75	11.9	7.39	47.2	0.08	0.6	11.5	0.54	0.31	16.7	96.9
745	hbl	0.75	11.9	7.32	47.3	0.08	0.53	11.5	0.54	0.36	16.5	96.9
745	hbl	0.77	11.9	7.67	46.8	0.1	0.61	11.1	0.52	0.34	16.6	96.3
745	hbl	0.64	12.1	7.42	47.3	0.09	0.55	11.7	0.57	0.32	16.3	96.9
759	hbl	0.72	10.3	7.35	46.4	0.06	0.56	10.7	1.03	0.41	18.8	96.4
759	hbl	0.72	10.4	7.26	46.2	0.06	0.59	10.9	1.02	0.4	18.9	96.5
759	hbl	0.75	10.7	7.06	46.1	0.05	0.58	10.7	1.07	0.38	19.2	96.6
759	hbl	0.77	10.7	7.25	46	0.07	0.65	10.9	1.11	0.39	19.1	96.9
759	hbl	0.8	10.5	7.67	45.4	0.09	0.69	11	1.51	0.39	19	97.1
759	hbl	0.71	10.6	7.61	46	0.07	0.64	11.1	1.38	0.32	18.4	96.9
759	hbl	0.77	10.7	7.67	45.6	0.07	0.67	11	1.39	0.35	19	97.2
759	hbl	0.75	10.9	6.95	46.1	0.08	0.61	10.9	1.25	0.32	18.6	96.5
759	hbl	0.8	11	7	46	0.07	0.62	10.8	1.26	0.3	18.8	96.6
759	hbl	0.71	10.4	7.37	46.1	0.04	0.58	10.9	1.06	0.48	19.7	97.4
759	hbl	0.77	10.7	7.15	46.3	0.04	0.6	10.9	1.01	0.42	19.4	97.2
759	hbl	0.79	10.7	7.02	46.1	0.06	0.58	10.8	1.01	0.42	19.4	96.8
759	hbl	0.82	10.5	7.47	45.3	0.08	0.72	10.9	1.44	0.42	19.1	96.6
759	hbl	0.77	10.5	7.49	45.3	0.05	0.6	10.8	1.26	0.44	19.4	96.6
759	hbl	0.81	10.6	7.25	45.8	0.06	0.62	10.7	1.37	0.43	18.9	96.4
759	hbl	0.47	10.9	6.98	46.1	0.05	0.42	10.7	1.02	0.46	19.4	96.5
759	hbl	0.73	11	6.77	46	0.07	0.57	10.6	1.18	0.35	18.8	96
759	hbl	0.71	9.96	7.6	45.8	0.07	0.59	11	1.38	0.39	19.4	96.9
759	hbl	0.66	10.2	7.56	46	0.07	0.63	11	1.35	0.38	19.2	97
759	hbl	0.73	10.2	7.5	45.4	0.08	0.61	10.9	1.41	0.38	18.8	96
759	hbl	0.61	10.4	6.6	48.2	0.05	0.5	10.9	1.15	0.41	18.2	97
759	hbl	0.58	11.1	6.74	46.7	0.05	0.59	11	1.22	0.45	18.7	97

Table A-5, continued: Microprobe analyses (wt% oxides) from Liese & Football plutons

smpl#	min	Na_2O	MgO	Al_2O_3	SiO_2	K_2O	CaO	TiO_2	MnO	FeO	sum	%An
768	Pl	5.61	0.01	28.2	53.8	0.18	10.9	0.01	-0	0.22	99	52
768	Pl	6.28	0.02	27.3	55.7	0.12	9.56	-0	0.01	0.16	99.1	46
768	Pl	6.02	0.08	27.5	54.4	0.18	10.2	0	0.01	0.34	98.7	48
PUC13	Pl	6.01	0.01	27.4	54.1	0.16	10	0	0.02	0.24	98.1	48
PUC14	Pl	5.4	0.01	28.1	52.4	0.14	11.1	-0	-0	0.28	97.4	53
PUC15	Pl	6.31	0.01	27.2	54.9	0.13	9.62	-0	-0	0.23	98.4	46
PUC16	Pl	5.64	0	27.9	52.7	0.13	10.7	0.01	-0	0.18	97.2	51
PUC17	Pl	5.68	0.01	27.6	53.2	0.14	10.5	0.01	0	0.19	97.3	51
15PWT07	Pl	5.64	0.01	28.7	54	0.11	11.1	0	0	0.17	99.7	52
15PWT07	Pl	4.85	0.02	29.5	51.9	0.1	12.4	0.01	0.01	0.28	99.1	59
15PWT07	Pl	5.52	0.01	28.7	53.7	0.11	11.2	0.01	0	0.13	99.4	53
15PWT07	Pl	5.59	0.02	28.4	53.6	0.11	11	0.01	0.01	0.25	99	52
15PWT14	Pl	4.68	0.01	29.3	51.3	0.05	12.5	0.02	0	0.3	98.1	60
15PWT14	Pl	5.02	0.03	29.1	52.5	0.07	12	0.02	-0	0.4	99.1	57
15PWT14	Pl	5.17	0.02	28.6	52.1	0.08	11.7	0.02	0.01	0.39	98	56
15PWT14	Pl	5.22	0.01	28.9	52.4	0.1	11.7	0.02	0.02	0.39	98.7	55
761	Pl	7.74	0.02	27.9	55.1	0.13	9.76	-0	0	0.23	101	41
761	Pl	7.27	0.01	27.7	54	0.16	9.8	0	-0	0.22	99.2	43
761	Pl	6.43	0.02	29.3	52.5	0.11	11.6	-0	-0	0.22	100	50
771	Pl	6.25	0.01	27.8	55.6	0.16	9.12	-0	0.02	0.16	99.1	45
771	Pl	6.04	0.01	27.7	55	0.17	9.04	0.01	-0	0.22	98.2	45
771	Pl	6.69	0.02	26.9	57.2	0.15	8.05	-0	-0	0.28	99.3	40
771	Pl	6.4	0.01	27.4	57.1	0.2	8.42	0.01	0.01	0.19	99.6	42
771	Pl	6	0.01	27.9	55.9	0.14	9.46	-0	0.01	0.28	99.6	47
15PWT87	Pl	7.03	0.01	28.4	53.9	0.14	10.4	0.03	-0	0.23	100	45
15PWT87	Pl	7.63	0.02	27.7	54.6	0.15	9.47	-0	-0	0.39	99.9	41
15PWT87	Pl	7.76	0	27.1	55.5	0.19	8.97	0.03	0.02	0.24	99.9	39
56	Pl	6.71	0.01	26.7	57.2	0.13	8.43	0.03	0.06	0.39	99.6	41
56	Pl	5	0.02	29.3	53.3	0.14	11.4	0	-0	0.34	99.4	55
56	Pl	4.56	0.02	29.8	52.6	0.19	11.8	-0	0.02	0.34	99.2	58
56	Pl	5.43	0.02	28.7	54.4	0.24	10.5	0.01	0	0.34	99.6	51
56	Pl	5.11	0.09	28.8	53.4	0.18	10.7	0.02	0.06	0.57	98.9	53
56	Pl	6.58	-0	26.4	56.7	0.17	8.28	-0	0.02	0.2	98.3	41
56	Pl	6.45	0	26.5	56.7	0.21	8.3	-0	0.04	0.21	98.4	41
56	Pl	6.65	0.02	26.4	56.7	0.15	8.2	0.01	0.05	0.19	98.4	40
56	Pl	6.64	-0	26.3	57.3	0.18	8.16	0.01	-0	0.21	98.8	40
56	Pl	6.61	0.01	26.6	57.3	0.23	8.25	0	0.02	0.24	99.3	40
56	Pl	6.73	0.01	26.6	56.9	0.15	8.35	-0	0.04	0.19	99	40
56	Pl	6.7	0.02	26.3	57.3	0.2	8.18	0.01	0.06	0.32	99.1	40
56	Pl	6.7	0.04	26.2	57	0.18	8.11	0.02	-0	0.22	98.4	40

Table A-5, continued: Microprobe analyses (wt% oxides) from Liese & Football plutons

smpl#	min	Na_2O	MgO	Al_2O_3	SiO_2	K_2O	CaO	TiO_2	MnO	FeO	sum	%An
56	Pl	6.77	0.01	26.1	58	0.08	7.77	-0	0.02	0.11	98.9	39
56	Pl	6.65	0.01	26.3	57.5	0.16	8.08	-0	0.02	0.28	99	40
56	Pl	6.1	0.02	27.5	56.3	0.12	9.21	-0	-0	0.25	99.4	45
744B	Pl	6.23	-0	27	56.5	0.33	8.69	0.01	0.06	0.1	98.9	43
744B	Pl	5.22	-0	28.8	54	0.23	10.9	0	-0	0.18	99.3	53
744B	Pl	5.68	0	27.7	55.1	0.28	9.73	0.01	0.02	0.09	98.6	48
744B	Pl	6.26	0	27	56.5	0.24	8.81	0	0.03	0.12	98.9	43
744B	Pl	6.18	0	27.2	56.1	0.22	8.97	0	0.03	0.09	98.8	44
744B	Pl	5.49	0.01	28	55	0.24	10.1	0.01	0.01	0.16	99	50
744B	Pl	5.57	0.01	27.9	55.3	0.25	9.87	0	0.04	0.14	99.1	49
744B	Pl	5.88	0.02	27.7	55.2	0.21	9.48	0.02	0.07	0.06	98.6	47
744B	Pl	5.17	0.02	28.4	53.9	0.2	10.9	-0	-0	0.14	98.7	53
744B	Pl	5.02	0.08	24.3	48.8	0.26	8.87	0	0.23	4.55	92.3	49
745	Pl	5.1	-0	28.6	53.6	0.16	11	0.03	0.02	0.17	98.6	54
745	Pl	5.08	0	28.7	54.1	0.18	10.9	0.02	0.02	0.19	99.2	54
745	Pl	5.17	0.01	28.9	54.4	0.14	10.9	0.02	-0	0.18	99.8	53
745	Pl	4.8	0	29.5	53.2	0.13	11.6	-0	-0	0.23	99.5	57
745	Pl	4.77	0.01	29.3	53.1	0.12	11.6	0.01	-0	0.2	99	57
745	Pl	4.75	0.01	29.5	52.6	0.12	11.9	0.01	-0	0.14	99.1	58
745	Pl	5.07	-0	28.8	53.6	0.13	11.2	0.01	-0	0.24	99	55
745	Pl	5.02	0	28.9	53.7	0.13	11.3	0.04	-0	0.23	99.3	55
745	Pl	4.99	0.01	29.1	53.3	0.13	11.4	0	0.04	0.27	99.3	55
745	Pl	4.9	0.02	29.2	53.5	0.13	11.5	0.02	0.01	0.24	99.5	56
745	Pl	4.92	-0	29.3	53.1	0.11	11.5	0.02	0.04	0.2	99.2	56
745	Pl	4.84	0.01	29.1	53.2	0.13	11.3	0.03	-0	0.24	98.9	56
745	Pl	4.99	0.02	29.1	53.3	0.13	11.3	-0	-0	0.18	98.9	55
745	Pl	5.05	0.09	28.8	53.5	0.19	11.1	0.02	-0	0.26	99.1	54
745	Pl	5.92	0	27.6	55.8	0.17	9.56	0	-0.1	0.22	99.2	47
745	Pl	6.21	0.02	27.4	56.2	0.17	9.27	0.01	0.02	0.2	99.5	45
745	Pl	5.16	-0	28.9	53.8	0.13	11	0.02	0.02	0.27	99.2	54
745	Pl	5.17	0.02	28.9	53.8	0.11	11.1	0.04	0.01	0.22	99.4	54
745	Pl	5.25	0.02	29	53.9	0.12	11	0.04	0.01	0.19	99.5	53
745	Pl	5.17	0.02	28.9	53.7	0.11	10.9	0.04	-0	0.24	99.1	53
745	Pl	5.16	0.03	28.8	53.8	0.13	11	0.03	-0	0.24	99.1	54
759	Pl	5.03	0.02	29	53.1	0.09	11.2	0.01	0.02	0.28	98.7	55
759	Pl	4.71	0.03	29.8	52.2	0.09	11.7	0.02	0.01	0.25	98.8	58
759	Pl	5.01	0.06	28.9	53.1	0.09	11.1	0.01	0	0.42	98.7	55
759	Pl	3.98	-0	30.9	50.8	0.14	13.1	0.01	0.01	0.21	99.1	64
759	Pl	4.33	0	30.3	51.4	0.08	12.5	0.02	0.04	0.22	98.9	61
759	Pl	5.56	0	28.1	54.5	0.1	10.1	0	0.03	0.16	98.5	50

Table A-5, continued: Microprobe analyses (wt% oxides) from Liese & Football plutons

smpl#	min	Na_2O	MgO	Al_2O_3	SiO_2	K_2O	CaO	TiO_2	MnO	FeO	sum	%An
759	Pl	5.83	0.01	27.9	54.7	0.11	9.76	0.01	0	0.29	98.6	48
759	Pl	5.33	0.01	28.7	53.9	0.08	10.7	0.03	0.05	0.19	98.9	52
759	Pl	5.41	0.01	28.7	53.9	0.13	10.5	0.01	0.02	0.23	98.9	51
759	Pl	5.19	0.05	28.9	53.3	0.19	10.8	0.01	-0	0.24	98.6	53
759	Pl	4.67	0.01	29.4	52.2	0.11	11.6	0.01	-0	0.21	98.1	58
759	Pl	4.83	0.01	29.3	52.9	0.11	11.4	0.02	0.01	0.18	98.8	56
759	Pl	4.71	0.01	29.7	52.5	0.09	11.7	-0	0.01	0.17	98.9	58

I analyzed zircons using two different routines. For both I used a 15 kV, 70 nA, < 1 micron beam, and counting times of 20 seconds on peak and 10 seconds each on the high and low background positions. My initial routine, which I employed on zircons from sample 4021A, analyzed for Th on spectrometers 1-4 (PET) and then analyzed for Hf on spectrometers 1-3 (LiF). I input ZrO2 and SiO2 concentrations for pure zircon (for the purposes of ZAF corrections) and averaged the 4 different Th and 3 different Hf concentrations. I used an artificial thorite standard for Th and Chuck Taylor zircon for Hf. I estimate a detection limit of 0.04% for ThO2.

I modified the routine for some additional analyses on zircons from 4021A and also zircons from the FZ samples. For the modified routine, I analyzed for Hf on spectrometers 1 and 2 (LiF) and Th on spectrometers 3 and 4 (PET), using the same counting times and beam. I analyzed for SiO2, ZrO2, and UO2 using the energy dispersive spectrometer, but used Zr and Si concentrations for pure zircon for ZAF corrections. I estimate a detection limit of 0.1% ThO2 for this version.

In the following tables, I list only ThO2 and HfO2 concentrations using the first routine, but all the elements using the second one.

Table A-6: Microprobe analyses (wt% oxides) of zircons from sample 4021A

zircon	ThO_2	HfO_2	zircon	ThO_2	HfO_2	zircon	ThO_2	HfO_2
2	0.01	0.02	18	0.00	1.8	37	0.96	1.9
2	0.00	0.07	18	0.02	2.1	37	0.04	1.9
2	0.01	0.08	18	0.02	2.2	37	0.06	2.0
2	0.00	0.08	18	0.00	2.4	37	0.08	2.0
2	0.00	0.11	18	0.00	2.6	37	0.31	2.0
2	0.01	0.11	25	0.00	0.01	37	0.15	2.1
8	0.01	0.14	25	0.00	0.01	37	0.02	2.1
8	0.01	1.2	25	0.00	0.02	37	0.06	2.1
8	0.01	1.2	25	0.01	0.03	37	0.01	2.1
8	0.00	1.2	25	0.00	0.04	37	0.14	2.1
8	0.02	1.3	25	0.01	0.05	37	0.00	2.2
8	0.04	1.4	25	0.01	0.14	37	0.15	2.2
8	0.12	1.6	26	0.01	0.00	37	0.10	2.2
8	0.00	1.7	26	0.00	0.01	37	0.19	2.3
8	0.02	2.0	26	0.00	0.01	37	0.05	2.3
8	0.07	2.0	26	0.01	0.01	37	0.13	2.3
8	0.05	2.0	26	0.00	0.03	37	0.05	2.3
8	0.03	2.0	26	0.00	0.10	37	0.13	2.4
8	0.07	2.2	26	0.02	0.11	37	0.21	2.4
8	0.02	2.2	26	0.00	0.11	37	0.11	2.5
8	0.03	2.2	27	0.01	0.05	37	0.01	2.6
8	0.01	2.3	27	0.00	0.07	37	0.04	2.7
8	0.02	2.5	27	0.01	0.10	37	0.22	2.8
8	0.04	2.6	27	0.01	0.12	37	0.08	3.1
8	0.03	2.6	37	0.01	0.02	44	0.01	0.02
8	0.06	3.1	37	0.02	0.09	44	0.01	0.05
8	0.16	3.5	37	0.00	0.13	44	0.00	0.10
8	0.05	4.2	37	0.00	0.15	44	0.00	0.13
12	0.01	0.02	37	0.01	0.68	44	0.01	0.17
12	0.00	0.05	37	0.94	0.68	44	0.01	0.19
12	0.00	0.13	37	0.85	0.89	44	0.00	0.20
12	0.00	0.17	37	0.77	1.0	48	0.00	0.01
15	0.02	0.02	37	0.62	1.2	48	0.00	0.02
15	0.00	0.41	37	0.09	1.5	48	0.00	0.04
15	0.05	1.5	37	0.07	1.7	48	0.00	0.04
15	0.06	1.7	37	0.17	1.7	48	0.00	0.04
15	0.02	2.1	37	0.34	1.8	48	0.00	0.05
18	0.01	1.2	37	0.39	1.8	48	0.00	0.08
18	0.02	1.7	37	0.05	1.9	48	0.00	0.11
			37	0.29	1.9	48	0.00	0.12

Table A-7: Microprobe analyses (wt% oxides) of zircons from FZ & 4021Asamples

zircon	SiO_2	ZrO_2	HfO_2	ThO_2	UO_2
FZ 41	36.4	62.9	0.41	0.2	0.12
FZ 41	36.2	62.6	0.97	0.0	0.23
FZ 41	36.6	62.5	0.8	0.04	0.02
FZ 41	37.6	61.1	1.08	0.13	0.13
FZ 41	38.1	60.4	0.73	0.29	0.46
FZ 41	38.3	60.8	0.48	0.1	0.35
FZ 41	36.2	62.7	1.06	0.03	0.06
FZ 41	36.2	63.1	0.52	0.07	0.06
FZ 41	37.1	61.7	0.68	0.14	0.36
FZ 41	38.1	60.8	0.93	0.0	0.19
FZ 41	35.8	62.4	1.04	0.43	0.3
FZ 41	36.1	62.5	1.24	0.04	0.13
FZ 41	36.2	62.4	1.07	0.2	0.1
FZ 41	37.2	61.6	1.1	0.08	0.08
FZ 41	37.2	61.6	0.88	0.1	0.24
FZ 41	36.6	61.8	1.23	0.21	0.13
FZ 41	36.6	62.2	0.63	0.22	0.37
FZ 41	36.3	62.7	0.92	0.06	0.0
FZ 41	36.1	62.1	1.1	0.3	0.33
FZ 41	36.1	62.2	0.61	0.58	0.46
FZ 41	36.2	61.8	1.56	0.16	0.34
FZ 41	36.3	62.6	1.0	0.0	0.09
FZ 41	37.8	60.7	1.17	0.16	0.15
FZ 41	37.4	61.4	1.02	0.1	0.18
FZ 41	37.3	61.5	1.03	0.11	0.09
FZ 41	36.4	62.2	1.31	0.08	0.07
FZ 41	36.8	61.9	0.82	0.23	0.19
FZ 41	36.2	62.8	0.42	0.36	0.26
FZ 41	36.8	62.2	0.81	0.05	0.08
FZ 41	36.8	61.8	1.29	0.12	0.0
FZ 41	36.1	62.8	1.04	0.04	0.02
FZ 41	36.0	62.5	1.17	0.08	0.18
FZ 41	37.0	61.1	1.27	0.31	0.31
FZ 41	36.1	62.8	0.84	0.13	0.09

zircon	SiO_2	ZrO_2	HfO_2	ThO_2	UO_2
FZ-3	36.4	60.8	1.46	0.62	0.76
FZ-3	36	61.6	1.59	0.33	0.5
FZ-3	36.1	62.3	1.12	0.23	0.26
FZ-3	36.3	62.6	1	0.06	0
FZ-3	36.2	63.2	0.44	0.17	0.01
FZ-3	36.2	62.7	1.1	0.04	0
FZ-3	39.4	58.5	1.24	0.35	0.51
FZ-3	36.3	62.4	1.11	0.1	0.09
FZ-3	35.7	62.8	1.34	0.02	0.14
FZ-3	36	62.5	1.09	0.25	0.2
FZ-3	42.9	56.4	0.62	0.14	0
FZ-3	36	62.6	1.19	0.12	0.06
FZ-3	36.4	62.7	0.89	0	0.08
FZ-3	36.3	62.2	1.41	0	0.14
FZ-3	36	62.5	1.53	0	0
FZ-3	36.6	61.9	1.31	0.01	0.11
FZ-3	36.4	62.7	0.85	0	0
FZ-3	36.1	62.8	1.03	0.03	0.07
FZ-3	36.5	60.8	1.83	0.33	0.52
FZ-3	36.2	61.6	1.67	0.18	0.27

zircon	SiO_2	ZrO_2	HfO_2	ThO_2	UO_2
FZ-21	37.1	59.9	1.44	1.0	0.64
FZ-21	37.5	60.6	1.71	0.06	0.15
FZ-21	36.3	61.7	1.76	0.18	0.14
FZ-21	37.3	60.4	2.23	0	0.11
FZ-21	38.1	60.5	1.22	0.11	0.1
FZ-21	36.5	61.8	1.48	0.06	0.14
FZ-21	36.5	62.1	1.16	0.17	0.14
FZ-21	35.7	61.5	2.55	0.02	0.2
FZ-21	35.9	61.4	2.29	0.15	0.3
FZ-21	37.7	60.7	1.35	0.17	0.06
FZ-21	36.5	61.2	2.28	0	0.06
FZ-21	35.7	62.2	2.07	0	0.07
FZ-21	36.2	61.5	2.17	0.17	0
FZ-21	36.8	60.1	3.02	0	0.06
FZ-21	38.1	60.4	1.51	0	0.02
FZ-21	36.1	61.7	2.04	0.05	0.18
FZ-21	36.3	61.5	1.72	0.17	0.29
FZ-21	36.8	60.8	1.5	0	0.44
FZ-21	36.8	61	1.11	0.75	0.4
FZ-21	36.1	62.1	1.75	0.06	0
FZ-21	36.2	62	1.63	0	0.18
FZ-21	36.7	62	0.93	0.16	0.24

Table A-7, continued: Microprobe analyses (wt% oxides) of zircons from sample 4021A

zircon	SiO_2	ZrO_2	HfO_2	ThO_2	UO_2
4021A-40	35.5	61.1	2.49	0.05	0.82
4021A-40	35.8	62.1	1.76	0.16	0.16
4021A-40	38.4	59.3	2.04	0.13	0.18
4021A-40	36.2	61.3	2.31	0.05	0.14
4021A-40	35.8	62	1.95	0.14	0.14
4021A-40	35.6	60.8	2.63	0.56	0.45
4021A-40	36	61.3	2.47	0	0.26
4021A-40	35.9	60.9	3.15	0	0
4021A-40	35.7	59.8	3.91	0.28	0.26
4021A-40	36.1	61.3	2.52	0.04	0.07
4021A-40	35.9	61.5	2.1	0.23	0.25
4021A-40	35.8	60.3	3.6	0.01	0.24
4021A-40	36.3	61.4	1.77	0.16	0.35
4021A-40	37.8	59.9	1.89	0.15	0.25
4021A-40	35.8	60.8	2.62	0.55	0.27
4021A-40	35.5	60.7	3.41	0.22	0.2
4021A-40	35.7	61.6	2.48	0	0.21

zircon	SiO_2	ZrO_2	HfO_2	ThO_2	UO_2
4021A-6	39.2	58	2.75	0.0	0.09
4021A-6	38.7	59.5	1.72	0.02	0.11
4021A-6	36.1	61.1	2.6	0.20	0.02
4021A-6	36.5	61.1	2.02	0.17	0.16
4021A-6	36.0	61.8	2.08	0.05	0.12
4021A-6	38.5	58.9	2.36	0.15	0.09
4021A-6	36.3	61.4	2.27	0.0	0.06
4021A-6	36.7	60.8	2.44	0.0	0.0
4021A-6	37.9	59.7	2.04	0.14	0.17
4021A-6	36.1	61.1	2.7	0.0	0.08
4021A-6	38.3	58.7	3.01	0.0	0.05
4021A-6	36.2	61.5	2.25	0.0	0.0
4021A-6	36.2	62.1	1.65	0.12	0.0
4021A-6	40.9	57.2	1.83	0.06	0.1
4021A-6	37.2	60.4	2.35	0.04	0.0

zircon	SiO_2	ZrO_2	HfO_2	ThO_2	UO_2
4021A-7	36.8	60.1	2.43	0.38	0.34
4021A-7	40.1	58.9	0.86	0.0	0.15
4021A-7	39.9	58.2	1.84	0.0	0.0
4021A-7	39.1	58.8	1.87	0.1	0.18
4021A-7	36.6	61.1	1.54	0.22	0.51
4021A-7	32.7	66.3	2.52	0.0	0.0
4021A-7	32.9	65.2	1.18	0.66	0.84
4021A-7	32.8	65.5	2.49	0.07	0.12
4021A-7	32.6	65.1	3.47	0.01	0.0
4021A-7	32.5	65.6	2.05	0.19	0.62
4021A-7	36.3	61.4	1.9	0.17	0.25
4021A-7	36	61.5	2.57	0.0	0.0
4021A-7	36.2	61.1	1.85	0.26	0.55
4021A-7	36.4	60.3	1.82	0.51	0.82
4021A-7	37.2	59.5	1.43	0.78	1.07
4021A-7	38.8	59.7	1.49	0.05	0.0
4021A-7	37.2	59.1	1.54	1.04	1.1
4021A-7	37.2	60.5	1.2	0.44	0.63
4021A-7	36.5	61.5	2	0.0	0.02
4021A-7	38.4	59	1.73	0.49	0.38
4021A-7	36.8	61.5	1.6	0.07	0.01
4021A-7	37.3	60.6	1.49	0.29	0.31
4021A-7	36.1	61.6	2.29	0.02	0.0
4021A-7	36.3	61	2.31	0.11	0.3
4021A-7	37.6	60.1	1.42	0.0	0.0
4021A-7	38	58.8	1.16	0.92	1.14
4021A-7	39.6	58.7	1.19	0.13	0.39

Appendix B: Rock chemical analyses

I developed an XRF routine for analyzing major oxides and selected trace elements on relatively fine-grained Pogo rocks, as described in Chapter 1. I calibrated it from commercial chemical analyses of selected rocks combined with well-characterized international standards made into pressed pellets. In addition, I had a few commercial chemical analyses of selected drill core intervals supplied by the Chief Geologist at Pogo. For rocks that I suspected hydrothermal alteration, I also analyzed for S, As, Pb, and Zn using a separate routine. For some orthogneiss samples, I also analyzed for Th.

In these tables I use the following abbreviations: FB = Football, pgn = paragneiss, otg = orthogneiss, WP = within-plate, VA = volcanic arc, alt'd = altered, QD = quartz diorite, ton = tonalite, grd = granodiorite, peral = peraluminous, metal = metaluminous, serp = serpentinite, T = Tertiary, syen = syenite, dk = dike. For CIPW normative minerals I use these abbreviations: Qtz = quartz, Alb = alb, Orth = or, Anor = an, Cor = corundum, Di = diopside, Hyp = hypersthene, Ilm = ilmenite, Mt = magnetite, Ap = apatite, Pyr = pyrite.

Drill hole depths are in feet, UTMs are in meters.

Table B-1: location and selected trace element data for analyzed Pogo rocks

Sample #	rock type	UTM E	UTM N	Drill Hole	Elev/ Depth	Cr	Nb	Rb	Sr	V	Y	Zr
753 SA	FB Ton	600275	7149104	UG		2	10	49	341	24	20	36
753 SA-am	amphib					274	1	62	258	153	7	12
765	pgn					49	8	94	226	79	9	122
1023 SA	peral gr	600509	7149051	UG		3	4	184	64	1	9	29
1170ED RA	LieseQD	600882	7149033	UG		84	6	60	340	191	18	87
1170ufEDRA	LieseQD	601076	7149217	UG		71	6	51	310	226	16	83
1250 SA	peral gr	600176	7149212	UG		3	10	361	24	1	11	20
1271 Cut #8A	peral gr	600371	7149455	UG		0	12	278	159	10	21	41
1271 Cut#8B	LieseTon	600371	7149455	UG		47	8	78	260	121	19	143
1352	amphib					197	13	40	360	226	28	151
1637	peral gr	600447	7149616	UG	966	0	8	225	80	2	18	43
1660	peral gr	600484	7149616	UG	949	0	8	197	69	2	13	31
1703	peral gr	600566	7149618	UG	905	0	7	153	107	1	11	29
1744	peral gr	600649	7149621	UG	867	0	12	299	31	0	5	23
1745	peral gr	600667	7149622	UG	859	0	8	164	91	3	14	53
1745#2	peral gr	600667	7149622	UG	859	0	9	175	93	3	17	49
1759	peral gr	600686	7149622	UG	852	0	4	233	89	0	13	34
2100-4	peral gr	600686	7148717	UG	2096	0	14	215	10	1	9	22
RN831B	maf dike	606693	7146306			210				148		
MBW765A	maf dike	605007	7147799			205				121		
09U031A	amphib			09U031	182'	212	24	23	265	264	63	318
10U007A	amphib			10U007	311'	286	2	6	134	250	23	51
11RN338A	amphib	608185	7145088			166	1	7.3	187	409	29	75
11RN341A	amphib					264	2	46	489	178	4	10
14-739A	LieseTon			14-739	370'	20	5	53	335	139	17	104
14WT17	FB Ton	604839	7147841			6	8	62	396	94	20	130
14WT18	FB Ton	604853	7147931			1	8	66	347	59	14	132
14WT35	LieseTon	603257	7147365			18	9	76	308	82	22	120
14WT55B	FB Ton	603397	7147913			0	8	48	307	77	15	73
14WT56	FB grd	603357	7147962			1	8	93	274	70	17	98
14WT61	FB Ton	603341	7148054			0	9	84	298	58	17	123
14WT62	FB Ton	603415	7148005			3	10	78	370	63	18	116
14WT63	FB Ton	603415	7148217			4	9	68	291	59	17	113
14WT66A	peral gr	603356	7148288			0	7	153	164	23	15	102
14WT70	LieseTon	604799	7147327			85	8	66	316	153	20	147
14WT742A	FB Ton	601106	7149336			0	9	104	239	53	21	154
14WT742B	LieseQD	601106	7149336			33	6	50	335	195	19	88
14WT742C	LieseQD	601222	7149187			136	6	42	333	184	17	124
14WT744A	FB Ton	602540	7148410			0	7	68	298	31	16	113
14WT744B	LieseQD	602540	7148410			94	6	33	422	227	16	37
14WT745	LieseQD	602428	7147856			95	6	58	317	237	17	52
14WT746	LieseTon	601930	7148211			73	6	50	358	166	18	94

Table B-1, continued: location and selected trace element data for analyzed Pogo rocks

Sample #	rock type	UTM E	UTM N	Drill Hole	Elev/ Depth	Cr	Nb	Rb	Sr	V	Y	Zr
14WT748	LieseQD	602279	7148545			137	3	22	445	288	14	33
14WT753	peral gr	603044	7146839			0	9	153	204	17	12	113
14WT754	LieseQD	603264	7147354			55	5	50	375	245	19	78
14WT755	FB grd	603313	7147650			1	7	80	280	51	19	100
14WT755	FB Ton	603313	7147650			1	9	83	311	44	16	127
14WT756	FB grd	603374	7147799			0	8	84	308	27	12	115
14WT757	FB grd	603459	7147814			0	8	95	298	12	8	119
14WT758	FB grd	603379	7147919			1	6	78	286	52	17	100
14WT759	LieseTon	603299	7147939			15	7	48	429	93	19	142
14WT760	FB grd	603322	7148049			0	8	99	278	43	15	125
14WT761	FB Ton	603369	7148179			4	9	68	320	65	18	124
14WT763	FB Ton	603360	7148283			0	8	75	283	60	12	113
14WT764	FB Ton	603369	7148384			4	7	59	340	70	19	115
14WT767	metal gr	604711	7147321			0	7	103	164	4	25	87
14WT768	LieseTon	604809	7147554			56	7	70	310	179	18	126
14WT769A	LieseQD	604809	7147724			67	6	96	333	248	28	55
14WT769B	maf dk	604809	7147724			213	23	53	339	140	39	261
14WT770	LieseTon	604899	7147939			12	7	75	402	89	17	139
14WT771	LieseTon	604894	7147994			82	7	39	335	175	18	104
14WT772	FB Ton	604907	7148244			0	13	69	372	51	20	149
14WT773	FB Ton	604929	7148704			0	7	67	296	61	18	124
14WT82	FB Ton	604841	7147848			2	7	57	340	42	8	107
14WT84A	FB Ton					0	6	67	400	50	15	158
14WT85	FB Ton	604894	7148199			0	10	73	387	48	16	128
14WT86	FB Ton	604925	7148329			0	19	55	355	40	19	173
14WT87	FB Ton	604910	7148449			0	12	61	350	38	14	144
14WT89	FB Ton					0	9	66	374	41	14	125
14WT90A	maf dk	604917	7148611			197	24	59	342	154	39	263
14WT90B	FB Ton	604917	7148611			0	8	65	314	65	19	130
14WT91A	FB Ton	604913	7148644			1	8	61	330	68	29	103
1525-mfd1	Liese dk					54	8	62	300	147	20	137
1525-mfd2	Liese dk					65	8	45	296	192	20	137
15-791A	Liese dk			15-791	916'	122	9	58	874	206	19	125
15-878A	LieseQD			15-878	1169'	130	8	60	311	207	28	28
15-878A	LieseTon			15-878	1087'	135	6	75	320	164	19	89
15-885-1356	VAgr otg			15-885	1356	0	11	76	263	7	30	87
15DL04	LieseTon	603161	7148021			29	8	73	321	100	19	186
15DL05	FB grd	603255	7148057			3	7	88	266	47	13	102
15PUC01	peral gr					0	5	226	21	1	6	23
15PUC02	peral gr					0	8	264	92	3	17	33
15PUC03	metal gr					0	5	65	227	2	18	83
15PUC05	VAgr otg					0	10	113	180	32	18	92
15PUC06	WPgr otg					0	32	132	328	13	28	46

Table B-1, continued: location and selected trace element data for analyzed Pogo rocks

Sample #	rock type	UTM E	UTM N	Drill Hole	Elev/ Depth	Cr	Nb	Rb	Sr	V	Y	Zr
15PUC07	LieseQD	600831	7149164	15EXP8	82	43	4	49	358	153	12	72
15PUC08	LieseTon	600780	7149156	15EXP8	277	43	4	52	308	150	13	56
15PUC09	LieseTon	600632	7149143			38	14	108	354	118	14	155
15PUC10	metal gr	600632	7149143	15EXP8	840	0	7	142	79	4	14	36
15PUC11	LieseTon	601124	7148154	15-859	1142	88	7	54	391	144	18	81
15PUC13	LieseTon	601122	7148125	15-859	1287	45	7	60	358	144	15	110
15PUC14	FB Ton	600036	7149756	15-786	157	0	9	61	247	65	20	186
15PUC15	FB Ton	600041	7149752	15-786	212	0	12	59	228	56	19	186
15PUC16	WPgr otg	600152	7150071	15-849	740	0	52	160	136	5	65	54
15PUC17	VAgr otg	600152	7150072	15-849	745	0	16	146	159	2	9	62
15PUC19	alt'd otg	601133	7148380	15-860	115	0	9	169	81	7	18	124
15PUC20	Liese dk	601132	7148379	15-860	144	33	6	94	279	102	29	117
15PUC21	peral gr	600198	7150062	15-834	279	0	10	236	57	2	14	32
15PUC22	peral gr	600203	7150069	15-834	324	0	10	232	57	1	12	27
15PUC23	peral gr	600214	7150084	15-834	413	0	9	210	70	3	16	38
15PUC24	ALT'D!	600225	7150101	15-834	513	0	9	195	31	2	15	34
15PUC25	ALT'D!	600233	7150113	15-834	583	0	13	154	42	3	15	39
15PUC26	peral gr	600238	7150120	15-834	626	0	10	190	79	2	18	38
15PUC27	peral gr	600248	7150135	15-834	715	0	6	189	83	3	16	39
15PUC28	serp					1522			5	21		
15PUC29	VAton ot	600193	7150054	15-851	812	0	17	51	462	22	14	77
15PUC30	VAgr otg	600199	7150063	15-851	1001	0	10	200	177	10	36	43
15PUC31	VAgr otg	600199	7150063	15-851	1013	0	19	205	87	15	18	100
15PUC32	WPgr otg	600200	7150064	15-851	1022	0	36	209	89	15	66	142
15PUC33	WPgr otg	600202	7150067	15-851	1079		41	206	104	14	85	145
15PUC34	WPgr otg	600204	7150071	15-851	1163	0	63	219	73	3	56	202
15PUC35	syen otg	600205	7150071	15-851	1178	0	99	209	53	0	90	164
15PUC36	amphib	600507	7149324			415	4	122	853	217	43	72
15PUC37	alt'd pgn	600558	7149280	15U259	362	92		35	32	105	21	30
15PUC38	LieseQD	600559	7149278			98	6	55	303	199	24	91
15PUC40	LieseQD	600576	7149257	15U259	463	54	6	43	328	181	35	46
15PUC41	peral gr	599994	7149916	15-828	797	0	11	276	19	1	23	61
15PUC42	peral gr	599993	7149922	15-828	828	0	8	322	14	0	6	16
15PUC43	peral gr	599993	7149926	15-828	850	0	12	248	42	2	22	32
15PUC44	FB Ton	600273	7150009	15-836	556	0	14	69	248	69	18	210
15PUC45	LieseQD	601986	7147058	15-878	231	107	9	80	284	173	21	84
15PUC46	LieseTon	601884	7147171	15-878	1010	100	8	85	306	147	19	97
15PUC47	LieseTon	601880	7147176	15-878	1040	83	4	82	298	162	26	85
15PUC48	LieseQD	601818	7147245	15-878	1517	86	8	64	325	211	19	86
15PUC49	peral gr			15EXP14	393.5	0	5	193	44	2	15	37
15PUC50	pgn			15EXP14	399	0	6	153	12	1	24	26
15PUC51	LieseQD			15EXP09	228	73	6	55	282	205	27	59
15PUC52	amphib			15EXP09	365	368	2	15	271	227	25	18

Table B-1, continued: location and selected trace element data for analyzed Pogo rocks

Sample #	rock type	UTM E	UTM N	Drill Hole	Elev/ Depth	Cr	Nb	Rb	Sr	V	Y	Zr
15PUC53	alt'd ampib			15EXP9	378	197	4	27	377	313	14	21
15PUC54	LieseQD			15EXP9	493	91	6	54	292	371	19	64
15PUC55	peral gr			15EXP9	936	0	4	188	90	1	18	34
15PUC56	peral gr			15EXP9	983	0	5	227	68	2	13	34
15PUC57	LieseTon			15EXP9	1772	22	11	93	327	102	19	149
15PUC58	syen otg	600063	7150054	15-845	1243	0	53	193	22	0	42	320
15PUC59	syen otg	600059	7150056	15-845	1288	0	42	133	20	0	56	74
15PUC60	VAgr otg	603055	7146611	15-885	1356	0	9	77	255	12	30	116
15PUC61	Liese dk			15EX16	549	22	8	99	298	117	24	136
15PUC62	peral gr			15EX16	566	0	5	216	30	0	14	40
15PUC63	peral gr			15EP15	595	0	3	199	89	1	14	33
15PUC64	peral gr	600200	7150013	15-836	177	0	10	223	85	4	18	37
15PUC65	ALT'D!	600237	7150011	15-836	370	0	22	358	108	20	50	103
15PUC66	LieseTon	601312	7148216	15-857	1157	62	7	57	323	159	18	68
15PUC67	pgn			15EX17	520	0	5	97	137	9	20	118
15PUC68	VAgr otg			15EX17	559	0	7	170	155	11	26	66
15PUC69	LieseTon			15EX17	639	24	8	56	359	118	23	131
15PUC70	LieseTon			15EX17	641	33	7	75	328	119	21	145
15PUC71	LieseTon			15EX17	655.5	24	8	51	349	122	22	132
15PUC72	alt'd Liese			15EX17	668	13	10	240	21	98	23	145
15PUC73	peral gr	600192	7150003	15-839	134	0	8	224	57	1	13	30
15PUC74	peral gr	600201	7149999	15-839	177	0	5	156	38	1	11	41
15PUC75	ser alt'd	600214	7149993	15-839	246	0	10	314	81	13	22	70
15PUC76	alt'd FB	600219	7149991	15-839	273	0	20	182	80	66	22	239
15PUC77	alt'd FB	600221	7149990	15-839	280	0	16	139	117	72	19	210
15PUC78	alt'd FB	600221	7149990	15-839	281	0	19	80	140	67	23	238
15PUC79	FB Ton	600221	7149990	15-839	281	0	15	64	233	62	17	199
15PUC80	FB Ton	600222	7149990	15-839	286	0	10	71	227	67	22	210
15PUC81	FB Ton	600222	7149990	15-839	288	0	14	56	217	61	18	191
15PUC82	peral gr			15-839	368	0	3	172	144	4	8	20
15PUC83	peral gr			15-839	523	0	5	168	297	15	7	53
15PUC84	FB grd			15-839	558	0	13	89	219	59	28	173
15PUC85	peral gr			15-839	578	0	26	343	18	2	5	21
15PUC86	peral gr	600281	7149964	15-839	592	0	30	389	37	2	6	39
15PUC87	LieseTon	602045	7147025	15-880	145	90	8	83	286	147	19	99
15PUC88	LieseTon	602085	7147027	15-880	348	86	9	96	281	152	19	103
15PUC89	LieseTon	602091	7147027	15-880	378	91	7	81	276	143	18	90
15PUC90	LieseTon	602096	7147027	15-880	405	91	8	83	263	145	20	100
15PUC91	LieseTon	602120	7147028	15-880	526	92	8	82	264	178	19	121
15PUC92	WPgr otg					0	38	90	414	24	22	114
15PUC94	VAgr otg					0	5	80	176	10	11	93
15PUC95	VAgr otg					0	8	89	219	40	18	108

Table B-1, continued: location and selected trace element data for analyzed Pogo rocks

Sample #	rock type	UTM E	UTM N	Drill Hole	Elev/ Depth	Cr	Nb	Rb	Sr	V	Y	Zr
15PUC96	metal gr					0	8	128	141	20	22	102
15PUC97	WPgr otg					0	37	78	184	17	27	72
15PUC98	FB Ton					0	8	91	254	43	15	124
15PUC99	peral gr					0	9	219	40	2	19	28
15PUC100	metal gr	601126	7148389	15-905	127	0	7	159	136	8	26	131
15PUC101	alt'd gr	601125	7148389	15-905	147	0	7	189	103	9	24	133
15PUC103	Pgn					0	12	118	80	8	24	125
15PUC104	Pegmatite	too	coarse	15-905	763	0	2	162	267	4	9	15
15PUC105	peral gr			15-905	823	0	8	312	172	5	26	30
15PUC106	VAgrd otg			15-905	954	0	3	72	357	8	14	28
15PUC107	peral gr	601056	7148402	15-905	1037	0	2	135	236	3	7	140
15PUC108	Pegmatite	too	coarse	15-905	1296	0	2	37	126	5	4	51
15PUC109	peral gr	601035	7148406	15-905	1297	0	5	224	81	2	13	14
15PUC110	peral gr			15-892	527	0	6	189	105	2	6	29
15PUC111	metal gr	601747	7149636	15-892	840	0	7	116	227	12	13	75
15PUC112	VAgr otg	601749	7149636	15-892	861	0	12	109	194	34	28	130
15PUC113	LieseTon					31	8	45	262	103	17	81
15PUC114	WPgr otg					0	32	102	260	13	30	72
15PUC115	WPgr otg					0	41	155	207	11	29	31
15PUC116	WPgr otg					0	57	118	273	16	23	102
15PUC117	WPgr otg	604303	7147153	11-639	101	0	76	81	294	34	70	128
15PUC118	WPgr otg	603026	7146567	15-885	1629	0	54	135	255	33	77	101
15PUC119	WPgr otg	604499	7147077	11-656	423	0	58	88	203	11	37	50
15PUC120	WPgr otg	604337	7147168	11-640	154	0	48	104	309	13	59	43
15puc121A	WPgr otg	604298	7147153	11-639	140		51	112	265	20	61	35
15puc121B	WPgr otg	604298	7147153	11-639	140		49	109	266	9	47	61
15PUC122	WPgr otg	604512	7146927	11-655	770	0	87	93	281	19	34	75
15PUC123	WPgr otg	604500	7147074	11-656	371	0	40	111	386	19	36	60
15PUC124	syen otg	600117	7150230	13-590	3271	1	28	280	77	1	40	44
15PUC125	WPgr otg	604501	7147068	11-656	283	1	78	96	276	15	41	82
15PUC126	syen otg	599837	7150197	15-846	2008	3	19	111	32	0	46	46
15puc127A	syen otg	600050	7150059	15-845	1400	1	44	124	93	9	32	75
15puc127B	syen otg	600050	7150059	15-845	1400	2	37	122	99	1	33	84
15PUC128	LieseTon	600630	7148402	15E13	486	20	7	57	323	119	21	127
15PUC129	peral gr					0	8	363	19	1	12	23
15PUC130	metal gr	601082	7148603	15-853	473	0	8	105	197	6	18	119
15PUC131	LieseTon	601150	7148384	15-856	181	30	8	84	383	134	22	138
15PUC132	Liese dk	601345	7148184	15-857	1376	54	6	45	339	174	17	115
15PUC133	Liese dk	601106	7148380	15-888	165	16	8	62	323	116	23	139
15PUC134	metal gr	600924	7148613	15-852	1291	0	8	92	193	7	17	112
15PUC135	LieseTon	601104	7148645	15-853	1171	97	7	50	316	166	20	121
15PUC136	LieseTon	604298	7147153	11-639	145	11	10	66	385	116	23	131

Table B-1, continued: location and selected trace element data for analyzed Pogo rocks

Sample #	rock type	UTM E	UTM N	Drill Hole	Elev/ Depth	Cr	Nb	Rb	Sr	V	Y	Zr
15PUC137	LieseTon	604303	7147153	11-639	103	11	19	47	296	109	21	121
15PUC138	LieseTon	604334	7147166	11-640	133	11	23	70	312	83	13	72
15PUC139	LieseTon	604337	7147168	11-640	154	5	11	55	467	104	25	128
15PUC141	LieseTon	604500	7147076	11-656	408	10	15	106	287	77	27	151
15PUC143	LieseTon	603884	7147442	13-609	531	78	8	117	288	185	19	127
15PUC144	LieseTon	604003	7147443	13-624	300	51	7	75	326	157	18	92
15PUC145	LieseTon	603954	7147445	13-625	250	61	6	57	364	172	18	85
15PUC146	FB Ton	599966	7149592	15-793	986	2	15	72	231	72	22	204
15PUC147	LieseQD	601130	7148694	15-853	1975	136	5	41	327	164	17	101
15PUC148	LieseQD	601242	7148544	15-855	1714	72	5	49	346	191	13	59
15PUC149	LieseTon	601228	7148369	15-856	1189	48	7	70	320	95	18	99
15PUC150	LieseTon	601225	7148301	15-857	585	83	5	62	468	117	25	59
15PUC151	LieseTon	601312	7148217	15-857	1155	65	6	65	488	130	17	74
15PUC152	LieseTon	601122	7148126	15-859	1278	60	7	56	318	156	17	98
15PUC153	LieseTon	601105	7148318	15-860	1192	48	7	63	334	146	18	104
15PUC154	LieseTon	601115	7148339	15-860	817	49	6	57	343	132	18	110
15PUC155	LieseTon	602088	7147171	15-879	830	52	6	48	374	125	16	105
15PUC156	LieseTon	600152	7150023	15-846	90	58	8	70	334	151	18	106
15PUC157	LieseTon	603877	7147562	13-610	839	65	7	67	309	155	19	82
15PUC158	LieseTon	600033	7149718	15-791	300	54	7	67	306	153	16	84
15PUC159	VAton ot	604381	7147143	11-641	466	3	15	60	249	86	18	227
15PUC160	peral gr	600300	7149862	14-631	1394	3	9	212	78	1	17	37
15PUC161	peral gr	600447	7150003	14-681	1110	2	8	231	79	1	19	24
15PUC162	peral gr	600061	7149608	15-791	950	3	6	178	22	1	7	21
15PUC163	peral gr	600005	7149827	15-827	672	4	13	233	29	1	16	36
15PUC164	peral gr	600084	7149775	15-831	298	3	21	358	24	1	20	43
15PUC165	peral gr	600284	7149994	15-837	1198	3	11	203	85	3	16	40
15PUC166	peral gr	600215	7149988	15-838	271	2	10	223	73	0	15	32
15PUC167	peral gr	599955	7150050	15-844	1364	2	14	225	82	2	15	39
15PUC168	metal gr	600925	7148612	15-852	1281	0	6	137	308	11	24	72
15PUC169	metal gr	601156	7148383	15-856	263	2	10	123	143	12	28	69
15PUC170	pgn	601113	7148336	15-860	871	28	2	94	163	26	21	106
15PUC171	WPgr otg	602651	7146424	15-882	472	0	89	107	222	16	48	107
15PUC172	metal gr	603094	7146670	15-885	998	0	8	139	185	2	19	38
15PUC173	metal gr	603324	7146750	15-886	765	0	12	172	87	2	14	36
15PUC174	metal gr	603413	7146691	15-886	1308	3	19	135	77	2	19	31
15PUC175	VAgr otg	603419	7146687	15-886	1346	0	10	93	143	2	34	105
15PUC176	alt'd gr	600835	7148317	15-888	1645	2	13	127	78	2	18	21
15PUC177	peral gr	601462	7149899	15-893	996	3	10	173	81	3	13	35
15PUC178	peral gr	601456	7149909	15-893	909	3	6	168	45	1	16	80
15PUC179	peral gr	601284	7150201	15-897	3201	3	8	190	44	1	9	19
15PUC180	VAgr otg	601174	7148349	15-857	253	1	8	165	95	4	25	84
15PUC181	VAgr otg	603959	7147429	13-625	566	4	11	95	234	75	20	120

Table B-1, continued: location and selected trace element data for analyzed Pogo rocks

Sample #	rock type	UTM E	UTM N	Drill Hole	Elev/ Depth	Cr	Nb	Rb	Sr	V	Y	Zr
15PUC182	VAgrd ot	603662	7147370	13-634	604	9	12	102	212	88	23	140
15PUC183	VAgr otg	604376	7147197	11-640	507	4	10	178	149	12	14	100
15PUC184	pgn	604504	7147052	11-656	47	1	7	114	119	1	28	128
15PUC185	VAgr otg	603878	7147441	13-609	575	3	9	97	196	21	27	110
15PUC186	VAgr otg	603170	7146787	15-885	286	1	9	94	273	1	27	109
15PUC187	VAgrd ot	604250	7147151	11-639	513	4	8	89	224	54	16	97
15PUC188	VAG otg	604380	7147199	11-640	540	4	12	179	89	10	36	75
15PUC189	VAG otg	601095	7148629	15-853	896	3	11	279	63	3	39	66
15PUC190	VAgrd ot	604243	7147076	11-642	521	5	9	78	193	39	11	85
15PUC191	VAgrd ot	603959	7147429	13-625	568	4	10	90	257	63	18	122
15PUC192	WPgr otg	604381	7147143	11-641	466	3	28	168	107	9	52	77
15PUC193	VAgrd ot	600650	7149947	13-737	600	8	10	106	218	63	21	139
15PUC194	WPgr otg	599857	7149734	15-825	1294	3	26	169	14	0	61	21
15PUC195	VAgrd ot	604282	7147152	11-639	263	2	11	95	212	49	30	110
15PUC196	VAgr otg	604065	7147427	13-624	650	5	11	95	283	13	24	127
15PUC197	VAgr otg	601095	7148629	15-853	897	3	11	260	61	1	36	80
15PUC198	WPgr otg	604291	7147153	11-639	196	0	24	67	308	3	57	129
15PUC199	LieseQD	601687	7148064	16-935	1798	65	6	64	362	121	17	104
15PUC200	LieseQD	600920	7148100	16-975	845	27	6	63	331	96	17	123
15WT01	LieseTon	601980	7147400			61	6	66	318	153	24	73
15WT02	FBgrd dk	601945	7147382			4	10	81	437	49	17	197
15WT03	FB grd	601310	7147090			2	10	112	245	27	25	134
15WT04	FB Ton	601310	7147090			3	18	63	200	64	23	147
15WT05	VAgrd ot	600480	7147680			1	16	78	194	55	23	149
15WT06	Pgn	600480	7147680			53	15	127	269	70	9	164
15WT07	LieseTon	601860	7147990			62	8	64	319	141	17	86
15WT08	LieseTon	601825	7148065			67	6	56	328	149	19	107
15WT09	metal gr	601070	7148575			0	7	117	183	9	13	84
15WT10	Pgn	601070	7148575			29	10	76	126	38	16	216
15WT11	Pgn	601615	7149765			88	9	92	151	76	16	131
15WT12	VAgr otg	601375	7150200			0	9	109	204	28	27	135
15WT13	Pgn	601290	7150445			76	6	83	54	60	24	148
15WT14	LieseQD	601120	7149200			97	4	52	321	197	15	72
15WT15	LieseTon	601473	7148295			74	6	55	307	130	22	70
15WT16	LieseTon	601370	7148253			39	8	65	369	123	26	95
15WT17	LieseTon	601690	7148219			42	5	47	337	138	14	79
15WT18	LieseQD	601874	7147957			41	6	59	348	147	21	49
15WT19	LieseTon	602687	7147627			76	5	51	365	136	15	88
15WT20	LieseTon	601622	7147642			74	6	50	358	138	15	94
15WT21	VAgr otg	601628	7147706			1	6	134	172	9	29	69
15WT22A	peral gr	601669	7147820	S. Pogo		0	5	164	276	24	11	137
15WT22B	peral gr	601669	7147820	S. Pogo		1	5	161	275	19	12	146
15WT23	LieseTon	601583	7147165			52	7	91	286	124	17	109

Table B-1, continued: location and selected trace element data for analyzed Pogo rocks

Sample #	rock type	UTM E	UTM N	Drill Hole	Elev/ Depth	Cr	Nb	Rb	Sr	V	Y	Zr
15WT24	pgn	601429	7147128			18	8	70	159	28	12	200
15WT25	LieseTon	601512	7147128			55	8	95	317	136	18	133
15WT26	VAgrd ot	600490	7150165			23	10	79	239	48	26	31
15WT27#1	VAG otg	604506	7147045	4021B			8	136	168	2	23	69
15WT27#2	VAG otg	604506	7147045	4021B			10	145	143	2	26	72
15WT28B	VAton ot	604475	7147027			22	5	70	175	90	21	145
15WT28C	peral gr	604475	7147027			2	5	169	60	1	14	36
15WT29	VAgrd otg	603805	7147307			2	8	97	244	46	22	120
15WT30	FB Ton	603621	7147427			8	7	91	291	55	15	128
15WT31	LieseTon	603513	7147537			63	5	65	301	168	15	49
15WT32	LieseQD	603497	7147699			39	4	69	510	205	14	52
15WT33	FB Ton	603308	7147983			6	7	75	279	65	18	100
15WT34	FB Ton	603285	7147993			6	8	63	320	75	23	105
15WT35	FB Ton	603356	7148006			6	7	82	268	58	16	96
15WT36	FB Ton	603411	7148050			5	8	67	300	55	18	97
15WT37	FB Ton	603289	7147937			2	7	58	347	31	7	125
15WT38	LieseTon	603254	7147960			8	7	59	360	85	13	79
15WT39	LieseTon	603152	7147916			12	6	63	313	77	19	96
15WT40	FB Ton	603201	7148013			4	8	66	307	65	22	123
15WT41	FB Ton	603140	7148156			2	7	78	323	50	18	117
15WT42	FB Ton	603229	7148133			2	8	83	307	45	20	115
15WT43	T maf dk	604913	7148608			198	16	53	411	146	38	251
15WT44	Pgn	604859	7148805			78	11	83	138	103	15	207
15WT45	Pgn	604857	7148827			42	7	71	101	55	16	112
15WT46	FB grd	601499	7149164			2	13	97	251	15	12	115
15WT47	peral gr	600495	7149308			2	8	188	77	0	10	27
15WT48	peral gr	600671	7149427			1	10	218	11	6	7	23
15WT49	peral gr	600694	7149432			3	5	205	61	1	10	32
15WT50	peral gr	600700	7149469			3	6	195	64	2	7	38
15WT51	peral gr	600701	7149379			2	5	132	52	1	14	27
15WT52	peral gr	600721	7149322			3	14	189	22	0	8	20
15WT53	metal gr	600319	7148930			3	9	195	218	13	43	27
15WT54	metal gr	600274	7148905			0	4	48	362	0	18	35
15WT55	peral gr	600177	7150006			3	12	227	65	2	13	31
15U259a	Liese dk			15U259	129'	114	10	88	1116	192	19	127
15U368A	alt'd liese			15U368	13'	117	5	116	122	218	16	72
16WT01	LieseQD	602476	7147316			72	6	48	333	175	24	60
16WT02	LieseQD	602633	7147199			59	5	62	322	153	12	94
16WT03	LieseTon	602817	7147003			54	5	78	303	134	15	66
16WT04	LieseTon	602996	7146849			46	8	95	275	144	22	101
16WT05	WPgr otg	602998	7146845			0	22	183	33	20	89	113
16WT06	VAgrd ot	603030	7146794			3	12	117	188	36	22	119

Table B-1, continued: location and selected trace element data for analyzed Pogo rocks

Sample #	rock type	UTM E	UTM N	Drill Hole	Elev/ Depth	Cr	Nb	Rb	Sr	V	Y	Zr
16WT08	LieseTon	603200	7147030			64	7	78	326	157	15	87
16WT08	LieseTon	601825	7148065			46	6	85	346	121	15	83
16WT09	LieseTon	603319	7147166			40	6	73	300	161	21	130
16WT10	VAgrd otg	603944	7147271			3	8	95	192	66	30	133
16WT11	LieseTon	603664	7147306			86	6	61	326	205	24	108
16WT12	FB Ton	603187	7148350				6	84	294	49	23	71
16WT13	VAgr otg	603162	7148469				7	136	211	20	19	92
16WT15	peral gr					0	8	163	113	8	12	64
16WT16	VAgr otg	603217	7149167			0	11	105	225	21	18	140
16WT17	VAgrd otg	603183	7149208			0	15	73	208	58	24	123
16WT18	VAgr otg	603147	7149284			0	10	102	274	18	19	135
16WT19	VAgr otg	603080	7149259			0	10	105	256	25	32	136
16WT20	peral gr	602674	7149221			0	5	194	65	4	13	56
16WT-935A	LieseTon	601687	7148064	16-935	1798	121	7	60	340	163	27	70
16WT-935B	amphib					368	10	74	452	179	20	126
16WT-975	LieseTon	600920	7148100	16-975	845	61	7	56	297	142	16	95
17P04-242	pgn			17-004	242	81	36	349	198	105	31	214
17PGN01	pgn	601028	7149514	17EXP04		115	21	140	178	138	23	209
DL04	LieseTon	603161	7148021			45	7	77	304	102	30	168
DL10A	amphib			08-440	1267	372	6	97	296	225	26	179
DL11	WPgr otg			08-440	1284	262	24	144	206	76	44	647
DL11A	pgn			08-440	727	166	7	115	278	104	28	359
DL12A	pgn			08-440	1295	334	21	152	199	95	11	179
DL13A	pgn			08-440	497	395	35	112	263	96	26	289
DL1A	amphib			08-440	1058	234	2	47	115	270	33	66
DL2A	amphib			08-440	1277	267	2	43	411	173	63	203
DL3A	amphib			08-440	999	353	22	17	46	283	6	67
DL4A	amphib			08-440	794	204	2	90	323	301	44	229
DL5A	amphib			08-440	773	234	39	97	327	247	9	323
DL6A	amphib			08-440	1269	652	7	137	233	218	34	121
DL7A	amphib			08-440	562	410	3	152	143	254	41	116
DL82	FB Ton					0	5	63	350	31	6	102
DL8A	amphib			08-440	927	325	14	89	262	183	44	242
DL9A	amphib			08-440	1117	265	14	130	298	165	44	209
MAF1	Liese dk			UG		129	6	71	350	281	22	89
S Pogo1	peral gr	601669	7147820	S. Pogo		0	7	186	265	16	10	134
S Pogo2	peral gr	601669	7147820	S. Pogo		0	7	188	270	17	11	143

Table B-2: major oxide data for analyzed Pogo rocks

Sample #	SiO_2	Al_2O_3	Na_2O	CaO	K_2O	FeO	MgO	MnO	TiO_2	P_2O_5	BaO	S	sum
753 SA	69.2	17.4	5.1	4.4	2.0	0.9	0.5	0.02	0.15	0.28	0.05	0.01	100.1
753 SA-am	53.8	16	3.5	13	1.1	5.4	5.7	0.1	0.23	0.01	0.02		99
765	71.7	11.6	1.8	2.5	2.2	6.1	1.8	0.1	0.9	0.1	0.1		
1023 SA	75.7	12.9	2.1	1.3	4.3	0.6	0.2	0.02	0.05	0.19	0.03	0.1	97.6
1170ED RA	55.7	15.9	2.2	7.9	1.6	6.8	4.4	0.13	0.68	0.1	0.12		95.6
1170ufEDRA	58.3	17.3	2.6	8.4	1.4	6.2	4.4	0.11	0.78	0.10	0.10	0.04	99.7
1250 SA	72.5	13.3	3.4	0.5	4.4	0.9	0.1	0.24	0.01	0.2	0.01		95.5
1271Cut #8A	70.7	14.9	1.4	1.0	9.2	0.3	0.3	0.01	0.18	0.24	0.23	0.02	98.4
1271Cut#8B	66.9	15.1	2.3	5.6	1.8	4.4	2.6	0.07	0.62	0.12	0.10	0.04	99.6
1352	58.4	16.7	3.3	8.1	1.1	6.4	4.3	0.12	1.2	0.24	0.05	0.06	99.9
1637	76.3	13.7	2.8	0.6	5.1	0.8	0.2	0.02	0.10	0.21	0.03	0.04	100.0
1660	75.3	14.2	2.8	0.5	5.8	0.7	0.2	0.02	0.08	0.13	0.03		99.8
1703	76.8	14	2.2	1.5	5.8	0.6	0.2	0.02	0.08	0.19	0.03		101.5
1744	75.6	14.3	3.5	0.7	5.5	0.5	0.2	0.07	0.01	0.27	0.02		100.7
1745	75.1	14	2.7	1	5.4	0.9	0.3	0.03	0.08	0.13	0.04		99.7
1745#2	75.4	14.3	2.9	1.1	5.3	0.8	0.3	0.03	0.06	0.12	0.04		100.3
1759	76.7	13.1	3.1	0.9	5.0	0.6	0.2	0.02	0.05	0.17	0.03	0.12	99.8
2100-4	75.9	14.3	3.8	0.6	4.6	0.5	0.1	0.06	0.02	0.05	0.01		99.9
RN831B	53.6	14.2	2.7	7.9	2.1	10	6.3	0.16	2.11	0.49	0.06		99.8
MBW765A	51.5	14.3	2.8	8.8	1.2	11	5.5	0.18	2.36	0.61	0.08		98.4
09U031A	51.5	15.2	4.2	8.3	1	10.6	4.6	0.2	2.01	0.65	0.06		98.3
10U007A	50.9	17.1	2.7	11	0.2	7.7	7.7	0.16	1.02	0.1	0.01		99
11RN338A	56.7	16.2	4.5	7.9	0.4	8.7	4.1	0.16	1.05	0.21	0.02	0.05	99.9
11RN341A	49.9	18	1.3	13	1	6.4	10	0.12	0.2	0.03	0.03	0.01	99.8
14-739A	58.4	16.1	2.5	7.6	1.4	7.8	4.6	0.12	0.85	0.12	0.11		99.4
14WT17	62.8	17.2	2.8	6.3	1.7	5.0	2.0	0.10	0.86	0.18	0.14	0.06	99.2
14WT18	63.7	16	2.5	5.6	2	4.7	1.8	0.09	0.81	0.17	0.2		97.5
14WT35	59.3	16.6	2.4	7	2.1	5.9	3.1	0.11	0.92	0.15	0.19		97.9
14WT55B	59.9	17.6	2.4	7.1	1.4	5.9	2.2	0.11	0.97	0.18	0.15		97.8
14WT56	65.8	14.7	2.5	4.3	3.1	4.3	1.7	0.09	0.62	0.11	0.18		97.5
14WT61	66.3	15.4	2.5	4.5	2.6	4	1.6	0.09	0.68	0.16	0.27		98.1
14WT62	64.8	15.8	2.5	4.9	2.4	4.5	1.7	0.09	0.7	0.15	0.22		97.9
14WT63	66.4	14.8	2.4	5.1	2.3	4.2	1.6	0.08	0.68	0.15	0.2		97.9
14WT66A	73.5	13.7	2.4	1.2	4.5	1.8	0.6	0.03	0.25	0.14	0.1		98.1
14WT70	59.3	16.2	2.3	7.2	1.9	6.1	4.1	0.12	0.76	0.12	0.15		98.3
14WT742A	68	13	2.1	2.4	3.7	2.3	0.8	0.03	0.47	0.07	0.13		93.0
14WT742B	52.7	15.5	2.2	7.7	1.4	7.5	4.6	0.14	0.81	0.11	0.12		92.8
14WT742C	55.2	13.3	2.2	10.2	0.5	7.4	5.1	0.19	1.35	0.23	0.15		95.9
14WT744A	68.1	14.9	2.8	4.1	2.5	3.4	1	0.06	0.42	0.09	0.19		97.5
14WT744B	50.7	17.8	1.4	11	0.7	9.3	7.3	0.18	0.86	0.15	0.03		99.5
14WT745	55.2	16.4	2.2	8.4	1.6	7.8	5.3	0.15	0.78	0.11	0.11		98.0
14WT746	58.1	16.2	2.2	7.4	1.5	7	4.5	0.14	0.79	0.11	0.15		98.2

Table B-2, continued: major oxide data for analyzed Pogo rocks

Sample #	SiO_2	Al_2O_3	Na_2O	CaO	K_2O	FeO	MgO	MnO	TiO_2	P_2O_5	BaO	S	sum
14WT748	48	18.1	1.1	11	0.4	10	8.2	0.21	0.88	0.15	0.03		98.8
14WT753	74.4	14	2.8	1.2	4.5	1.3	0.4	0.02	0.21	0.08	0.12		99.1
14WT754	54.5	17.8	2.5	7.9	1.3	7.8	4.6	0.15	0.84	0.14	0.1		97.6
14WT755	69.6	14.7	3.0	4.9	2.4	2.9	1.3	0.04	0.58	0.16	0.18	0.06	99.8
14WT755	67.1	15.1	2.6	4.6	2.4	3.7	1.5	0.05	0.61	0.13	0.2		98.0
14WT756	68.1	14.5	2.6	3.7	2.8	2.9	1.1	0.05	0.52	0.12	0.19		96.6
14WT757	68.6	14.5	2.7	3.3	3.6	2.1	0.7	0.03	0.37	0.09	0.24		96.2
14WT758	66.9	15.3	3.0	4.5	2.8	3.5	1.6	0.07	0.59	0.12	0.13	0.04	98.6
14WT759	59.5	16.7	2.4	6.8	1.4	6.2	2.7	0.12	0.99	0.21	0.16		97.2
14WT760	66.7	14.4	2.4	3.7	3.1	3.4	1.3	0.07	0.54	0.13	0.28		96.0
14WT761	63.9	15.4	2.4	5.2	2.4	4.6	1.8	0.09	0.76	0.15	0.21		97.0
14WT763	67.5	14.8	2.4	4.5	2.5	4	1.5	0.08	0.64	0.13	0.28		98.3
14WT764	62.4	15.4	2.4	5.8	2.2	4.9	1.9	0.1	0.73	0.12	0.16		96.2
14WT767	73.2	13.8	3.2	2	4	1	0.2	0.03	0.08	0.01	0.07		97.7
14WT768	58.6	15.3	2.2	7	2.1	6.9	4.4	0.13	0.89	0.11	0.24		97.9
14WT769A	54.1	16.5	1.5	8.6	1.9	8.4	5.5	0.17	0.9	0.14	0.16		97.9
14WT769B	54.4	12.6	2	7.7	1.4	8.7	5.9	0.13	1.9	0.36	0.07		95.2
14WT770	61.7	16.5	2.4	6.1	1.5	5.4	2.3	0.1	0.81	0.17	0.21		97.3
14WT771	60.3	14.8	2.5	7	1.2	6.2	4.4	0.13	0.73	0.12	0.18		97.5
14WT772	63.8	15	2.4	4.4	2.1	4.8	1.5	0.1	0.76	0.17	0.29		95.4
14WT773	66.6	15.2	2.4	4.4	2.4	4.1	1.5	0.08	0.67	0.13	0.27		97.7
14WT82	67.8	14.6	2.5	4.1	1.7	3.7	1.4	0.06	0.59	0.13	0.16		96.7
14WT84A	64.1	15.9	2.4	6.7	1.7	4.4	1.9	0.14	1.04	0.17	0.24		98.7
14WT85	64.6	15.4	2.6	4.9	2.5	4.5	1.4	0.09	0.71	0.17	0.32		97.4
14WT86	66.1	15.3	2.3	5	1.8	4.7	1.4	0.09	0.84	0.18	0.21		98.1
14WT87	65.4	15.7	2.6	5	2	4	1.3	0.08	0.72	0.17	0.23		97.2
14WT89	65.8	15.2	2.6	4.3	2.2	4.3	1.4	0.08	0.7	0.17	0.24		97.0
14WT90A	53.4	13.6	2.2	8.6	1.7	8.8	5.1	0.21	2.04	0.34	0.09		96.1
14WT90B	64.4	15.2	2.3	5.8	2	4.7	1.8	0.1	0.82	0.16	0.24		97.6
14WT91A	63.4	14.8	2.4	5.1	1.9	4.9	1.9	0.11	0.66	0.14	0.2		95.6
1525-mfd1	65.2	16	2.4	5.7	1.5	5.7	2.3	0.11	0.77	0.12	0.11	0.10	99.9
1525-mfd2	65.6	15.6	2.1	6	0.9	6	2.7	0.12	0.69	0.12	0.09	0.11	99.9
15-791A	54.3	14.2	2.1	9.3	1.2	8.1	8.9	0.16	0.92	0.14	0.16		99.5
15-878A	55.3	16	2.9	8.9	1.5	8	6	0.15	0.91	0.13	0.09		99.7
15-878A	60.4	15.3	2.2	7.2	2.1	6.5	4.7	0.13	0.71	0.11	0.17		99.5
15-885-1356	77.1	11.1	3.2	2.2	3.3	2.0	0.4	0.0	0.1	0.0	0.1		99.4
15DL04	57.8	15.3	2.6	5.2	2.3	5.2	2	0.09	0.87	0.1	0.13		91.6
15DL05	66.9	14.7	2.6	3.9	2.8	3.6	1.4	0.08	0.46	0.11	0.16		96.7
15PUC01	76.9	13.7	3.9	0.5	4.2	0.3	0.3	0.07	0.03	0.23	0.02		100.1
15PUC02	75.7	13.9	2.5	1.2	5.4	0.6	0.4	0.02	0.13	0.22	0.05		100.0
15PUC03	74.5	12.1	3.8	2.4	2.7	0.9	0.3	0.04	0.10	0.01	0.05		96.8
15PUC05	76.4	10.6	2.1	2.4	3.2	2.1	0.7	0.07	0.35	0.05	0.10		98.2
15PUC06	74.3	12.9	3.5	1.1	4.9	0.8	0.6	0.02	0.18	0.09	0.22		98.6

Table B-2, continued: major oxide data for analyzed Pogo rocks

Sample #	SiO_2	Al_2O_3	Na_2O	CaO	K_2O	FeO	MgO	MnO	TiO_2	P_2O_5	BaO	S	sum
15PUC07	56.2	17.0	2.0	9.3	1.2	6.8	5.1	0.21	0.79	0.10	0.11		98.7
15PUC08	58.4	16.2	2.1	8.4	1.3	6.2	4.2	0.19	0.87	0.09	0.11		98.1
15PUC09	60.8	16.7	2.6	6.3	1.0	5.7	3.3	0.2	1.0	0.22	0.09		98
15PUC10	75.4	12.6	2.8	2.1	5.9	0.6	0.4	0.04	0.14	0.14	0.03		100.2
15PUC11	61.2	15.9	2.4	7.4	1.7	6.0	4.4	0.1	0.9	0.14	0.17	0.03	100.2
15PUC13	57.2	15.8	2.2	7.5	1.9	6.3	3.4	0.1	0.8	0.11	0.13		95.5
15PUC14	71.2	14.2	2.8	4.7	2.1	2.7	1.0	0.05	0.64	0.26	0.09	0.02	99.7
15PUC15	73.2	13.7	2.7	4.2	1.8	2.4	0.9	0.03	0.55	0.14	0.06	0.01	99.7
15PUC16	71.1	11.5	1.8	3.1	6.5	0.4	0.5	0.02	0.08	0	0.1		95.0
15PUC17	75.6	11.8	1.6	1	6.4	0.6	0.3	0.01	0.1	0	0.16		97.6
15PUC19	77.2	12.1	2.0	1.1	6.1	1.0	0.3	0.01	0.18	0.06	0.04	0.44	100.6
15PUC20	62.1	16.4	2.5	7.1	2.0	5.8	2.9	0.10	0.83	0.12	0.12	0.19	100.1
15PUC21	73.2	13.4	3	0.5	5.1	0.7	0.2	0.03	0.07	0.16	0.02		96.4
15PUC22	73.3	13.2	2.9	0.6	4.6	0.7	0.3	0.03	0.07	0.19	0.02		95.9
15PUC23	76.4	13.9	3.2	0.5	4.5	0.7	0.3	0.03	0.08	0.24	0.03	0.02	100.0
15PUC24	78.4	13.6	0.1	1.8	4.3	0.9	0.4	0.05	0.08	0.26	0.02	0.23	100.1
15PUC25	78.1	13.7	2.4	1.5	3.3	0.4	0.3	0.01	0.08	0.19	0.01	0.07	100.1
15PUC26	74.2	12.9	2.6	0.7	4.7	0.8	0.3	0.03	0.09	0.11	0.04		96.5
15PUC27	77.2	13.3	3.2	0.9	4.2	0.6	0.3	0.02	0.06	0.24	0.02	0.09	100.0
15PUC28	42.1	0.57	0.3	0.2	0.1	10	41	0.15	0.04	0.02	0		94.2
15PUC29	73.6	13.3	4.3	3.3	1.4	2.0	1.6	0.03	0.42	0.06	0.04	0.08	100.1
15PUC30	71.7	14.5	3.6	2.1	6.1	0.8	0.3	0.01	0.17	0.46	0.10	0.12	99.9
15PUC31	71.7	12.6	2.8	1.3	4.9	1.8	0.4	0.04	0.27	0.04	0.04		95.8
15PUC32	75.4	12.9	3.3	1.3	5.1	1.2	0.3	0.02	0.29	0.10	0.04	0.28	100.2
15PUC33	71.8	14.3	4.0	2.0	5.0	2.3	0.6	0.04	0.54	0.18	0.04	0.02	100.7
15PUC34	71.0	15.2	5.6	1.4	4.7	2.1	0.3	0.06	0.32	0.06	0.04	0.06	100.7
15PUC35	65.3	17.7	6.1	1.5	6.2	2.8	0.2	0.08	0.37	0.05	0.06	0.03	100.3
15PUC36	56.1	15.2	2.4	7.7	2.2	7.5	7.0	0.12	0.90	0.21	0.16	0.33	99.9
15PUC37	93.1	3.1	0.7	0.5	1.4	0.7	0.2	0.01	0.14	0.01	0.03	0.30	100.2
15PUC38	59.2	16.6	2.8	8.4	1.8	5.7	4.6	0.12	0.71	0.11	0.11	0.04	100.0
15PUC40	59.0	17.5	2.8	8.3	1.4	6.0	4.0	0.12	0.74	0.12	0.10	0.02	100.1
15PUC41	75.3	15.3	3.0	0.5	4.4	0.7	0.2	0.04	0.05	0.25	0.01	0.02	99.9
15PUC42	72.4	13.4	3.2	0.4	5.1	0.4	0.1	0.05	0.03	0.17	0.01		95.3
15PUC43	75.2	14.8	4.1	0.7	4.4	0.5	0.1	0.01	0.07	0.20	0.01	0.16	100.2
15PUC44	71.6	14.0	2.7	4.5	2.0	3.0	1.1	0.04	0.68	0.22	0.10	0.03	99.8
15PUC45	59.9	15.7	2.5	7.6	2.4	5.7	4.8	0.12	0.80	0.14	0.14	0.04	99.8
15PUC46	62.6	14.9	2.7	7.2	2.3	4.9	4.1	0.10	0.68	0.13	0.14	0.14	100.0
15PUC47	63.1	15.5	2.5	6.7	2.5	5.0	3.8	0.09	0.72	0.13	0.16	0.02	100.2
15PUC48	54.8	15.2	1.8	7.7	1.7	7.5	4.6	0.14	0.92	0.13	0.15		94.6
15PUC49	77.9	12.9	3.5	0.8	4.1	0.5	0.1	0.04	0.01	0.03	0.01	0.03	100.0
15PUC50	80.2	12.3	0.1	0.2	3.8	2.2	0.3	0.20	0.01	0.06	0.01	0.10	99.5
15PUC51	57.8	18.0	2.6	8.7	1.6	6.0	4.4	0.12	0.75	0.13	0.09	0.03	100.2
15PUC52	48.2	19.1	1.6	12	0.4	8.9	9.0	0.18	1.16	0.10	0.04	0.03	100.2

Table B-2, continued: major oxide data for analyzed Pogo rocks

Sample #	SiO_2	Al_2O_3	Na_2O	CaO	K_2O	FeO	MgO	MnO	TiO_2	P_2O_5	BaO	S	sum
15PUC53	51.1	20.7	2.1	11	0.8	7.9	4.9	0.14	0.94	0.96	0.07	0.66	100.5
15PUC54	54.2	16.2	1.5	9.2	1.3	8.7	7.2	0.16	1.03	0.03	0.04	0.10	99.6
15PUC55	76.0	13.8	3.3	0.9	4.6	0.7	0.2	0.02	0.09	0.17	0.03	0.07	99.8
15PUC56	75.6	14.2	3.6	0.9	5.0	0.3	0.1	0.01	0.07	0.18	0.02	0.05	100
15PUC57	67.3	15.7	3.6	5.0	1.9	3.6	1.7	0.05	0.64	0.15	0.04	0.04	99.7
15PUC58	65.2	17.7	5.0	1.2	7.7	3.2	0.1	0.10	0.24	0.03	0.01	0.10	101
15PUC59	66.0	17.4	6.7	1.5	5.2	2.7	0.1	0.09	0.27	0.02	0.01	0.13	100
15PUC60	76.4	12.3	4.0	2.1	2.6	1.1	0.2	0.02	0.15	0.01	0.05	0.04	98.9
15PUC61	61.2	16.3	3.1	7.2	2.1	6.1	3.0	0.11	0.86	0.15	0.11	0.24	100.4
15PUC62	76.1	14.4	3.5	0.8	4.7	0.4	0.1	0.02	0.02	0.04	0.01	0.04	100.2
15PUC63	75.7	14.3	2.0	0.7	6.4	0.3	0.1	0.03	0.01	0.05	0.03	0.05	99.7
15PUC64	72.5	13.5	3	0.8	4.7	0.9	0.2	0.04	0.1	0.14	0.06		95.9
15PUC65	50	22.7	0.8	2.3	7	1.3	1.3	0.04	0.25	0.66	0.05		86.4
15PUC66	61.1	15.8	2.7	7.6	1.8	5.6	3.8	0.10	0.81	0.12	0.10	0.09	99.7
15PUC67	74.3	14.9	1.7	0.8	3.5	3.0	1.6	0.06	0.22	0.08	0.10	0.02	100
15PUC68	73.8	13.7	2.6	1.3	6.8	1.0	0.4	0.01	0.15	0.18	0.11	0.02	99.9
15PUC69	62.3	16.2	2.8	7.0	1.2	6.2	3.1	0.12	0.86	0.14	0.09	0.02	100
15PUC70	63.8	16.1	2.6	6.6	1.4	5.9	3.1	0.11	0.80	0.18	0.10	0.05	101
15PUC71	62.7	16.5	2.7	7.0	1.2	5.8	2.9	0.11	0.79	0.15	0.10	0.11	100
15PUC72	66.6	17.6	0.2	0.5	5.0	7.7	1.2	0.52	0.83	0.14	0.06	0.38	101
15PUC73	75.9	13.9	3.7	0.6	4.3	0.4	0.1	0.02	0.05	0.18	0.02	0.05	99.3
15PUC74	76.1	14.2	3.3	0.9	3.0	0.4	0.3	0.01	0.06	0.55	0.01	0.16	99.0
15PUC75	60.6	21.9	3.3	1.4	8.7	0.8	0.4	0.03	0.12	0.69	0.08	0.05	98.1
15PUC76	72.8	14.7	2.0	2.5	3.9	2.0	0.8	0.04	0.74	0.26	0.04	0.03	99.9
15PUC77	70.2	15.7	1.4	1.3	3.2	1.4	1.0	0.02	0.69	0.20	0.11	0.02	95.1
15PUC78	64.5	15.9	0.2	3.7	2.1	4.2	1.4	0.10	0.71	0.21	0.09	0.02	93.1
15PUC79	73.1	13.8	2.7	4.2	1.9	2.5	0.9	0.03	0.62	0.19	0.08	0.05	100
15PUC80	71.3	14.1	3.0	4.4	1.9	2.8	1.0	0.04	0.62	0.23	0.08	0.06	99.5
15PUC81	72.6	13.7	2.7	4.1	2.0	2.6	0.9	0.03	0.58	0.18	0.09	0.01	99.4
15PUC82	75.3	14.7	1.4	1.2	6.2	0.5	0.2	0.01	0.05	0.08	0.14	0.03	99.8
15PUC83	72.6	14.9	2.2	1.4	6.8	0.8	0.4	0.01	0.17	0.07	0.30	0.02	99.7
15PUC84	71.7	13.7	3.1	3.7	2.9	2.5	0.8	0.04	0.58	0.19	0.11	0.02	99.4
15PUC85	76.4	14.6	2.0	0.5	4.7	0.6	0.1	0.07	0.03	0.15	0.01	0.01	99.2
15PUC86	75.2	14.5	4.1	0.7	4.5	0.3	0.1	0.03	0.01	0.32	0.04	0.02	99.8
15PUC87	62.5	15.4	2.7	6.9	2.4	4.9	3.6	0.09	0.75	0.12	0.15	0.03	99.5
15PUC88	62.3	15.4	2.6	6.7	2.7	5.2	4.0	0.10	0.76	0.14	0.15	0.06	100
15PUC89	63.4	15.2	2.6	6.9	2.4	4.6	3.5	0.08	0.72	0.11	0.13	0.03	99.8
15PUC90	63.6	15.2	2.4	6.7	2.5	4.8	3.6	0.10	0.72	0.13	0.14	0.02	99.9
15PUC91	63.5	14.8	2.3	7.1	2.5	5.1	3.7	0.08	0.73	0.13	0.15	0.04	100
15PUC92	72.4	12.7	3.2	3.8	3.7	1.8	0.8	0.07	0.35	0.12	0.26		99.1
15PUC94	76.8	12.1	2.3	2.1	3.5	1.2	0.4	0.04	0.21	0.08	0.11		98.9
15PUC95	73.8	12.8	2.1	3.5	3.1	2.7	0.8	0.09	0.44	0.06	0.11		99.4

Table B-2, continued: major oxide data for analyzed Pogo rocks

Sample #	SiO_2	Al_2O_3	Na_2O	CaO	K_2O	FeO	MgO	MnO	TiO_2	P_2O_5	BaO	S	sum
15PUC96	75.7	11.3	2.3	2.3	4.2	1.7	0.5	0.05	0.31	0.03	0.09		98.4
15PUC97	77.1	11.7	2.9	1.4	3.6	0.9	0.5	0.04	0.25	0.08	0.16		98.7
15PUC98	69.4	13.1	2.3	4.1	3.4	4.4	0.8	0.09	0.41	0.06	0.11		98.1
15PUC99	77.1	14.3	3.1	1.1	3.5	0.6	0.1	0.02	0.04	0.05	0.01		99.9
15PUC100	77.1	12.4	2.0	1.7	5.3	0.4	0.2	0.01	0.13	0.03	0.09	0.03	99.3
15PUC101	74.8	12.9	2.4	1.2	6.3	0.9	0.2	0.01	0.17	0.17	0.07	0.14	99.2
15PUC103	77.8	12.4	2	1.1	3.9	0.7	0.5	0.02	0.33	0.04	0.06		98.9
15PUC104	71.9	12.5	1.4	0.9	8	0.1	0.1	0.01	0.02	0.05	0.32		95.3
15PUC105	70.6	15.9	2.0	1.0	8.8	0.3	0.1	0.01	0.07	0.65	0.09	0.07	99.7
15PUC106	75.1	13.9	3.5	3.0	3.2	0.7	0.2	0.0	0.27	0.04	0.17	0.06	100.1
15PUC107	76.2	13.8	2.7	1.6	3.7	0.4	0.3	0.02	0.04	0.13	0.1	0	100.0
15PUC108	81.2	7.51	1.8	1.7	1.4	0.4	0.3	0.02	0.02	0.02	0.03		94.3
15PUC109	74.4	14.8	2.3	0.5	7.2	0.3	0.1	0.04	0.01	0.13	0.02	0.04	99.9
15PUC110	72.4	14.5	3	1.4	2.6	1	0.2	0.01	0.03	0.18	0.03		95.4
15PUC111	71.2	13	2.6	1.9	5.3	1.1	0.4	0.02	0.16	0.09	0.11		95.8
15PUC112	73.5	13.4	3.0	2.6	4.0	1.6	0.6	0.03	0.34	0.13	0.11	0.11	99.4
15PUC113	69.6	13.8	2.3	6.0	1.7	3.4	2.3	0.06	0.40	0.08	0.06		99.6
15PUC114	76.2	11.6	3.5	1.7	4	0.9	0.6	0.05	0.23	0.05	0.32		99.1
15PUC115	77.2	11.1	2.6	1	5.8	0.7	0.4	0.04	0.17	0.01	0.16		99.2
15PUC116	75.5	11.9	3.6	1.7	3.9	1	0.7	0.05	0.31	0.03	0.19		98.8
15PUC117	77.1	11.9	2.8	1.8	3.7	1.4	0.5	0.02	0.32	0.11	0.20	0.02	99.8
15PUC118	76.4	12.2	3.8	1.4	4.0	1.1	0.4	0.03	0.19	0.10	0.16	0.08	99.8
15PUC119	78.1	11.2	3.9	1.6	2.8	0.6	0.2	0.01	0.11	0.1	0.13	0	98.8
15PUC120	75.2	13.3	3.6	1.7	5.0	0.7	0.2	0.02	0.13	0.05	0.26	0.01	100
15puc121A	74.9	13.6	3.5	1.5	4.7	0.8	0.3	0.01	0.14	0.02	0.16		99
15puc121B	75.6	13.3	3.6	1.5	4.6	0.8	0.3	0.01	0.14	0.02	0.16		100
15PUC122	77.5	11.7	3.6	1.5	3.4	1	0.3	0.03	0.23	0.02	0.13	0	99.5
15PUC123	73.3	14.1	4.1	1.8	4.6	0.7	0.3	0.02	0.15	0.06	0.20	0.1	99.5
15PUC124	63.9	17.5	4.4	1.7	8.5	2.8	0.3	0.11	0.38	0.17	0.06	0.04	99.7
15PUC125	77.7	11.9	3.9	1.7	2.9	0.8	0.4	0.02	0.17	0.05	0.17	0	99.8
15PUC126	66.4	17.6	7.5	1.3	4.4	2.0	0.1	0.09	0.14	0.00	0.01	0.08	99.5
15puc127A	64.3	17.9	6.2	2.1	5.2	3	0.3	0.12	0.37	0.06	0.08		99.5
15puc127B	63.9	18.0	6	2.0	5.7	2.7	0.2	0.1	0.41	0.15	0.09		99.2
15PUC128	57.9	16.4	2.2	7.3	1.5	6.6	3.1	0.12	0.86	0.1	0.13		96.3
15PUC129	75.0	13.7	3.8	0.7	5.4	1.0	0.4	0.1	0.1	0.2	0.0		100
15PUC130	73.4	12.9	3	2	3.3	1.8	0.3	0.03	0.11	0.04	0.2		97.2
15PUC131	62.5	15.0	2.3	7.9	1.7	6.4	2.5	0.12	0.90	0.14	0.09	0.07	99.6
15PUC132	57.2	15.5	2.1	9.1	1.1	7.3	3.9	0.14	0.8	0.11	0.11		97.4
15PUC133	58.3	15.9	2.3	6.7	1.6	7	3.1	0.13	0.85	0.11	0.13		96.1
15PUC134	75.3	13.4	3.7	2.0	3.7	1.2	0.3	0.01	0.13	0.06	0.18	0.01	100.0
15PUC135	57.9	15.8	2.2	7.8	1.6	6.5	4.2	0.13	0.81	0.12	0.13		97.2
15PUC136	58.7	17	2.6	6.8	1.7	5.3	2.5	0.1	0.77	0.13	0.09		95.7

Table B-2, continued: major oxide data for analyzed Pogo rocks

Sample #	SiO_2	Al_2O_3	Na_2O	CaO	K_2O	FeO	MgO	MnO	TiO_2	P_2O_5	BaO	S	sum
15PUC137	62.2	16.5	2.5	6.9	1.2	4.4	2.3	0.08	0.7	0.1	0.08		96.9
15PUC138	64.9	15.7	2.4	5.4	1.5	3.8	2.1	0.08	0.59	0.08	0.09		96.6
15PUC139	59.3	17.5	2.4	7	1.7	5.6	2.4	0.12	0.75	0.2	0.09		96.9
15PUC141	66.2	14.6	3.4	4.8	1.3	3.7	1.5	0.07	0.54	0.09	0.09		96.3
15PUC143	63.3	14.1	2.8	7.6	1.9	5.4	3.2	0.09	0.84	0.16	0.07	0.18	99.6
15PUC144	58.5	15.2	2	7.9	2.1	6.1	3.5	0.11	0.71	0.1	0.16		96.4
15PUC145	57	14.7	2.1	10	1.4	6.5	3.2	0.12	0.79	0.11	0.14		96.2
15PUC146	68.4	14.2	2.3	4.1	2.1	3.7	1.1	0.06	0.71	0.18	0.1		97.1
15PUC147	55.8	16.3	2.2	8.2	1.5	6.3	4.4	0.12	0.69	0.11	0.12		95.6
15PUC148	54	17.9	1.9	8.7	1.3	7.6	4.5	0.15	0.86	0.12	0.09		97.2
15PUC149	63.3	14.9	2.2	5.7	2.1	4.9	2.7	0.1	0.68	0.1	0.14		96.9
15PUC150	62.1	16.1	2.6	6.9	1.9	5.4	3.6	0.11	0.82	0.21	0.17	0.04	99.9
15PUC151	59.2	15.3	2.1	6.5	1.9	6.3	3.5	0.13	0.82	0.13	0.2		96.1
15PUC152	58.5	15	2	7.2	1.7	6.4	4	0.13	0.8	0.1	0.13		96.0
15PUC153	57.9	15.5	2.1	7.2	1.9	6.7	3.9	0.14	0.86	0.12	0.13		96.3
15PUC154	59	15.6	2.1	7	1.9	6.4	3.3	0.13	0.86	0.13	0.13		96.5
15PUC155	59	16.6	2.2	7.7	1.5	6.2	3.3	0.13	0.82	0.13	0.12		97.6
15PUC156	59	15.8	2.2	7.3	1.9	6.1	3.7	0.12	0.76	0.11	0.13		97.0
15PUC157	61.4	15.7	2.6	7.4	2.2	5.4	3.7	0.10	0.80	0.49	0.12	0.09	99.9
15PUC158	59.3	15.5	2.1	7	2	6.2	3.9	0.12	0.79	0.1	0.14		97.1
15PUC159	68.3	14.3	2	4.8	1.9	3.8	1.3	0.05	0.81	0.2	0.1		97.5
15PUC160	73.5	14.4	3.1	0.8	4.5	0.9	0.2	0.04	0.08	0.14	0.03		97.6
15PUC161	73.9	13.8	2.9	1	5.7	0.7	0.2	0.04	0.07	0.48	0.03		98.8
15PUC162	75.6	13.9	3.1	0.6	4.7	0.7	0.1	0.07	0.03	0.13	0.01		98.9
15PUC163	75.5	13.6	2.7	0.7	3.1	0.9	0.3	0.04	0.05	0.18	0.02		97.0
15PUC164	75.2	14.5	2.8	0.4	5.2	0.9	0.1	0.03	0.05	0.2	0.01		99.4
15PUC165	75.2	13.1	2.7	0.9	4.9	0.9	0.2	0.03	0.08	0.15	0.03		98.1
15PUC166	74.9	13.4	3.1	0.7	4.6	0.8	0.2	0.04	0.09	0.15	0.03		97.9
15PUC167	72.7	13.7	2.4	0.8	6.9	0.4	0.2	0.02	0.07	0.13	0.04		97.2
15PUC168	74.3	13.5	2.9	1.7	6.1	1.0	0.3	0.02	0.18	0.07	0.30	0.03	100.1
15PUC169	74.1	13.9	3.9	2.0	4.8	0.9	0.3	0.03	0.16	0.09	0.07	0.02	100.3
15PUC170	85.0	8.1	1.7	1.6	2.5	0.8	0.3	0.01	0.19	0.01	0.07	0.04	100.4
15PUC171	77.5	12	4.4	1.6	2.8	1	0.4	0.03	0.21	0.05	0.09	0	100.2
15PUC172	70.9	13.3	2.8	1.9	5.2	0.7	0.2	0.02	0.07	0.04	0.09		95.1
15PUC173	72.6	14	3.5	2	5.2	0.7	0.1	0.02	0.05	0.05	0.06		97.2
15PUC174	73.1	14	4	1.7	5	0.7	0.2	0.02	0.04	0.06	0.02		97.8
15PUC175	78.6	11.6	2.5	1.7	3.4	1.3	0.2	0.02	0.08	0.02	0.05		99.3
15PUC176	77.0	13	3	1.3	4	0.7	0.2	0.01	0.06	0.03	0.01	0.2	99.3
15PUC177	75.4	13.6	2.9	0.8	4.8	0.7	0.2	0.02	0.08	0.13	0.04		98.6
15PUC178	72.7	14.2	3.9	0.8	3.6	0.7	0.2	0.02	0.07	0.13	0.01		96.4
15PUC179	75	13.3	2.4	0.7	5.3	0.6	0.2	0.02	0.06	0.1	0.01		97.7
15PUC180	72.6	13.6	2.1	1.2	6.5	1.6	0.3	0.07	0.16	0.04	0.07		98.2
15PUC181	71.1	12.8	1.7	2.6	3.6	3.6	0.8	0.06	0.42	0.08	0.18		96.9

Table B-2, continued: major oxide data for analyzed Pogo rocks

Sample #	SiO_2	Al_2O_3	Na_2O	CaO	K_2O	FeO	MgO	MnO	TiO_2	P_2O_5	BaO	S	sum
15PUC182	69.6	12.7	2	3.5	3.2	4.4	1.1	0.09	0.5	0.09	0.1		97.2
15PUC183	74	13.4	2.7	1.7	4.6	1.1	0.3	0.02	0.16	0.04	0.08		98.0
15PUC184	79.9	11.9	2.6	1.2	3.0	0.8	0.1	0.03	0.07	0.00	0.05	0.01	99.7
15PUC185	75.3	11.5	2.2	3.4	4.0	2.3	0.6	0.05	0.29	0.05	0.15	0.02	99.8
15PUC186	78.6	12.0	2.8	1.6	3.2	1.1	0.1	0.03	0.07	0.01	0.08		99.6
15PUC187	73.8	12.1	1.9	3	3.2	2.6	0.7	0.05	0.31	0.06	0.11		97.8
15PUC188	76.5	11.8	2.4	1.2	4.4	1.2	0.2	0.03	0.11	0.02	0.03		98.0
15PUC189	78.7	11.8	1.9	0.7	6.5	0.5	0.2	0.02	0.09	0.02	0.03		100.4
15PUC190	74.1	12.4	2.3	2.7	2.7	2.2	0.6	0.05	0.28	0.04	0.1		97.4
15PUC191	72.1	12.8	1.9	3	3.3	3.2	0.7	0.05	0.4	0.07	0.13		97.6
15PUC192	76.7	12.3	3.0	1.4	5.0	0.9	0.2	0.03	0.09	0.01	0.03	0.07	99.7
15PUC193	69.3	14.1	2.4	3.4	3.2	3.4	0.8	0.06	0.38	0.07	0.08		97.0
15PUC194	77.8	12.1	4.2	0.9	3.3	0.7	0.1	0.02	0.05	0.15	0.01	0.13	99.5
15PUC195	73.2	13.1	2.7	3.5	3.1	2.8	0.8	0.05	0.38	0.10	0.08	0.05	99.9
15PUC196	76.5	12.4	2.6	1.6	4	1.3	0.3	0.02	0.17	0.04	0.08		98.9
15PUC197	78.5	11.2	2.2	0.6	6.2	0.5	0.1	0.02	0.07	0.01	0.02	0.1	99.6
15PUC198	76.8	12.0	4.5	1.8	2.5	1.1	0.2	0.05	0.08	0.01	0.12	0.1	99.2
15PUC199	57	16.4	2.1	8.1	1.7	8.6	4.4	0.16	0.9	0.1	0.15		99.6
15PUC200	58.4	16.9	2.3	7.7	1.8	8	3.4	0.16	0.87	0.09	0.13		99.7
15WT01	61.2	17.8	2.9	7.6	2.0	4.6	3.2	0.08	0.65	0.10	0.13	0.05	100.2
15WT02	67.8	15.0	3.3	3.7	2.6	3.5	1.8	0.04	0.58	0.51	0.23	0.11	99.3
15WT03	72.9	13.5	3.1	2.6	3.5	1.3	0.5	0.03	0.27	0.30	0.10	0.05	98.2
15WT04	70.8	13.8	2.8	3.4	2.2	2.3	0.9	0.03	0.45	0.08	0.07		96.7
15WT05	72.3	13.2	2.4	3	2.8	2.5	0.7	0.05	0.43	0.1	0.12		97.5
15WT06	68.6	13.7	2.2	1.7	4.4	4.2	1.5	0.07	0.69	0.03	0.22		97.3
15WT07	60.3	15.2	2.1	6.5	1.8	5.8	3.4	0.11	0.74	0.1	0.13		96.2
15WT08	58.6	15	2	7.4	1.9	6.4	3.7	0.13	0.8	0.11	0.17		96.2
15WT09	75.4	12.6	2.2	1.5	4.5	0.7	0.3	0.02	0.12	0.05	0.11		97.5
15WT10	79.9	8.43	1.2	0.8	1.9	2.8	1.3	0.04	0.48	0.1	0.14		97.2
15WT11	73.5	13.3	1.2	1.6	2.8	3.7	1.8	0.04	0.55	0.07	0.07		98.8
15WT12	76.2	13.1	2.9	2.2	3.6	1.6	0.6	0.03	0.34	0.12	0.13	0.01	100.8
15WT13	74.8	12.1	0.5	0.6	2.6	5	2.9	0.1	0.39	0.02	0.04		99.1
15WT14	54.3	15.8	2	8.6	1.3	7.6	5.4	0.15	0.67	0.07	0.1		95.8
15WT15	61.9	16.2	2.4	7.5	1.8	5.2	3.2	0.10	0.82	0.14	0.11	0.07	99.5
15WT16	63.5	16.0	2.5	6.7	1.9	4.9	2.9	0.10	0.75	0.13	0.11	0.03	99.6
15WT17	58.9	15.7	2.1	7.2	1.5	6	3.4	0.11	0.7	0.11	0.11		95.9
15WT18	60.8	17.2	3.1	7.8	1.7	5.0	3.6	0.10	0.63	0.13	0.11	0.03	100.2
15WT19	57.1	15.3	2.2	6.7	1.7	6.2	3.6	0.12	0.8	0.1	0.13		93.9
15WT20	58.1	16.3	2.2	7.3	1.6	6.3	3.8	0.12	0.83	0.12	0.13		96.8
15WT21	76.9	12.9	2.6	1.3	5.2	0.4	0.2	0.00	0.12	0.11	0.09	0.02	99.8
15WT22A	73.3	14.9	3.1	1.7	3.4	1.3	0.5	0.02	0.25	0.11	0.11	0.02	99.2
15WT22B	74.3	14.7	3.2	1.8	3.2	1.2	0.5	0.02	0.26	0.08	0.10	0.02	99.9
15WT23	62.3	15.4	2.3	5.8	2.8	4.9	2.8	0.09	0.67	0.11	0.17		97.3

Table B-2, continued: major oxide data for analyzed Pogo rocks

Sample #	SiO_2	Al_2O_3	Na_2O	CaO	K_2O	FeO	MgO	MnO	TiO_2	P_2O_5	BaO	S	sum
15WT24	88.5	7.72	0.9	1.1	2.5	1.7	0.7	0.03	0.3	0.04	0.1		103.7
15WT25	60.5	14.7	2.2	5.6	2.7	5.4	3	0.1	0.72	0.1	0.2		95.2
15WT26	74.6	13.0	2.6	3.5	2.5	2.1	1.3	0.04	0.30	0.01	0.08	0.02	100.0
15WT27#1	74.9	13.9	3.3	1.9	4.7	0.9	0.14	0.03	0.07	0.01	0.07		99.9
15WT27#2	75.4	13.4	3.3	1.8	4.6	0.9	0.12	0.03	0.06	0.01	0.06		99.6
15WT28B	71.6	13.1	1.6	4.7	2.4	3.8	1.4	0.06	0.63	0.08	0.03	0.03	99.4
15WT28C	75	12.6	3.1	0.9	2.9	1	0.3	0.05	0.03	0.05	0.01		96.0
15WT29	76.1	12.3	2.9	2.4	3.1	2.2	0.6	0.04	0.30	0.07	0.11	0.04	100.1
15WT30	64.6	15	2.4	5.1	2.4	4	1.5	0.07	0.62	0.11	0.21		96.0
15WT31	58	14.9	2.1	7.3	1.8	6.2	3.9	0.12	0.68	0.11	0.11		95.3
15WT32	53.8	17.2	2.3	7.7	1.7	7.4	4.4	0.14	0.83	0.1	0.13		95.6
15WT33	65.3	14.9	2.5	4.7	2.6	4.1	1.6	0.08	0.61	0.12	0.16		96.7
15WT34	63.1	16.1	2.5	5.9	2.2	5	2	0.1	0.72	0.12	0.15		97.8
15WT35	66	15.2	2.6	4.7	2.6	4	1.6	0.08	0.6	0.11	0.14		97.6
15WT36	64.6	15.4	2.8	5.4	1.9	4.4	1.7	0.09	0.72	0.13	0.13		97.2
15WT37	68	15.5	2.6	4.5	2.3	3	1.1	0.05	0.53	0.15	0.21		98.0
15WT38	58.2	16.8	2.4	6.3	1.7	6.4	2.5	0.12	0.94	0.16	0.13		95.6
15WT39	59.4	17	2.5	6.8	1.9	5.5	2.5	0.11	0.82	0.14	0.15		96.7
15WT40	66.8	15.1	2.8	5.4	2.4	4.1	1.9	0.08	0.69	0.16	0.12	0.05	99.7
15WT41	66.4	14.9	2.2	4.7	2.7	4	1.5	0.07	0.65	0.13	0.23		97.4
15WT42	66.9	15.2	2.3	4.8	2.7	3.9	1.3	0.08	0.63	0.12	0.19		98.1
15WT43	54.0	14.7	2.8	11	1.7	7.4	4.3	0.19	2.10	0.57	0.05	0.14	99.2
15WT44	73.1	13.5	1.1	0.4	3.3	5.3	2	0.07	0.78	0.04	0.12		99.6
15WT45	77.5	13	0.7	0.3	3.1	4.2	1.8	0.04	0.3	0.18	0.11		101.1
15WT46	71.1	13.5	3	2.2	3.6	1.1	0.4	0.02	0.19	0.06	0.13		95.4
15WT47	76.7	13.9	2.5	0.7	6	0.3	0.2	0.01	0.05	0.17	0.03		100.5
15WT48	75.5	14.5	4.2	0.6	4.0	0.5	0.1	0.04	0.03	0.23	0.01	0.06	99.8
15WT49	77.8	13.2	2.5	0.6	5.2	0.6	0.2	0.02	0.05	0.12	0.02		100.3
15WT50	75.5	14.5	2.0	0.6	6.0	0.4	0.2	0.00	0.03	0.22	0.02	0.18	99.6
15WT51	76.6	14	3.3	1.2	2.6	0.7	0.2	0.03	0.06	0.16	0.02		98.8
15WT52	76.8	14.2	2.9	0.6	4.9	0.6	0.1	0.01	0.05	0.15	0.01		100.3
15WT53	66	15.2	2.6	2.3	7.4	1.3	0.8	0.03	0.19	0.76	0.23		96.8
15WT54	76.5	13.5	4.2	2.5	2.4	0.0	0.2	0.0	0.01	0.10	0.13	0.05	99.6
15WT55	76.5	13.7	2.7	0.5	4.9	1	0.2	0.03	0.12	0.15	0.03		99.8
15U259a	57.9	15.5	2.2	8.4	1.7	6.7	5.2	0.1	0.9	0.2	0.2		98.9
15U368A	51.7	10.4	0.3	11	1.5	11	14	0.21	0.8	0.15	0.04		101
16WT01	58.9	17.1	2.8	8.0	1.4	5.9	3.6	0.12	0.77	0.12	0.10	0.06	98.8
16WT02	60.3	17.7	2.8	8.0	1.7	4.9	3.2	0.09	0.70	0.12	0.10	0.06	99.6
16WT03	61.6	16.2	2.7	7.1	2.3	4.9	3.6	0.10	0.63	0.12	0.13	0.06	99.3
16WT04	62.2	16.3	2.6	6.8	2.6	4.7	3.1	0.08	0.75	0.09	0.13	0.05	99.5
16WT05	73.9	13.3	3.2	2.2	4.3	1.1	0.4	0.02	0.22	0.14	0.13	0.04	98.9
16WT06	74.8	13.1	3.1	2.4	3.5	1.6	0.6	0.03	0.35	0.11	0.10	0.03	99.7

Table B-2, continued: major oxide data for analyzed Pogo rocks

Sample #	SiO_2	Al_2O_3	Na_2O	CaO	K_2O	FeO	MgO	MnO	TiO_2	P_2O_5	BaO	S	sum
16WT08	60.6	16.1	2.7	7.1	2.0	5.4	3.7	0.10	0.79	0.14	0.11	0.11	98.9
16WT08	59.1	14.4	2.0	7.0	2.1	8.0	4.0	0.18	0.94	0.11	0.15		98.0
16WT09	61.3	16.5	2.8	7.3	2.2	4.9	3.1	0.09	0.72	0.11	0.11	0.05	99.2
16WT10	72.9	13.1	2.9	3.7	2.8	2.6	0.8	0.06	0.38	0.11	0.07	0.03	99.4
16WT11	60.3	15.2	2.5	8.7	1.5	6.3	4.0	0.11	0.89	0.14	0.15	0.11	99.9
16WT12	67.9	15.3	3.2	4.9	2.4	3.6	1.7	0.08	0.59	0.15	0.14	0.05	99.9
16WT13	76.3	13.0	2.9	1.6	4.8	1.0	0.3	0.03	0.18	0.07	0.10	0.04	100.3
16WT15	74.4	15.1	2.9	1	4.7	1.1	0.3	0.03	0.11	0.11	0.06		99.7
16WT16	75.2	13.2	3.0	2.5	3.8	1.6	0.5	0.03	0.33	0.14	0.12	0.05	100.4
16WT17	73.1	14.2	3.1	3.4	3.2	1.8	0.7	0.04	0.39	0.13	0.09	0.02	100.2
16WT18	75.2	13.5	3.4	2.1	3.6	1.4	0.5	0.03	0.24	0.10	0.10	0.04	100.3
16WT19	75.9	12.6	3.3	2.1	3.7	1.3	0.4	0.02	0.25	0.10	0.12	0.05	99.8
16WT20	75.3	13.9	3.8	0.9	4.5	0.8	0.2	0.02	0.08	0.14	0.02	0.02	99.6
16WT-935A	60.3	15.9	2.8	8.0	1.7	5.8	4.1	0.09	0.79	0.11	0.10	0.16	99.8
16WT-935B	54.8	16.2	2.6	8.9	1.7	6.8	7.7	0.12	0.90	0.29	0.13	0.10	100.2
16WT-975	62.7	16.0	2.6	7.0	2.0	5.3	3.3	0.10	0.79	0.13	0.12	0.06	100.1
17P04-242	55.9	18.5	2.0	1.0	6.0	8.8	2.4	0.1	1.5	0.0	0.5	96.9	
17PGN01	50.7	26.3	1.1	1.1	2.9	9.5	3.8	0.2	1.8	0.1	0.3	97.8	
DL04	62.5	16.4	3.1	5.5	2.4	4.9	2.3	0.07	0.93	0.13	0.12	0.06	98.4
DL1A	47.0	14.5	1.61	12.6	0.46	10.9	8.34	0.18	1.32	0.09	0.00	0.11	99.05
DL2A	49.6	15.7	2.67	8.9	1.09	9.5	5.35	0.13	2.09	0.43	0.06	<.05	99.19
DL3A	50.9	14.3	2.61	10.5	0.33	9.3	7.67	0.15	1.10	0.07	0.01	0.26	99.57
DL4A	51.8	13.8	2.42	7.04	2.60	10.0	5.30	0.15	2.30	0.30	0.11	0.42	98.56
DL5A	54.4	14.7	2.75	7.11	1.85	8.63	4.20	0.13	1.85	0.26	0.11	0.18	99.14
DL6A	54.7	14.3	1.52	7.56	2.17	8.05	7.02	0.15	1.09	0.13	0.03	<.05	99.08
DL7A	56.0	13.3	1.47	5.90	2.42	8.54	6.16	0.12	1.12	0.12	0.06	0.20	98.68
DL82	67.7	13.3	2.4	4.2	1.7	5.6	1.4	0.09	0.67	0.12	0.17		97.4
DL8A	56.9	14.8	2.77	6.82	1.77	7.52	3.84	0.11	1.36	0.25	0.06	0.08	99.19
DL9A	56.9	15.3	3.10	6.48	2.34	7.02	3.46	0.10	1.18	0.56	0.08	0.13	98.57
DL10A	57.7	14.3	1.68	7.20	1.85	7.21	5.29	0.13	1.24	0.17	0.03	<.05	99.33
DL11	68.9	12	2.1	2.3	3.1	4.7	2.6	0.05	0.53	0.15	0.03	0.1	98.4
DL11A	64.5	15.42	2.67	2.40	2.99	6.79	2.22	0.07	0.94	0.04	0.08	0.06	99.54
DL12A	67.1	13.32	2.13	2.11	3.31	4.73	1.46	0.03	0.71	0.16	0.09	0.15	98.24
DL13A	61.8	15.69	2.15	2.63	3.05	6.14	2.21	0.06	0.80	0.07	0.06	0.07	98.44
MAF1	56.7	16.6	2.4	9	1.1	7.8	4.9	0.16	0.81	0.14	0.09		99.7
S Pogo1	75.1	14.3	3.1	1.7	3.1	1.3	0.6	0.04	0.32	0.11	0.12		99.9
S Pogo2	74.8	14.7	3.1	1.6	3.3	1.3	0.6	0.04	0.33	0.09	0.12		99.9

Table B-3: CIPW norms and selected trace element data for analyzed Pogo rocks

Sample #	Qtz	Alb	Or	An	Cor	Di	Hyp	Ilm	Mt	Ap	Pyr	Ni	Pb	Zn	As	Th
753 SA	22	43	12	18	0	1.6	1.5	0.3	0.3	0.6	0	2	26	12		
753 SA-am	0.0	29	6	25	0	33	0	0	2	0		72				
765	43	17	14	12	1.9	0.0	15	1.7		0.2		6	31	46	27	
1023 SA	45	19	26	5.2	2.9		1.2	0.1	0.2	0.5	0.2	0	34	13	47	14
1170ED RA	13	19	9.8	30	0	8.1	16	1.4	2.1	0.2		13	156	59		
1170ufEDRA	13	22	8	32	0	7.6	14	1.5	2	0.2	0.1	13	30	62		
1250 SA	37	30	27	1	2.8	0	2	0	0.3	0.5		0	11	27		
1271Cut #8A	26	12	55	3.4	1.4	0	0.7	0.4	0.1	0.6	0	0	28	4	50	
1271Cut#8B	29	20	11	26	0	1.3	11	1.2	1.4	0.3	0.1	7	29	48	92	
1352												44	20	77	9	
1637	39	24	30	1.7	3.0	0	1.4	0.2	0.3	0.5	0.1	1	28	26		
1660	36	24	34	1.8	2.7	0	1.3	0.2	0.2	0.3		0	32	15		
1703	37	19	34	6.3	1.6	0	1.3	0.2	0.2	0.4		0	40	12		
1744	33	30	32	1.6	2	0	1.1	0	0.1	0.6		0	10	33		
1745	36	23	32	4.2	2.2	0	1.8	0.2	0.3	0.3		0	24	14		
1745#2	36	24	31	4.6	2.2	0	1.7	0.1	0.2	0.3		0	27	14		
1759	38	26	29	3.4	2.5	0	1	0.1	0.2	0.4	0.3	2	33	15		
2100-4	34	32	27	2.6	2.1	0	1	0	0.1	0.1		0	13	31		
RN831B	4	25	13	21		13	16	3	3.9	1.1		88				
09U031A	0.0	36	6	20	0	15	12	4	3	2		28				
10U007A	0.0	23	1	34	0	18	18	2	3	0		93				
11RN338a												11		42		
11RN341a												172	43	69	3	
14-739A	15	21	8	29	0	6	17	2	3	0		7				
14WT17	22	24	10	30	0	0.5	10	1.7	1.6	0.4	0.1	6	10	76	22	
14WT18	26	22	12	27	0.1	0	9.8	1.6	1.4	0.4		3	14	64		
14WT35	16	21	13	29	0	4.8	12	1.8	1.8	0.4		7	18	82		
14WT55B	21	20	8.2	34	0	0.4	12	1.9	1.8	0.4		5	16	85		
14WT56	27	22	19	20	0	0.9	8.9	1.2	1.3	0.3		3	24	52		
14WT61	29	22	16	22	0.7	0	8.5	1.3	1.2	0.4		5	14	56		
14WT62	27	22	14	24	0.4	0	9.5	1.4	1.4	0.4		5	11	62		
14WT63	30	21	14	23	0	1.6	8	1.3	1.2	0.4		4	13	67		
14WT66A	40	20	27	4.9	3.3	0	3.4	0.5	0.5	0.3		2	44	30		
14WT70	16	20	12	29	0	5.7	15	1.5	1.8	0.3		19	41	61		
14WT742A	37	19	23	12	1.5	0	4.5	1	0.7	0.2		4	84	26		
14WT742B	10	20	8.8	31	0	8	18	1.7	2.4	0.3		19	45	78		
14WT742C	11	20	2.8	26	0	21	13	2.7	1.3	0.6		16				
14WT744A	32	24	15	20	0.4	0	6.5	0.8	1	0.2		2	15	37		
14WT744B	5.6	12	3.9	40	0	11	24	1.6	2.7	0.4		45	24	90		
14WT745	9	19	9.4	31	0	8.8	19	1.5	2.3	0.3		16	25	70		

Table B-3, continued: CIPW norms & selected trace element data for analyzed Pogo rocks

Sample #	Qtz	Alb	Or	An	Cor	Di	Hyp	Ilm	Mt	Ap	Pyr	Ni	Pb	Zn	As	Th
14WT748	6.6	9.4	2.7	44	0	11	28	1.7	2.9	0.4		47	21	105		
14WT753	38	24	27	5.6	2.6	0	2.5	0.4	0.4	0.2		0	50	14		
14WT754	8.9	21	7.7	34	0	3.9	19	1.6	2.3	0.3		10	21	74		
14WT755	31	26	14	20	0	3.1	4.4	1.1	0.9	0.4	0.1	5	15	53	37	
14WT755	30	23	15	23	0	0	7.8	1.2	1.1	0.3		3	12	36		
14WT756	33	23	17	18	0.7	0	6.1	1	0.9	0.3		5	14	42		
14WT757	32	23	22	16	0.5	0	4.1	0.7	0.6	0.2		1	17	20		
14WT758	26	25	17	20	0	1.4	7	1.1	1.2	0.3	0.1	5	16	52		
14WT759	20	21	8.3	32	0	1.3	13	1.9	1.9	0.5		6	13	82		
14WT760	31	21	19	18	0.8	0	7.3	1.1	1	0.3		3	17	54		
14WT761	26	21	15	25	0	0.8	9.4	1.5	1.4	0.4		3	12	67		
14WT763	31	20	15	22	0.4	0	8.3	1.2	1.2	0.3		2	14	58		
14WT764	24	21	13	26	0	2.7	9.5	1.4	1.5	0.3		5	16	67		
14WT767	35	28	24	10	0.6	0	1.7	0.2	0.3	0		2	57	11		
14WT768	15	19	13	26	0	7.1	16	1.7	2	0.3		14	17	67		
14WT769A	9.3	13	12	33	0	7.8	20	1.8	2.5	0.3		17	5	82		
14WT769B												126	9	93		
14WT770	24	21	9	30	0.3	0	12	1.6	1.6	0.4		7	14	85		
14WT771	19	22	7.4	26	0	7.1	15	1.4	1.9	0.3		19	10	66		
14WT772	29	22	13	22	1.2	0	9.6	1.5	1.5	0.4		7	14	92		
14WT773	31	21	14	21	1.1	0	8.5	1.3	1.2	0.3		4	15	65		
14WT82	36	22	10	20	1.7	0	7.9	1.2	1.1	0.3		3	10	44		
14WT84A	27	20	10	28	0	3.9	7.1	2	1.5	0.4		3				
14WT85	26	23	15	23	0	0.7	8.5	1.4	1.4	0.4		3	15	72		
14WT86	32	20	11	24	0.8	0	8.7	1.6	1.4	0.4		4	11	79		
14WT87	29	23	12	25	0.4	0	7.7	1.4	1.2	0.4		4	11	67		
14WT89	30	23	13	21	1.2	0	8.5	1.4	1.3	0.4		3	17	75		
14WT90A												109	12	100		
14WT90B	28	20	12	26	0	2.3	8.8	1.6	1.4	0.4		4	11	74		
14WT91A	27	21	12	25	0	0.7	11	1.3	1.5	0.4		5	11	68		
1525-mfd1	18	20	8.9	28	0.4		13		1.5	0.9	0.3	30	39	61	10	
1525-mfd2	20	18	5.1	29	0.7		15		1.3	1	0.3	26	23	78	1	
15-791A	8	18	7	26	0	16	24	2	3	0		130				
15-878A	5	28	10	28	0	12	14	1	1	0		33				
15-878A	17	18	13	26	0	8	16	1	2	0		24				
15-885-1356	41	27	20	6.3	0.0	3.8	2.0	0.3	0.3	0.1		0				
15DL04	20	24	15	26	0	1.3	11	1.8	1.7	0.3		4	17	59		
15DL05	30	23	17	20	0.5	0	7.9	0.9	1.1	0.3		3	18	45		
15PUC01	37	33	25	1.2	2.4	0	1.3	0.1	0.1	0.5		0				
15PUC02	38	21	32	4.6	2.3	0	1.5	0.3	0.2	0.5		0				

Table B-3, continued: CIPW norms & selected trace element data for analyzed Pogo rocks

Sample #	Qtz	Alb	Or	An	Cor	Di	Hyp	Ilm	Mt	Ap	Pyr	Ni	Pb	Zn	As	Th
15PUC03	37	34	18	8	0	2.5	0.3	0.1	0.2	0		0				
15PUC05	44	18	20	10	0	1.5	3.4	0.7	0.7	0.1		0				
15PUC06	32	30	29	5	0	0	2.2	0.4	0.3	0.2		0				
15PUC07	12	17	7	36	0	9.6	16	1.5	2.2	0.2		8				
15PUC08	17	18	7.8	32	0	8.7	13	1.7	2	0.2		8				
15PUC09	21	22	6	31	0	0	16	2	1	1		8				
15PUC10	32	24	35	4.2	0	3.2	0	0.3	0.2	0.3		0				
15PUC11	18	20	9.8	28	0	6.6	14	1.6	1.9	0.3	0.1	7	14	64		
15PUC13	16	19	12	29	0	7.8	13	1.6	1.9	0.3		8	28	65		
15PUC14	36	24	12	20	0	1.2	4.3	1.2	0.9	0.6	0	2	7	37		
15PUC15	39	23	11	20	0	0	4.4	1.1	0.8	0.3	0	4	10	36		
15PUC16	28	20	36	15	0	1.4	0.2	0.1	0.1	0.1	0.1	0	29	6		89
15PUC17	40	14	39	5.1	0.5	0	1.5	0.2	0.2	0		0	19	7		
15PUC19	39	17	36	5.2	0.3	0	0.8	0.3	0.3	0.1	0.9	0	54	21	52	
15PUC20	20	21	12	28	0	5.4	10	1.6	1.9	0.3	0.4	19	12	80	82	
15PUC21	36	26	31	1.7	2.5	0	1.5	0.1	0.2	0.4		0	25	27		
15PUC22	39	25	29	1.9	2.9	0	1.8	0.1	0.2	0.5		0	19	23		
15PUC23	39	27	27	1.1	3.3	0	1.5	0.2	0.2	0.6	0	0	19	32		
15PUC24	57	1.3	25	7.3	6	0	1.5	0.2	0.3	0.6	0.5	0	36	99		
15PUC25	48	20	19	6.2	4.4	0	1.1	0.2	0.1	0.4	0.2	0	172	410	25	
15PUC26	41	23	29	2.7	2.7	0	1.7	0.2	0.3	0.3		0	21	24		
15PUC27	41	27	25	3.4	2.5	0	1.2	0.1	0.2	0.6	0.2	0	34	28		
15PUC28												2150		49		
15PUC29	34	36	8	13	0	2.6	4.5	0.8	0.6	0.1	0.2	1	21	18		
15PUC30	24	30	36	5.6	0	1.4	0.6	0.3	0.3	1.1	0.3	1	50	12		
15PUC31	34	25	30	6.5	0.5	0	3.2	0.5	0.6	0.1		0	11	20		
15PUC32	34	28	30	5.5	0	0.3	1.2	0.6	0.4	0.2	0.6	0	24	53		32
15PUC33	24	34	29	6.3	0	2.2	2.4	1	0.7	0.4	0	0	23	33		13
15PUC34	17	47	27	2.6	0	3.3	1.1	0.6	0.7	0.1	0.1	1	28	28		21
15PUC35	2.5	51	37	2.8	0	3.8	1.5	0.7	0.9	0.1	0.1	2	22	40		
15PUC36	6.6	20	13	24	0	10	20	1.7	2.4	0.5	0.7	47	29	66		
15PUC37	82	5.8	8.1	1.4	0	0.9	0.2	0.3	0.2	0	0.6	1	23	13	59	
15PUC38	12	23	10	28	0	11	13	1.4	1.8	0.3	0.1	4	40	50	19	
15PUC40	13	24.0	8.2	31	0	7.6	13	1.4	1.9	0.3	0	2	44	67		
15PUC41	39	26	26	1.1	5.1	0	1.4	0.1	0.2	0.6	0	0	26	38		
15PUC42	35	29	31	0.9	2.4	0	1	0.1	0.1	0.4		0	14	17		
15PUC43	34	34	26	2.1	2.6	0	0.6	0.1	0.2	0.5	0.3	0	37	15		
15PUC44	37	23	12	20	0	0.4	5.1	1.3	1	0.5	0.1	1	7	41		
15PUC45	13	21	14	24	0	10	13	1.5	1.8	0.3	0.1	21	27	52		

Table B-3, continued: CIPW norms & selected trace element data for analyzed Pogo rocks

Sample #	Qtz	Alb	Or	An	Cor	Di	Hyp	Ilm	Mt	Ap	Pyr	Ni	Pb	Zn	As	Th
15PUC46	17	23	14	22	0	11	10	1.3	1.6	0.3	0.3	12	9	40		
15PUC47	19	21	15	23	0	7.1	11	1.4	1.6	0.3	0	17	31	47		
15PUC48	13	16	11	30	0	8	17	1.8	2.3	0.3		12	22	73		
15PUC49	39	30	24	3.7	1.3	0	1	0	0.2	0.1	0.1	0	40	23	22	
15PUC50	63	1.2	23	0.6	7.7	0	3.8	0	0.7	0.1	0.2	0	16	24		
15PUC51	11	22	9.4	33	0	7.8	14	1.4	1.9	0.3	0.1	11	31	61		
15PUC52	0	14	2.5	43	0	10	19	2.2	2.8	0.2	0.1	79	19	73		
15PUC53	5.3	17	4.6	45	0	1.5	20	1	2.5	2.2	1.4	36	27	63	167	
15PUC54	8.8	12	7.4	34	0	9.4	23	2	2.8	0.1	0.2	13	26	81		
15PUC55	37	28	27	3.2	2.2	0	1.1	0.2	0.2	0.4	0.2	0	40	21		
15PUC56	34	30	30	3.1	1.7	0	0.6	0.1	0.1	0.4	0.1	0	34	22		
15PUC57	25	31	11	21	0	2.2	6.8	1.2	1.2	0.4	0.1	2	44	50	46	
15PUC58	3	42	45	3.3	0	2.3	2.8	0.5	1	0.1	0.2	2	9	48		
15PUC59	3.9	56	31	2.3	0	4.6	0.7	0.5	0.9	0.1	0.3	1	12	40		17
15PUC60	39	34	16	8.2	0	1.8	0.7	0.3	0.4	0	0.1	0	14	25		
15PUC61	15	26	12	24	0	8.4	9.4	1.6	1.9	0.4	0.5	18	12	74		
15PUC62	36	30	28	3.7	2.2	0	0.7	0	0.1	0.1	0.1	0	46	11		
15PUC63	38	17	38	3.4	2.9	0	0.6	0	0.1	0.1	0.1	0	29	21		
15PUC64	37	26	29	3	2.6	0	1.7	0.2	0.3	0.4		0	21	25		
15PUC65	15	8.2	48	8.2	13	0	5.4	0.6	0.4	1.8		2	12	7		
15PUC66	16	23	11	26	0	9.4	11	1.5	1.8	0.3	0.2	8	24	67		
15PUC67	46	15	20	3.2	7.1	0	7.5	0.4	1	0.2	0	1	36	45		
15PUC68	30	22	40	5.1	0.3	0	1.9	0.3	0.3	0.4	0	0	36	17		
15PUC69	20	23	7.3	28	0	4.7	12	1.6	2	0.3	0	4	10	86		
15PUC70	23	21	8.4	28	0	2.7	13	1.5	1.9	0.4	0.1	4	12	59		
15PUC71	21	23	7.3	29	0	3.8	12	1.5	1.9	0.4	0.2	4	10	76		
15PUC72	40	1.4	29	1.4	11	0	12	1.6	2.5	0.3	0.8	4	31	24	75	
15PUC73	37	32	26	1.9	2.4	0	0.7	0.1	0.1	0.4	0.1	0	41	37		
15PUC74	45	28	18	0.9	5.3	0	0.9	0.1	0.1	1.3	0.3	0	32	17		
15PUC75	6.2	28	53	2.3	6.4	0	1.9	0.2	0.3	1.6	0.1	0	13	60	27	
15PUC76	40	17	23	11	3.3	0	3.4	1.4	0.7	0.6	0.1	2	12	44	31	
15PUC77	48	13	20	5.3	8.5	0	3.2	1.4	0.5	0.5	0	0	15	57		
15PUC78	47	1.7	13	18	7.6	0	8.5	1.4	1.5	0.5	0	3	27	37		
15PUC79	39	23	11	19	0.1	0	4.4	1.2	0.8	0.4	0.1	0	12	40		
15PUC80	36	25	11	20	0	0.8	4.6	1.2	0.9	0.5	0.1	1	9	41		
15PUC81	39	23	12	19	0.2	0	4.7	1.1	0.8	0.4	0	1	9	38		
15PUC82	41	12	37	5.5	3.7	0	1	0.1	0.1	0.2	0.1	0	45	15		
15PUC83	30	19	40	6.6	1.5	0	1.8	0.3	0.3	0.2	0	2	46	22		
15PUC84	33	27	17	15	0	2.2	3.2	1.1	0.8	0.4	0	2	11	39		
15PUC85	45	18	28	1.6	5.7	0	1.2	0.1	0.2	0.8	0	0	18	47		

Table B-3, continued: CIPW norms & selected trace element data for analyzed Pogo rocks

Sample #	Qtz	Alb	Or	An	Cor	Di	Hyp	Ilm	Mt	Ap	Pyr	Ni	Pb	Zn	As	Th
15PUC86	33	35	27	1.3	2.4	0	0.7	0	0.1	0.7	0	0	22	18		
15PUC87	18	23	14	23	0	8.5	10	1.4	1.6	0.3	0.1	9	36	58		
15PUC88	17	22	16	23	0	8	11	1.4	1.7	0.3	0.1	13	35	56		
15PUC89	19	22	14	23	0	9	9.2	1.4	1.5	0.3	0.1	12	38	46		
15PUC90	20	20	15	24	0	7.3	11	1.4	1.6	0.3	0	14	35	58		
15PUC91	20	19	15	23	0	9.5	10	1.4	1.6	0.3	0.1	18	34	53		
15PUC92	32	27	22	9.8	0	7	0.5	0.7	0.6	0.3		0				
15PUC94	43	20	21	10	0.8	0	2.3	0.4	0.4	0.2		0				
15PUC95	40	18	18	17	0	0.2	4.8	0.8	0.9	0.2		0				
15PUC96	39	19	27	8.3	0	2.7	1.7	0.6	0.6	0.1		0				
15PUC97	43	26	22	6.1	0.5	0	1.6	0.3	0.2	0.2		0				
15PUC98	32	20	21	16	0	4.1	5.2	0.8	1.4	0.1		0				
15PUC99	44	26	21	5	4	0	1	0	0	0		0				
15PUC100	42	17	31	8.2	0.4	0	0.8	0.3	0.1	0.1	0.1	0	56	9		
15PUC101	35	20	37	4.8	0.5	0	1.1	0.3	0.3	0.4	0.3	2	39	16	657	
15PUC103	50	17	23	5.2	3	0	1.7	0.7	0.2	0.1		0				
15PUC104	33	12	50	4.6	0	0.2	0.4		0	0		1	44	5		
15PUC105	25	17	52	0.9	2.8	0	0.5	0.1	0.1	1.5	0.2	0	47	12		
15PUC106	36	29	19	13	0	1.5	0.1	0.5	0.2	0.1	0.1	0	39	12		6
15PUC107	41	23	24	10	1.8	0	1.3	0.1	0.1	0.3	0.1	0	39	18	28	12
15PUC108	65	16	8.7	8.7	0	0	1.4		0	0.1		0	13	16		
15PUC109	28	18	49	2.2	1.2	0	1.2		0	0.2	0.1	1	25	49		12
15PUC110	44	27	16	6.1	4.9	0	2		0.1	0.3		0	251	8		
15PUC111	33	23	33	8.9	0	0.5	2	0.3	0.3	0.2		1	23	9		
15PUC112	35	25	24	11	0	0.7	2.5	0.7	0.5	0.3	0.2	0	26	25		8
15PUC113	29	20	9.8	26	0	5.7	6.7	0.8	1.1	0.2		4	18	22		
15PUC114	37	30	24	4	0	3	1.2	0.4	0.1	0.1		0	14	9		29
15PUC115	38	23	35	1	0	3	0	0	0	0		0	32	23		20
15PUC116	36	31	23	5	0	3	1.4	0.6	0.2	0.1		0	16	21		36
15PUC117	42	24	22	8	0.4	0	2.5	0.6	0.5	0.3	0	0	20	12	67	62
15PUC118	36	32	24	4.7	0	1.5	1.2	0.4	0.4	0.2	0.2	1	11	10	37	21
15PUC119	42	33	17	5	0	1.8	0.2	0.2	0.2	0.2	0	0	24	18	24	28
15PUC120	32	30	29	5.6	0	2.2	0.1	0.3	0.2	0.1	0	1	16	6		37
15puc121A	33	29	28	7.3	0.3		1.5	0.3	0.3	0.1		8	35	19		17
15puc121B	34	30	27	6.8	0	0.3	1.4	0.3	0.3	0.1		8	28	11		22
15PUC122	40	31	20	5.9	0	1.2	1.2	0.4	0.3	0.1	0	0	18	18	22	18
15PUC123	28	35	27	6.6	0	1.5	0.7	0.3	0.3	0.1	0.2	1	29	9		23
15PUC124	2.1	37	50	3.2	0	3.4	2	0.7	0.9	0.4	0.1	2	35	34		18
15PUC125	40	33	17	6.5	0	1.3	1.1	0.3	0.3	0.1	0	0	10	13		14

Table B-3, continued: CIPW norms & selected trace element data for analyzed Pogo rocks

Sample #	Qtz	Alb	Or	An	Cor	Di	Hyp	Ilm	Mt	Ap	Pyr	Ni	Pb	Zn	As	Th
15PUC126	3.3	63	26	1.6	0	4.2	0.4	0.3	0.7	0	0.2	0	15	23		18
15puc127A	3.5	52	32	5	0	3.5	2	0.7	1.2	0.1		2	21	44		18
15puc127B	2.5	52	35	4.2	0	3.1	1.6	0.8	1.1	0.4		3	17	47		
15PUC128	17	20	9.3	31	0	4.5	14	1.7	2	0.2		5	38	84		
15PUC129	25	32	32	2	2.7	0.0	3	0.1		0.4		0	21	35	0	
15PUC130	39	26	20	10	0.3	0	3.2	0.2	0.5	0.1		0	23	23		
15PUC131	22	19	9.9	26	0	10	7.9	1.7	2.1	0.3	0.2	6	33	85		11
15PUC132	15	18	6.9	30	0	13	13	1.6	2.2	0.3		10	14	65		
15PUC133	18	20	9.6	30	0	3.4	15	1.7	2.1	0.3		5	19	85		
15PUC134	34	32	22	8.9	0	0.7	1.7	0.3	0.4	0.1	0	0	20	13	37	12
15PUC135	15	19	9.8	29	0	8.1	15	1.6	2	0.3		20	36	58		
15PUC136	18	23	10	31	0	2.7	11	1.5	1.6	0.3		5	8	55		
15PUC137	24	22	7.5	31	0	3.3	9.2	1.4	1.3	0.2		3	29	41		
15PUC138	30	21	9.4	28	0.4	0	9.8	1.2	1.1	0.2		3	16	34		
15PUC139	19	21	10	33	0	1.1	12	1.5	1.7	0.5		3	10	66		
15PUC141	29	29	8.2	22	0	1.9	7.3	1.1	1.1	0.2		2	7	32		
15PUC143	20	24	11	20	0	13	6.9	1.6	1.7	0.4	0.4	15	25	55		8
15PUC144	17	18	13	27	0	11	11	1.4	1.8	0.2		15	25	54		
15PUC145	15	18	8.8	28	0	20	6.7	1.6	2	0.3		18	24	59		
15PUC146	36	20	13	20	1	0	6.8	1.4	1.1	0.4		3	9	41		
15PUC147	13	19	9.3	32	0	8.1	15	1.4	1.9	0.3		27	44	56		
15PUC148	10	17	7.8	37	0	5.2	18	1.7	2.3	0.3		24	31	72		
15PUC149	25	19	13	26	0	2.6	11	1.3	1.5	0.2		5	30	52		
15PUC150	19	22	11	27	0	5	12	1.6	1.7	0.5	0.1	4	33	65		8
15PUC151	19	19	12	28	0	4.2	15	1.6	1.9	0.3		9	19	67		
15PUC152	18	18	11	28	0	7.2	15	1.6	1.9	0.2		9	20	62		
15PUC153	16	18	12	28	0	6.7	15	1.7	2	0.3		8	28	70		
15PUC154	19	19	11	29	0	5.6	13	1.7	1.9	0.3		8	25	68		
15PUC155	18	19	9.3	32	0	5.5	13	1.6	1.8	0.3		6	20	66		
15PUC156	17	19	12	28	0	6.7	13	1.5	1.8	0.3		11	33	54		
15PUC157	18	22	13	25	0	6.9	12	1.5	1.8	1.1	0.2	8	9	49	32	10
15PUC158	18	18	12	28	0	6.1	14	1.5	1.9	0.2		15	29	55		
15PUC159	37	17	12	23	0.7	0	7.1	1.6	1.1	0.5		1	27	33		
15PUC160	37	27	27	3.4	3.3	0	1.6	0.2	0.3	0.3		0	26	25		
15PUC161	35	24	34	2	2.3	0	1.4	0.1	0.2	1.1		0	24	15		
15PUC162	39	26	28	2	3	0	1.4	0.1	0.2	0.3		0	17	21		
15PUC163	48	23	19	2.4	5.2	0	1.9	0.1	0.3	0.4		0	23	435		
15PUC164	39	23	31	0.7	4.2	0	1.6	0.1	0.3	0.5		0	18	15		
15PUC165	39	23	30	3.5	2.1	0	1.6	0.2	0.3	0.4		0	21	10		
15PUC166	39	26	28	2.4	2.6	0	1.5	0.2	0.2	0.4		0	19	22		

Table B-3, continued: CIPW norms & selected trace element data for analyzed Pogo rocks

Sample #	Qtz	Alb	Or	An	Cor	Di	Hyp	Ilm	Mt	Ap	Pyr	Ni	Pb	Zn	As	Th
15PUC167	32	20	42	3.1	2.3	0	0.9	0.1	0.1	0.3		0	21	3		
15PUC168	31	24	36	6	0	0.5	1.6	0.3	0.3	0.2	0.1	1	29	16		15
15PUC169	29	33	28	6.2	0	2.7	0.3	0.3	0.3	0.2	0	0	45	21		8
15PUC170	61	15	15	6.9	2.2	0.8	1.1	0.4	0.3	0	0.1	1	21	15		10
15PUC171	37	37	16	4.7	0	2.4	0.9	0.4	0.3	0.1	0	1	21	15		17
15PUC172	32	25	32	8.5	0	0.9	0.8	0.1	0.2	0.1		0	26	11		
15PUC173	30	31	32	4.6	0.4	0	1.2	0.1	0.2	0.1		0	21	14		
15PUC174	29	35	30	3.3	0.3	0	1.4	0.1	0.2	0.1		0	16	6		
15PUC175	47	21	20	8.2	0.9	0	2	0.2	0.4	0.1		0	14	12		
15PUC176	41	26	24	6.2	1.5	0	1.3	0.1	0.2	0.1		0	35	8	87	
15PUC177	39	24	28	3.3	2.6	0	1.4	0.2	0.2	0.3		0	19	17		
15PUC178	35	34	22	3.4	2.8	0	1.4	0.1	0.2	0.3		0	18	17		
15PUC179	40	21	32	3	2.5	0	1.1	0.1	0.2	0.2		0	23	12		
15PUC180	32	18	39	5.6	1.2	0	2.8	0.3	0.5	0.1		0	31	16		
15PUC181	40	15	22	13	1.6	0	6.4	0.8	1.1	0.2		3	15	34		
15PUC182	36	17	20	17	0	0.4	8	1	1.3	0.2		5	15	46		
15PUC183	37	23	28	8.5	0.9	0	1.9	0.3	0.3	0.1		1	19	11		
15PUC184	50	22	18	6	2.1	0	1.2	0.1	0.3	0	0	0	16	14		6
15PUC185	40	19	24	9.8	0	5.6	1.3	0.6	0.7	0.1	0	2	25	33		15
15PUC186	46	24	19	8.2	0.9	0	1.7	0.1	0.3	0		0	16	11		
15PUC187	43	17	19	15	0.2	0	4.9	0.6	0.8	0.1		1	12	27		
15PUC188	43	21	26	6.1	0.9	0	2.1	0.2	0.4	0.1		0	26	10		
15PUC189	41	16	38	3.6	0.4	0	1	0.2	0.2	0.1		1	26	11		
15PUC190	44	20	17	14	0.8	0	4	0.6	0.7	0.1		2	19	25		
15PUC191	41	16	20	15	0.9	0	5.5	0.8	0.9	0.2		3	12	27		
15PUC192	37	25	30	5.2	0	1.3	0.7	0.2	0.3	0	0.2	0	29	19		24
15PUC193	34	21	19	17	0.8	0	6.1	0.7	1	0.2		4	12	34		
15PUC194	39	36	19	3.3	0.4	0	1	0.1	0.2	0.4	0.3	0	16	25		20
15PUC195	36	23	18	14	0	2	4	0.7	0.9	0.2	0.1	2	9	41		
15PUC196	42	22	24	7.8	1.0	0	2.3	0.3	0.4	0.1		0	138	12		
15PUC197	41	19	37	2.4	0	0.6	0.5	0.1	0.2	0	0.1	0	29	19		6
15PUC198	38	38	15	5.5	0	3	0.2	0.2	0.4	0	0.1	0	27	17	31	20
15PUC199	12	18	10	31	0	7.6	17	1.7	2.8	0.2		11				
15PUC200	14	19	10	31	0	5.6	15	1.7	2.6	0.2		6				
15WT01	16	24	12	30	0	5.8	9.9	1.2	1.5	0.2	0.1	11	30	33		
15WT02	28	28	16	15	1.1	0	8	1.1	1.2	1.2	0.2	8	15	42		
15WT03	36	27	21	11	0.7	0	2.6	0.5	0.4	0.7	0.1	1	22	35		
15WT04	38	24	13	17	0.9	0	4.6	0.9	0.7	0.2		0	69	19		
15WT05	40	21	17	15	1.1	0	4.7	0.8	0.7	0.2		2	54	31		
15WT06	42	19	27	8.8	2.2	0	8.5	1.4	1.3	0.1		10	101	41		
15WT07	21	19	11	28	0	4.6	13	1.5	1.8	0.2		7	21	59		
15WT08	18	18	12	27	0	8.3	13	1.6	1.9	0.3		11	28	65		

Table B-3, continued: CIPW norms & selected trace element data for analyzed Pogo rocks

Sample #	Qtz	Alb	Or	An	Cor	Di	Hyp	Ilm	Mt	Ap	Pyr	Ni	Pb	Zn	As	Th
15WT09	43	19	27	7.6	0.5	0	1.5	0.2	0.2	0.1		1	29	11		
15WT10	63	10	12	3.6	3.2	0	6.6	0.9	0.8	0.2		11	18	43		
15WT11	48	10	17	7.7	5.6	0	8.7	1.1	1.1	0.2		11	10	47		
15WT12	39	24	21	10	0.7	0	2.9	0.7	0.5	0.3	0	2	12	29		
15WT13	54	4.4	16	3	7.4	0	13	0.7	1.5	0.1		8	10	55		
15WT14	10	17	7.9	32	0	10	19	1.3	2.3	0.2		25	24	66		
15WT15	20	21	11	28	0	6.8	10	1.6	1.7	0.3	0.2	7	20	70		
15WT16	22	21	12	27	0	4.7	10	1.4	1.6	0.3	0.1	4	33	70		
15WT17	19	19	9.4	30	0	5.3	14	1.4	1.8	0.3		8	23	59		
15WT18	14	26	9.9	28	0	8	11	1.2	1.6	0.3	0.1	4	14	63		
15WT19	17	20	10	29	0	4.9	15	1.6	1.9	0.3		16	22	64		
15WT20	17	19	9.5	31	0	4.6	15	1.6	1.9	0.3		17	24	65		
15WT21	39	22	31	5.6	0.9	0	0.8	0.2	0.1	0.3	0	0	34	11	145	
15WT22A	37	26	22	8.1	2.5	0	2.5	0.5	0.5	0.3		1	25	23		
15WT22B	38	27	21	9.6	2.4	0	2.5	0.5	0.4	0.2	0	1	23	25		
15WT23	21	20	17	24	0	4.1	11	1.3	1.5	0.3		13	38	46		
15WT24	67	7.2	14	5.2	2.5	0	3.6	0.6	0.5	0.1		3	20	21		
15WT25	21	19	17	24	0	4.2	12	1.4	1.7	0.3		14	26	52		
15WT26	40	22	15	16	0	0.8	5.2	0.6	0.7	0	0	6	15	27		
15WT27#1	33	28	28	9			1.3	0.1	0.4	0		2	22	13		
15WT27#2	35	28	27	8		0.3	1.2	0.1	0.4	0		1	21	16		
15WT28B	40	13	14	22	0	1	7	1.2	1.2	0.2	0.1	7	8	35		
15WT28C	45	27	18	4.6	2.8	0	2.1	0.1	0.3	0.1		0	22	14	46	
15WT29	41	24	18	11	0.2	0	3.8	0.6	0.7	0.2	0.1	1	18	25		
15WT30	28	21	15	24	0	1.3	8	1.2	1.2	0.3		5	17	43		
15WT31	17	19	11	27	0	8.3	14	1.4	1.9	0.3		15	24	55		
15WT32	9.2	20	10	33	0	5	18	1.7	2.3	0.2		13	12	67		
15WT33	28	22	16	23	0	0.6	8.6	1.2	1.3	0.3		3	13	46		
15WT34	23	22	13	27	0	2	10	1.4	1.5	0.3		3	11	56		
15WT35	28	23	16	23	0	0.5	8.4	1.2	1.2	0.3		3	13	48		
15WT36	26	24	11	25	0	1.6	8.5	1.4	1.3	0.3		2	25	57		
15WT37	33	22	14	22	0.9	0	6.2	1	0.9	0.4		3	11	41		
15WT38	19	21	10	32	0	0.1	14	1.9	1.9	0.4		5	16	74		
15WT39	18	22	12	31	0	2.8	11	1.6	1.7	0.3		6	9	62		
15WT40	26	24	14	22	0	3.5	7.4	1.3	1.3	0.4	0.1	3	11	57		
15WT41	30	19	17	23	0	0.1	8.2	1.3	1.2	0.3		1	13	54		
15WT42	30	20	16	23	0	0	7.8	1.2	1.2	0.3		3	21	60		
15WT43	6	24	10	23	0	24	5.2	4	2.4	1.3	0.3	94	14	97		
15WT44	48	8.9	19	2	7.5	0	11	1.5	1.5	0.1		27	15	57		
15WT45	56	5.8	18	0.1	8.4	0	9.5	0.6	1.2	0.4		16	17	42		
15WT46	35	27	23	11	0.6	0	2.4	0.4	0.4	0.1		0	20	16		
15WT47	38	21	35	2.3	2.5	0	0.7	0.1	0.1	0.4		0	24	4		

Table B-3, continued: CIPW norms & selected trace element data for analyzed Pogo rocks

Sample #	Qtz	Alb	Or	An	Cor	Di	Hyp	Ilm	Mt	Ap	Pyr	Ni	Pb	Zn	As	Th
15WT48	35	35	24	1.7	2.8	0	0.8	0.1	0.2	0.5	0.1	0	18	113		
15WT49	42	21	30	2.4	2.6	0	1.1	0.1	0.2	0.3		0	22	15		
15WT50	40	17	35	1.3	4.2	0	0.5	0.1	0.1	0.5	0.4	0	51	8		
15WT51	46	28	15	4.8	4.2	0	1.4	0.1	0.2	0.4		0	3	8		
15WT52	40	24	29	1.9	3.5	0	1	0.1	0.2	0.4		0	22	18		
15WT53	19	23	45	6.7	0.6	0	3.7	0.4	0.4	1.8		6	51	15		
15WT54	38	35	14	11	0	0.8	0	0	0	0.2	0.1	6	30	1	34	
15WT55	41	23	29	1.5	3.3	0	1.6	0.2	0.3	0.4		0	24	25		
15U259a	13	21	11	29		9.3	14	1.0	0.6	0.3		29				
15U368A	0	2	9	23	0	25	32	2	4	0		162				
16WT01	14	24	8.4	30	0	7.2	12	1.5	1.9	0.3	0.1	13	25	60		
16WT02	16	24	9.8	31	0	6.7	10	1.3	1.6	0.3	0.1	11	29	65	33	
16WT03	17	23	14	26	0	7.3	11	1.2	1.6	0.3	0.1	15	25	46		
16WT04	18	22	15	25	0	6.7	9.4	1.4	1.5	0.2	0.1	12	26	53		
16WT05	34	27	26	9.7	0	0.3	2	0.4	0.4	0.3	0.1	1	37	28	12	17
16WT06	37	26	21	11	0	0	2.8	0.7	0.5	0.3	0.1	2	29	30		
16WT08	16	23	12	26	0	7.2	11	1.5	1.7	0.3	0.2	14	21	69		
16WT08	17	17	12	26	0	8.4	15	1.8	2.6	0.3		14				
16WT09	16	24	13	26	0	7.9	9.1	1.4	1.6	0.3	0.1	7	34	51		
16WT10	36	24	17	15	0	2.6	3.5	0.7	0.9	0.3	0.1	2	11	41		
16WT11	16	21	8.7	26	0	14	9.9	1.7	2	0.3	0.2	8	19	66		
16WT12	27	27	14	20	0	2.4	6.6	1.1	1.2	0.4	0.1	7	19	41		
16WT13	37	24	28	7.3	0.4	0	1.8	0.3	0.3	0.2	0.1	3	67	29		
16WT15	37	24	28	4.3	3.6	0	2.3	0.2	0.2	0.3		0	23	22		
16WT16	37	25	23	11	0	0.1	2.6	0.6	0.5	0.3	0.1	1	25	30		
16WT17	34	26	19	15	0	0.7	3	0.7	0.6	0.3	0	2	15	32		
16WT18	36	29	21	10	0.3	0	2.6	0.5	0.5	0.2	0.1	0	39	26		
16WT19	38	28	22	8.8	0	0.9	1.8	0.5	0.4	0.2	0.1	1	19	32		
16WT20	34	32	27	3.5	1.6	0	1.4	0.2	0.3	0.3	0	0	27	20	21	
16WT-935A	15	23	10	26	0	11	11	1.5	1.9	0.3	0.3	13	28	72	43	
16WT-935B	3.5	22	9.9	28	0	11	21	1.7	2.2	0.7	0.2	35	23	50	28	
16WT-975	19	22	12	26	0	6.6	11	1.5	1.7	0.3	0.1	5	36	64	31	
17P04-242	34	18	27	4.7	7.3	0.0	5.0	2.9	4.4	0.1		33				
17PGN01	24	11	21	5.4	16	0.0	19	2.3	0.9	0.3		35				
DL04	19	27	14	24	0	2.1	9.7	1.8	1.6	0.3	0.1	7	30	74	42	
DL1A	0.0	14	2.8	32	0	26	11	2.6	1.8	0.2	0.2	105	5.3	84	12	1
DL2A	1.8	24	6.7	29	0	11	20	4.2	1.6	1	0	88	6.6	128	6	5
DL3A	0.6	23	2	27	0	21	22	2.2	1.5	0.2	0.6	102	4.4	76	72	1
DL4A	3.6	21	16	20	0	12	20	4.5	1.7	0.7	0.9	46	9.1	124	15	9
DL5A	8.6	24	11	23	0	9.8	17	3.7	1.5	0.6	0.4	15	11	114	5	13
DL6A	8.8	13	13	27	0	9.1	25	2.2	1.3	0.3	0	59	5.3	87	7	5
DL7A	13	13	15	24	0	5	25	2.2	1.4	0.3	0.5	108	7.3	99	6	5

Table B-3, continued: CIPW norms & selected trace element data for analyzed Pogo rocks

Sample #	Qtz	Alb	Or	An	Cor	Di	Hyp	Ilm	Mt	Ap	Pyr	Ni	Pb	Zn	As	Th
DL82	35	21	10	21	0.2	0	10	1.3	1.9	0.3		1				
DL8A	13	24	11	24	0	8.1	16	2.7	1.3	0.6	0.2	30	13	99	2	15
DL9A	10	27	14	22	0	6.4	15	2.3	1.2	1.3	0.3	30	16	92	44	21
DL10A	16	15	11	27	0	7.3	20	2.4	1.2	0.4	0	32	7.2	88	10	17
DL11	36	19	19	10	0.6	0	13	1	0.8	0.4	0.2	23	7	51	6	23
DL11A	40	19	16	10	4.6	0	15	1.8	1.1	0.1	0.1	43	18	107	1	12
DL12A	40	17	21	9.9	3.9	0	10	1.4	0.8	0.4	0.3	19	9.6	43	36	25
DL13A	38	16	19	13	5	0	8.8	1.6	3.1	0.2	0.2	44	18	104	5	9
MAF1												15	13	97		
S Pogo1	41	26	19	7.6	3	0	2.4	0.6	0.6	0.3		0				
S Pogo2	40	26	19	7.3	3.6	0	2.4	0.6	0.6	0.2		0				

Appendix C: Laser Ablation ICP-MS U-Pb zircon age data for Pogo Samples

Table C-1: U-Pb data for sample 4021A

#	ppm U	ppm Th	U/Th	$^{206}Pb/^{238}U$	±2 s	$^{207}Pb/^{235}U$	±2 s	$^{208}Pb/^{232}Th$	±2 s	$^{206}Pb/^{238}U$ Age (Ma)	±2 s
1	1240	865	1.4	0.0576	0.0010	0.42	0.01	0.0181	0.0004	361	6
2	1032	673	1.5	0.0597	0.0009	0.46	0.01	0.0194	0.0005	374	6
3	1850	1859	1.0	0.0547	0.0014	0.40	0.01	0.0174	0.0004	343	9
4	2092	1071	2.0	0.0566	0.0014	0.42	0.01	0.0189	0.0004	355	8
5	434	302	1.4	0.0521	0.0013	0.38	0.02	0.0197	0.0006	327	8
6	1937	802	2.4	0.0484	0.0012	0.36	0.01	0.0158	0.0004	305	8
7	2094	1175	1.8	0.0486	0.0010	0.35	0.01	0.0158	0.0004	306	6
8	234	18	13	0.0174	0.0005	0.12	0.02	0.0077	0.0012	111	3
9	1787	837	2.1	0.0559	0.0011	0.42	0.01	0.0176	0.0004	350	7
10	1846	808	2.3	0.0504	0.0013	0.37	0.01	0.0169	0.0004	317	8
11	935	415	2.3	0.0513	0.0009	0.38	0.02	0.0170	0.0004	322	6
12	911	629	1.4	0.0578	0.0010	0.43	0.02	0.0185	0.0004	362	6
13	2291	1480	1.5	0.0570	0.0012	0.42	0.01	0.0181	0.0004	357	7
14	962	883	1.1	0.0532	0.0010	0.40	0.02	0.0179	0.0004	334	6
15	1352	3725	0.4	0.0577	0.0012	0.42	0.02	0.0182	0.0004	361	7
16	352	152	2.3	0.0542	0.0013	0.40	0.02	0.0180	0.0007	340	8
17	856	465	1.8	0.0552	0.0011	0.42	0.02	0.0188	0.0005	347	7
18	309	2	141	0.0183	0.0005	0.13	0.02	0.0119	0.0056	117	3
19	633	767	0.8	0.0533	0.0009	0.39	0.02	0.0177	0.0004	335	6
20	1379	761	1.8	0.0569	0.0012	0.42	0.01	0.0186	0.0004	356	7
21	265	266	1.0	0.0569	0.0013	0.43	0.03	0.0189	0.0006	357	8
22	509	1012	0.5	0.0567	0.0011	0.43	0.02	0.0179	0.0005	355	7
23	1364	511	2.7	0.0565	0.0011	0.41	0.01	0.0184	0.0005	354	7
24	1074	585	1.8	0.0578	0.0010	0.42	0.01	0.0188	0.0005	362	6
25	502	871	0.6	0.0564	0.0011	0.41	0.02	0.0186	0.0004	354	7
26	797	261	3.0	0.0580	0.0010	0.43	0.02	0.0187	0.0005	364	6
27	2428	1043	2.3	0.0565	0.0012	0.41	0.01	0.0185	0.0004	354	8
28	1164	563	2.1	0.0569	0.0010	0.42	0.01	0.0181	0.0004	357	6
29	918	996	0.9	0.0586	0.0011	0.44	0.02	0.0186	0.0004	367	7
30	1784	910	2.0	0.0542	0.0013	0.40	0.01	0.0175	0.0004	340	8
31	1054	931	1.1	0.0568	0.0012	0.42	0.02	0.0188	0.0004	356	8
32	1090	503	2.2	0.0574	0.0013	0.42	0.01	0.0188	0.0005	360	8
33	1926	683	2.8	0.0559	0.0011	0.41	0.01	0.0180	0.0004	351	7
34	766	342	2.2	0.0568	0.0012	0.41	0.01	0.0182	0.0005	356	8
35	698	295	2.4	0.0552	0.0009	0.41	0.02	0.0178	0.0005	346	6
36	1045	813	1.3	0.0550	0.0010	0.40	0.02	0.0179	0.0004	345	6
37	2059	1350	1.5	0.0564	0.0011	0.42	0.01	0.0182	0.0004	354	7
38	1218	608	2.0	0.0519	0.0012	0.39	0.02	0.0155	0.0005	326	7
39	531	197	2.7	0.0482	0.0011	0.35	0.02	0.0175	0.0006	303	7
40	1540	989	1.6	0.0502	0.0011	0.36	0.01	0.0168	0.0003	316	6
41	928	291	3.2	0.0552	0.0010	0.41	0.02	0.0176	0.0005	347	6

Table C-1, continued: U-Pb data for sample 4021A

#	ppm U	ppm Th	U/Th	$^{206}Pb/^{238}U$	±2 s	$^{207}Pb/^{235}U$	±2 s	$^{208}Pb/^{232}Th$	±2 s	$^{206}Pb/^{238}U$ Age (Ma)	±2 s
42	921	482	1.9	0.0562	0.0010	0.42	0.02	0.0177	0.0004	352	6
43	1492	994	1.5	0.0567	0.0012	0.41	0.01	0.0179	0.0004	355	7
44	882	427	2.1	0.0575	0.0010	0.42	0.01	0.0179	0.0005	360	6
45	1118	658	1.7	0.0574	0.0010	0.43	0.02	0.0183	0.0004	360	6
46	1397	429	3.3	0.0571	0.0014	0.42	0.01	0.0187	0.0005	358	9
47	1585	474	3.3	0.0558	0.0010	0.41	0.01	0.0180	0.0004	350	6
48	524	2	228	0.0172	0.0004	0.12	0.01	0.0391	0.0091	110	3
49	1069	331	3.2	0.0476	0.0009	0.34	0.01	0.0177	0.0005	300	5
50	668	902	0.7	0.0516	0.0012	0.38	0.02	0.0178	0.0005	324	7

Table C-2: U-Pb data for sample 4021B

#	ppm U	ppm Th	U/Th	$^{206}Pb/^{238}U$	±2 s	$^{207}Pb/^{235}U$	±2 s	$^{208}Pb/^{232}Th$	±2 s	$^{206}Pb/^{238}U$ Age (Ma)	±2 s
1	260	50	5.2	0.0583	0.0025	0.418	0.034	0.0183	0.0012	365	15
2	1006	227	4.4	0.0599	0.0023	0.444	0.020	0.0189	0.0009	375	14
3	140	56	2.5	0.0557	0.0025	0.429	0.037	0.0179	0.0011	350	16
4	391	235	1.7	0.0568	0.0022	0.423	0.028	0.0182	0.0008	356	14
5	129	145	0.9	0.0611	0.0026	0.460	0.044	0.0180	0.0009	382	16
6	587	304	1.9	0.0573	0.0020	0.417	0.020	0.0179	0.0007	359	12
7	247	98	2.5	0.0563	0.0025	0.424	0.030	0.0168	0.0011	353	15
8	171	116	1.5	0.0575	0.0023	0.431	0.033	0.0186	0.0009	361	14
9	2866	491	5.8	0.0560	0.0018	0.413	0.016	0.0181	0.0006	351	11
10	635	172	3.7	0.0555	0.0021	0.409	0.020	0.0176	0.0008	348	13
11	417	122	3.4	0.0591	0.0025	0.447	0.026	0.0179	0.0009	370	15
12	563	122	4.6	0.0573	0.0019	0.430	0.022	0.0191	0.0009	359	12
13	384	269	1.4	0.0555	0.0029	0.417	0.028	0.0186	0.0010	348	18
14	730	347	2.1	0.0579	0.0028	0.438	0.023	0.0190	0.0010	369	16
15	141	26	5.4	0.0172	0.0009	0.120	0.021	0.0056	0.0009	110	5
16	189	229	0.8	0.0559	0.0023	0.421	0.036	0.0189	0.0009	351	14
17	458	283	1.6	0.0573	0.0020	0.431	0.026	0.0184	0.0007	359	12
18	820	206	4.0	0.0597	0.0019	0.443	0.020	0.0199	0.0008	374	11
19	268	84	3.2	0.0591	0.0026	0.446	0.029	0.0187	0.0010	370	16
20	624	209	3.0	0.0572	0.0024	0.423	0.024	0.0185	0.0010	359	14
21	802	16	50	0.0176	0.0010	0.118	0.009	0.0077	0.0012	113	7
22	643	289	2.2	0.0597	0.0024	0.439	0.023	0.0189	0.0009	374	15
23	419	106	4.0	0.0606	0.0027	0.451	0.028	0.0192	0.0010	379	17
24	194	55	3.5	0.0565	0.0016	0.422	0.032	0.0179	0.0010	354	10
25	362	83	4.4	0.0598	0.0014	0.442	0.023	0.0200	0.0008	374	8
26	129	60	2.2	0.0176	0.0011	0.128	0.022	0.0058	0.0007	112	7
27	587	113	5.2	0.0567	0.0013	0.414	0.019	0.0183	0.0008	355	8
28	301	140	2.2	0.0552	0.0012	0.397	0.026	0.0183	0.0007	346	8

Table C-2, continued: U-Pb data for sample 4021B

#	ppm U	ppm Th		$^{206}Pb/^{238}U$	±2 s	$^{207}Pb/^{235}U$	±2 s	$^{208}Pb/^{232}Th$	±2 s	$^{206}Pb/^{238}U$ Age (Ma)	±2 s
29	334	141	2.4	0.0576	0.0009	0.418	0.022	0.0188	0.0006	361	6
30	539	120	4.5	0.0589	0.0011	0.431	0.021	0.0188	0.0007	369	7
31	263	40	6.6	0.0575	0.0014	0.432	0.028	0.0192	0.0012	361	8
32	787	199	4.0	0.0537	0.0010	0.400	0.017	0.0185	0.0006	337	6
33	563	377	1.5	0.0555	0.0010	0.412	0.019	0.0175	0.0004	348	6
34	385	256	1.5	0.0583	0.0011	0.432	0.024	0.0179	0.0005	365	6
35	2400	568	4.2	0.0572	0.0012	0.421	0.013	0.0181	0.0005	358	7
36	167	85	2.0	0.0571	0.0017	0.425	0.038	0.0184	0.0009	358	10
37	482	120	4.0	0.0565	0.0018	0.420	0.025	0.0185	0.0008	354	11
38	1578	298	5.3	0.0568	0.0025	0.421	0.023	0.0180	0.0008	356	15
39	698	191	3.7	0.0588	0.0023	0.438	0.023	0.0186	0.0009	368	14
40	765	485	1.6	0.0582	0.0023	0.428	0.020	0.0177	0.0007	365	14
41	80	69	1.2	0.2867	0.0120	4.070	0.209	0.0804	0.0036	1648	42
42	565	235	2.4	0.0584	0.0011	0.430	0.018	0.0186	0.0006	366	7
43	607	132	4.6	0.0574	0.0011	0.431	0.019	0.0189	0.0007	360	7
44	183	85	2.2	0.0481	0.0016	0.359	0.034	0.0192	0.0010	303	10
45	537	205	2.6	0.0554	0.0020	0.412	0.025	0.0184	0.0010	348	12
46	382	87	4.4	0.0574	0.0026	0.433	0.030	0.0183	0.0010	360	16
47	398	86	4.6	0.0580	0.0021	0.437	0.030	0.0186	0.0025	364	13
48	167	145	1.1	0.0578	0.0012	0.462	0.057	0.0184	0.0006	363	7
49	387	153	2.5	0.0599	0.0012	0.456	0.044	0.0196	0.0025	375	7
50	860	144	6.0	0.0460	0.0009	0.332	0.017	0.0176	0.0007	290	5

Table C-3: U-Pb data for sample S. Pogo

#	ppm U	ppm Th	U/Th	$^{206}Pb/^{238}U$	±2 s	$^{207}Pb/^{235}U$	±2 s	$^{208}Pb/^{232}Th$	±2 s	$^{206}Pb/^{238}U$ Age (Ma)	±2 s
1	170	127	1.3	0.2513	0.0119	3.60	0.23	0.0779	0.0043	1550	50
2	445	26	17	0.0237	0.0013	0.174	0.023	0.0182	0.0024	151	8
3	166	84	2.0	0.0167	0.0010	0.114	0.019	0.0050	0.0006	107	6
4	34	12	2.8	0.0167	0.0020	0.124	0.052	0.0063	0.0018	107	12
5	389	83	4.7	0.0165	0.0006	0.114	0.020	0.0058	0.0006	106	4
6	487	87	5.6	0.0166	0.0007	0.114	0.010	0.0052	0.0005	106	4
7	51	40	1.3	0.0156	0.0012	0.118	0.034	0.0060	0.0008	100	8
8	75	64	1.2	0.0163	0.0012	0.113	0.033	0.0052	0.0006	104	8
9	94	50	1.9	0.0167	0.0009	0.122	0.025	0.0058	0.0005	107	6
10	356	4	92	0.0178	0.0008	0.125	0.013	0.0120	0.0039	114	5
11	323	252	1.3	0.0168	0.0010	0.118	0.015	0.0055	0.0004	107	7
12	97	79	1.2	0.0172	0.0010	0.125	0.027	0.0056	0.0007	110	6
13	111	24	4.7	0.1984	0.0200	2.65	0.52	0.0643	0.0139	1166	108
14	173	130	1.3	0.0165	0.0009	0.118	0.020	0.0054	0.0004	106	5

Table C-3, continued: U-Pb data for sample S. Pogo

#	ppm U	ppm Th	U/Th	$^{206}Pb/^{238}U$	±2 s	$^{207}Pb/^{235}U$	±2 s	$^{208}Pb/^{232}Th$	±2 s	$^{206}Pb/^{238}U$ Age (Ma)	±2 s
15	129	60	2.2	0.0176	0.0011	0.128	0.022	0.0058	0.0007	112	7
16	276	240	1.2	0.0167	0.0011	0.121	0.016	0.0053	0.0005	107	7
17	98	65	1.5	0.0163	0.0009	0.115	0.033	0.0061	0.0007	104	6
18	99	68	1.5	0.0171	0.0010	0.123	0.029	0.0055	0.0006	109	7
19	288	173	1.7	0.0176	0.0006	0.124	0.016	0.0055	0.0004	113	4
20	136	86	1.6	0.0564	0.0015	0.433	0.034	0.0181	0.0008	354	9
21	150	28	5.4	0.0250	0.0012	0.194	0.033	0.0231	0.0020	159	8
22	323	195	1.7	0.0169	0.0008	0.117	0.015	0.0054	0.0004	108	5
23	209	106	2.0	0.0168	0.0010	0.116	0.015	0.0053	0.0005	108	7
24	103	54	1.9	0.0171	0.0014	0.139	0.034	0.0077	0.0007	110	9
25	88	60	1.5	0.2074	0.0209	2.81	0.47	0.0640	0.0095	1215	112
26	744	705	1.1	0.0580	0.0016	0.421	0.018	0.0186	0.0006	363	10
27	141	26	5.4	0.0172	0.0009	0.120	0.021	0.0056	0.0009	110	5
28	152	76	2.0	0.0167	0.0006	0.119	0.023	0.0057	0.0006	106	4
29	89	26	3.4	0.0166	0.0009	0.127	0.033	0.0069	0.0010	106	6
30	123	74	1.7	0.0165	0.0008	0.116	0.025	0.0055	0.0005	106	5
31	434	345	1.3	0.0166	0.0005	0.115	0.010	0.0053	0.0003	106	3
32	78	45	1.7	0.0166	0.0010	0.122	0.031	0.0052	0.0006	106	6
33	85	39	2.2	0.0164	0.0010	0.129	0.035	0.0050	0.0010	105	6
34	66	30	2.2	0.0160	0.0011	0.116	0.031	0.0057	0.0012	102	7
35	164	94	1.7	0.0526	0.0014	0.392	0.030	0.0173	0.0010	331	9
36	60	36	1.6	0.0162	0.0008	0.118	0.036	0.0058	0.0009	104	5
37	107	140	0.8	0.0166	0.0007	0.115	0.027	0.0053	0.0004	106	4
38	173	157	1.1	0.0161	0.0007	0.111	0.018	0.0053	0.0004	103	4
39	68	28	2.5	0.0160	0.0013	0.115	0.037	0.0055	0.0009	102	8
40	1178	304	3.9	0.0379	0.0008	0.270	0.011	0.0173	0.0005	240	5
41	243	135	1.8	0.0562	0.0012	0.413	0.024	0.0180	0.0007	352	8
42	95	66	1.4	0.0171	0.0011	0.129	0.026	0.0059	0.0006	109	7
43	283	326	0.9	0.0161	0.0004	0.114	0.016	0.0053	0.0003	103	3
44	69	46	1.5	0.0168	0.0010	0.137	0.031	0.0060	0.0007	108	6
45	49	47	1.1	0.3135	0.0060	4.75	0.19	0.0896	0.0027	1758	29
46	186	112	1.7	0.0166	0.0006	0.119	0.018	0.0054	0.0005	106	4
48	66	34	2.0	0.0172	0.0009	0.113	0.036	0.0064	0.0008	110	6
49	238	226	1.1	0.0163	0.0005	0.113	0.014	0.0053	0.0003	104	3
50	260	2	108	0.0173	0.0006	0.125	0.015	0.0127	0.0047	111	4

Table C-4: U-Pb data for sample Fun Zone

#	ppm U	ppm Th	U/Th	$^{206}Pb/^{238}U$	±2 s	$^{207}Pb/^{235}U$	±2 s	$^{208}Pb/^{232}Th$	±2 s	$^{206}Pb/^{238}U$ Age (Ma)	±2 s
3	1066	723	1.5	0.0544	0.0011	0.396	0.018	0.0170	0.0004	342	6
5	356	4	92	0.0178	0.0008	0.125	0.013	0.0120	0.0039	114	5
9	455	192	2.4	0.0512	0.0012	0.372	0.023	0.0175	0.0006	322	7
11	804	2	334	0.0171	0.0004	0.116	0.007	0.0051	0.0089	109	2
13	1131	641	1.8	0.0352	0.0013	0.255	0.014	0.0124	0.0007	223	8
18	787	390	2.0	0.0531	0.0010	0.386	0.016	0.0176	0.0005	334	6
21	1156	957	1.2	0.0379	0.0010	0.268	0.012	0.0100	0.0005	240	6
23	540	262	2.1	0.0528	0.0010	0.383	0.017	0.0162	0.0005	331	6
25	737	215	3.4	0.0359	0.0006	0.250	0.012	0.0172	0.0006	227	4
26	343	2	155	0.0183	0.0005	0.127	0.011	0.0126	0.0053	117	3
28	802	16	50	0.0176	0.0010	0.118	0.009	0.0077	0.0012	113	7
29	234	18	13	0.0174	0.0005	0.122	0.018	0.0077	0.0012	111	3
31	816	215	3.8	0.0452	0.0009	0.326	0.015	0.0165	0.0006	285	6
32	331	7	50	0.0185	0.0006	0.131	0.016	0.0062	0.0025	118	4
33	306	71	4.3	0.0527	0.0011	0.393	0.024	0.0174	0.0009	331	7
34	555	204	2.7	0.0506	0.0010	0.374	0.032	0.0171	0.0009	318	6
35	661	361	1.8	0.0521	0.0011	0.382	0.018	0.0168	0.0005	327	7
37	428	255	1.7	0.0539	0.0010	0.397	0.020	0.0172	0.0005	338	6
39	260	2	108	0.0173	0.0006	0.125	0.015	0.0127	0.0047	111	4
40	258	5	47	0.0183	0.0006	0.122	0.013	0.0069	0.0029	117	4
41	1648	1462	1.1	0.0531	0.0012	0.390	0.014	0.0172	0.0004	334	7
42	948	525	1.8	0.0468	0.0009	0.339	0.013	0.0171	0.0005	295	6
43	309	2	141	0.0183	0.0005	0.131	0.016	0.0119	0.0056	117	3
44	371	92	4.0	0.0546	0.0012	0.403	0.022	0.0174	0.0008	343	7
45	512	246	2.1	0.0540	0.0011	0.395	0.018	0.0174	0.0006	339	7
46	454	239	1.9	0.0446	0.0010	0.322	0.017	0.0175	0.0006	281	6
47	800	546	1.5	0.0545	0.0009	0.406	0.015	0.0172	0.0004	342	6
50	142	67	2.1	0.0546	0.0015	0.406	0.036	0.0184	0.0010	343	9

Appendix D: Images of zircon grains used for U-Pb dating (excluding those in Chapter 3)

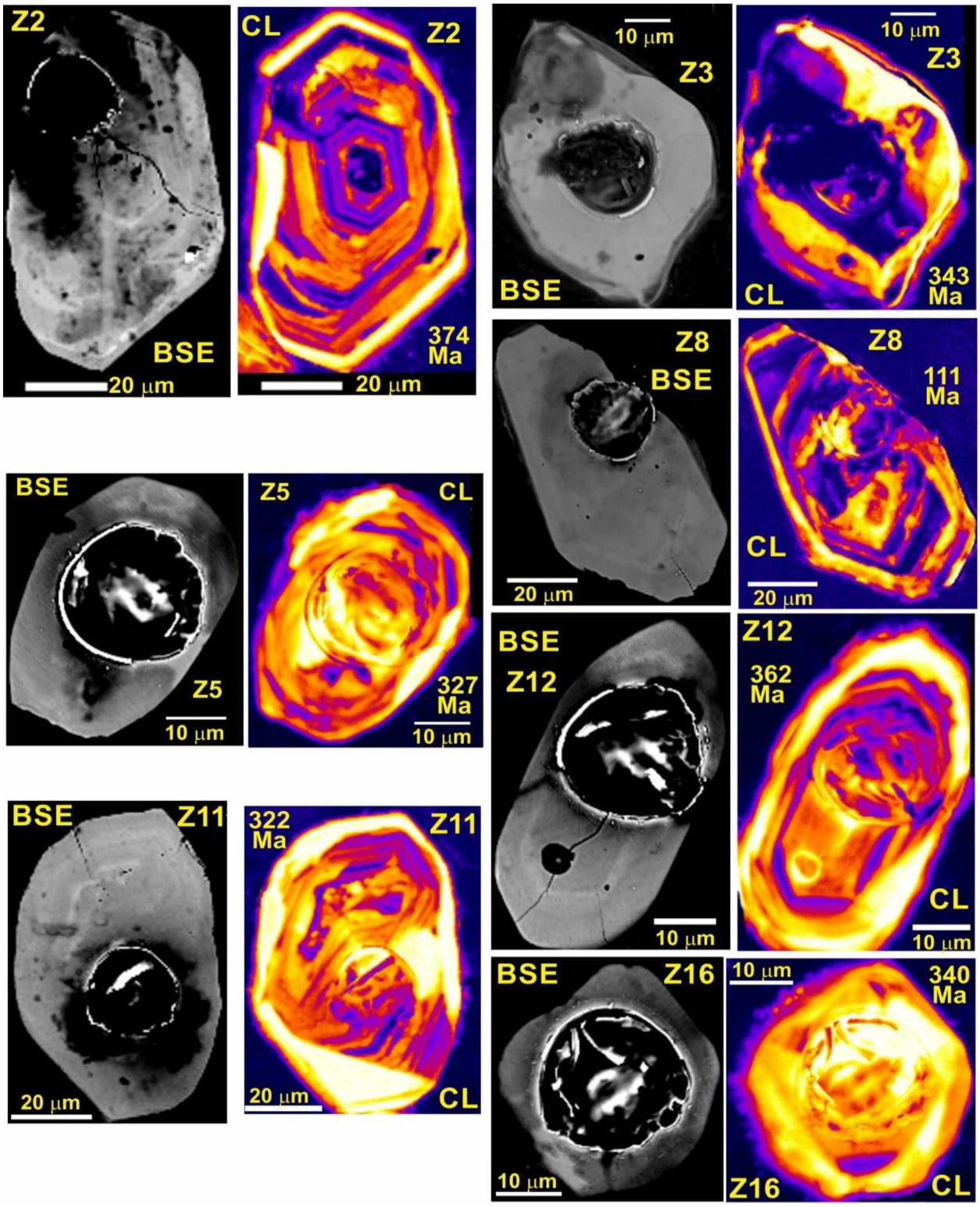

Figure D-1: Back-scattered electron (BSE) and cathodoluminescence (CL) images from 4021A

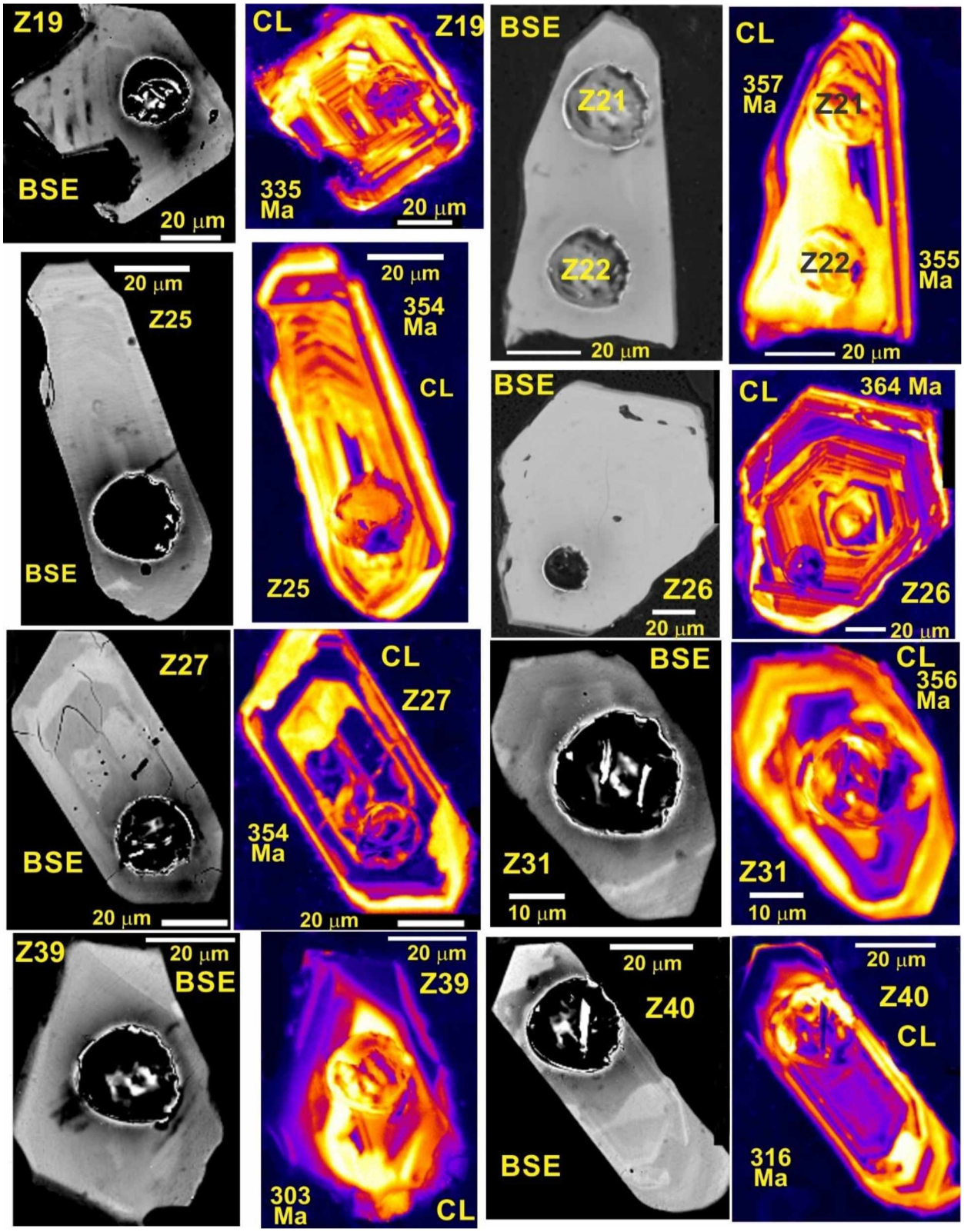

Figure D-1, continued: Back-scattered electron (BSE) and cathodoluminescence (CL) images from sample 4021A, excluding those shown in Chapter 3

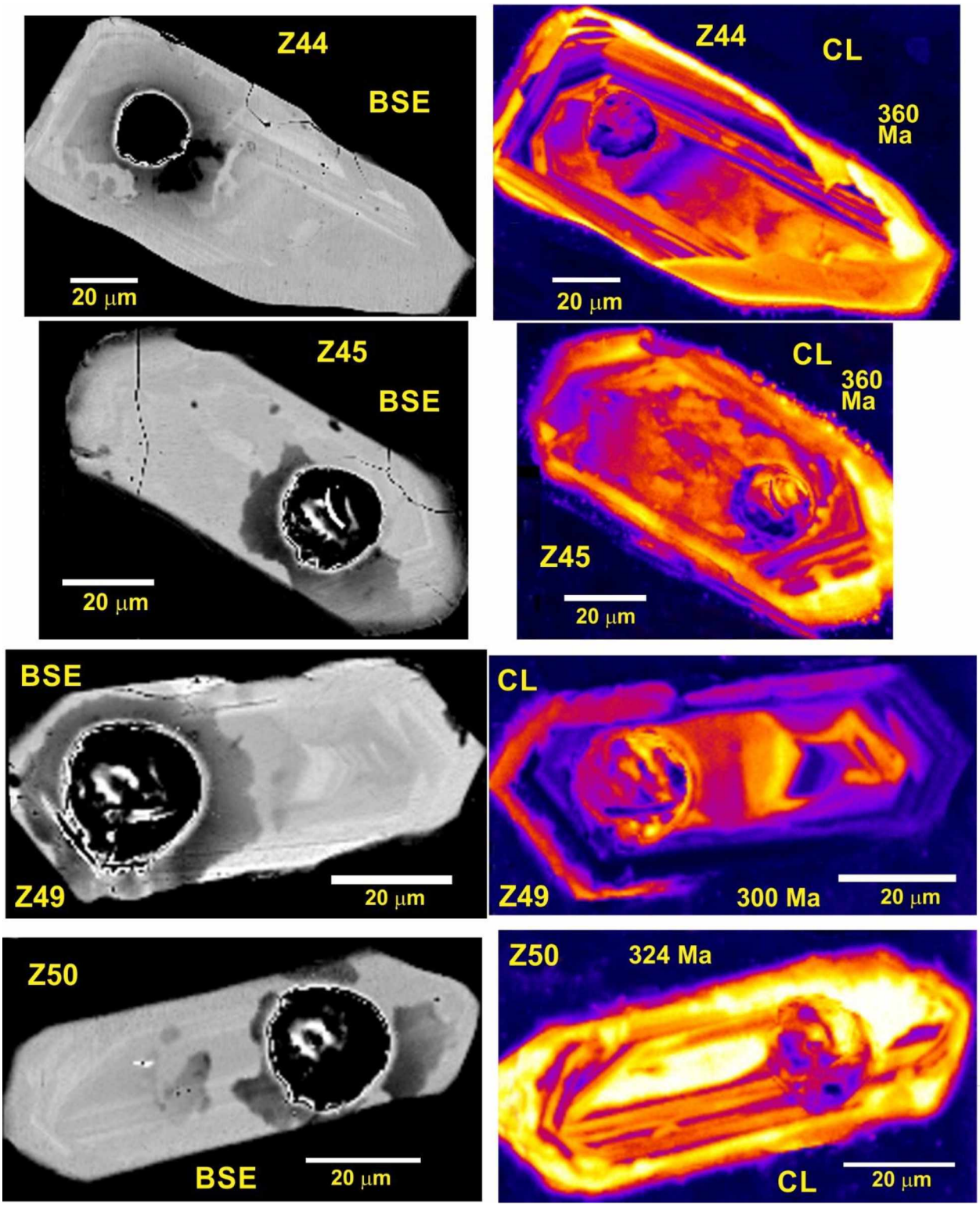

Figure D-1, continued: Back-scattered electron (BSE) and cathodoluminescence (CL) images from sample 4021A, excluding those shown in Chapter 3

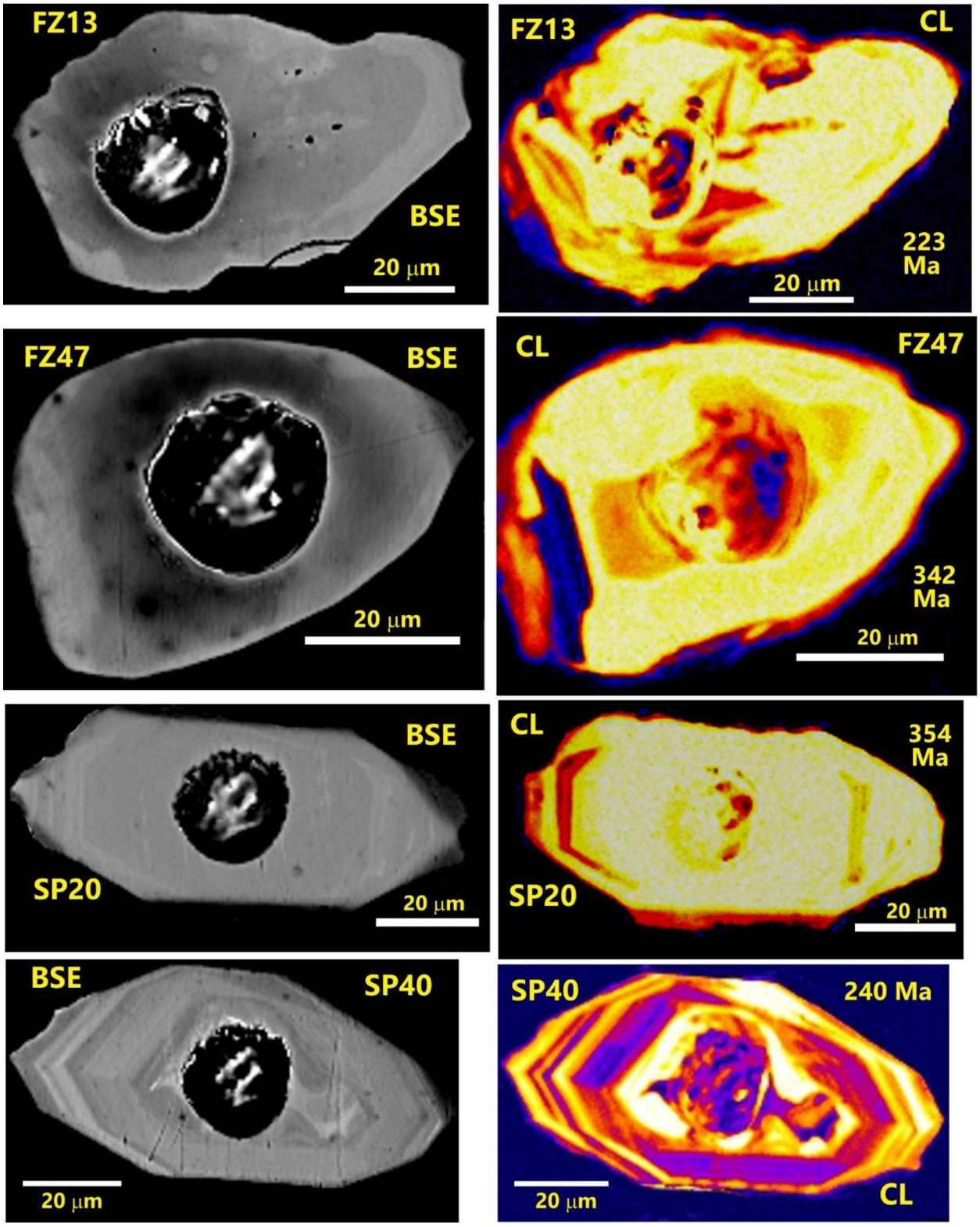

Figure D-2: Back-scattered electron (BSE) and cathodoluminescence (CL) images from samples Fun Zone (FZ) and S. Pogo (SP), excluding those shown in Chapter 3